UNIVERSITY OF SOUTHAMPTON

FACULTY OF ENGINEERING, SCIENCE AND MATHEMATICS

School of Ocean and Earth Science

Neogene paleomagnetism and geodynamics of the Hikurangi margin, East Coast, New Zealand

by

Christopher James Rowan

MSci (Hons.), MA (Hons.)

Thesis for the degree of Doctor of Philosophy

March 2006

UNIVERSITY OF SOUTHAMPTON

ABSTRACT

FACULTY OF ENGINEERING, SCIENCE AND MATHEMATICS
SCHOOL OF OCEAN AND EARTH SCIENCE

Doctor of Philosophy

NEOGENE PALEOMAGNETISM AND GEODYNAMICS OF THE HIKURANGI MARGIN, EAST COAST, NEW ZEALAND

by Christopher James Rowan

Vertical-axis rotations are an important component of Neogene deformation in the New Zealand plate boundary region, and potentially offer fundamental insights into the rheology of continental crust. Extensive paleomagnetic sampling along the Hikurangi margin, on the East Coast of the North Island, has provided new insights into the patterns, rates and timings of tectonic rotation, and also an improved understanding of the magnetic signature of New Zealand Cenozoic mudstones. Rigorous field tests reveal numerous late remagnetizations, which have often formed several million years after deposition and can be irregularly distributed within an outcrop. Scanning electron microscopy and rock magnetic analyses indicate that the remanence carrier is predominantly the ferrimagnetic iron sulphide, greigite, which is present as a mixed population of single domain and superparamagnetic grains that are characteristic of arrested authigenic growth. Strong viscous overprints are the result of later, usually recent, oxidation of these sulphides. The recognition of late-forming magnetizations leads to a completely new view of the Neogene tectonic evolution of the Hikurangi margin, with no tectonic rotations being evident prior to 8–10 Ma; coherent rotation of most of the Hikurangi margin since that time refutes the existence of the independently rotating 'domains' that were inferred from earlier paleomagnetic data. This pattern is more consistent with the short-term velocity field, and allows all Neogene rotation to be more simply explained as a large-scale response to realignment of the subducting Pacific plate. Tectonic rotations have been accommodated by a variety of structures since 10 Ma; in the Late Miocene and Pliocene, rates of tectonic rotation were 3–4 times faster than presently observed and possibly involved a much larger region, before initiation of the North Island Dextral Fault Belt and the Taupo Volcanic Zone at 1-2 Ma instigated the current tectonic regime. Collision of the Hikurangi Plateau in the Late Miocene is interpreted to have caused both the initiation of tectonic rotation, and the widespread remagnetization of sediments, making it a key event in the Neogene evolution of the plate boundary region.

Some thoughts on the nature of scientific research

"It doesn't matter how beautiful your theory is, it doesn't matter how smart you are. If it doesn't agree with experiment, it's wrong."

Richard Feynman

"Our work is like this doughnut. Sure, it's all fluff, has no nutritional value, and there's a gaping hole in the middle... but, if you sugar coat it, and add colourful little sprinkles, people will eat it up."

Mike Slackenerny (as immortalised by Jorge Cham)

Contents

List of Figures

List of Tables

Graduate School of the National Oceanography Centre, Southampton

This PhD. dissertation by

Christopher James Rowan

has been produced under the supervision of Professor Andrew P. Roberts, with additional supervision provided by Dr. Geoff Rait of Talisman Energy Inc.

External Examiner: Dr. John Haines, University of Cambridge.

Internal Examiner: Dr. Adrian Muxworthy.

The research was supported by contributions from the UK Natural Environment Research Council (grant NER/S/2001/06363), the Leverhulme Trust, and the Royal Society of London.

Declaration

The work presented in this thesis is my own, and was done wholly whilst in candidature for a research degree at this University. Where I have consulted or quoted from the published work of others, the source is always clearly attributed. I have acknowledged all main sources of help, and where parts of this work have been published, or have been submitted for publication, this has been clearly stated; in such cases co-authors have contributed in an advisory capacity only.

Signed:

Date:

Acknowledgements

This tome represents an enterprise which has dominated the last 15% of my life. It's disappointingly thin, considering. Nonetheless, in the last four years a cast of tens, nay, dozens, has helped to make this thesis what it is. Of these, a good many are owed a beer or three; others will be the first against the wall when the revolution comes. In either case, they will be remembered. Oh yes.

However, the individuals awarded below deserve particular thanks for their professional and/or moral support during the making of this thesis.

The Llyne Truss Prize (for excellence in the field of pedantry)
Awarded to Andy, my supervisor *par excellence*, for his unerring ability to find a typo or formatting error in even the most stringently edited manuscript. I just hope that he wasn't ignoring obvious scientific errors so that he could properly concentrate on my abject failure to grasp the finer points of spelling Maori place names. But just for the record, Andy: pronouns are *good*. Really, they are.

The Walter E. Kurtz Medal (for services in the cause of sanity retention)
Awarded jointly to Naoise, for feeding me coffee; Jenny, for feeding me chocolate; and Jude, for feeding me cake. All three have, at one time or another, put up with enough misanthropic ranting to power a small town of Victor Meldrews.

The Carpe Jugulum Trophy (for notable domestic tolerance)
Awarded to the many housemates who have had to live with me in the last four years, for tolerating my various foibles and idiosyncrasies. This includes those who, in the end, couldn't. And no, that's not all of them.

The Igor Novello Award (for services in the laboratory)
Jointly awarded with profuse thanks to Yoshi, the mysterious Prof. Shau, and Richard, for instilling me into the dark arts of the SEM; to Bob and John, for their Scotty-like attitude to sample preparation (it cannae be done, but there it is); and to Kev, for teaching me the true meaning of "manaña, manaña".

Special Commendations
To Sandy, Jane and the rest of the canteen staff, for their much-needed, and often unappreciated, humanity; to Gillian, for responding so superbly to a phone call out of the blue; to NERC, for paying me to go to Middle Earth; and last but not least, to everyone I met in New Zealand, particularly those who let me drill holes in their land (I think most of them thought I was looking for gold, which, given all that pyrite, is a tad ironic). Great people. Great country.

And to anyone else who hasn't been mentioned, but thinks they should have been: get over it. And thank you.

Chapter 1

Introduction

1.1 Rationale

New Zealand straddles a region of the convergent plate boundary between the Pacific and Indo-Australian plates (referred to hereafter as the Australian plate), across which there are significant changes in the nature of deformation (Fig. 1.1). Trench-normal, westward subduction of the Pacific plate beneath oceanic crust at the Tonga-Kermadec Trench slows and becomes increasingly oblique to the south as it is subducted beneath the continental crust of the North Island of New Zealand (Hikurangi margin). On the South Island, the plate boundary becomes a zone of intra-continental, dextral transpression, formed by the Marlborough and Alpine-Wairau fault zones. These changes are caused by rapid lateral variations in the azimuth of the relative plate motion vector, and in the lithology and structure of both plates.

The presence of a large range of deformation modes within a relatively small region make New Zealand an ideal natural laboratory for investigating how large-scale plate motions are accommodated by brittle deformation within the crust. Plate tectonics strictly requires the lithosphere to behave rigidly, except within narrow zones at the plate boundaries. However, whilst this is a reasonable approximation for oceanic lithosphere, it has long been recognised that this is not the case for continental lithosphere, where inter-plate motions are commonly broadly distributed over a wide plate boundary zone (Molnar, 1988). A key question is whether there is a practical length scale below which the continental crust is effectively rigid, allowing a 'microplate' treatment, or whether deformation is distributed at all length scales, requiring a quasi-continuous flow model. In reality, aspects of both models are observed, and to different degrees in different tectonic situations (Thatcher, 1995). What causes and controls this spectrum of behaviour depends to a large extent on what is controlling the deformation of the brittle upper crust.

Paleomagnetic, structural and geodetic studies have revealed that vertical-axis rotations of fault-bounded blocks are a common feature of deforming continental crust, especially in areas of oblique convergence. Examples include the western Transverse Ranges of California (Hornafius, 1985; Hornafius et al., 1986; Jackson and Molnar, 1990; Sorlien et al., 1999), the Aegean arc (Kissel et al., 1986; Kissel and Laj, 1988), Sakhalin off the northwest Pacific coast of Russia (Fournier et al., 1994; Takeuchi et al., 1999; Weaver et al., 2003) and also the New Zealand plate boundary region, where clockwise vertical-axis rotations of the Hikurangi margin have been confirmed by numerous paleomagnetic studies (Walcott et al., 1981; Walcott and Mumme, 1982; Mumme and Walcott, 1985; Wright and Walcott, 1986; Lamb, 1988; Mumme et al., 1989; Roberts, 1992, 1995a; Vickery and Lamb,

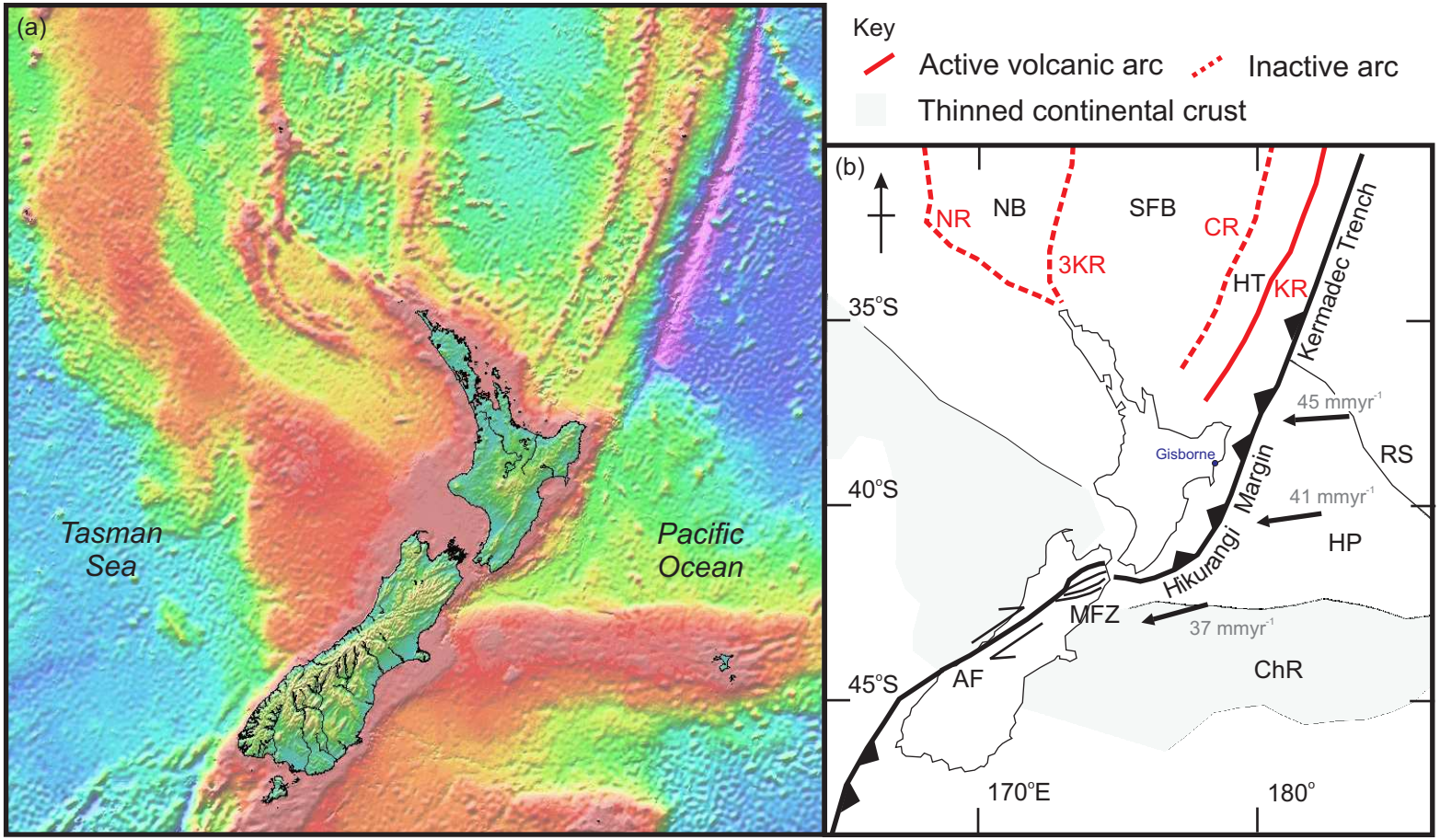

Figure 1.1: (a) Bathymetry of the southwest Pacific in the New Zealand region, from combined satellite gravity measurements and bathymetric soundings (Sandwell and Smith, 1997). (b) Interpretive map of (a), illuminating bathymetric features discussed in the text. The thickened oceanic crust of the Hikurangi Plateau can be clearly seen to the east of the North Island. To the north is a series of volcanic arcs, separated by back-arc basins. AF = Alpine Fault, MFZ = Marlborough Fault Zone, HP = Hikurangi Plateau, RS = Rapuhia Scarp, ChR = Chatham Rise, HT = Havre Trough, SFB = South Fiji Basin, NB = Norfolk Basin, NR = Norfolk Ridge, 3KR = 3 Kings Rise, CR = Colville Ridge, KR = Kermadec Ridge.

1995; Thornley, 1996; Little and Roberts, 1997). Apparent lateral variations in the rates and timings of rotations within the Hikurangi forearc since the Early Miocene have been interpreted in terms of fault-bounded 'domains' (Lamb, 1989; Walcott, 1989)(Section 1.3). Geodetic studies of short-term deformation also indicate contemporary clockwise rotation of the forearc (Walcott, 1984a; Beanland and Haines, 1998; Beavan and Haines, 2001; Wallace et al., 2004), but suggest a much more coherent rotation of the entire forearc (Section 1.4). These contrasting length scales of deformation mean that it is unclear how geodetically and paleomagnetically inferred rotations are related. Better knowledge of the rates, timings, and magnitudes of rotation on the Hikurangi margin, and the mechanisms by which large differential rotations have been accommodated, potentially offer significant insights not only into the tectonic history of the New Zealand plate boundary region, but also into the underlying mechanisms of continental deformation.

1.2 Geological development of the New Zealand region

The basement terranes that make up New Zealand chiefly originated in a subduction setting as part of Gondwana in the Triassic to early Cretaceous. Along with other continental blocks, such as the Lord Howe Rise, these terranes were rifted from the eastern Australian margin by the opening of the Tasman Sea in the late Cretaceous-early Cenozoic (84–52 Ma; Gaina et al., 1998).

A major plate reorganisation, possibly a consequence of the collision of India with SE Asia (Hall, 2002), affected the whole SW Pacific region between 50 and 40 Ma, and initiated the development of the present-day Pacific-Australian plate boundary. Convergent tectonics in the region to the north of New Zealand as early as the mid-Eocene are indicated by a collisional event that culminated in ophiolite obduction in New Caledonia from ∼48 Ma (Aitchison et al., 1995). However, there was an extensional regime in New Zealand itself, with the development of several N– to NE–trending basins in the mid-late Eocene (King, 2000, and references therein), linked to seafloor spreading in the Emerald Basin to the south (Sutherland, 1995; Wood et al., 1996). The nature of the Paleogene plate boundary in the intervening region is poorly constrained, possibly due to the Pacific-Australian Euler pole being located in southern New Zealand at this time (Sutherland, 1995), which would have resulted in low convergence rates, and possibly diffuse tectonism.

Increased convergence rates resulting from the subsequent SE migration of the Euler pole from 30 Ma (Sutherland, 1995) led to the southward propagation of a subduction boundary into the New Zealand region by late Oligocene-early Miocene time. The initiation of subduction along the Hikurangi margin is marked by the

20–25 Ma obduction of the Northland and East Coast allochthons, with coeval thrusting in the Wairarapa and Marlborough regions (Chanier and Férrière, 1989; Lamb, 1989; Rait et al., 1991). Initiation of subduction also coincided with the beginning of widespread volcanic activity on the Three Kings Ridge and Northland arc, from ∼22 Ma (Herzer, 1995).

The precise configuration of the Early Miocene plate boundary in northern New Zealand remains controversial. A proposed reconstruction is shown in Figure 1.2a, after Rait et al. (1991), with the nascent subduction margin trending NW–SE. This orientation is supported by several lines of geological evidence, including the southwestward transport directions of the Northland and East Coast allochthons (Stoneley, 1968; Rait, 2000) and the trend of the Northland arc (Herzer, 1995). However, in the Wairarapa region of the southern North Island, the Early Miocene fold and thrust belt associated with initiation of subduction presently has a NE–SW trend (Chanier and Férrière, 1989), indicating that this part of the Hikurangi margin has rotated by ≥90° to its present orientation during the Neogene (Rait et al., 1991) (Fig. 1.2b).

The region behind the currently active Kermadec-Tonga arc to the north of New Zealand contains a number of relict Cenozoic arcs and ocean basins (Fig. 1.1). Although early Miocene volcanic activity seems to have been concentrated on the Three Kings Ridge and in Northland, microfossil studies of dredge samples have established that the Kermadec and Colville ridges also date back to ∼25 Ma (Ballance et al., 1999). This suggests that all of the volcanic arcs north of New Zealand may once have formed a single ridge, that has been subsequently dismembered by a series of back-arc rifting events in the Neogene, in response to eastward roll-back of the Pacific plate. At the southern end of the subduction zone, underthrusting of buoyant continental crust has resulted in a long-term locking of the plate interface (Section 2.1.2), that has effectively pinned the plate boundary. Clockwise rotation of the Hikurangi margin can therefore be explained by a reorientation of the subducting Pacific plate, driven by the couple arising from this transition (Walcott, 1989) (Fig. 1.2c). Similar forces appear to be driving contemporary rotation of the Hikurangi margin (Section 1.4), therefore this mechanism is geodynamically plausible over longer timescales. However, a number of problems remain with this model. First, the relatively simple scenario of sequential back-arc basin opening driven by roll-back of the subducting plate is challenged by the Oligocene age assigned to the South Fiji Basin, based on the interpretation of magnetic anomalies (Malahoff et al., 1982; Sdrolias et al., 2003). If correct, this would complicate the history of subduction and back-arc basin formation to the north of New Zealand and significantly reduce inferred Neogene roll-back of the Pacific plate. However,

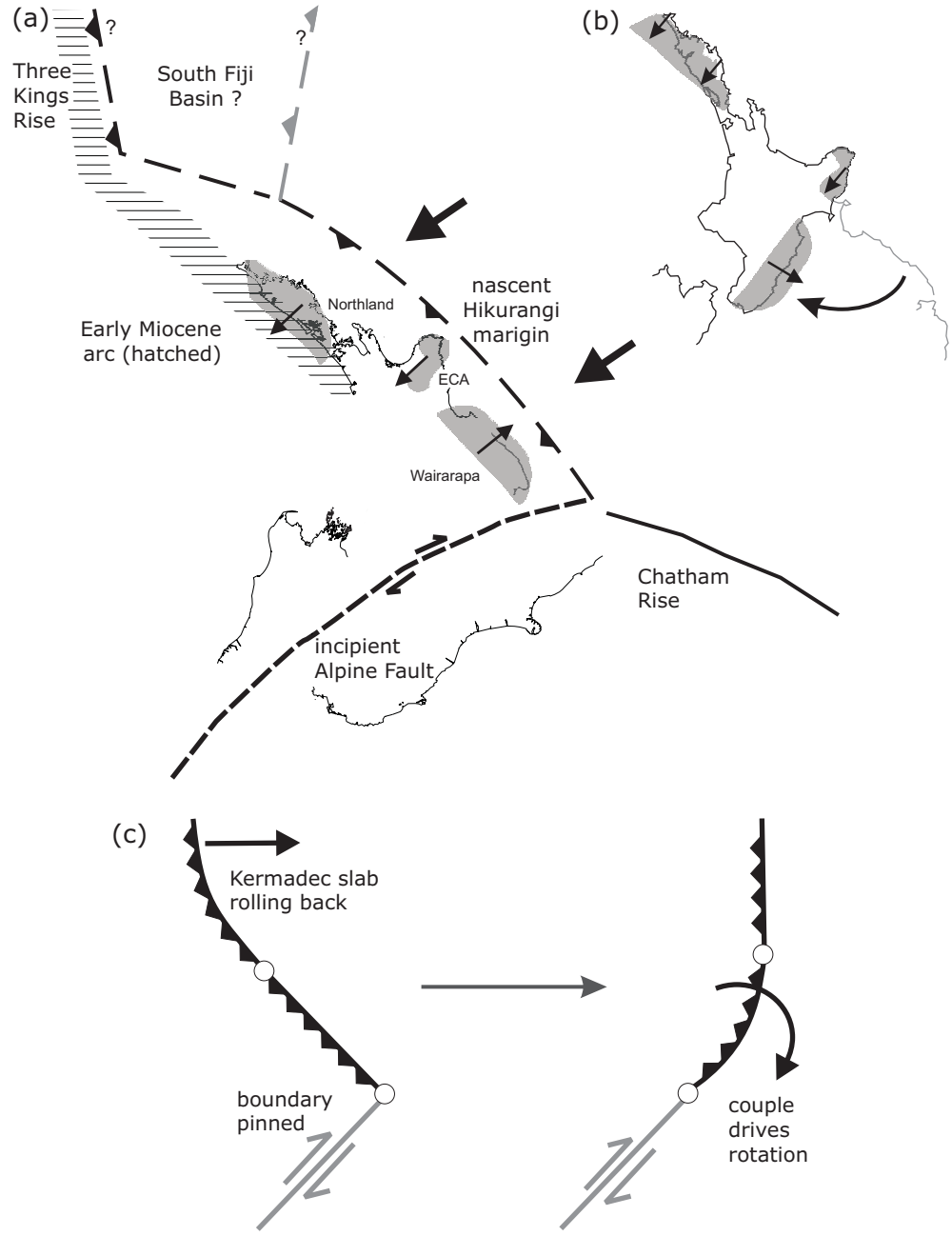

Figure 1.2: (a) Reconstruction of the Hikurangi margin at 20–23 Ma, according to Rait et al. (1991). Realigning Early Miocene thrust belts (ECA = East Coast Allochthon) indicates that the margin was oriented NW–SE. Back-arc basins to the north of New Zealand (cf. Fig. 1.2) have been closed, allowing subduction of the Pacific plate beneath Northland and the Three Kings Rise. However, the age of the South Fiji Basin is currently disputed. (b) Present-day orientation of Early Miocene thrust belts, depicting the inferred 90° clockwise rotation of the Hikurangi margin. (c) Proposed driving mechanism for the tectonic rotation: the transition from subduction, with roll-back and back-arc spreading, to intra-continental transpression creates a couple that causes clockwise rotation of the subducting slab.

recent seismic surveys on the Northland margin of the basin indicate that the basement is continuous with a volcanic plateau that overlies the Northland Allochthon (Herzer et al., 2000). This suggests Mid–Late Miocene spreading, which is easier to reconcile with the inferred ages of adjacent basins: to the west, dredge samples in the Norfolk Basin suggest Early Miocene spreading (Mortimer et al., 1998), which may have continued into the Late Miocene (Sdrolias et al., 2004); to the east, extension in the Havre Trough is thought to have initiated in the Pliocene (Wright, 1993). Second, it is presently unclear how the proposed 90° rotation of the Hikurangi margin has been accommodated within the New Zealand region. Such large tectonic rotations would appear to require substantial shortening in the southern part of the Hikurangi margin. In contrast, estimates of long-term deformation from seismic reflection lines indicate <30 km of shortening across the southern forearc since 5 Ma (Nicol and Beavan, 2003), and the low metamorphic grade of rocks in the East Coast region is also inconsistent with intense tectonism (Field et al., 1997). However, because the limits of the rotating forearc are poorly defined by paleomagnetic data (Section 1.3), it is difficult to constrain which regions are likely to have been deforming in response to tectonic rotation of the forearc.

Since the beginning of subduction in the Early Miocene, the tectonic regime appears to have been dominated by shortening (Field et al., 1997), although significant dextral displacements have been proposed by some authors (Delteil et al., 1996; Field et al., 1997). However, at least two tectonic reorganisations have taken place since the Late Miocene. An abrupt southwestward shift in the position of the Pacific-Austalian Euler rotation pole at 6.5–5 Ma (Cande et al., 1995; Sutherland, 1995; Walcott, 1998) increased convergence across the plate boundary in the New Zealand region, and appears to have triggered a number of tectonic changes, including development of the Marlborough Fault Zone (MFZ) (Little and Roberts, 1997), and uplift and subaerial exposure of the inner forearc of the Hikurangi margin (Kelsey et al., 1995; Buret et al., 1997). Further changes occurred at 2–1 Ma, with the beginning of extension in the Taupo Volcanic Zone (TVZ) (Wilson et al., 1995) and initiation of strike-slip displacement on the North Island Dextral Fault Belt (NIDFB; see Section 1.4) (Beanland, 1995; Beanland et al., 1998). The presently observed tectonic regime has therefore only persisted since the beginning of the Quaternary, and prior to this different structures must have been involved in accommodating motion across the plate boundary region. This ongoing tectonic evolution must be taken into account when developing rotation models for the Hikurangi margin.

1.3 Paleomagnetic investigations of the Hikurangi margin

Vertical-axis tectonic rotations on the Hikurangi margin are determined by measuring the declination anomaly, which is the deviation of the paleomagnetic mean declination for a sampling locality from that expected from large-scale motions of the Australian and Pacific plates. The apparent polar wander path (APWP) of the Pacific plate, determined both from standard paleomagnetic measurements and also from marine magnetic anomaly skewness (Petronotis et al., 1994; Johnson and Gordon, 1996), indicate that it has remained relatively stationary, with a small to negligible northward drift, during the Neogene. Motion of the Australian plate about the SW Pacific Euler pole should therefore lead to clockwise rotations of about 1°/Myr on the Australian plate. This is confirmed by measured Australian APWPs (Idnurm, 1985; Musgrave, 1989).

Large rotations of the forearc of the Hikurangi margin have been confirmed by numerous paleomagnetic studies (Walcott et al., 1981; Walcott and Mumme, 1982; Mumme and Walcott, 1985; Wright and Walcott, 1986; Mumme et al., 1989; Roberts, 1992, 1995a; Vickery and Lamb, 1995; Thornley, 1996; Little and Roberts, 1997). These data have been further interpreted to indicate that the margin is divided into a number of rotational domains, with separate tectonic histories (Lamb, 1988, 1989; Walcott, 1989) (Figs. 1.3, 1.4).

The apparent lateral variations in the rates, timings and magnitudes of tectonic rotation are not a feature of the short-term velocity field (Section 1.4), which may indicate fundamental differences between long- and short-term deformation patterns on the Hikurangi margin. Alternatively, they may reflect deformation in an earlier tectonic regime prior to formation of the NIDFB and TVZ (Section 1.2). To test these hypotheses, the boundaries of the domains must be rigorously delineated, and the structures that have accommodated large differential rotations at the boundaries between adjacent domains must be identified.

The extant paleomagnetic data presented in Figures 1.3 and 1.4 are discussed in the following sections. The Cenozoic mudstones from which most of these data have been extracted are weakly magnetized and are commonly affected by strong present-day field overprints, which make it difficult to isolate primary remanence components. These rocks have undergone multiple cycles of erosion, deposition and uplift, causing the dissolution of ferrimagnetic Fe-Ti oxides such as magnetite; in most cases, the remanence carrier has not been conclusively identified (Turner, 2001). These uncertainties could potentially impact the reliability of paleomagnetic data from the Hikurangi margin.

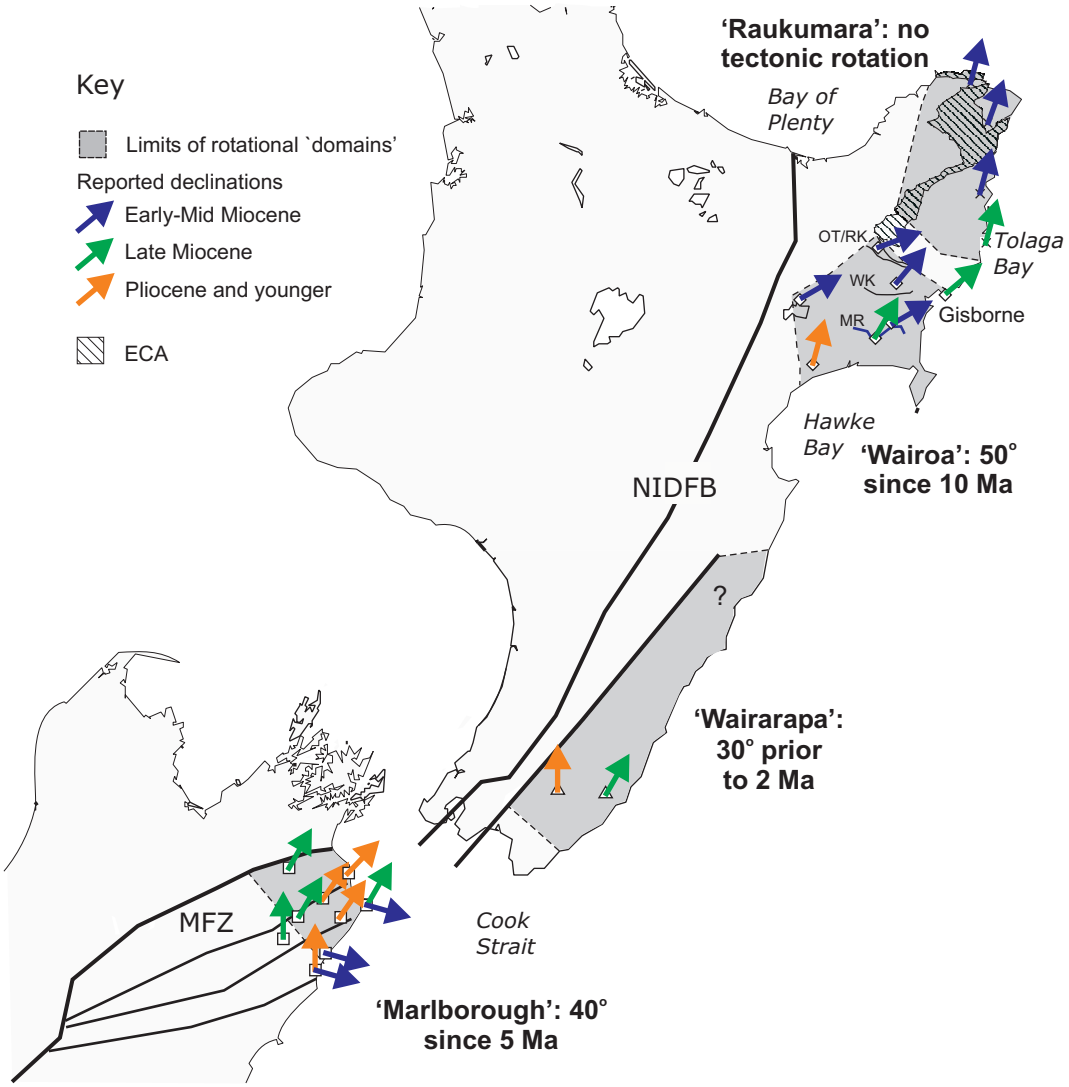

Figure 1.3: Rotational domains of the Hikurangi margin, according to Lamb (1988, 1989) and Walcott (1989). Representative declinations from previously published studies, colour coded according to age, are also plotted, to illustrate the distribution of data used to delimit these domains. ECA = East Coast Allochthon, OT = Otoko-Totangi Fault, RK = Rakauroa Fault, WK = Waerengaokuri Fault, MR = Mangapoike River. Declination anomalies are from Walcott et al. (1981); Walcott and Mumme (1982); Mumme and Walcott (1985); Wright and Walcott (1986); Mumme et al. (1989); Roberts (1992, 1995a); Vickery and Lamb (1995); Thornley (1996) and Little and Roberts (1997).

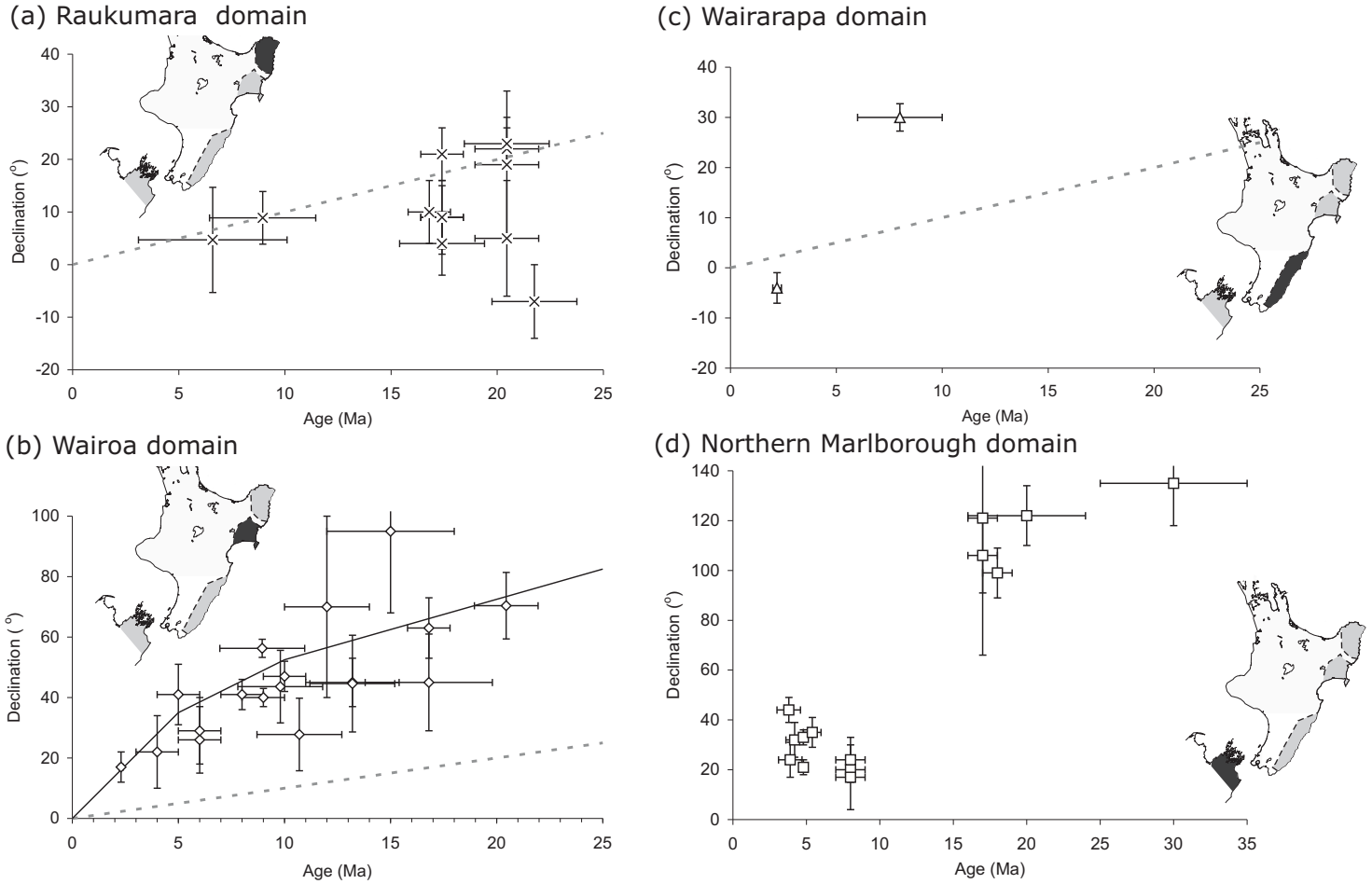

Figure 1.4: Summary of published paleomagnetic data from: (a) the Raukumara domain, (b) the Wairoa domain (solid line is the fit of Wright and Walcott (1986), depicting accelerating rates of tectonic rotation since the Early Miocene), (c) the Wairarapa domain, and (d) the Northern Marlborough domain. The dashed line on (a-c) depicts the 1°/Myr rotation due to large-scale motion of the Australian plate (Idnurm, 1985; Musgrave, 1989); this line is irrelevant for data in (d), which are from the Pacific plate. Data sources are as for Fig. 1.3.

1.3.1 Raukumara

Extensive sampling of Early Miocene (18–20 Ma) rocks (Walcott and Mumme, 1982; Mumme et al., 1989) on the northern Raukumara Peninsula indicate negligible rotations with respect to the Australian plate during the Neogene (Figs. 1.3, 1.4a). This is in clear contrast to the large clockwise rotations reported from sites further south on the Hikurangi margin. One potentially worrying feature of the paleomagnetic data from many localities is their anomalously shallow inclinations (as little as 25°, compared to expected inclinations of ∼60°), although this has been argued to result from sediment compaction (Mumme et al., 1989). However, the presence of reversed polarity directions at several sites imparts confidence that these data are not strongly contaminated by present-day field overprints. The southern extent of this non-rotated region is not precisely defined; sampling from over 20 localities in the southern Raukumara Peninsula failed to yield stable magnetizations (Mumme et al., 1989), although unrotated declinations have been reported from a Late Miocene coastal locality near Tolaga Bay (Thornley, 1996) (Fig. 1.3).

1.3.2 Wairoa

A number of studies (Walcott and Mumme, 1982; Mumme and Walcott, 1985; Wright and Walcott, 1986; Thornley, 1996) provide data with a broad temporal range from 24 to 2 Ma (Fig. 1.4b), much of which come from a 5000 m mid Miocene–early Pliocene (16–4 Ma) section from the Mangapoike River (MR, Fig. 1.3). These data consistently indicate large clockwise rotations with respect to both the Australian plate and the Raukumara Peninsula to the north (Fig. 1.3), and have been further interpreted as indicating a steadily accelerating rate of tectonic rotation with respect to the Australian plate during the Neogene, from 3–4°/Myr in the Early Miocene to 7–8°/Myr from the Pliocene onward (Wright and Walcott, 1986; Walcott, 1989) (Fig. 1.4b). However, there is significant scatter in Early and Middle Miocene data, which results in the proposed best-fit curve being poorly constrained beyond 12 Ma.

The substantial (∼60°) discrepancy in net rotations between the Wairoa and Raukumara regions implied by these data requires that a major structural boundary exists between the two 'domains'. Within the broad, geologically complex area defined by the paleomagnetic results, there is a significant change in structural trends, from NW–SE to SW–NE; however, structures that have accomodated large differential rotations have proven difficult to identify. Several studies have proposed a corridor of dextral strike-slip between Gisborne and the Bay of Plenty (Fig. 1.3), involving movement on the Otoko-Totangi, Rakauroa and Waerengaokuri faults (e.g. Lamb, 1988). The history of displacement on these

faults remains ambiguous, however, and evidence for large dextral offsets is weak. Thornley (1996) reported both anomalously large and small declinations from samples collected around the Waerengaokuri Fault, which may indicate differential rotations across this structure. The data are of poor quality, however, with strong overprints complicating interpretation, which makes their significance uncertain, and for this reason they are not included on Figures 1.3 and 1.4. Correlating the paleomagnetic results with structural geology is further complicated by a large declination anomaly reported by Mumme and Walcott (1985) from a locality situated between the Otoko-Totangi and Rakauroa faults (Fig. 1.3). The large inferred tectonic rotation at this locality contradicts geological evidence that suggests it is unrotated (i.e. in this region, Early Miocene structures associated with emplacement of the ECA still trend NW–SE). Further data from this region are clearly needed to further constrain the position of the rotation boundary.

1.3.3 Wairarapa

Paleomagnetic data from the North Island south of northern Hawke Bay are sparse; only two stable primary magnetizations have been reported from this region (Figs. 1.3, 1.4c). A number of other sites have been sampled but have consistently been found to be overprinted by a hard spurious magnetization (Walcott and Mumme, 1982; Roberts, 1990).

The published results indicate 30° of clockwise rotation of Late Miocene (8 Ma) sediments (Walcott et al., 1981), whereas Late Pliocene (2 Ma) rocks are unrotated (Lamb, 1988). The former result is consistent with data from the Wairoa region; the latter may imply structural decoupling between the Wairarapa and Wairoa regions from the late Pliocene onward. This would require a further structural boundary south of the Wairoa region, which is not obvious from current patterns of deformation or surface geology. It could also be argued that extant paleomagnetic data are insufficient to conclusively establish a distinct tectonic history for this region.

1.3.4 Marlborough

Tectonic rotations on the northeastern South Island of New Zealand seem to be principally associated with the transition from subduction to transpression in the Marlborough region (Fig. 1.3). The whole of northeastern Marlborough has rotated clockwise by up to 30–50° since ∼4 Ma (Walcott et al., 1981; Roberts, 1992, 1995a) (Fig. 1.4d). Early–Middle Miocene coastal outcrops record additional rotations of ∼50° (Mumme and Walcott, 1985; Vickery and Lamb, 1995) (Figs. 1.3, 1.4). Middle–late Miocene depositional hiatuses divide these two phases of rotation (Roberts, 1992).

The paleomagnetic data from northern Marlborough have been augmented by structural data from basement rocks of the Torlesse Supergroup, which has near-vertical bedding fabric that can be used as a marker for vertical-axis rotations (Little and Roberts, 1997). A NW-trending kink in the structural trend of these basement rocks defines a 'migrating hinge', through which the northern Marlborough region has been translated during the Pliocene by strike-slip motion on the Marlborough Fault Zone (Little and Roberts, 1997). The much larger clockwise rotations recorded by Paleogene to Middle Miocene sediments in coastal regions (Vickery and Lamb, 1995) appear to be spatially restricted, and represent earlier deformation associated with the initial propagation of the plate boundary through New Zealand in the Early Miocene (Little and Roberts, 1997), or possibly oroclinal bending associated with Early-Middle Miocene strike-slip on the Alpine-Wairau Fault (Hall et al., 2004).

Major active faults cannot be traced across Cook Strait, and basement terranes are offset by ∼140 km across it, indicating that it is a major structural discontinuity (Walcott, 1978; Carter et al., 1988). These observations suggest that the inactive, rotated, termination of the Alpine-Wairau Fault may run through Cook Strait (Walcott, 1978; Lewis et al., 1994); differential motion across this structure may explain the later apparent initiation of rotations in this part of the margin, compared to those documented on the North Island.

1.4 Active faulting and deformation in the plate boundary region

Active faulting on the Hikurangi margin is principally divided between three regions: the subduction thrust and outer forearc, the NIDFB, and the TVZ. The obliquity of the plate motion vector to the margin increases between 40°S and 42°S: margin-normal convergence decreases from 34mm/yr to 22mm/yr, whilst the margin-parallel component remains constant at ∼31 mm/yr. However, it seems unlikely that this variation is entirely responsible for the observed lateral changes in the distribution of deformation, inferred from both geodetic data and estimates of geological slip rate (Fig. 1.5).

Earthquake focal mechanisms at the subduction interface consistently have slip vectors oriented normal to the trench, indicating that the plate interface accommodates little trench-parallel motion (Webb and Anderson, 1998). This is a common feature of oblique subduction zones, although in this case the 'strain partitioning' is not complete: on the southern Hikurangi margin, thrusts in the outer forearc are slightly oblique to trench-normal, which may account for 5–6mm/yr of margin-parallel motion, and offshore strike-slip faults have also been reported

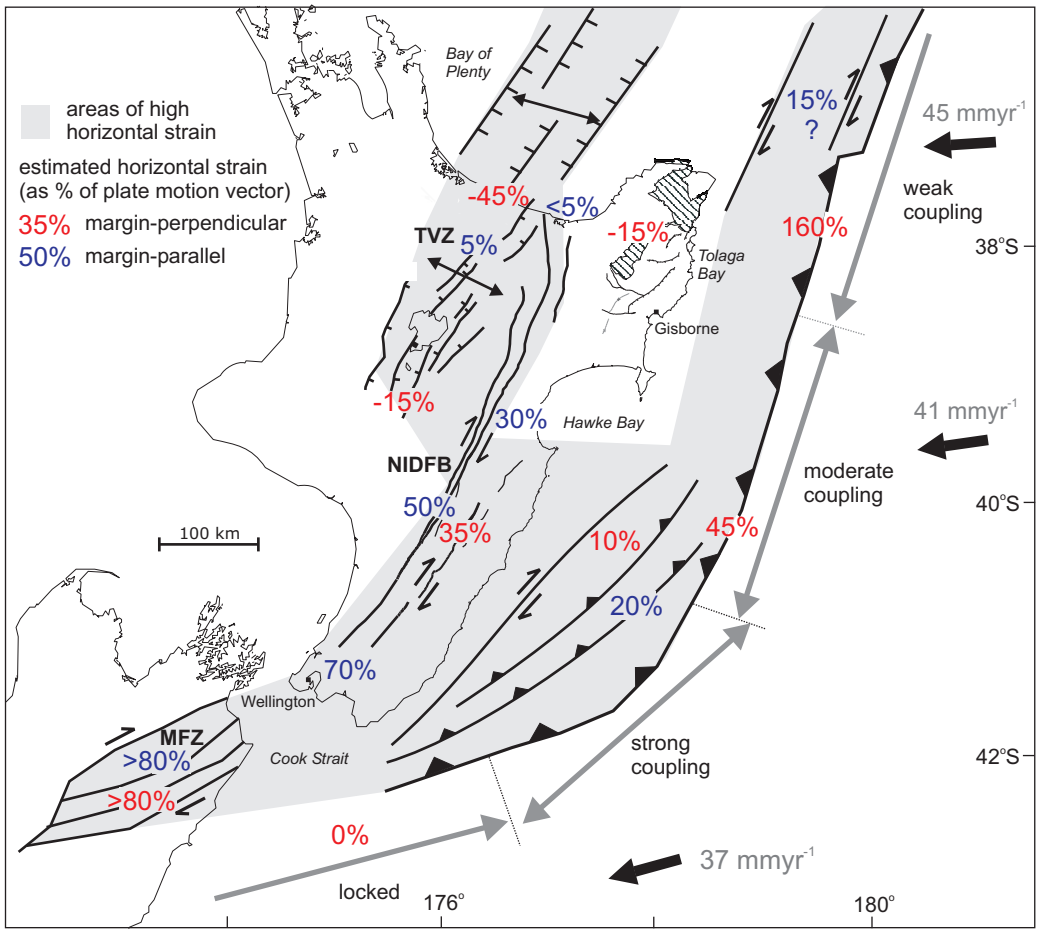

Figure 1.5: Distribution of active deformation in the New Zealand plate boundary region, indicating areas that are presently accommodating significant horizontal strain, and the major faults within them. The relative proportions of margin-normal (red) and margin-parallel (blue) motion being accommodated on known faults in these areas are given as a percentage of the Australian-Pacific convergence vector. See Section 1.4 for references.

east of the Raukumara Peninsula (Collot and Davy, 1998; Davey et al., 1997), although their slip rates are poorly constrained. A southward increase in inter-plate coupling (Reyners, 1998) means that at the southern Hikurangi margin a significant proportion of margin-normal motion is not accommodated at the trench, and is transferred onto the Australian plate (Fig. 1.5). Although a comparison of global positioning system (GPS) and geologically-derived strain rates indicates that some of this shortening is elastic deformation caused by temporary locking of the plate interface (Nicol and Beavan, 2003), uplift of the Coastal and Axial ranges on the North Island demonstrates that at least some of this shortening is being permanently accommodated in the forearc. Off the coast of the northern South Island, the subduction interface appears to be permanently locked (Collot et al., 1996; Barnes and Mercier de Lepinay, 1997) (Section 2.1.2), with >80% of relative plate motion being permanently accommodated by the Marlborough Fault zone (Beavan and Haines, 2001) (Fig. 1.5).

The amount of extension in the TVZ decreases southward, from 15mm/yr in the Bay of Plenty region to 5mm/yr in the central North Island (Stern, 1987; Acocella et al., 2003); this is probably also linked to increased coupling across the plate boundary, because back-arc extension can only occur where the interface is weak (Upton et al., 2003). Extension is oblique to the plate motion vector, resulting in 2–3 mm/yr of dextral strike-slip being accommodated in this region (Acocella et al., 2003) (Fig. 1.5).

The two strands of the NIDFB, the western Wellington-Mohaka fault system, and the eastern Wairarapa Fault, both consist of linked dextral-reverse faults, associated with the Axial Ranges (Beanland, 1995). Near Wellington, 21 mm/yr of margin-parallel motion is accommodated on these faults (Beanland, 1995); however, this decreases northward, with 5mm/yr of dextral strike-slip on the two main strands in Hawkes Bay, and only 1.6 mm/yr in the Bay of Plenty region (Beanland, 1995) (Fig. 1.5).

It is clear from Figure 1.5 that the transition from subduction to transpression along the Hikurangi margin is leading to significant changes in the distribution of deformation. In the north, faulting is confined to two narrow regions associated with the subduction interface and the TVZ; the intervening Raukumara Peninsula is not undergoing significant basement deformation, with normal faulting in this region being related to gravitational sliding of the sedimentary cover (Thornley, 1996). As inter-plate coupling increases to the south, deformation becomes more distributed, with faulting across the entire region between the trench and the NIDFB.

Whilst displacement on known faults can account for most of the margin-

normal motion, there is a significant amount of margin-parallel motion that cannot be accounted for. This strike-slip deficit increases to the north, as less margin-parallel motion is accommodated on the NIDFB (Fig. 1.5). Derived velocity fields indicate that this deficit is principally accounted for by bulk rotation of the margin (Walcott, 1984a; Beanland, 1995; Beanland and Haines, 1998; Beavan and Haines, 2001; Wallace et al., 2004). The modelling of Wallace et al. (2004) suggests that such rotation accounts for 65% of margin-parallel motion on the Raukumara Peninsula, resulting in a tectonic rotation rate of 3–4°/Myr. Although this is comparable to rotation rates estimated from paleomagnetic data (Section 1.3), geodetically-derived deformation fields indicate coherent rotation of the entire forearc region, showing no significant smaller scale variation in rotation rates associated with the proposed paleomagnetic 'domains'. Neither do the active faulting patterns in Figure 1.5 appear consistent with large differential rotations between adjacent parts of the Hikurangi margin.

1.5 Synthesis

In the decade since the majority of paleomagnetic data from the East Coast of the North Island have been published, high-resolution surveys of seismicity, bathymetry and gravity along the Hikurangi margin have vastly improved knowledge of its structure (Section 2.1), whereas new geodetic modelling, using GPS measurements and more accurate fault slip rate data, have provided a much clearer picture of contemporary deformation patterns. None of these new data support the proposed division of the deforming forearc into independent rotational domains (Lamb, 1989; Walcott, 1989). When the domains were originally proposed, their boundaries were correlated to postulated 'tears' in the subducting plate (Reyners, 1983; Smith et al., 1989). More detailed analysis of intra-plate seismicity has shown that these tears do not exist (Ansell and Bannister, 1996); although some lateral variations in the structure of the subducting plate are still apparent (Section 2.1), they no longer seem to directly correlate to the paleomagnetically inferred tectonic boundaries on the forearc, which also seem incompatible with the coherent rotation of the margin observed in the short-term velocity field (Beanland and Haines, 1998; Beavan and Haines, 2001; Wallace et al., 2004) (Section 1.4).

Differential rotations are clearly indicated by both paleomagnetic and structural data across Cook Strait. Changes in the structure of both plates near Gisborne (Section 2.1.2) are also associated with a change in intra-plate coupling that could have potentially allowed differential rotation (Reyners, 1998), and correlate with the paleomagnetically-defined boundary between the unrotated Raukumara Peninsula and the rotated Wairoa domain. In this case, however, the sub-surface

discontinuity inferred from geophysical data is not clearly expressed by surface geology. Along the rest of the Hikurangi margin, there are no clearly defined structural boundaries between Hawke Bay and Cook Strait, and the paucity of paleomagnetic data from the southern part of the margin makes it difficult to justify a division into distinct Wairoa and Wairarapa domains.

The poor coverage of the paleomagnetic data set makes meaningful comparison of long-term and short-term deformation patterns extremely difficult. Although it is clear that tectonic rotations have occurred, the rates, timings and distributions of these rotations are poorly constrained along much of the Hikurangi margin, particularly between Hawke Bay and Cook Strait. Therefore, although the domain hypothesis is poorly supported by present data, it cannot be completely rejected.

Another implication of recent geophysical results is that the rotation of the forearc region is dependent on the gradual southward increase in inter-plate coupling observed along the plate interface (Reyners, 1998), which produces a margin-normal shear gradient along the entire length of the margin. This increase is implicitly related to the gradually increasing thickness of the subducting Hikurangi Plateau (Davy and Wood, 1994). Numerical models of oblique subduction (Upton et al., 2003) indicate that more abrupt changes in the strength of the subduction thrust leads to a relatively confined zone of margin-normal dextral shear. Thus, prior to collision of the Hikurangi Plateau, the kinematic response of the forearc to rotation of the underlying Pacific plate was likely to have been different.

1.6 Aims and objectives of this study

The access provided by subaerial exposure of the Hikurangi forearc allows detailed paleomagnetic study of deformation that enables us to address questions regarding the timing, distribution and accommodation of vertical-axis rotations during the Neogene. The principal aims of this study can be summarised as follows.

- To improve the spatial and temporal resolution of the paleomagnetic data set for the Hikurangi margin through a field sampling campaign along the east coast of the North Island.

- To integrate paleomagnetic data and structural data in order to accurately constrain the rates and timing of vertical-axis rotations along the whole of the Hikurangi margin. This will enable a rigorous test of the hypothesis that the margin is divided into domains, which act as rigid blocks with discrete tectonic histories. Precisely delineating the boundaries of any such regions will also allow investigation of how differential rotations are accommodated.

- To properly integrate any tectonic rotations into reconstructions of the New

Zealand plate boundary region during the Neogene.

- To investigate the magnetic signature of New Zealand Cenozoic marine mudstones in an attempt to characterise the principal magnetic carriers, and to understand the origins of the strong viscous overprints that are common in these rocks.

Some further geological background is presented in Chapter 2, followed by a discussion of experimental methods in Chapter 3. Results of sampling undertaken specifically to examine and resolve an apparent discrepancy between published paleomagnetic and structural data are presented in Chapter 4, which highlights potential reliability issues in the published paleomagnetic data set. In Chapter 5, results are presented that first triggered the realisation that late authigenic growth of iron sulphide minerals has a potentially serious impact on paleomagnetic results from New Zealand. In Chapter 6, these results are expanded, and it is demonstrated that remagnetization is a regional problem. These issues are addressed in Chapter 7 to produce a coherent account of the Neogene tectonic development of the Hikurangi margin. The overall conclusions of this study, and suggestions for further work, are then presented in Chapter 8.

Chapter 2

Geological background

2.1 Structure of the present Hikurangi margin

The Hikurangi margin encompasses the region of the Australian-Pacific plate boundary between 38° and 42°S, where the Pacific Plate is being subducted beneath the continental crust of the North Island at the Hikurangi Trough (Fig. 1.1). It marks the transition between fast (60 mm/yr), intra-oceanic subduction in the Kermadec trench to the north, and a chiefly dextral transform boundary within continental crust (the Alpine-Wairau Fault) to the south. Relative motions between the Australian and Pacific plates are described by a clockwise rotation of 1.07°/Myr about an Euler pole situated at 60.1°S, 181.7°E (DeMets et al., 1994). The close proximity of this pole to the New Zealand section of the plate boundary leads to measurable changes in the magnitude and obliquity of the convergence vector along the margin, from 45 mm/yr at 266° off the Raukumara Peninsula in the north to 37 mm/yr at 258° in Marlborough to the south (Fig. 1.1). The arcuate form of the Hikurangi margin further magnifies the southward increase in the obliquity of the convergence vector to the trench.

2.1.1 Subducting plate

Seismic and gravity surveys (Davy and Wood, 1994; Wood and Davy, 1994) have shown that the Pacific crust currently being subducted at the Hikurangi margin (the Hikurangi Plateau) is anomalously thick (10–15 km), and contains numerous volcanic seamounts and intrusions. Geochemical analyses of basement rocks support the hypothesis that the Hikurangi Plateau consists of thickened oceanic crust, formed by a mantle plume on or near a mid-ocean ridge (Mortimer and Parkinson, 1996). The additional buoyancy resulting from thicker oceanic crust on the downgoing plate has led to uplift and subaerial exposure of the forearc on the eastern North Island, and to abrupt shallowing of the subduction trench, from 6000 m depth to 2500-3500 m (Collot et al., 1996). Pacific crust 11–14 km thick has been observed on the subducted slab at 15 to 30 km depth using teleseismic ScSp conversions, indicating that subduction of the Hikurangi Plateau has been occurring for at least 3 Ma (Bourne and Stuart, 2000). A low velocity zone at the top of the subducting plate, which may correspond to thickened oceanic crust, has been imaged by seismic tomography down to ∼75 km depth (Reyners et al., 2004); the whole of the shallow slab beneath the North Island may therefore be topped by abnormally thick oceanic crust, representing at least 6-8 Myr of subduction. These observations suggest that the excess buoyancy of the Hikurangi Plateau is responsible for the shallow 12–15° initial dip of the subducted slab, as defined by high-resolution surveys of plate seismicity (Smith et al., 1989, and references therein). Futhermore, the slab has a conical profile, with radius of curvature increasing from 240 km north of Hawke Bay to 280 km near Wellington (Ansell and

Bannister, 1996), which correlates with a southward increase in the thickness of the Hikurangi Plateau, from 10 to 15 km (Davy and Wood, 1994). The dip of the slab increases abruptly to 50° at 60–80 km depth, about 200 km west of the trench (Adams and Ware, 1977; Ansell and Bannister, 1996) which may the mark the down-dip extent of the Hikurangi Plateau and the transition to normal oceanic crust.

Seaward of the trench, the Hikurangi Plateau has been subdivided according to variations in basement structure (Wood and Davy, 1994) (Fig. 2.1); these divisions include regions of more abundant volcanic seamounts (Northern Volcanic Region) and of higher sediment accumulation (Central Basin, North Chatham Basin). However, these divisions are not reflected in basment structure; the southward increase in crustal thickness indicated by gravity surveys appears to be relatively gradual, with no abrupt changes or obvious structural discontinuities associated with, for example, the subsided Central Basin (Davy and Wood, 1994). Although lateral segmentation of the downgoing slab has been suggested, based on along-strike changes in the distribution of seismicity within the plate interface zone (Reyners, 1983; Smith et al., 1989), compiled high-resolution data from all recent studies reveal no compelling evidence for the sharp along-strike offsets in seismicity that this interpretation requires (Ansell and Bannister, 1996).

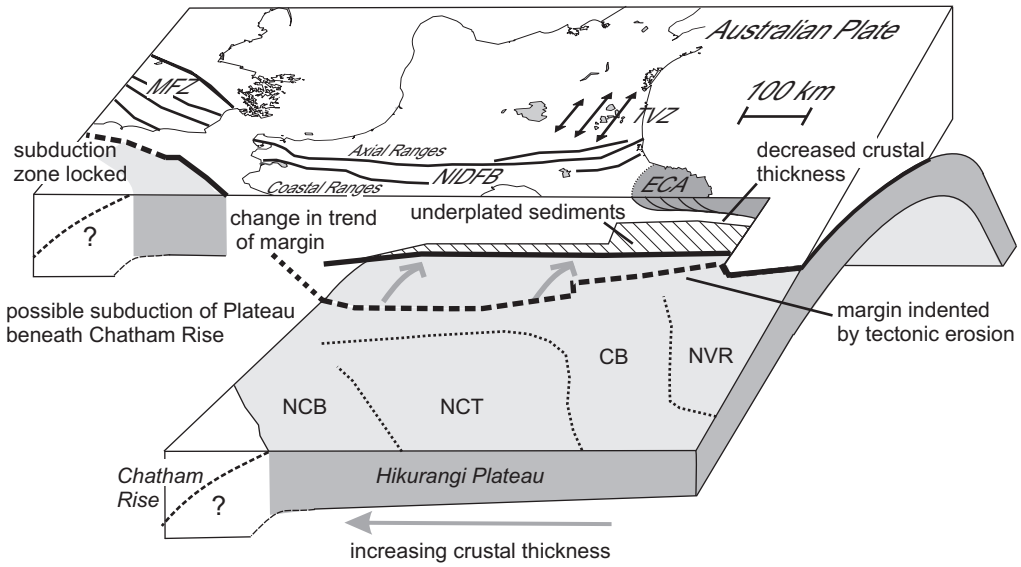

Figure 2.1: N–S cross section along the Hikurangi margin, illustrating lateral variations in the structure of the subducting and overiding plates. Vertical dimensions have been exaggerated for clarity. Dotted lines on the Hikurangi Plateau mark the structural divisions of Wood and Davy (1994) (NVR = Northern Volcanic Region, CB = Central Basin, NCT = North Chatham Terrace, NCB = North Chatham Basin). NIDFB = North Island Dextral Fault Belt, ECA = East Coast Allochthon, TVZ = Taupo Volcanic Zone.

2.1.2 Plate interface and forearc

The forearc of the Hikurangi margin (Fig. 2.1) can be subdivided into an offshore imbricate wedge of deforming Cenozoic sediments, with an actively accreting Quaternary wedge in the southeast; an outer arc high formed by the Coastal Ranges; and a subaerially exposed inner forearc, containing Early Miocene to Pliocene marine sediments (Cole and Lewis, 1981; Lewis and Pettinga, 1993). Uplifted Cretaceous greywackes of the Axial Ranges act as a backstop to the deforming zone. Back-arc extension in the Taupo Volcanic Zone is linked to offshore extension in the Havre Trough to the north of New Zealand (Fig. 1.1), and does not extend south of the central North Island.

The margin can also be divided laterally, according to structural changes along the subduction margin revealed by geophysical surveys (Collot and Davy, 1998). These divisions can also be correlated to changes in structure of the overlying plate, and the degree of coupling at the plate interface (Reyners, 1998).

Southern Kermadec margin

Subduction of the Hikurangi Plateau continues in an intra-oceanic setting to the north of New Zealand, until the Kermadec Trench intersects with the NW-trending, 1000 m-high Rapuhia scarp at 36°S (Fig. 1.1). There is an abrupt change to normal-thickness Pacific crust north of this feature (Davy and Wood, 1994); the resulting buoyancy contrast is inferred to have caused a tear fault in the subducting plate (Davey and Collot, 2000). Sediment transport from the New Zealand landmass to the trench north of New Zealand is impeded by a volcanic ridge near East Cape, resulting in limited active accretion at the inner trench (Collot and Davy, 1998). Dextral strike-slip faults have been identified on the middle and upper slope of the margin (Collot and Davy, 1998; Davey et al., 1997) (Fig. 1.5), behind which is a forearc basin containing up to 10 km of mainly Cenozoic sediment fill (Davey et al., 1997). The basin is floored by Cretaceous oceanic crust, which seismic surveys have shown to be obducted onto the Raukumara Peninsula as part of the East Coast Allochthon (Davey et al., 1997) (Fig. 2.1). Back-arc rifting, at rates of 15–20 mm/yr in the Havre Trough began at about 5 Ma (Wright, 1993); extension is slightly oblique to the plate motion vector (Delteil et al., 2002).

Northern Hikurangi Margin - the Raukumara Peninsula

Between 37°40'S and 40°20'S, there is no actively accreting wedge. Instead, the structural trench is indented by 10–25 km (Fig. 2.1), and the inner trench wall has a much steeper slope than other parts of the margin (12° as opposed to 2.5°). In this section of the plate boundary, the subducting Hikurangi Plateau has a rougher topography due to a higher abundance of volcanic seamounts (the Northern Volcanic region of Wood and Davy, 1994) (Fig. 2.1). Slumping and gravitational

collapse resulting from multiple collisions of these seamounts have led to the removal of the lower margin by tectonic erosion (Collot et al., 1996).

Significant changes in the structure of the overlying plate also occur along this section of the margin. In the northeast, 3D seismic models derived from inversion of earthquake arrival times (Reyners et al., 1999) reveal a low velocity zone in the lower crust, which thins abruptly north of Gisborne, and appear to represent a thick (>20 km) accumulation of subducted sediment (Fig. 2.1). Sediment underplating has previously been hypothesised to explain the uplift and extension through gravitational collapse of the Raukumara Range in the last 6 Ma (Thornley, 1996; Walcott, 1987), and is supported by the observation that the low velocity zone is most extensive beneath the most rapidly uplifting part of the range.

Large thicknesses of underplated sediments are often linked to tectonic erosion at a subduction margin (von Heune and Scholl, 1991). However, south of Gisborne there is a 50 km section of the indented (tectonically eroding) part of the margin with no significant underplating, suggesting additional controls on the accumulation of sediments beneath the forearc. The thickness of the over-riding Australian crust also increases abruptly in the Gisborne region, from 17–19 km in the north to 36–37 km in the south (Davey et al., 1997; Reyners et al., 1999). It is possible that thinner crust on the over-riding plate in the northeast allows the sediment to pond against stronger upper mantle (Reyners et al., 1999).

The increased subduction of sediments beneath Raukumara appears to have reduced coupling at the plate interface. Earthquake waveform modelling indicates 1–2 km of subducted sediments along the shallow interplate thrust, made weak by elevated pore fluid pressure (Eberhart-Phillips and Reyners, 1999). Velocity fields derived from geodetic data (Walcott, 1984b; Beavan and Haines, 2001; Wallace et al., 2004) and geological slip rates on major faults (Beanland and Haines, 1998) also indicate a major discontinuity in velocities across the plate boundary off Raukumara, supporting the idea that significant horizontal stresses are not being transferred into the overlying plate.

Central Hikurangi margin - Hawke Bay and the Wairarapa

From 40°30'S to 42°S, the presence of a Plio-Pleistocene accretionary wedge, consisting of an imbricate fold and thrust belt (Collot et al., 1996), indicates that active accretion is occuring at the trench. Outbuilding of this wedge has accelerated during the Quaternary (Barnes and Mercier de Lepinay, 1997). This section of the Hikurangi margin is arcuate, with the structural trend changing from 15° in the north to 50–70° in the south. Three NE-trending active fault scarps, the most landward of which appears to have accommodated significant dextral strike-slip, have been imaged by sidescan sonar on the upper margin behind the active wedge

(Barnes et al., 1998) (Fig. 1.5).

The topography of the plate interface beneath the Wairarapa region has been imaged in detail, using PS and SP converted arrivals to further constrain hypocentres (Reading et al., 2001). The depth to the plate interface increases by 2–4 km in the southern Wairarapa, but this change appears to be gradual rather than abrupt. More of these converted phases originate beneath the northern Wairaraipa, where the crust is thinner, suggesting that a small thickness (<2 km) of underplated sediments may be present (Fig. 2.1.)

Geodetic measurements indicate that up to 50% of contemporary inter-plate convergence is being accommodated on the Australian plate (Nicol and Beavan, 2003), and clustering of thrust earthquakes near the plate interface at depths of 20–25 km indicate the down-dip edge of a locked region (Ansell and Bannister, 1996; Reyners et al., 1997; Reyners, 1998). Much lower convergence rates within the Australian plate are indicated by the geologically derived velocity field (Beanland and Haines, 1998), suggesting that much of the short-term deformation is related to the accumulation of elastic strain and that this locking is not permanent.

Southern Hikurangi margin - Marlborough

Beneath the Marlborough region, strong coupling across the subduction interface is indicated by the absence of low angle thrust earthquakes at the interface itself, and by focal mechanisms of upper plate earthquakes being dominated by subhorizontal compression (Reyners et al., 1997). Marlborough marks the transition on the Pacific plate from thickened oceanic crust to the 23–26 km thick continental crust of Chatham Rise (Fig. 2.1). Partial subduction of the Hikurangi Plateau beneath Chatham Rise is indicated by seismic sections across this boundary (Wood and Davy, 1994), which is probably a result of its collision with the Gondwana margin at ∼105 Ma (Sutherland and Hollis, 2001).

Subduction of continental material to depths of at least 50 km is indicated by the presence of a low velocity slab in 3D seismic velocity models (Eberhart-Phillips and Reyners, 1997). However, velocity fields derived from GPS measurements (Beavan and Haines, 2001) and estimates of Quaternary fault slip rates (Holt and Haines, 1995) indicate that >80% of relative plate motion is currently being accommodated in the Marlborough Fault Zone. 3–4 km of turbidites have been deposited without the development of a significant accretionary wedge in the subduction trench off the Marlborough coast (Collot et al., 1996), and Quaternary slip rates at the subduction thrust are estimated at <1 mm/yr (Barnes and Mercier de Lepinay, 1997). These observations suggest that the underthursting of buoyant continental crust has permanently locked the interface in this region (Collot et al., 1996).

2.2 The New Zealand geological timescale

The unique faunal succession resulting from the relative biogeographical isolation of New Zealand makes it difficult to directly correlate its sedimentary sequences to the global geochronological timescale, which has led to the development of a local timescale. Neogene strata in New Zealand are principally dated using microfossils such as foraminifera; biostratigraphic datums can then be calibrated to the international timescale via the geomagnetic polarity timescale (GPTS), using paleomagnetic data (e.g. Lienert et al., 1972; Kennett and Watkins, 1974; Wright and Vella, 1988; Roberts et al., 1994) or by radiometric dating of tephra horizons. The latest New Zealand geological timescale, calibrated to the international timescale and the GPTS (Cooper, 2004), is shown in Figure 2.2.

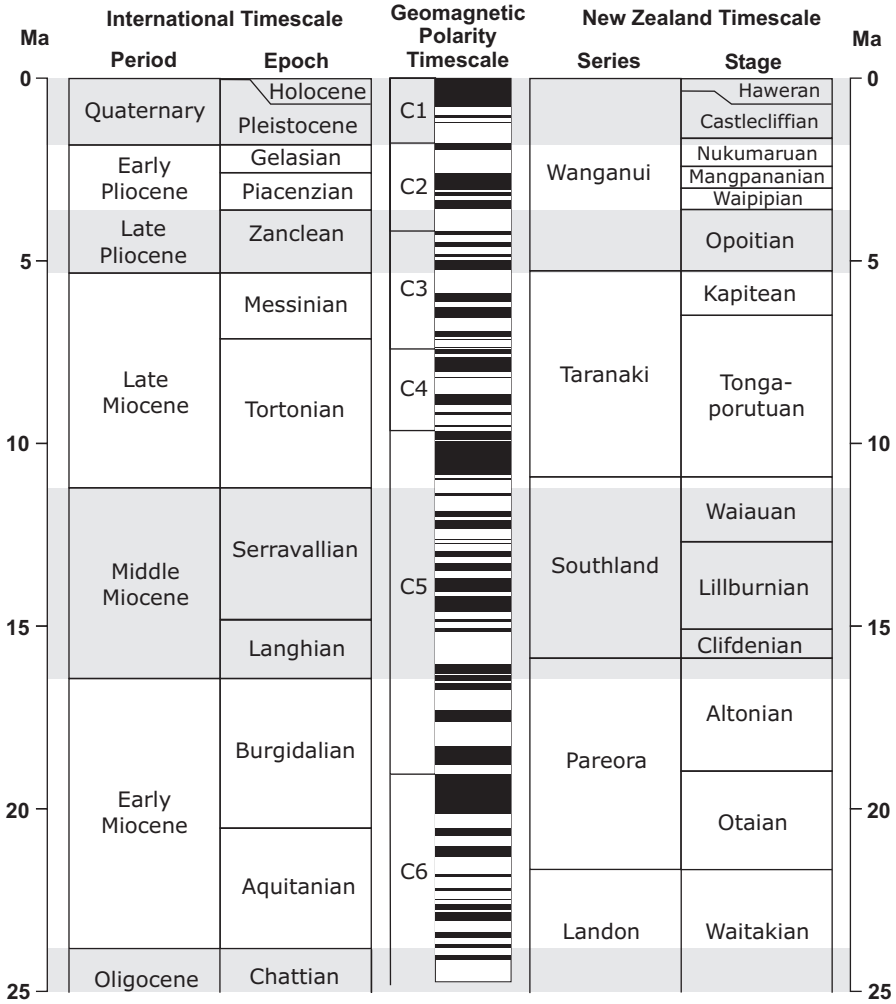

Figure 2.2: Comparison of the New Zealand and international geochronological timescales for the Neogene, from Cooper (2004). The GPTS (Cande and Kent, 1995)is also plotted for reference (C = chron).

This figure illustrates that whilst in many cases the series and stages of the New Zealand geological timescale roughly correspond to the periods and epochs

of the international timescale (e.g. there is a fairly good correspondence between the Taranaki and Southland stages, and the Late and Middle Miocene periods, respectively), the correlation is not exact (e.g. the Early Miocene includes both the Altonian and Otaian stages of the Pareora series, and also the upper part of the Waitakian stage in the older Landon series). Most of the ages and timings cited in this thesis are given in reference to the international timescale; however, it should be borne in mind that these age determinations are based on conversions from the New Zealand timescale (e.g. rocks referred to as being 'early Late Miocene' in age were originally assigned to the Tongaporutuan stage). In some cases this conversion has been done by the authors of the source material: many of the sedimentary sequences analysed in this thesis were assigned ages using the recently published 1:250000 QMAP sheets for the Wairarapa (Lee and Begg, 2002) and the Raukumara Peninsula (Mazengarb and Speden, 2000), which provide dates correlated to the international timescale. Other sources (e.g. the Southern Hawke Bay map of Kingma (1962) and papers published in regional journals such as the *New Zealand Journal of Geology and Geophysics*), which give ages in terms of the New Zealand timescale, have been similarly converted to the international timescale according to the calibration shown in Figure 2.2.

Chapter 3

Paleomagnetic theory and experimental methods

In addition to the explicit citations in this chapter, the textbooks of Butler (1992) and Tauxe (1998), and additionally the on-line guide of Moskowitz (1991), provide useful general references.

3.1 Principles of paleomagnetism

3.1.1 The Earth's magnetic field

To first order, the contemporary geomagnetic field can be approximated as a dipole inclined 11° away from Earth's axis of rotation, although there is also a significant (∼10%) non-dipole (quadrupole, octopole and other higher-order terms) contribution to the field. The magnetic field strength at the Earth's surface is 30–60 μT.

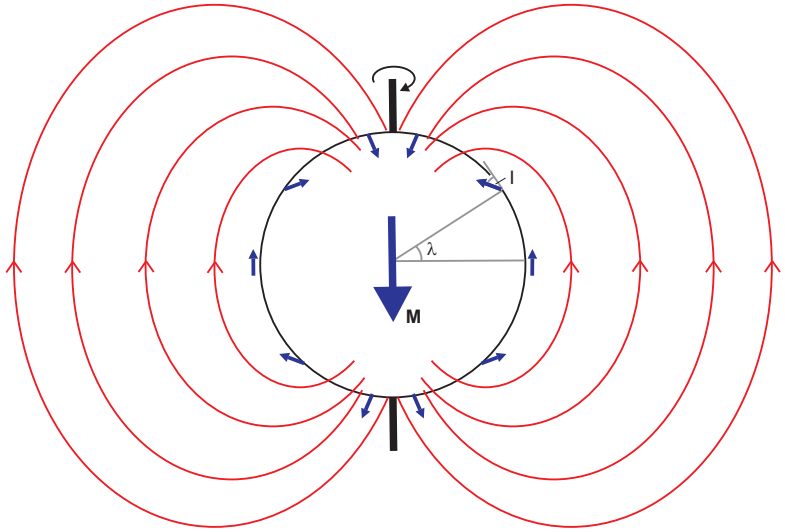

Figure 3.1: A normal polarity, geocentric axial dipole (GAD) field; small arrows depict the field direction at various points on the Earth's surface.

The ultimate source of the Earth's magnetic field is thought to be a 'self-sustaining dynamo' associated with convection of a conductive iron-nickel alloy in the liquid outer core. This convection is vigorous, allowing the geomagnetic field to vary in direction and strength over geologically rapid timescales. Fluctuations in the strength of the dipole and non-dipole fields over periods of 10^2–10^4 years lead to secular variation; the dipole field also switches polarity, sometimes several times per Myr. Studies of paleosecular variation indicate that, if time-averaged over a few thousand years, both normal and reversed polarity field configurations approximate to a simple dipole aligned with the axis of rotation (referred to as a geocentric axial dipole (GAD) field; Fig. 3.1). For a normal polarity GAD field, the horizontal component (or declination D) and vertical component (inclination I) of the magnetic field vector at any point on the Earth's surface will be:

$$D = 0, \qquad \text{and} \qquad I = \tan^{-1}(2\tan\lambda), \qquad \text{where } \lambda = \text{latitude}.$$

Paleomagnetism is concerned with studying the history of the ancient geomagnetic field recorded by permanently magnetized rocks. The origins and measurement of these remanent magnetizations are described below.

3.1.2 Types of magnetic behaviour

When a magnetic field **H** is applied to a material it induces a magnetization $\mathbf{M} = \chi\mathbf{H}$, where χ is the bulk magnetic susceptibility. The total measurable magnetic flux, from the combination of the applied field and the induced magnetization, is the magnetic induction $\mathbf{B} = \mu_0(\mathbf{H} + \mathbf{M})$.

Magnetism is a property arising from the orbital and spin motions of electrons; all matter is therefore magnetic, in the sense that it responds to the application of a magnetic field. However, the strength of this response varies greatly between different materials. There are three fundamental types of magnetic behaviour.

Diamagnetism An orbiting electron is effectively a small current loop, meaning that an external magnetic field will perturb the orbit, producing a small induced magnetization with strength inversely proportional to the applied field (Fig. 3.2a). Diamagnetism is a property of all materials, but it is a weak effect: for a purely diamagnetic material, χ is typically <-10^{-7} SI.

Paramagnetism In atoms with unfilled orbitals, the spin of unpaired electrons imparts a net magnetic moment, which will align with an applied field to produce a positive induced magnetization. At low fields, **M** is proportional to **H**, but it can reach a 'saturation magnetization' M_s at very high fields, as the atomic moments become fully aligned with the external field (Fig. 3.2b). Thermal lattice vibrations can destroy this alignment, hence $\chi \; \alpha \; 1/\mathrm{T}$.

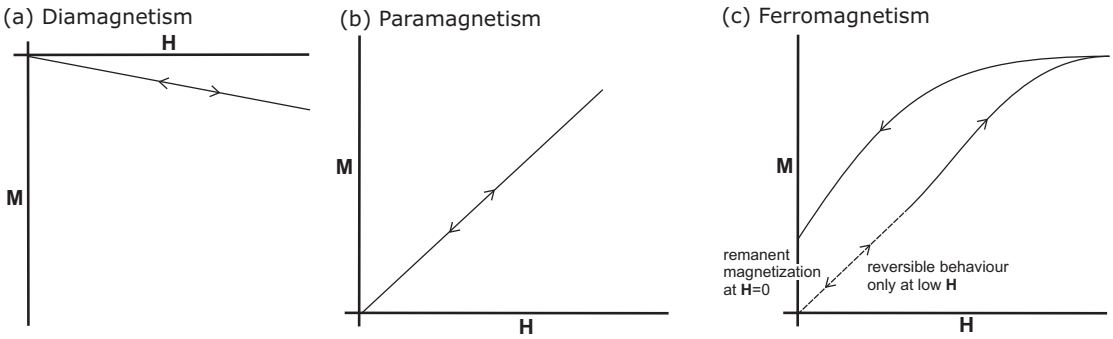

Figure 3.2: Magnetization **M** against applied field **H** for (a) diamagnetic, (b) paramagnetic, and (c) ferromagnetic materials.

'Ferromagnetism' The arrangement of atoms in some materials causes electron orbitals containing unpaired spins to overlap. Strong exchange forces between these interacting spins cause them to align with each other in order to minimize exchange energy. These interactions cause strong induced magnetizations in the presence of magnetic fields, which also lead to magnetic hysteresis: the alignment

of atomic moments is preserved even in the absence of an applied field, producing a remanent magnetization (Fig. 3.2c). Materials exhibiting these properties are referred to as 'ferromagnetic' (*sensu lato*), and have the potential to record information regarding the direction and intensity of the ancient geomagnetic field.

The way in which interacting spins align is determined by crystal structure. In ferromagnetic (*sensu stricto*) materials, the spins are parallel (Fig. 3.3a). In antiferromagnetic materials, the spins are anti-parallel (Fig. 3.3b); in such materials there will be no net magnetic moment unless the alignment is not perfect (canted antiferromagnetism; Fig. 3.3c) or the magnitudes of the opposing spins are unequal (ferrimagnetism; Fig. 3.3d).

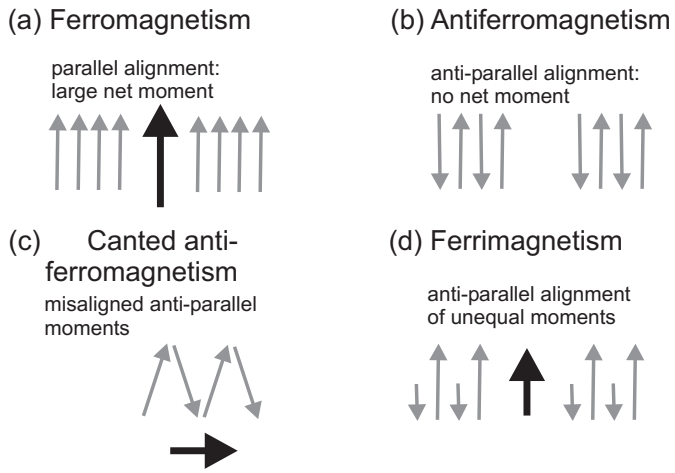

Figure 3.3: Forms of exchange coupling in ferromagnetic (*s.l.*) materials.

Ferromagnetic (*s.l.*) behaviour is also temperature dependent. Increased thermal energy increases inter-atomic spacing and reduces the overlap between electron orbits; above a characteristic Curie temperature (referred to as the Néel temperature for antiferromagnetic materials), inter-atomic spacing increases to the point that interactions are no longer possible, and the material becomes paramagnetic. Geologically common ferromagnetic (*s.l.*) minerals, mostly ferrimagnetic iron oxides and sulphides, are listed in Table 3.1.

3.1.3 Preservation of remanent magnetization

In order for ferromagnetic minerals to be useful in paleomagnetic studies, their magnetizations must be able to align with the geomagnetic field, and then preserve this remanence for millions of years without further realignment. The main factors influencing the fidelity of a ferromagnetic grain as a paleomagnetic recorder are its magnetic anisotropy and domain structure, which are controlled by grain size and shape as well as mineral structure.

Table 3.1: Geologically common ferromagnetic minerals, and their magnetic properties. Modified from Moskowitz (1991) and Tauxe (1998).

Mineral	Composition	Spin alignment	Curie/Néel Temp.	Coercivity
Magnetite	Fe_3O_4	Ferrimagnetic	580°C	10's of mT
Ulvospinel	Fe_2TiO_2	Antiferromagnetic	-153°C	
Hematite	αFe_2O_3	Canted antiferromagnetic	675°C	highly variable, can be 10's of T
Ilmenite	$FeTiO_2$	Antiferromagnetic	-233°C	
Maghemite	γFe_2O_3	Ferrimagnetic	590–675°C	
Greigite	Fe_3S_4	Ferrimagnetic	>330°C	60– >100 mT
Pyrrhotite	Fe_7S_8	Ferrimagnetic	320°C	highly variable, can be 100's of mT
Goethite	αFeOOH	Antiferromagnetic, but small net moment	120°C	10s of T

Magnetic anisotropy

The magnetic energy of a ferromagnetic grain is minimised by aligning its magnetic moment in the direction of the ambient magnetic field; in the absence of other controls on the orientation of their magnetization, ferromagnetic grains would always align with the geomagnetic field and no older remanence would be preserved. However, the energy required to magnetize a grain is usually not constant in all orientations; there are 'easy' directions of magnetization in which the associated energy is lower. There are three principal sources of magnetic anisotropy.

- Magnetocrystalline anisotropy. The exchange energy between coupled spins is minimized when spins are aligned along particular crystallographic axes.
- Shape anisotropy. If atomic magnetic moments are modelled as pairs of magnetic charges, a magnetized grain will have a surface distribution of these charges (Fig. 3.4a), which not only produces an external (dipole) field but also an internal demagnetizing field $\mathbf{H}_D$ which opposes the overall magnetization (Fig. 3.4b). Because the strength of this field depends on the surface charge distribution, an elongated grain has a smaller $\mathbf{H}_D$ along its long axis, resulting in an easy axis of magnetization, because a smaller percentage of the surface is covered by magnetic charges (Fig. 3.4c, d).
- Magnetostrictive anisotropy. Spin realignment exerts stresses on the magnetic crystal, changing its shape. Conversely, therefore, applied stresses, which further alter the shape of the crystal, can affect the spin alignment and give rise to magnetostrictive anisotropy.

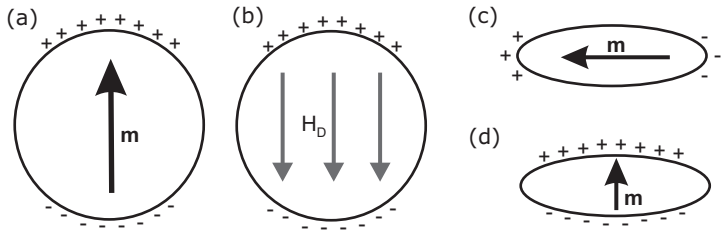

Figure 3.4: (a) Surface magnetic charge distribution for a uniformly magnetized spherical grain, and (b) the resultant internal demagnetizing field. (c, d) Charge distribution in an elongated grain with (c) a moment aligned along the long axis of the grain, and (d) a moment oriented perpendicular to the long axis. After Butler (1992).

The existence of magnetic anisotropy in ferromagnetic grains means that energy is required to shift the direction of their magnetic moment **m** from one 'easy' direction to another. Only a magnetic field greater than the switching or coercive field, h_c, can generate enough magnetostatic energy to overcome this anisotropy energy, forcing **m** through the intervening 'hard' directions. If h_c is large, details of an ancient magnetizing field can potentially be recorded for long periods of time.

Even at a constant temperature, however, thermal energy can eventually move **m** across these energy barriers into a new orientation, a phenomenon referred to as magnetic viscosity. From an initial magnetization M_0, the remanent magnetization of a population of ferromagnetic grains will decay exponentially:

$$M(t) = M_0\, e\left(\frac{-t}{\tau}\right),$$

where t is the elapsed time and τ is the characteristic relaxation time (the time for the remanence to decay to M_0/e). Technically, this equation is only valid for single domain grains (see Section 3.1.3) and only holds as a first approximation for multidomain systems. The probability that **m** will spontaneously change orientation is dependent on the ratio of magnetic anisotropy and thermal energies, hence:

$$\tau = \frac{1}{C}\, e\left(\frac{v h_c m}{2kT}\right),$$

where C = frequency factor ($\approx 10^8$ s^{-1}), v = grain volume, k = Boltzmann constant, and T = temperature. Relaxation time is therefore proportional to grain volume and the coercive field, and inversely proportional to temperature. The exponential relationship means that a small increase in grain size will increase τ by many orders of magnitude, from seconds to >1 Ga; above a particular 'blocking volume', τ becomes large enough that a remanent magnetization can be preserved over millions, or even billions of years.

In reality, thermal relaxation in a magnetized rock occurs in the presence of the geomagnetic field, which will cause particles with low h_c to align with the present day field direction. This viscous remanent magnetization (VRM) must be removed before any ancient components of magnetization can be measured.

Magnetic domains

Increasing grain size also increases the magnetostatic energy associated with the surface distribution of magnetic charges (Fig. 3.4). Above a certain size, it becomes energetically favourable for the grain to split into a number of uniformly magnetized domains, oriented along different easy directions of magnetization, which reduces the overall magnetization. The number of domains that form is determined by the balance between the resulting reduction in magnetostatic energy, and the energy required to form domain walls, the regions between adjacent domains across which spins must rotate from one easy direction to another. Three main types of domain structure are recognised:

- Single domain (SD). Below a critical grain size, the energy required to create a domain wall exceeds the reduction in magnetostatic energy achieved in forming one. An SD grain therefore has a uniform magnetization that can only be changed by rotation of its magnetic moment; when SD grains are relatively large and thermally stable, it is energetically difficult to change the direction of magnetization, resulting in high coercivities and magnetic stability (Fig. 3.5). Coercivity is reduced at smaller grain sizes, due to the randomising effect of thermal energy; eventually h_c is reduced to the point that the remanent magnetization rapidly decays to zero in the absence of an applied field (τ <100 s); these superparamagnetic (SP) grains are not stable enough to record paleomagnetic information (Fig. 3.5).

- Multi-domain (MD). The division of larger ferromagnetic grains into domains with differently aligned magnetizations leads to a low overall remanence. Additionally, rather than causing the realignment of magnetic moments, applying a field to a MD grain promotes preferential growth of domains with a magnetization parallel to the field. The movement of domain walls is a low energy process that can be accomplished in relatively low fields; thus MD grains also have low coercivities (Fig. 3.5), and are unstable over geological timescales.

- Pseudo-single domain (PSD). The transition from SD-like to MD-like behaviour is not abrupt (Fig. 3.5). For reasons that are still not fully understood, small MD particles, containing just a few domains, can still have SD-like

properties (large remanent magnetizations and, more crucially, high coercivities) and are capable of preserving a stable paleomagnetic signal.

The size of ferromagnetic grains is therefore of crucial importance in determining their magnetic stability; grains useful for paleomagnetic purposes are in the stable SD (τ >10^7–10^9 years) to PSD size range (Fig. 3.5).

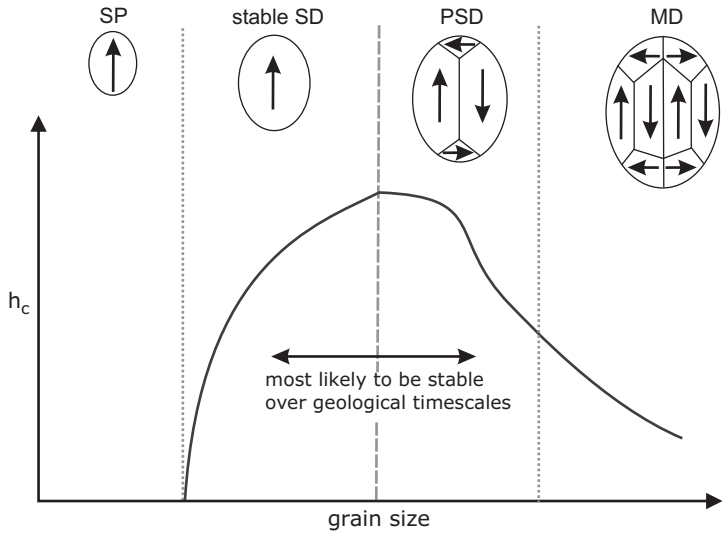

Figure 3.5: Variation in domain state and coercivity with increasing grain size. Stable SD grains, and PSD grains just above the critical SD grain size are the most likely to be stable over geological timescales. From Moskowitz (1991).

3.1.4 Remanence acquisition in sedimentary rocks

Depositional and post-depositional remanent magnetization (DRM/pDRM)

Remanent magnetization in sediments is in many cases caused by ferromagnetic grains aligning with the ambient geomagnetic field during deposition and lithification. Alignment can occur in the water column, where viscous forces that resist grain reorientation are low, and may be preserved upon settling to form a depositional remanent magnetization (DRM). However, processes operating after deposition, particularly bioturbation, are probably more important, realigning grains with the ambient field below the sediment-water interface to form a post-depositional remanent magnetization (pDRM).

A stable magnetization is therefore probably not locked into sediments before dewatering, compaction and lithification restrict the motion of ferromagnetic particles and prevent further realignment. The time interval before this lock-in occurs is dependent on grain size, and may be of the order of 10^2–10^3 years after deposition for smaller grains. As discussed in the previous section, the average grain size will also determine the stability of remanence. The SD–PSD size range varies for different ferromagnetic minerals, and is poorly characterised for iron sulphides

like greigite. However, for magnetite (a common carrier of DRM and pDRM) the SD–PSD transition occurs at ∼80 nm diameter; fine-grained siltstones and mudstones are therefore more likely to preserve a stable detrital remanence than coarse-grained sediments.

Chemical remanent magnetization (CRM)
An alternative source of remanent magnetization in sedimentary rocks is the authigenic growth of ferromagnetic minerals following deposition. Although initially small in size, and SP, with continued growth the mineral grains will pass through the critical blocking volume and become thermally stable. The ambient geomagnetic field at the time of this transition will then be preserved as a chemical remanent magnetization (CRM).

Examples of CRM acquisition include post-depositional hematite growth in red beds, and the growth of the iron sulphide greigite during reductive diagenesis of rapidly deposited marine sediments. An important consideration to bear in mind when dealing with CRMs is that they do not necessarily record a primary paleomagnetic signal. Although mineral growth during early diagenesis can lead to remanence acquisition over timescales similar to the lock-in of a pDRM, growth could potentially have occurred at any time after deposition.

3.2 Paleomagnetic measurements

3.2.1 Paleomagnetic sampling

The ultimate aim of most paleomagnetic sampling is to measure the direction of the ancient geomagnetic field. Because analysis of these directions assumes a GAD field, an important first step is to ensure that sampling covers a time interval $\geq 10^4$–10^5 years, so that secular variation is properly averaged out (Section 3.1.1). In sedimentary sequences, the stratigraphic thickness represented by this time interval depends on the average deposition rate, but is typically 10–20 m in most Neogene sedimentary environments in New Zealand; a sequence of >10 m was sampled at most localities in this study (Table 7.1). Another important criterion is that the sampled sediments have clearly discernible bedding, with a constant orientation consistent with local geological structures, so that measured paleomagnetic directions can be properly corrected for bedding tilt.

Sampling was undertaken using a portable petrol-powered drill, with a water-cooled diamond bit. At a typical locality, 4-6 cores were drilled at approximately 10 distinct stratigraphic levels within the section; weathered and fractured material was cleared from the surface of the outcrop prior to drilling. Before extraction, all cores were oriented and marked *in situ*, according to the scheme described in Figure 3.6. Following extraction, cores were wrapped in newspaper and immedi-

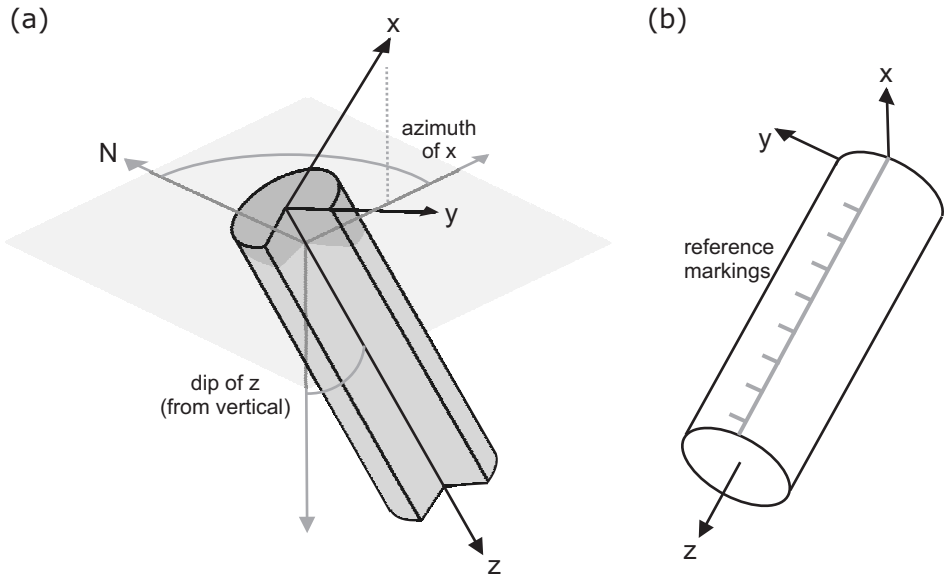

Figure 3.6: (a) Relation of the paleomagnetic core orientation to the sample coordinate system. The dip and dip azimuth of the core are measured to allow correction into geographic coordinates. (b) Relation of 'laboratory arrow', marked on the core prior to extraction, to the sample coordinate system.

ately transferred to a mu-metal shield for transportation back to the laboratory, to prevent the acquisition of viscous overprints (e.g. Walcott and Mumme, 1982). On average, 2–3 samples (21 mm length) were cut from each core; these were also kept in a low-field environment prior to, and during, paleomagnetic measurements.

3.2.2 Measurement of remanent magnetization

All measurements of remanent magnetization were made using a 2G-Enterprises 3-axis SQUID cryogenic magnetometer at the National Oceanography Centre, Southampton (NOCS). The superconducting quantum interference device (SQUID) is an extremely sensitive flux-to-voltage converter, which can theoretically detect single flux quantum changes in the intensity of the ambient magnetic field. In order to minimise sources of measurement noise, the magnetometer is situated in a magnetically shielded room, which reduces the intensity of the ambient magnetic field to <300 nT. Superconducting shields placed around the SQUID sensors further reduce the field to ∼1–2 nT in the measurement region of the magnetometer. This low-field environment gives the magnetometer a sensitivity of better than 10^{-6} Am^{-1}.

3.2.3 Stepwise demagnetization

The NRM of a sedimentary rock can be the vector sum of a number of different components: a DRM or pDRM from or near the time of deposition, one or more CRMs caused by mineral growth after deposition, and a VRM carrying a present day field overprint. In order to extract useful paleomagnetic information,

these different components must be isolated. This is usually achieved through the use of stepwise demagnetization, which relies on the principle that different magnetic components are carried by distinct populations of grains, with different mineralogies and grain sizes, and therefore different stabilities of remanence. Stepwise demagnetization progressively removes low stability components of NRM, and isolates the more stable components that are more likely to record an ancient magnetization. The most stable of these ancient components is referred to as the characteristic remanent magnetization (ChRM). The two techniques used in this study were thermal and alternating field (AF) demagnetization.

Thermal demagnetization The characteristic relaxation time τ is inversely proportional to temperature. Therefore, grains that are stable at room temperature ($\tau > 10^9$ years) will become unstable when heated to their unblocking temperature T_b, which is higher for larger, more stable grains. Thermal demagnetization involves heating a sample to temperature T then cooling back to room temperature in zero magnetic field. All grains with blocking temperature $T_b < T$ have their directions randomized, erasing the NRM carried by these grains and allowing more stable components to be isolated.

In this study, measurements of NRM were made after heating samples to $T = 80°$, 120°, 160°, 200°, 240°, 280°, 320°, 360°, 380° and 400°C; samples were held at T for 40 minutes before cooling. Low-field bulk magnetic susceptibility was measured after each heating step; elevated temperatures often caused thermal alteration and the growth of new magnetic minerals, indicated by a substantial increase in susceptibility above 360°C.

Alternating field demagnetization In AF demagnetization, the sample is exposed to a sinusoidal magnetic field, which is smoothly reduced to zero from a specified peak value. This process effectively randomises the magnetization of grains with coercivities below the peak AF intensity, allowing the remanence of higher coercivity grains to be isolated. This study utilised the in-line AF demagnetizer on the 2G-Enterprises cryogenic magnetometer, which at each measurement step sequentially applied an AF along three mutually perpendicular sample axes. Measurements of NRM were made at 5 mT steps up to 60 mT.

The relative effectiveness of thermal and AF techniques can differ, depending on the mineralogy of the remanence-carrying grains, and the distribution of coercivities and unblocking temperatures for the different components. For example, AF treatment would be ineffective at removing a CRM carried by hematite, which always has high coercivities, whereas thermal demagnetization would effectively

demagnetize all hematite grains above the Néel temperature of 680°C. For each locality in this study, pilot AF and thermal demagnetizations of single samples from each sampling level were undertaken to assess the relative effectiveness of each technique. Although in previous studies of weakly magnetized New Zealand Cenozoic mudstones, AF demagnetization has frequently proven ineffective (e.g. Turner et al., 1989; Pillans et al., 1994; Roberts et al., 1994; Turner, 2001), at a number of the sampled localities in this study the AF technique proved to be more or equally effective than thermal demagnetization. AF demagnetization can be performed more quickly than thermal demagnetization. Additionally, unlike thermally demagnetised samples, where high temperatures often alter the magnetic mineralogy, AF demagnetized samples can be used for further rock magnetic analyses (see sections 3.3, 3.4).

3.2.4 Display of stepwise demagnetization data

There are two principal methods of displaying stepwise demagnetization data.

- Vector component diagrams (Zijderveld, 1967; Dunlop, 1979). The cartesian components of the 3D magnetization vector ($x = M\cos I\cos D$, $y = M\cos I\sin D$, and $z = M\sin I$) are projected onto orthogonal horizontal and vertical planes. This technique allows the direction and intensity of the vector to be fully represented on a two-dimensional plot.

- Equal area stereographic plots. The direction of the normalised magnetic vector is plotted onto a lower hemisphere projection of the unit sphere, where:

$$x = \cos I \sin D \sqrt{1/(1+|sinI|)}; \quad y = \cos I \cos D \sqrt{1/(1+|sinI|)}.$$

  Upward and downward pointing vectors are represented by open and closed symbols, respectively. In this projection, the scatter of different data sets can be easily compared because regions of equal area on the unit sphere appear as equal areas on the projection.

Before interpretation, raw paleomagnetic measurements in sample coordinates (Fig. 3.6) must be transformed into a more useful coordinate system. Correction into geographic coordinates (known as a field correction) restores the original orientation of the specimen prior to sampling, which is useful for identifying present day field overprints. A further tilt correction can be made by restoring the beds sampled to the paleo-horizontal. This is usually the most appropriate system for analysing ancient components of remanence.

The most useful method for the display of demagnetization data depends upon the relative stability of the different remanence components within the sample.

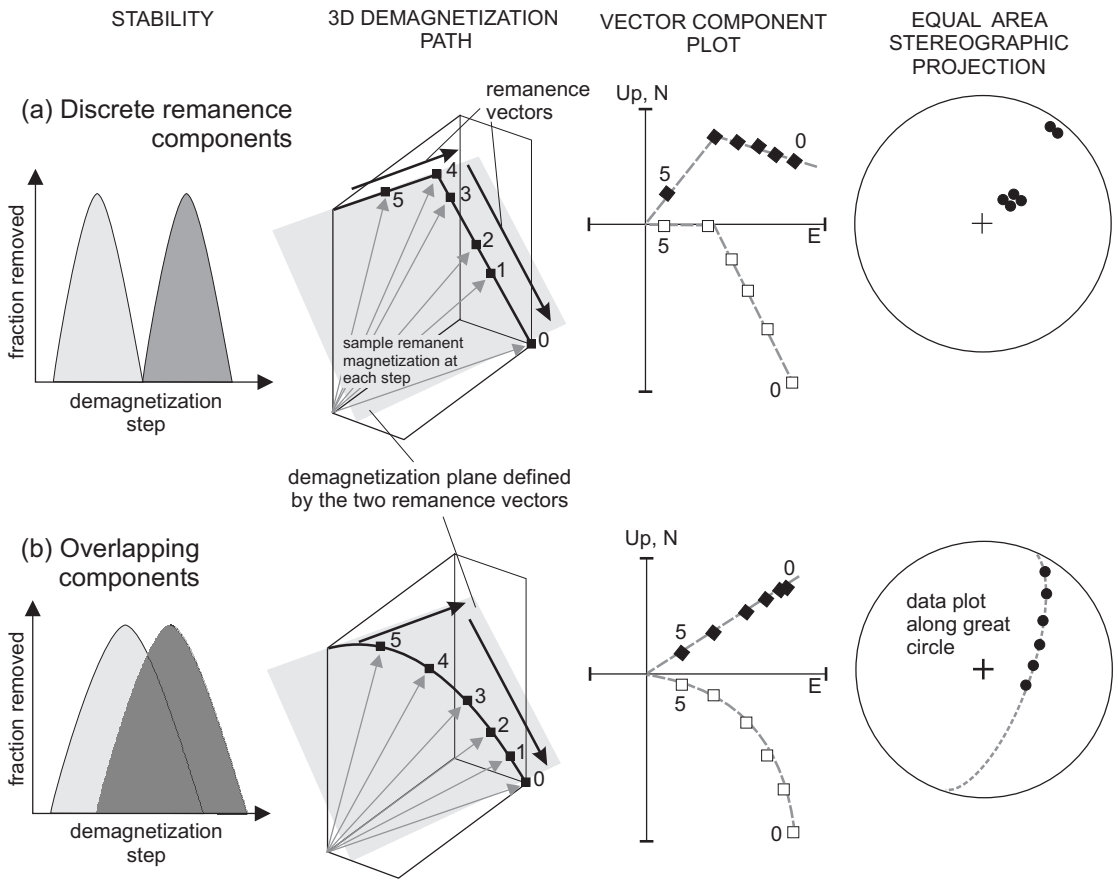

Figure 3.7: Methods of displaying demagnetization data. Stepwise demagnetization data are plotted on a vector component diagram (closed symbols = horizontal plane, open symbols = vertical plane) and an equal area stereographic projection, for: (a) two remanence components with discrete coercivity/unblocking temperature spectra, and (b) two components with overlapping spectra.

When separate components have discrete coercivity or unblocking temperature distributions (Fig. 3.7a), they will be progressively removed over a distinct range of demagnetization steps, and the demagnetization path will consist of a series of linear segments that are best displayed on a vector component diagram. However, when there is significant overlap between the two components, as indicated in Figure 3.7b, a fraction of both remanences will be removed concurrently at many demagnetization steps, and neither component may be isolated. However, all of the measured directions will fall within the plane defined by the two remanence vectors, and demagnetization data will plot along a great circle on a stereographic projection. This makes stereographic projections particularly useful for analysing demagnetization great circles (page 42). In practice, both methods of data display are routinely used.

3.2.5 Principal component analysis

Vector component plots of stepwise demagnetization data allow the various remanence components that make up the NRM to be separately identified. The directions of these different components are then calculated using principal component analysis (Kirschvink, 1980). This method analyses the variance of equally weighted data points about their 'centre of mass' $\mathbf{U} = (\overline{x},\ \overline{y},\ \overline{z})$, where:

$$\overline{x} = \frac{1}{N}\left(\sum_{1}^{N} x_i\right); \quad \overline{y} = \frac{1}{N}\left(\sum_{1}^{N} y_i\right); \quad \overline{z} = \frac{1}{N}\left(\sum_{1}^{N} z_i\right).$$

Where the highest stability component decays to the origin, an anchored fit can be obtained by setting the origin of the vector component plot as the centre of mass (i.e. $(\overline{x},\ \overline{y},\ \overline{z}) = 0$). The principal axes of maximum, minimum and intermediate variance for the data set parallel the eigenvectors of the orientation tensor $\mathbf{T}$:

$$\mathbf{T} = \begin{pmatrix} \sum(x_i-\overline{x})^2 & \sum(x_i-\overline{x})(y_i-\overline{y}) & \sum(x_i-\overline{x})(z_i-\overline{z}) \\ \sum(x_i-\overline{x})(y_i-\overline{y}) & \sum(y_i-\overline{y})^2 & \sum(y_i-\overline{y})(z_i-\overline{z}) \\ \sum(x_i-\overline{x})(z_i-\overline{z}) & \sum(y_i-\overline{y})(z_i-\overline{z}) & \sum(z_i-\overline{z})^2 \end{pmatrix}.$$

The eigenvectors are the axes of the coordinate system in which the non-diagonal terms of $\mathbf{T}$ are zero, i.e.:

$$\mathbf{TV} = \tau\mathbf{V},$$

where $\mathbf{V}$ is the matrix of eigenvectors $\mathbf{V}_1$, $\mathbf{V}_2$ and $\mathbf{V}_3$ and τ is the diagonal matrix of eigenvalues τ_1, τ_2 and τ_3. This equation is satisfied where:

$$det\,|\mathbf{T} - \tau| = 0$$

$\mathbf{V}_1$ represents the direction of maximum variance and is therefore equivalent to a line of best fit through the data. A large τ_1 compared to the other two eigenvalues indicates a linear distribution for the selected data points. This linearity can be assessed by calculating the maximum angular deviation (MAD):

$$MAD = \tan^{-1}\left(\sqrt{(\tau_2+\tau_3)/\tau_1}\right).$$

A good line fit is indicated by a MAD <10–15°. This method is only valid where linear components of the demagnetization path can be isolated (e.g. Fig. 3.7a). In the case of overlapping remanence components forming a demagnetization great circle (Fig. 3.7b), $\mathbf{V}_3$ defines the pole to this plane.

3.2.6 Calculation of mean directions

Fisher statistics

The ChRM directions isolated from a sampling locality can be used to calculate a paleomagnetic mean direction by converting them to unit vectors, summing them and scaling them by the resultant vector of the data set. However, statistical treatment is required to estimate how close this calculated direction is likely to be to the true mean direction. Paleomagnetists generally make use of the Fisher distribution, which is the Gaussian normal distribution mapped onto the surface of a unit sphere (Fisher, 1953). The probability of a measured direction falling within angle α of the true mean direction is given by the density function:

$$P(\alpha) = \frac{\kappa}{4\pi \sinh \kappa} e\left(\kappa \cos \alpha\right).$$

The precision parameter κ is a measure of the scatter of the paleomagnetic data, and can be approximated for N data points as

$$\kappa \approx k = \frac{N-1}{N-R},$$

which tends to infinity when scatter is low and the resultant R becomes similar in magnitude to N. A confidence angle $\alpha_{(1-p)}$ is given by:

$$\alpha_{(1-p)} = \cos^{-1}\left(1 - \frac{N-R}{R}\left(\left(\frac{1}{p}\right)^{\frac{1}{(N-1)}} - 1\right)\right).$$

The 95% confidence limit α_{95}, within which there is a 95% probability that the true mean occurs, is most commonly used. Where $k > 25$, α_{95} can be further approximated as:

$$\alpha_{95} \approx \frac{140}{\sqrt{kN}}.$$

In addition to measurement error, the scatter in paleomagnetic data can also be caused by other factors such as secular variation and the incomplete removal of secondary components. Some of these contributions can potentially lead to a non-symmetric data distribution that is not adequately represented by Fisher (1953) statistics. The use of bootstrap statistics (Tauxe, 1998) is one suggested approach for dealing with non-symmetric data whilst retaining the ability to calculate confidence intervals. Unfortunately, the paleomagnetic data sets from most localities in this study, as is the case in most paleomagnetic studies, are generally too small to properly represent the underlying data distribution. The data in this study are

therefore assumed to be normally distributed about the true mean direction.

Demagnetization great circles
At many localities in this study even stepwise demagnetization could not isolate a ChRM; strong viscous overprints had unblocking temperature and coercivity spectra that overlapped the ChRM to the extent that a stable endpoint could not be isolated. However, in such cases the stepwise demagnetization data trace out the great circle arc of the plane defined by the two remanence components (Fig. 3.7), and therefore still contains information about the higher stability component. Using the method developed by McFadden and McElhinny (1988), a probability distribution can be calculated for a set of great circle arcs, assuming that if endpoints had been reached they would have a Fisherian distribution about the true mean direction. This allows the great circle data to be combined with stable endpoints to produce a better constrained mean direction.

Determining tectonic rotations
As already discussed in Section 1.3, the declination anomaly for a particular locality is determined by comparing the mean paleomagnetic direction with the expected APWP. A further complication arises when calculating confidence limits for a declination anomaly. Because it is an angular confidence limit with two degrees of freedom, the α_{95} value is not directly equivalent to this confidence limit. Demarest (1983) demonstrated that the actual declination error is 80% of the α_{95} value. Uncertainties in the tectonic rotations reported in this study have had this correction applied.

3.2.7 Paleomagnetic field tests

Establishing the age of remanence acquisition in sedimentary rocks is particularly important where the presence of a CRM, which could potentially have formed at any point after deposition, is suspected. Paleomagnetic field tests can provide useful constrains in such cases. The principal tests used in this study were the fold test and, to a lesser extent, the reversals test; the lack of appropriate sampling localities meant that other commonly used field tests, such as the conglomerate test and the baked contact test, were not used.

Fold test
To apply the fold test it is necessary to isolate stable ChRMs from two or more localities with different bedding attitudes sampled across a fold, or within strata that have all been folded in a single tectonic episode. The timing of remanence acquisition can then be assessed by comparing the scatter of measured ChRM directions from these localities in geographic and tilt-corrected coordinates. When the directions are less scattered in tilt-corrected coordinates, the magnetization is likely

to have formed prior to folding; conversely, better clustering of directions before a tilt correction is applied indicates remanence acquisition after tilting (Fig. 3.8). In some cases, the least scatter is observed after a partial tilt correction, implying that remanence acquisition was contemporaneous with folding of the beds.

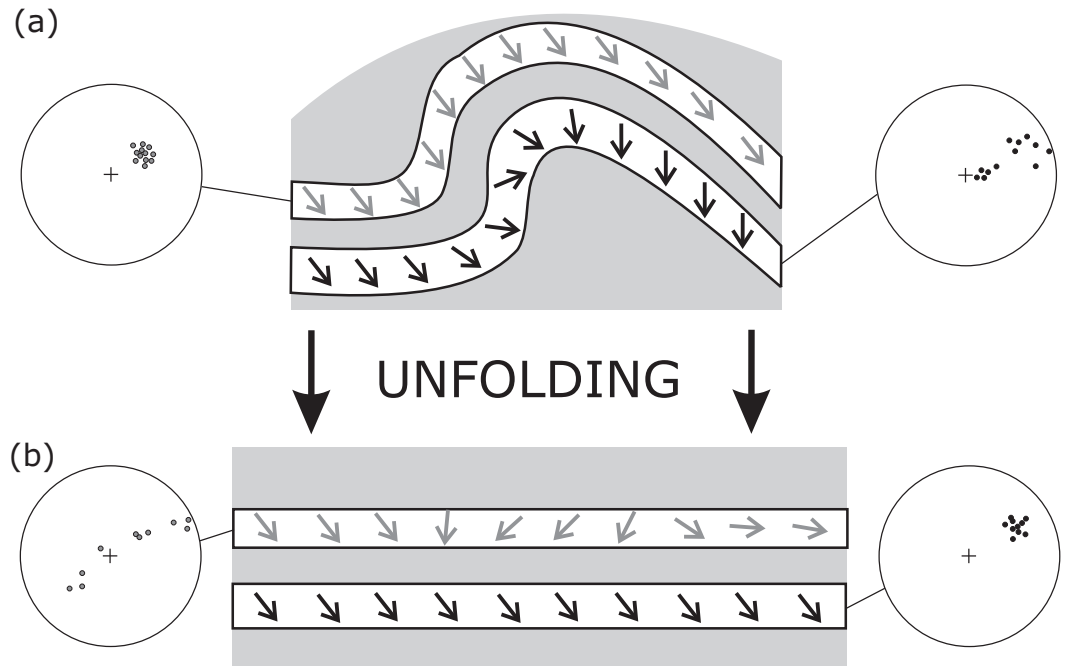

Figure 3.8: Illustration of the fold test. The stereoplots indicate directions of magnetization distributed across a fold in two beds, (a) before, and (b) after, correction for bedding tilt. In the lower bed, the measured directions are more clustered after tilt correction, indicating a pre-folding remanence acquisition. In contrast, in the upper bed better clustering of directions is observed before tilt correction, indicating a post-folding remagnetization.

Statistical tests must be applied in order to rigorously compare the scatter of data in different coordinate systems. In the fold test of Tauxe and Watson (1994), as used in this study, the eigenvalues of the data set (Section 3.2.5) are calculated at various degrees of unfolding; the principal eigenvector τ_1 reaches a maximum value at the point where the scatter in the data is minimised. Bootstrap statistics can then be used to calculate confidence intervals. The advantages of this method over earlier fold tests (e.g. McElhinny, 1964; McFadden, 1990) include the ability to deal with mixed polarity data, and also to rigorously constrain syn-folding magnetizations.

Reversals test

If a sequence with a primary NRM is sampled over a large enough stratigraphic thickness, the time interval covered may be long enough to recover ChRM direc-

tions from both normal and reversed polarity field configurations. Assuming a GAD field, in such cases the normal and reversed polarity mean directions should be antipodal. This forms the basis of the reversals test.

Although the presence of directions of both polarities is suggestive of a primary remanence, and is probably sufficient to demonstrate that a data set has not been unduly affected by strong systematic overprints, in order to formally pass a reversals test it is necessary to establish that when one of the mean directions is flipped, it is indistinguishable from the other (McFadden and McElhinny, 1990; Tauxe, 1998). To rigourously establish this, McFadden and McElhinny (1990) proposed a method of calculating a critical angle γ_c between the two mean directions, above which the hypothesis of a common mean would be rejected. The value of γ_c is dependent on the number of ChRMs contributing to the mean directions, and their k values, and will be larger when these parameters are larger for either direction, making it easier to pass the reversals test. A small critical angle therefore indicates a more robust reversals test, making a positive result more reliable (McFadden and McElhinny, 1990).

3.3 Rock magnetic measurements

3.3.1 Hysteresis properties

Ferromagnetic grains retain a remanent magnetization even when the magnetizing field is reduced to zero; this remanence can only be driven back to zero by a field in the opposite direction. A hysteresis loop (Fig. 3.9a) is generated by applying a varying magnetic field to a sample. The shape of this loop is dependent on the properties of the magnetic grains. Four parameters are particularly important for extracting information about the magnetic assemblage (Fig. 3.9a, b).

- Saturation magnetization (M_s). The maximum magnetization the sample can acquire in an applied magnetic field.
- Saturation remanent magnetization (M_r). The remanence when the applied field has been reduced to zero from saturation.
- Coercive force (B_c). The value of the reverse field at which the magnetization of the sample becomes zero.
- Coercivity of remanence (B_{cr}). The reverse field which, when applied and then removed, reduces the saturation remanence to zero. It is always larger than the coercive force.

As discussed on page 33, grain size is an important factor in determining the domain state, and hence the magnetic properties, of ferromagnetic minerals. Day

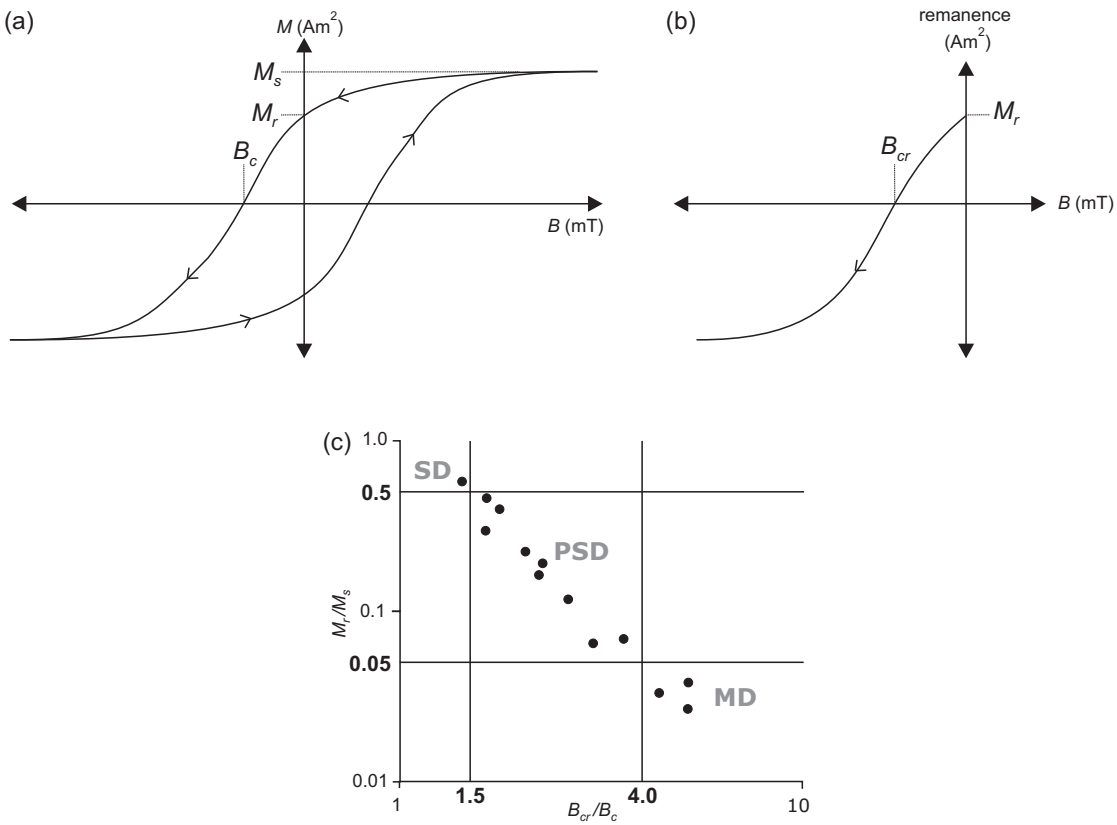

Figure 3.9: (a) Typical hysteresis loop, acquired by measuring the magnetization M in a varying magnetic field B, illustrating commonly measured parameters that can be used to characterise its shape. (b) Back-field remanence curve, acquired by measuring the remanence following removal of the applied magnetic field B, used to measure the coercivity of remanence B_{cr}. (c) Day plot of the ratios B_{cr}/B_c) against M_r/M_s, indicating the experimentally determined regions for single domain (SD), pseudo single domain (PSD) and multidomain (MD) magnetite (Day et al., 1977). Circles indicate typical measured values for magnetite of varying grain size.

et al. (1977) showed that the hysteresis properties of magnetite of known grain sizes follow a predictable trend on a plot of the ratios B_{cr}/B_c against M_r/M_s; small SD grains have high values of M_r/M_s and low values of B_{cr}/B_c, and larger MD grains have low values of M_r/M_s and high values of B_{cr}/B_c. This 'Day plot' can therefore provide useful information on the grain size of magnetic particles, although, as discussed in Chapter 6, hysteresis parameters become more difficult to interpret in samples with non-uniform grain size distributions.

In this study, measurement of the bulk magnetic hysteresis properties of $\sim$1 cm^3 sub-samples was undertaken using a Princeton Measurements Corporation Micromag 3900 vibrating sample magnetometer (VSM) at NOCS. Values of M_s, M_r, and B_c were obtained from hysteresis loops (0.5 T saturating field); B_{cr} was determined from back-field remanence curves.

3.3.2 First order reversal curve (FORC) diagrams

The fine control of the applied magnetic field provided by the VSM allows rapid and reliable measurement of first-order reversal curves (FORCs), which are a class of partial hysteresis loop measured by cycling between a positive saturation field and a reversal field B_a (Pike et al., 1999; Roberts et al., 2000). The magnetization $M(B_a, B_b)$ is measured for a series of field values B_b between B_a and positive saturation (Fig. 3.10a). Measuring a series of FORCs, with a range of different B_a values, provides a more complete sampling of the magnetic response of the sample than a single hysteresis loop. This is particularly useful for geological samples, which often contain mixtures of magnetic phases, both in terms of grain size or mineralogy, meaning that bulk hysteresis parameters often cannot be interpreted unambigously.

The FORC distribution is given by:

$$\rho\left(B_a, B_b\right) \equiv -\frac{\partial^2 M(B_a, B_b)}{\partial B_a \partial B_b},$$

which is well defined for $B_b > B_a$. A FORC diagram is a contour plot of the FORC distribution in the transformed co-ordinate system $B_u = \left(B_a + B_b\right)/2$, $B_c = \left(B_b - B_a\right)/2$. This transformation allows a more intuitive interpretation of the FORC distribution, based on the Néel (1954) interpretation of Preisach (1934) diagrams: the distribution along the B_c axis represents the coercivity distribution of magnetic grains in the sample, whereas the spread of contours along the B_u axis indicates the strength of magnetic interactions between them (Fig. 3.10b).

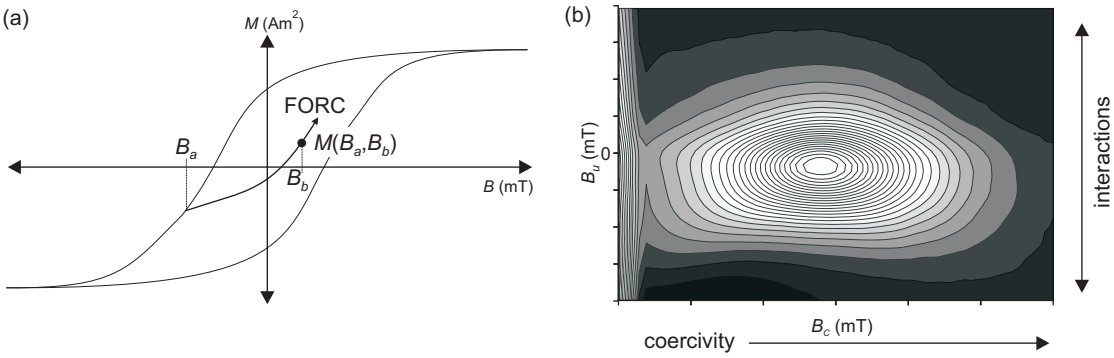

Figure 3.10: (a) Measurement of a first-order reversal curve (FORC). The magnetization $M(B_a, B_b)$ is measured at a series of field values B_a between a reversal field B_a and positive saturation. (b) Example of a FORC diagram, showing the FORC distribution obtained for a series of FORCs, which can be interpreted in terms of coercivity distribution and particle interaction field distribution.

In this study, samples were analysed by measuring 140 FORCs, with a field spacing of 1.85 mT, an averaging time of 250 ms, and a 0.5 T saturating field.

The FORC distributions were calculated using a smoothing factor (SF) of 5, as detailed in Pike et al. (1999) and Roberts et al. (2000).

3.4 Scanning electron microscopy

3.4.1 Basic principles

Electrons have a much smaller wavelength than visible light photons. The scanning electron microscope (SEM) takes advantage of this fact to acquire very high-resolution (of the order of nanometres) images of the morphology and topography of a specimen. The basic configuration of an SEM is shown in Figure 3.11. The electron gun produces a narrow beam of electrons, which is directed by electromagnets to scan over the specimen in a raster pattern. Because the magnets directing the beam are not involved in image formation, increased magnifications are simply achieved by scanning the electron beam over a smaller area. This allows the specimen to be imaged with a high depth of field, at a wide range of magnifications.

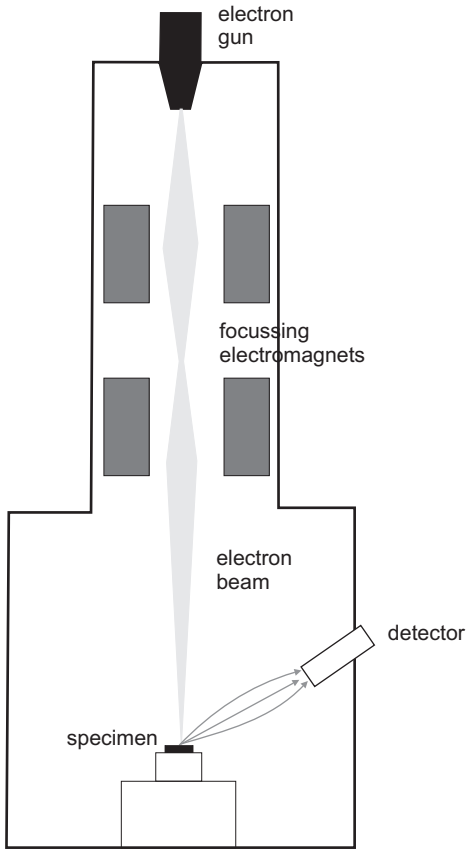

Figure 3.11: Schematic diagram illustrating the major components of a scanning electron microscope (SEM).

Within the small area being scanned at any given moment, some electrons in the beam are elastically reflected from the specimen with no loss of energy

(back-scattered electrons). Others are absorbed, producing low energy secondary electrons (so-called because they are a result of the transfer of energy from the electron beam to the specimen) and X-rays. These scattered electrons are collected by a positively charged detector grid, which converts the variations in the strength of scattering as the beam moves across the specimen into an electric signal, which can then be used to form an image. Secondary electrons are commonly used for imaging; because of their low energy, only electrons produced in the upper 5–50 nm of the sample are able to escape to the detector, meaning that they are derived from a smaller sampling volume than the higher energy back-scattered electrons. However, because the probability of back-scattering is a weak function of atomic number, areas with different chemical compositions can be more effectively distinguished if the sample is imaged using back-scattered electrons, at the cost of reduced topological contrast.

The energy and wavelength of the X-ray photons is dependent on the elemental composition of the samples. The energy dispersive X-ray spectrometer (EDS) is used to produce a histogram of the X-ray photon energies received by the detector when the beam is focussed on a particular spot on the surface of the sample (e.g. Fig. 3.12). Individual 'peaks' correlate to orbital energy levels within particular elements. The relative heights of these peaks, when compared to appropriate elemental standards, can be used to calculate the elemental composition of the region being excited by the electron beam.

Two systems were used in this study: a LEO 1450VP SEM, operated at 10–20 keV with an acceleration voltage of 17–20 pA, coupled with a Princeton Gamma Tech (IMIX-PTS) EDS system, at NOCS; and a JEOL JSM-6360LV SEM, operated at 15 keV with an 18 pA acceleration voltage, coupled with an Oxford Instruments Ltd INCA-300 EDS, at the Institute of Earth Sciences, Academia Sinica, Taipei, Taiwan.

3.4.2 Identification of magnetic iron sulphide minerals

The EDS system is particularly effective for examining the microstructure and growth patterns of authigenic iron sulphides, which have a high atomic mass and are therefore easily identified from their high electron backscatter. Different iron sulphide minerals have distinctive iron to sulphur ratios (Fe/S = 0.5 for pyrite (FeS_2), = 0.75 for greigite (Fe_3S_4), and = 0.88 for monoclinic pyrrhotite (Fe_7S_8)), which can be measured using the EDS system with a pyrite calibration standard. Numerous studies have demonstrated that, with careful analysis, these different sedimentary iron sulphides can be clearly distinguished (e.g. Jiang et al., 2001; Weaver et al., 2002; Roberts and Weaver, 2005; Sagnotti et al., 2005).

Observations in this study focussed on iron sulphide aggregates, with an av-

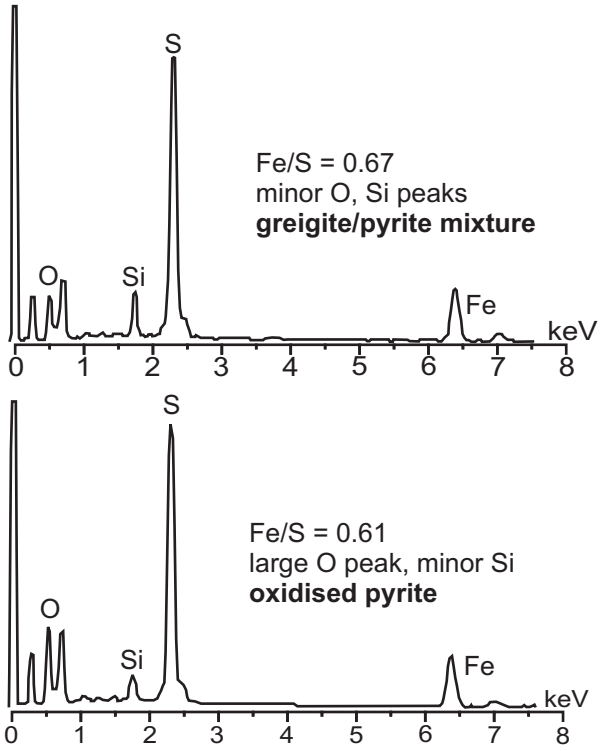

Figure 3.12: Example of energy dispersive X-ray spectra for regions of an iron sulphide aggregate within a silica matrix. Fe/S ratios intermediate between greigite and pyrite have resulted from: (a) a greigite/pyrite mixture, and (b) oxidised pyrite (indicated by the large O peak in the absence of an accompanying major Si peak).

erage grain size that was often small with respect to the diameter of the electron beam ($\sim$1 μm). In such cases, observed elemental ratios reflect an average of several grains and the matrix between them. This makes the interpretation of Fe/S ratios more difficult, because intermediate ratios ($0.5 < \mathrm{Fe/S} < 0.75$) are often observed. These values could indicate a mixture of greigite and pyrite grains within the area stimulated by the electron beam; however, oxidation of pyrite grains also leads to $\mathrm{Fe/S} > 0.5$. Inferring the composition of the matrix minerals, by comparitive analyses at the edge and centre of the sulphide aggregates, was often useful in distinguishing between these two possibilities, which required careful analysis. For example, Figure. 3.12 shows two EDS analyses of sulphide grains within a silicate matrix (indicated by the Si peak). In Figure 3.12a, the oxygen peak is relatively small, and is therefore likely to be mainly bound into silicate, with the intermediate Fe/S ratio resulting from a mixture of greigite and pyrite. In contrast, Figure 3.12b has a larger oxygen peak, some of which is likely to be in the form of iron oxides because the Si peak remains small. The intermediate ratio is therefore probably due to the presence of oxidised pyrite.

Chapter 4

Relocation of the tectonic boundary between the Raukumara and Wairoa domains (East Coast, North Island, New Zealand): Implications for the rotation history of the Hikurangi margin

This chapter appeared in *New Zealand Journal of Geology and Geophysics*, Volume 48, Rowan, C. J. A. P. Roberts, and G. J. Rait, Relocation of the tectonic boundary between the Raukumara and Wairoa domains (East Coast, North Island, New Zealand): Implications for the rotation history of the Hikurangi margin, pages 185-196.

Abstract Paleomagnetic studies of Neogene marine sediments have documented large clockwise rotations of the Hikurangi margin (East Coast, North Island) during the Neogene, with the exception of the Raukumara Peninsula, which is unrotated with respect to the Australian plate. Immediately south of the Raukumara Peninsula, the Wairoa region has been rotated clockwise by 50–60°; the boundary between these domains is associated with a change in regional structural trends. However, a declination of 70 ± 14° reported from Otaian (19–22 Ma) sediments in the Rakauroa area is located to the north of this change. Characterisation of how differential rotations have been accommodated along the Hikurangi margin has been frustrated by this apparent mismatch between paleomagnetic and structural data. Paleomagnetic analysis of two new Rakauroa localities has yielded declinations of 16 ± 5° and 19 ± 7°, consistent with expected values for the Australian plate. This region is therefore not part of the Wairoa domain. A strong viscous magnetic overprint was observed in many samples, the incomplete removal of which resulted in the misidentification of a large declination anomaly in the previous study. The paleomagnetically defined boundary between the Raukumara and Wairoa domains now coincides with the area where regional structural trends alter. Reassignment of the Rakauroa area to the Raukumara domain also results in a revised rotation history for the Wairoa domain, suggesting rotation rates of 4–6°/Myr since the Late Miocene (5–10 Ma), and potentially no earlier rotation. No reliable record of Early and Middle Miocene vertical-axis rotation on the Hikurangi margin now exists north of Marlborough; further studies are required to properly constrain the rotation history for this time interval.

4.1 Introduction

At the Hikurangi margin on the east coast of the North Island of New Zealand, westward-directed subduction of the Pacific plate occurs at a rate of ∼40 mm/yr (DeMets et al., 1994) (Fig. 4.1a). Subduction of the anomalously thick (12-15 km) oceanic crust of the Hikurangi Plateau (Davy and Wood, 1994) has led to the subaerial exposure of forearc basins throughout eastern New Zealand. Paleomagnetic studies of tectonically uplifted Neogene marine sediments along the entire Hikurangi margin (Walcott et al., 1981; Walcott and Mumme, 1982; Mumme and Walcott, 1985; Wright and Walcott, 1986; Mumme et al., 1989; Roberts, 1992, 1995a; Vickery and Lamb, 1995; Thornley, 1996; Little and Roberts, 1997) have documented clockwise vertical-axis rotations of up to 90° at a number of sites. These data support plate tectonic reconstructions of the New Zealand region, which suggest substantial clockwise rotations of the Pacific-Australian plate boundary as a whole since its propagation into the New Zealand region at 23–20 Ma (Rait et al.,

1991; King, 2000). The couple resulting from roll-back of the subducted Pacific plate in the north and 'pinning' of the boundary due to underthrusting of buoyant continental crust (the Chatham Rise) in the south has led to a change in the orientation of the subducted plate (Walcott, 1989). However, paleomagnetic data from the Raukumara Peninsula, the northernmost onshore part of the margin, show no rotation with respect to the Australian plate since the Early Miocene (Walcott and Mumme, 1982; Mumme et al., 1989; Thornley, 1996). This, combined with evidence of different rates of rotation in areas farther to the south, has resulted in the hypothesis that the margin is divided into discrete domains with independent tectonic histories (Lamb, 1988; Walcott, 1989). This interpretation requires crustal-scale basement structures that accommodate differential rotations between adjacent domains. The paleomagnetic data suggest that the boundary between the unrotated 'Raukumara domain' and the northernmost rotated block (the 'Wairoa domain') is located at about the latitude of Gisborne (38.5°S; Fig. 4.1b), an inference consistent with regional structural patterns.

The initiation of subduction in the early Miocene coincided with the southwestward obduction of a late Early Cretaceous–Paleogene passive margin sequence onto the Raukumara Peninsula (Stoneley, 1968; Rait et al., 1991), forming the East Coast Allochthon (ECA), and onto Northland (Ballance and Spörli, 1979; Spörli, 1982; Rait, 2000), forming the Northland Allochthon. At that stage, the margin was therefore oriented NW-SE, a determination supported by the parallel NW–SE trend of the Early Miocene Northland volcanic arc (Herzer, 1995). On the Raukumara Peninsula, the faults and folds associated with the emplacement of the ECA still have this trend, which implies that substantial vertical-axis rotations have not occurred in this region during the Neogene, consistent with the aforementioned paleomagnetic studies. In contrast, the rotated 'Wairoa domain' to the southwest of Gisborne is dominated by structures that have the SW–NE orientation of the present day margin.

The structural change between the Raukumara and Wairoa domains coincides with major changes in both the topography of the subduction margin (Collot et al., 1996) and the crustal structure of the overlying plate (Reyners et al., 1999); however, basement structures that have accommodated large differential rotations have proved difficult to identify. Attempts to use paleomagnetic methods to further constrain the location of the rotation boundary in the critical region between Gisborne and Opotiki have been frustrated by the paucity of stably magnetized rocks (Mumme et al., 1989; Thornley, 1996). However, Mumme and Walcott (1985) reported a mean declination of 70 ± 14° from Early Miocene (Otaian; Colin Mazengarb, IGNS, Lower Hutt, pers. comm., 2002) rocks in the Rakauroa

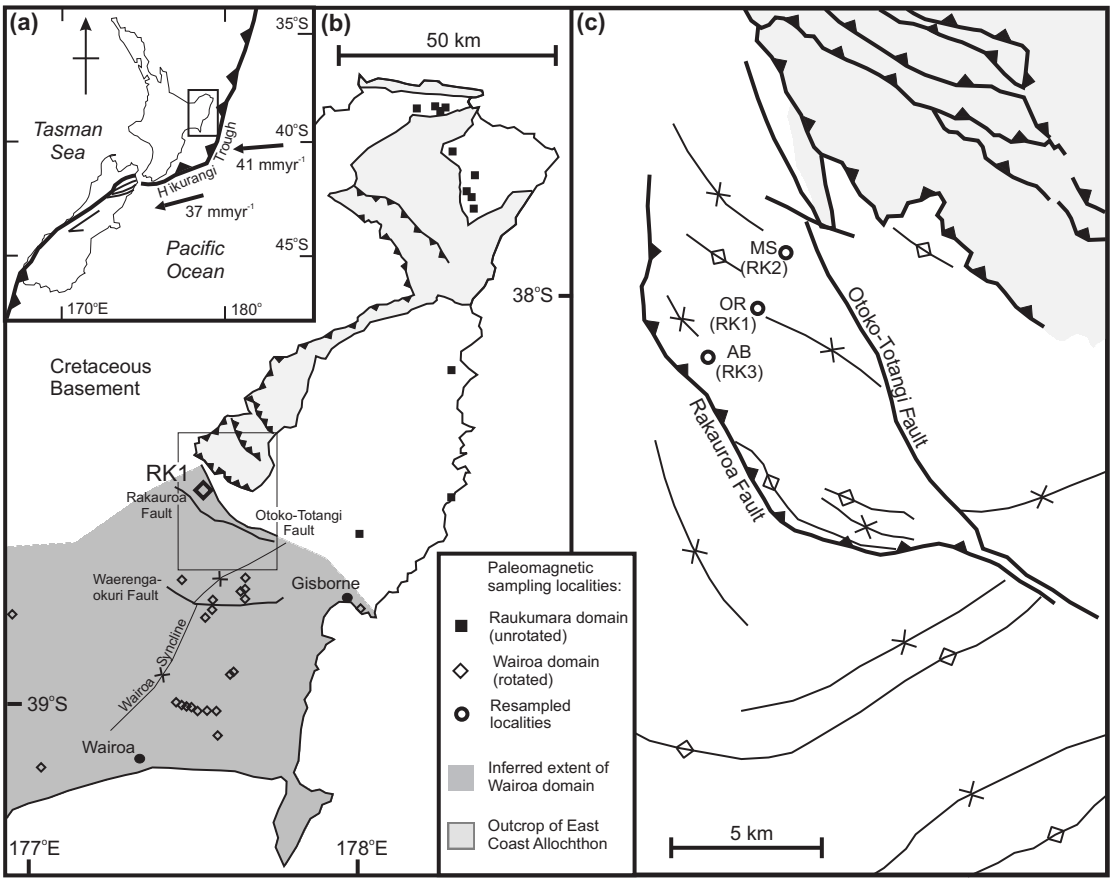

Figure 4.1: (a) Tectonic setting of the New Zealand region, showing the boundary between the Pacific and Australian plates. Local plate motion vectors are from DeMets et al. (1994). (b) Detail of northeastern North Island, including the locations of sites from which paleomagnetic data have been reported. The boundaries of the Wairoa domain are inferred from sites where large declination anomalies have been measured. The RK1 locality of Mumme and Walcott (1985) (large diamond) is the northernmost of these. (c) Tectonic map of the study area, showing the principal structures and the location of the localities sampled by Mumme and Walcott (1985), that were resampled in this study. Adapted from Mazengarb and Speden (2000).

area (referred to in later literature as the 'RK1' locality; Fig. 4.1b). The implied clockwise rotation of ∼50° relative to the Australian plate makes this the northernmost locality reported to belong to the rotated Wairoa domain, and provides an important constraint on the location of any structural boundary. Its age confers additional significance: most rotated sites on the east coast of the North Island are dated as Middle–Late Miocene, making RK1 a primary support for the hypothesis that the rate of rotation of the Hikurangi margin with respect to the Australian plate has steadily increased over time, from 2–3°/Myr in the early Miocene to 7–8°/Myr from the Pliocene onward (Wright and Walcott, 1986; Walcott, 1989).

The large clockwise rotations reported from Rakauroa become somewhat problematic when the regional geology is considered. The RK1 declination anomaly is based on data compiled from three sampling localities, distributed across a syncline located just to the south of the frontal thrust of the ECA (RK1–3, Fig. 4.1c). This fold has a NW–SE trend, as do other nearby folds (Mazengarb and Speden, 2000), and is clearly associated with emplacement of the allochthon. Thus, from a geological perspective, one would expect this area to be unrotated with respect to the Australian plate.

Good paleomagnetic data are needed from the Rakauroa area to properly constrain the Neogene tectonic evolution of the Hikurangi margin. We present the results from new sampling, undertaken as close as possible to the original three localities described by Mumme and Walcott (1985), in an effort to reconcile the paleomagnetic data with the regional geology. The data published by Mumme and Walcott (1985) are also reassessed in the light of more recent insights into the magnetization of New Zealand Cenozoic sediments.

4.2 Geological background

The area investigated in this study is bounded by the Otoko-Totangi and Rakauroa Faults, to the north and south, respectively (Fig. 4.1c). Thickness variations in Early Cretaceous and Paleogene sediments revealed by seismic data (Field et al., 1997) demonstrate that both faults predate the current tectonic regime. The Otaian units sampled were deposited in a flexural basin associated with obduction of the ECA, and were folded soon after deposition; Altonian strata were unconformably deposited on the anticline directly northwest of the Rakauroa Fault. The trend of the folds suggests southwestward-directed shortening, supporting the inference that they formed contemporaneously with emplacement of the allochthon.

The folds have subsequently been disrupted by probable post-Early Miocene dextral strike-slip on the reactivated Otoko-Totangi Fault, but the overall structural grain is still oriented NW-SE, which precludes any significant vertical-axis

rotations in the Neogene. Evidence for any recent tectonism is equivocal, although observations of tilted Pleistocene beds along strike from the Otoko-Totangi Fault are reported by Field et al. (1997).

4.3 Sampling and methods

Paleomagnetic sampling was carried out by drilling 25 mm diameter cores from three localities with good exposure and clear, measurable bedding structures, as close as possible to the original RK sites studied by Mumme and Walcott (1985).

OR - Oliver Road (NZMS 260 grid reference: X17/118988) A roadcut/ verge outcrop of moderately weathered, shallowly dipping grey and brown sandy mudstones and siltstones was sampled, on the highest point on Oliver Road before it descends to Matawai Station. This is a direct resampling of the RK1 locality described by Mumme and Walcott (1985). Seventy cores were collected across a total stratigraphic thickness of 27.1 m.

MS - Matawai Station (Grid reference: X17/128009) A fairly continuous exposure of light blue-grey calcareous mudstones with massive sandstone interbeds was sampled in the bed of the Waikohu River, 100-200 m west and upstream of where it is bridged by Oliver Road north of Matawai Station. The RK2 locality described by Mumme and Walcott (1985) is just downstream from this bridge; it was not directly resampled due to a lack of clear bedding structures. A total stratigraphic thickness of 58.5 m was sampled (63 cores).

AB - Anzac Bridge (Grid reference: X17/096972) Outcrops of fractured, massive blue-grey mudstones with rare massive sandstone beds were sampled from the banks of the Waihuka River, where a tributary joins it 200 m east and downstream of where it is crossed by State Highway 2 (Anzac Bridge), 2-3 km southeast of the Oliver Road turn-off. The RK3 locality described by Mumme and Walcott (1985) was identified just downstream from the bridge, but was not resampled due to a lack of clearly identifiable bedding structures. It is possible that Mumme and Walcott (1985) measured joint surfaces rather than bedding, since their reported variable bedding measurements are not consistent with the clear regional structural trend. A total stratigraphic thickness of 52.6 m was sampled (41 cores).

Weathered surficial material was removed from each outcrop before sampling. Cores were stored and transported to the laboratory in a mu-metal shield and were cut into samples of 21 mm length. Stepwise demagnetization of the samples was undertaken using a 2G-Enterprises cryogenic magnetometer at the National

Oceanography Centre, Southampton (NOCS). The instrument is situated in a magnetically shielded room, which reduces the level of the ambient magnetic field to <300 nT, which is further reduced to ∼1–2 nT in the measurement region of the magnetometer. This enables measurement of the magnetic moment with a sensitivity of better than 10^{-12} Am^2.

Thermal demagnetization has frequently proven to be more effective than alternating field (AF) demagnetization at isolating primary remanence directions in weakly magnetized New Zealand Cenozoic sediments (Pillans et al., 1994; Turner, 2001). A pilot study involving detailed stepwise AF (5 mT steps to 60 mT) and thermal (steps of 20°, 80°, 120°, 160°, 200°, 240°, 280°, 320°, 360°, 380° and 400°C) demagnetizations of individual samples from each stratigraphic level confirmed that thermal methods yielded more stable demagnetization paths; all subsequent samples were therefore thermally treated. Low-field bulk magnetic susceptibility was measured after each heating step to monitor for thermal alteration effects. Vector-component diagrams were used to identify samples where characteristic remanent magnetization (ChRM) directions could be isolated and analysed using principal component analysis (Kirschvink, 1980). Fisher (1953) statistics were used to calculate mean paleomagnetic directions; declination errors were calculated according to Demarest (1983). The stepwise demagnetization data for many samples follow great circle paths, which can be combined with ChRM directions using the method of McFadden and McElhinny (1988). Great circle analysis has been utilised for magnetostratigraphic studies of New Zealand Cenozoic mudstones (Pillans et al., 1994; Roberts et al., 1994), but not for tectonic studies, where a precise direction, rather than simply a polarity determination, is required. However, this technique is certainly adequate to fulfil the minimum requirement of this study: that is, to distinguish between substantial clockwise rotations (a declination of 70°) and no net rotation with respect to the Australian plate (a declination of 20°).

4.4 Results

4.4.1 Stepwise demagnetization

The NRM intensities of all samples from the three study sites are weak, ranging from 1×10^{-4} to 8×10^{-3} Am^{-1}. In a large proportion of the samples, the low temperature remanence component has an orientation close to that of the present-day field in geographic coordinates (Declination (D) = 20.5°, Inclination (I) = -63.7°) and is therefore interpreted as a viscous overprint. This component unblocked at temperatures of 200–240°C. No meaningful data were collected above temperatures of 360–380°C, due either to the magnetic intensity falling below the noise

level of the magnetometer, or to thermal alteration (indicated by large increases in low-field bulk magnetic susceptibility) producing new magnetic minerals that obscured the primary paleomagnetic signal. There was therefore only a small range over which ancient higher temperature components could potentially be observed. Samples from Anzac Bridge do not exhibit systematic behaviour within this range, which indicates that any primary magnetization has been completely obscured by overprinting (NRMs from this locality are particularly strongly clustered around the present-day field direction); data from this locality are therefore excluded from further analysis.

In 21% of the samples from Matawai Station, a stable component (defined by three or more collinear points, with maximum angular deviation (MAD) values of $<15°$) with reversed polarity is observed at temperatures of 200–380°C (Figs. 4.2a, 4.3a). A component with a similar trend can also be isolated from 11% of the Oliver Road samples, but in most cases only where there is no obvious viscous overprint (Figs. 4.2b, 4.3b). This component can generally be anchored to the origin of the vector-component plot (Fig. 4.2), but in some samples it misses the origin (Fig. 4.3), which may indicate the presence of a further component with unblocking temperatures >400°C. Samples exhibiting both types of behaviour can be identified from the same stratigraphic level at both localities.

In a further 50% of the samples, the blocking temperature (T_b) spectra of the viscous and intermediate components overlap to the extent that the latter cannot be isolated. Nevertheless, there is a consistent trend toward a reversed polarity direction along a great circle demagnetization path (Fig. 4.4). Despite the possible presence of a higher T_b component in some samples, the reversed polarity, intermediate T_b component is interpreted here as a primary ChRM. Its presence is discernible in all samples with stable demagnetization behaviour; the combined data from the two sites also pass a fold test (Fig. 4.5), implying that the magnetization predates the Early Miocene tilting of the sampled units. The magnetic behaviour of these samples is therefore comparable to that of Pliocene sediments from the Wanganui Basin described by Turner (2001), where an intermediate T_b (150–250°C) component was found to carry the primary remanence. A higher T_b (>250°C) component, carried by a distinct higher coercivity population of magnetic grains, was considered to be diagenetic in origin, probably related to weathering.

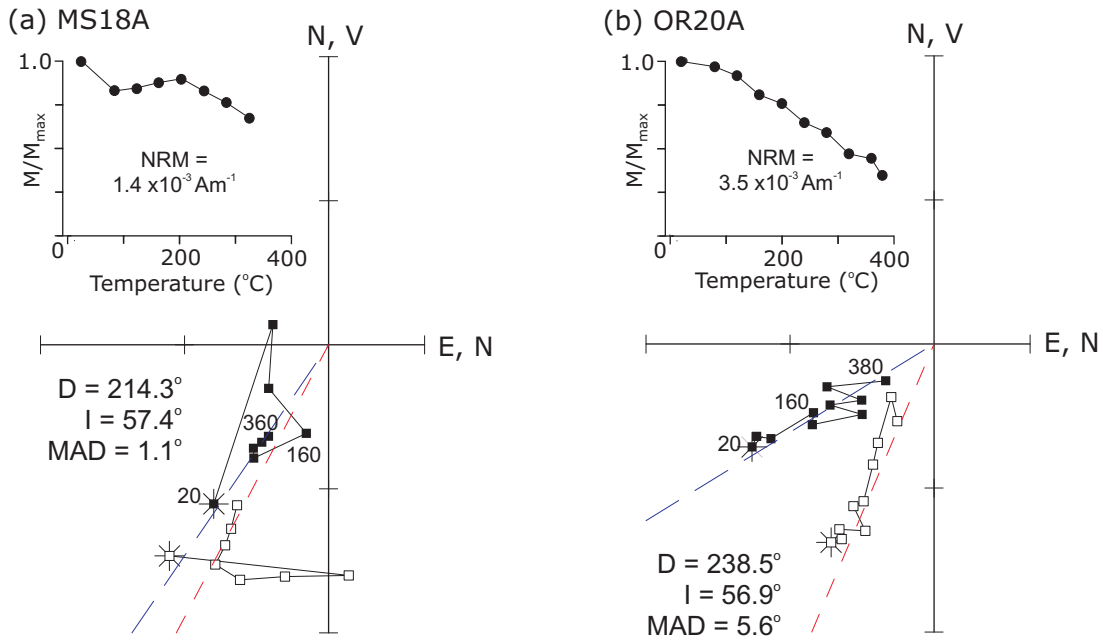

Figure 4.2: Vector-component plots of thermal demagnetization data showing anchored best-fit ChRM determination (blue = declination, red = inclination), from: (a) Matawai Station, following removal of a secondary overprint that unblocks at 200°C, and (b) Oliver Road, where no overprint is observed. Labelled points indicate the demagnetization step in °C. Solid symbols denote projections onto the horizontal plane (declinations); open symbols denote projections onto the vertical plane (inclinations).

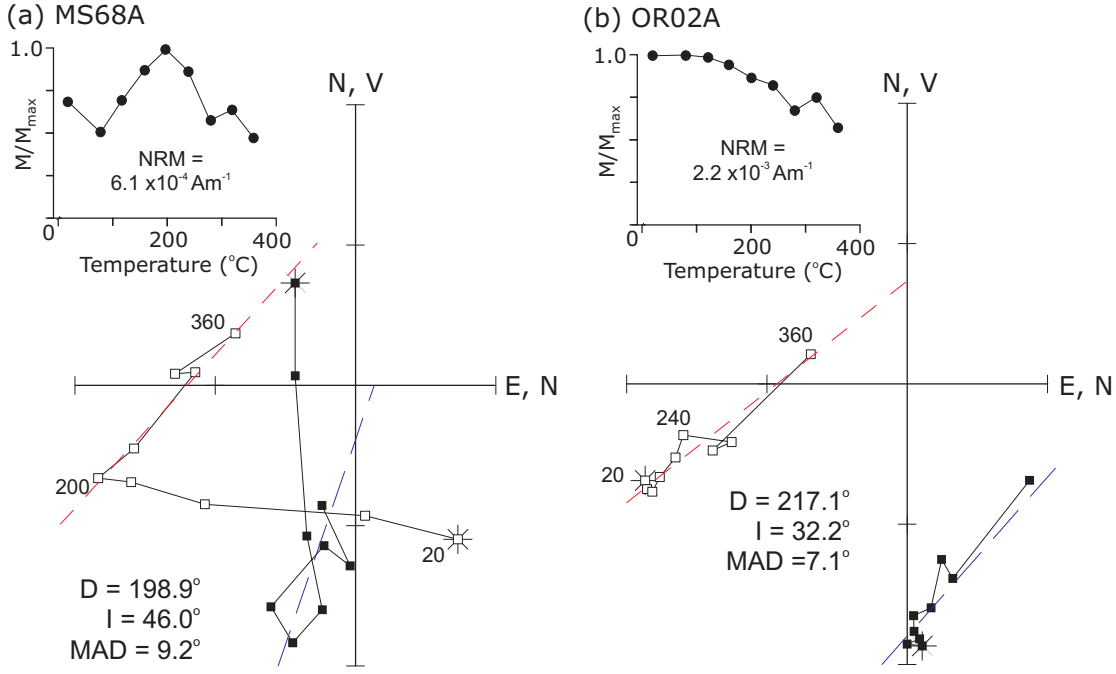

Figure 4.3: Vector-component plots of thermal demagnetization data from: (a) Matawai Station, and (b) Oliver Road, that exhibit an unanchored ChRM fit due to the presence of a higher T_b diagenetic component, that is interpreted to result from weathering. The trends of these intermediate components are similar to those of samples without higher T_b components (Fig. 4.2). Symbols are as in Figure 4.2

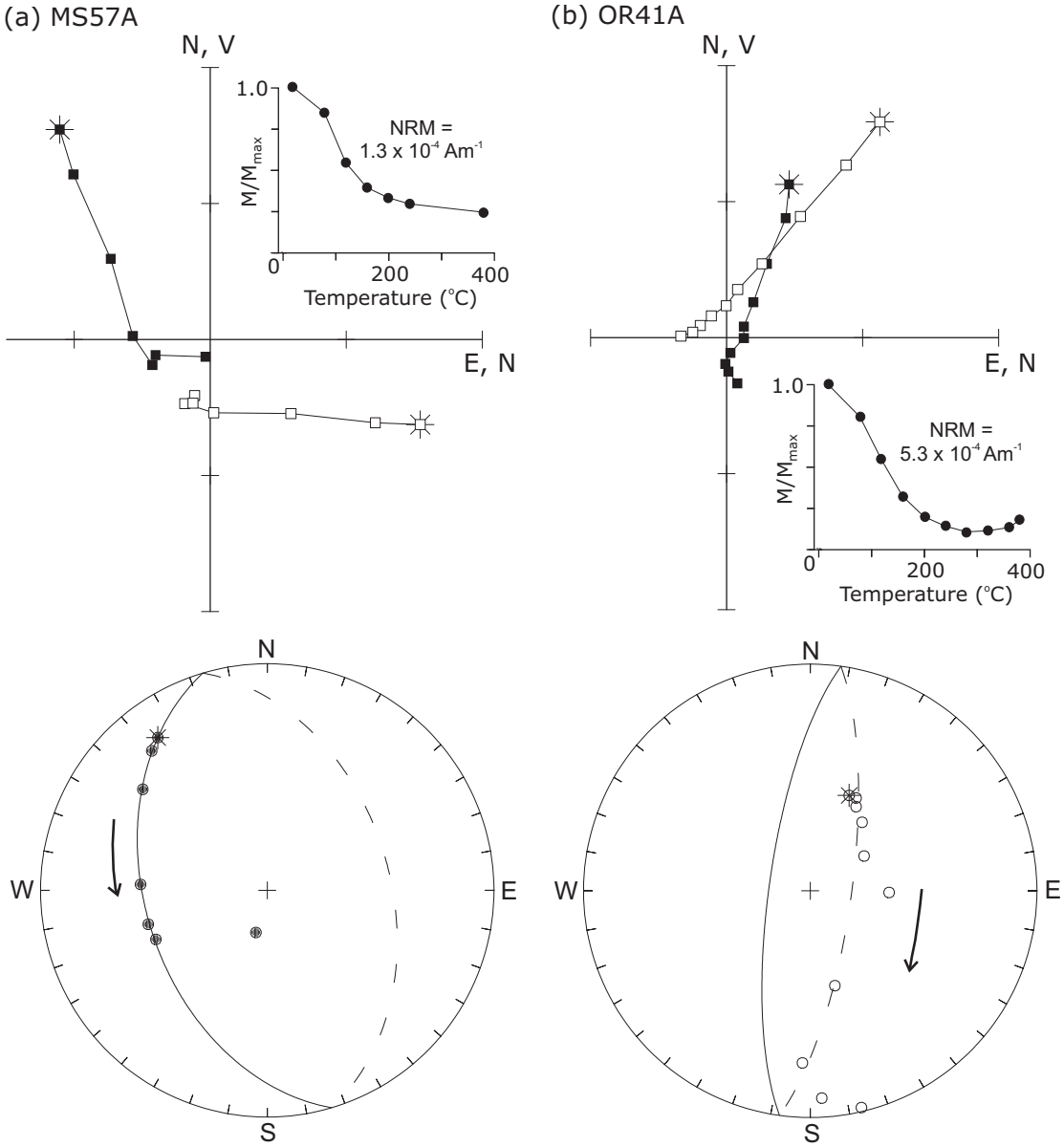

Figure 4.4: Vector-component and equal area stereographic plots of thermal demagnetization data from: (a) Matawai Station, and (b) Oliver Road, demonstrating removal of secondary overprints along a great circle path. Symbols for vector-component plots are as in Figure 4.2. Solid (open) circles on the stereoplots represent projections onto the lower (upper) hemisphere.

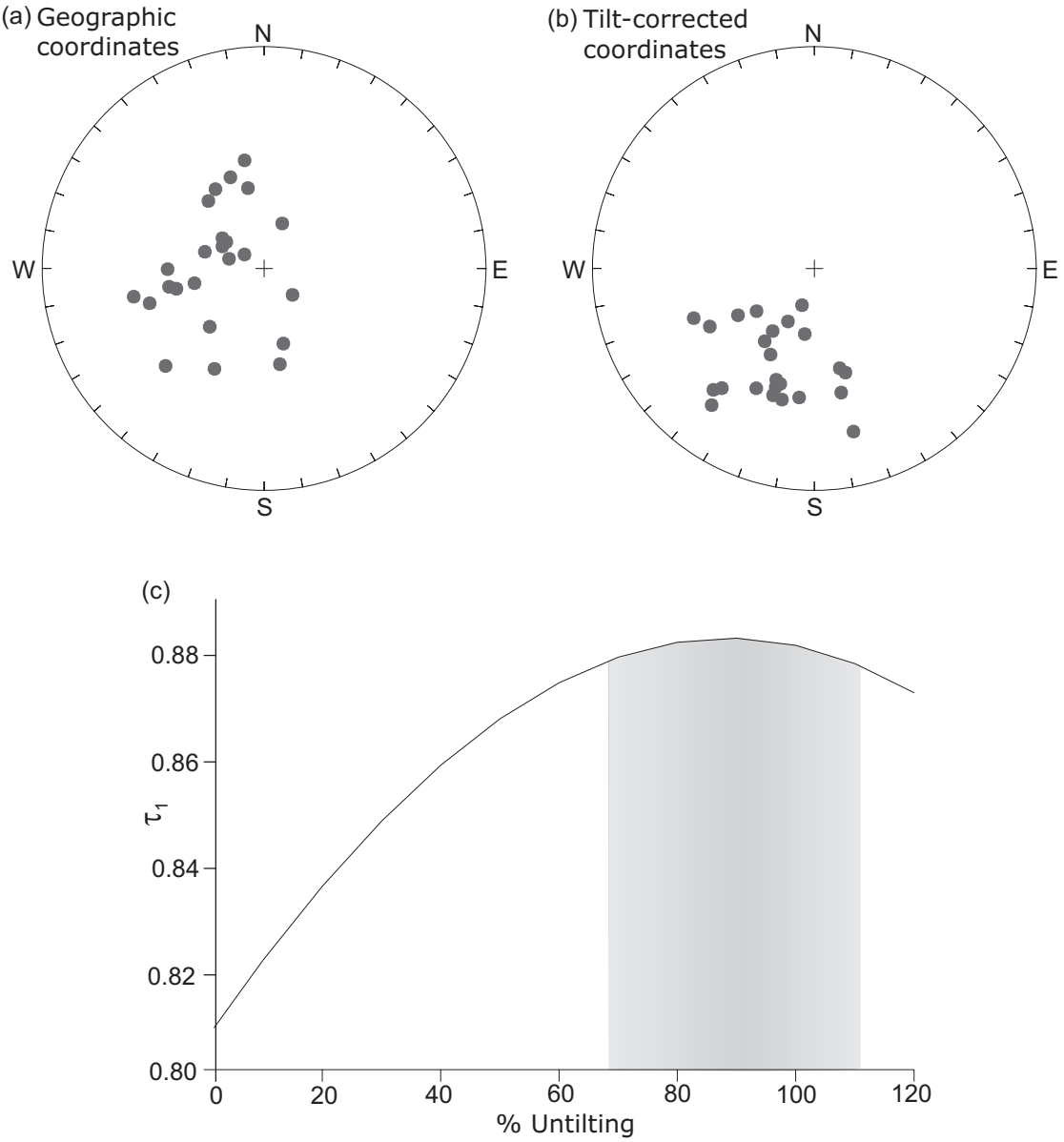

Figure 4.5: Combined ChRM data for both Matawai Station and Oliver Road, in: (a) geographic, and (b) tilt-corrected, coordinates. (c) Fold test of Tauxe and Watson (1994). The 95% confidence interval of the maximum value of the principal eigenvector τ_1 (shaded) encompasses 100% unfolding, consistent with remanence acquisition prior to tilting of the beds.

4.4.2 Paleomagnetic directions

Combination of the isolated ChRM directions from each site, after correction for bedding tilt, yielded a mean direction of D = 197.8°, I = 48.8°, α_{95} = 9.4° for Matawai Station (Fig. 4.6a), and D = 212.4°, I = 51.1°, α_{95} = 14.9° for Oliver Road (Fig. 4.6b). These directions are indistinguishable at the 95% confidence level (Fig. 4.7a); however, the small number of samples may not adequately average out secular variation and random measurement errors (Van der Voo, 1993).

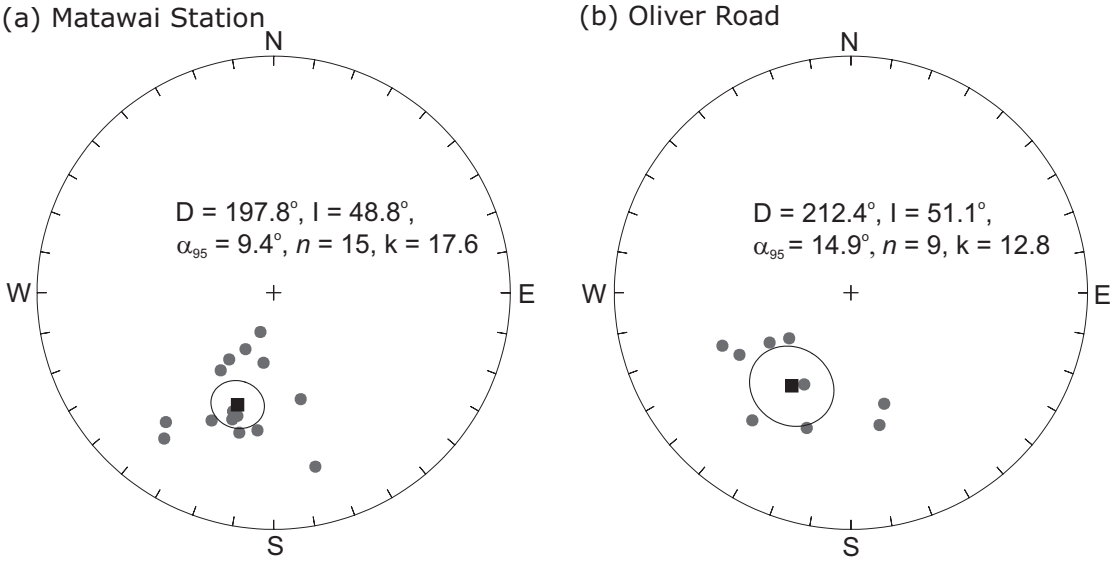

Figure 4.6: Equal area stereographic plot of ChRM directions (solid circles) obtained for: (a) Matawai Station, and (a) Oliver Road, with calculated mean directions (solid squares) and α_{95} confidence ellipses.

To further constrain the mean direction, the stable endpoints were combined with great circle arcs, according to the method of McFadden and McElhinny (1988). Although the T_b spectrum of the high temperature component does not overlap with the ChRM below 400°C (Fig. 4.3), the demagnetization paths of samples in which this third component is present will not directly converge on the ChRM directions (because they do not decay to the origin, unanchored ChRMs will plot away from their own demagnetization paths on a stereographic projection). Therefore, only great circles from sites where the ChRM could be consistently anchored to the origin, which were defined by four or more points and which had MAD values <15°, were included in the analysis. Addition of the great circle data gave a mean direction of D = 198.9°, I = 43.3°, α_{95} = 8.1° for Matawai Station, and D = 195.5°, I = 47.5°, α_{95} = 5.8° for Oliver Road. The resulting mean directions from the two sites are better constrained individually, and are still indistinguishable at the 95% confidence level (Fig. 4.7b).

As discussed above, great circle analysis has not been commonly used in tectonic studies of New Zealand Cenozoic sediments. However, use of the great circle

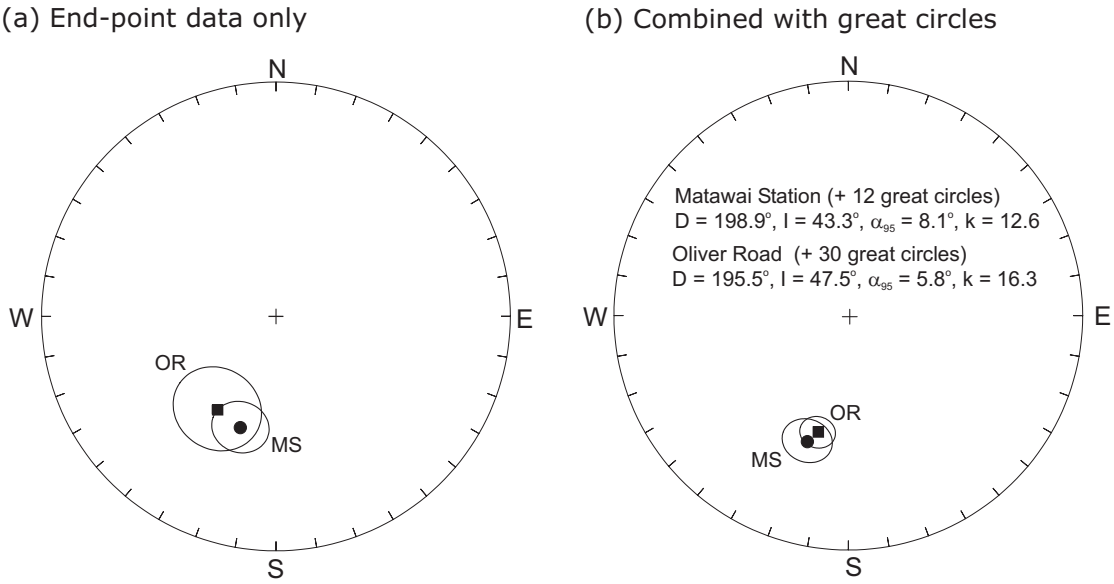

Figure 4.7: Comparison of palaeomagnetic directions determined for Matawai Station and Oliver Road using: (a) ChRM data alone, and (b) ChRM data combined with demagnetization great circles using the method of McFadden and McElhinny (1988).

data in the present study does not result in directions that lie outside the 95% confidence limits of the means calculated from stable endpoint data alone; in the case of Matawai Station, there is no appreciable change in the directions derived from the combined and endpoint-only datasets (Fig. 4.7). This confers confidence in the reliability of the results presented here.

4.5 Discussion

The Oliver Road and Matawai Station localities record declinations that are deflected clockwise with respect to the expected axial dipole field direction by $16 \pm 5°$ and $19 \pm 7°$, respectively. According to the apparent polar wander path of Idnurm (1985), Neogene motions of the Australian plate have led to clockwise rotations of $\sim 1°$/Myr. Thus the Otaian (19–22 Ma) declination anomalies reported here do not require the Rakauroa area to have undergone any vertical axis rotations, being fully explained by large-scale plate motions (Fig. 4.8). The new data also compare well with declinations reported from farther north on the Raukumara Peninsula (Walcott and Mumme, 1982; Mumme et al., 1989). Both localities record inclinations of $\sim 50°$, which is less than the 60° inclination expected for Otaian rocks; however, shallow inclinations are quite common in the East Coast region, and possibly result from the effects of sediment compaction (Mumme et al., 1989).

Our new data indicate that the Rakauroa area should be regarded as part of the unrotated Raukumara domain, in agreement with the regional structural trends discussed above. However, they conflict with the large rotations reported from the

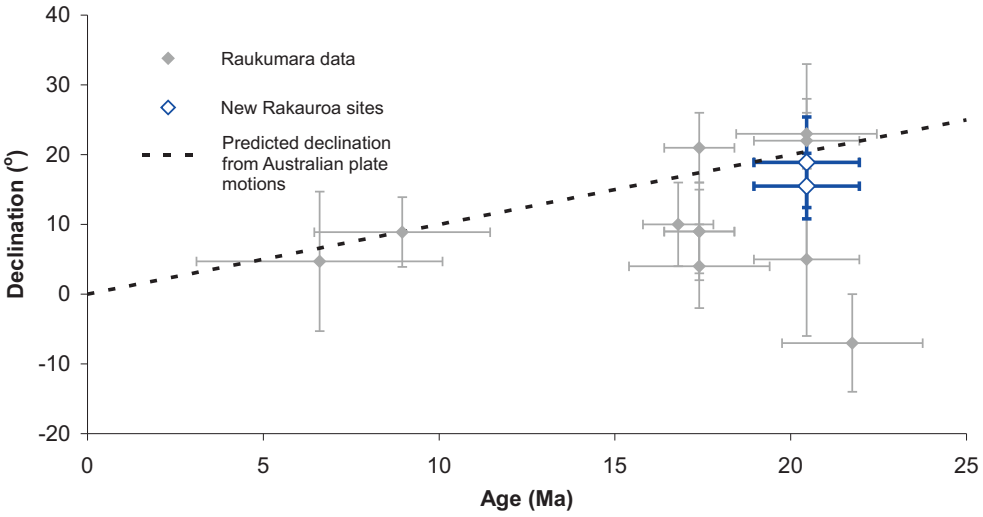

Figure 4.8: Declinations for the new Rakauroa data (open symbols), plotted with previously reported data from the Raukumara domain (closed symbols) (Walcott and Mumme, 1982; Mumme et al., 1989). Declination errors were calculated according to Demarest (1983).

same sites by Mumme and Walcott (1985). Data published in their appendix show that 50% of samples were AF demagnetized at only 10–20 mT, the level at which stable behaviour had been observed in pilot samples demagnetized to 30 mT. This blanket demagnetization approach is no longer considered adequate (Opdyke and Channell, 1996), especially in the presence of the strong magnetic overprints common in New Zealand Cenozoic mudstones; several studies have demonstrated that detailed stepwise thermal demagnetization of all samples is required to properly isolate primary components in such rocks (Turner et al., 1989; Turner and Kamp, 1990; Roberts, 1992; Pillans et al., 1994; Roberts et al., 1994; Roberts, 1995a; Turner, 2001).

The limited AF demagnetization data obtained in this study indicate that the viscous overprint observed in the Rakauroa localities has a high coercivity, typically >20 mT (Fig. 4.9a), which would have been incompletely removed in the fields used by Mumme and Walcott (1985). Vector-component plots indicate that many of their samples, particularly those that were demagnetized at lower peak fields, have yet to demonstrably converge onto a stable endpoint (Fig. 4.9b), and thus may not accurately represent the ChRM. The overprint appears to be weakest at the RK2 locality, where a normal polarity ChRM could be isolated in six samples (Fig. 4.10), giving a mean direction of D = 21.4°, I = -64.9°, $\alpha_{95} = 15.2°$. Whilst there are too few samples for this to be a statistically rigorous result, it is antipodal to the reversed polarity direction from the nearby Matawai

Station locality. It therefore appears that the large declination anomaly reported by Mumme and Walcott (1985) from the Rakauroa localities is due to the inclusion of data from incompletely demagnetized samples.

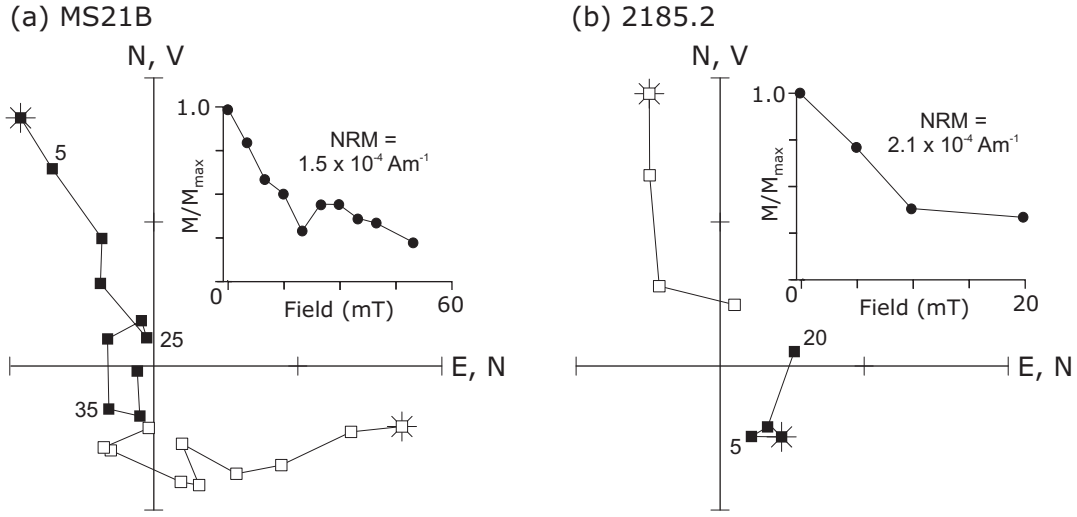

Figure 4.9: Vector-component plots of: (a) AF demagnetization data from Matawai Station. A viscous overprint is removed above 35 mT. (b) AF demagnetization data reported by Mumme and Walcott (1985). At the maximum demagnetization step of 20 mT, a stable endpoint has yet to be reached. Labelled points indicate the demagnetization step in mT; other symbols are as in Figure 4.2.

Demonstrating that the Rakauroa area is unrotated with respect to the Australian plate removes a major obstacle to the reconciliation of existing paleomagnetic data with regional geology. Both are now consistent with the boundary between the Wairoa and Raukumara domains being associated with a 20 km wide zone between the Rakauroa and Waerengaokuri Faults (Fig. 4.11). Structures that have accommodated the differential rotations between these two domains are still not immediately obvious within this corridor. However, now that a clear structural difference has been demonstrated between unrotated and rotated parts of the margin, further structural work should enable the filling in of gaps left by paleomagnetic measurements.

Reassignment of the Rakauroa locality to the Raukumara domain also has a bearing on the assumed rotation history of the Wairoa domain. Previously reported paleomagnetic data (Fig. 4.12a) indicate clockwise rotations of 40–60° with respect to the Australian plate since 10 Ma. The data for the Early and Middle Miocene are less coherent; the line of best fit used by Wright and Walcott (1986) and Walcott (1989) is significantly constrained by the RK1 declination anomaly reported by Mumme and Walcott (1985), which requires further clockwise rotation, albeit at a reduced rate, during the Early and Middle Miocene. With the removal of the RK1 constraint, this interpretation needs to be reassessed.

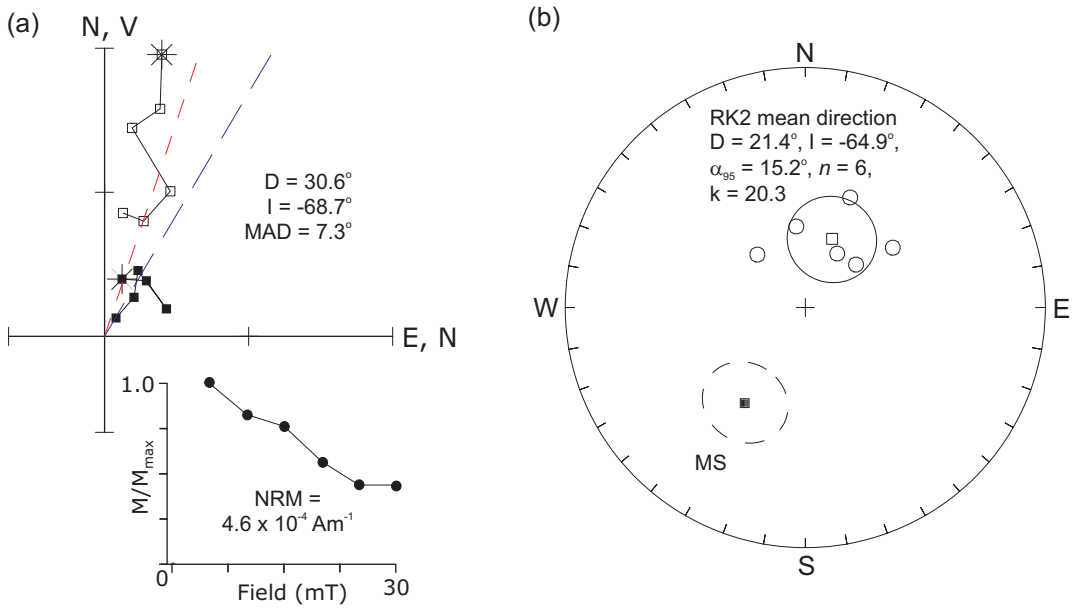

Figure 4.10: (a) Vector-component plot of data from the RK2 locality of Mumme and Walcott (1985), showing a normal polarity ChRM direction. (b) Equal area stereographic plot of ChRM directions (open circles) and mean direction (open square) for RK2. The mean direction is antipodal to the mean direction for Matawai Station (closed square). Ellipses indicate α_{95} confidence intervals.

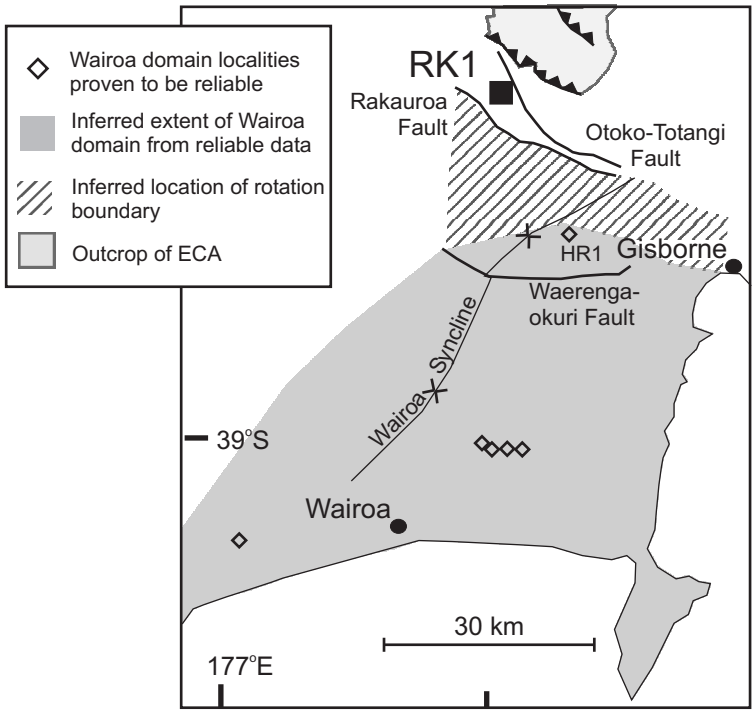

Figure 4.11: New paleomagnetic constraints on the rotation boundary between the Raukumara and Wairoa domains. Reassignment of the RK1 locality to the Raukumara domain, and the removal of potentially unreliable data (see discussion and Table 1 for details), has shifted the inferred boundary south, to a zone between the Rakauroa and Waerengaokuri Faults

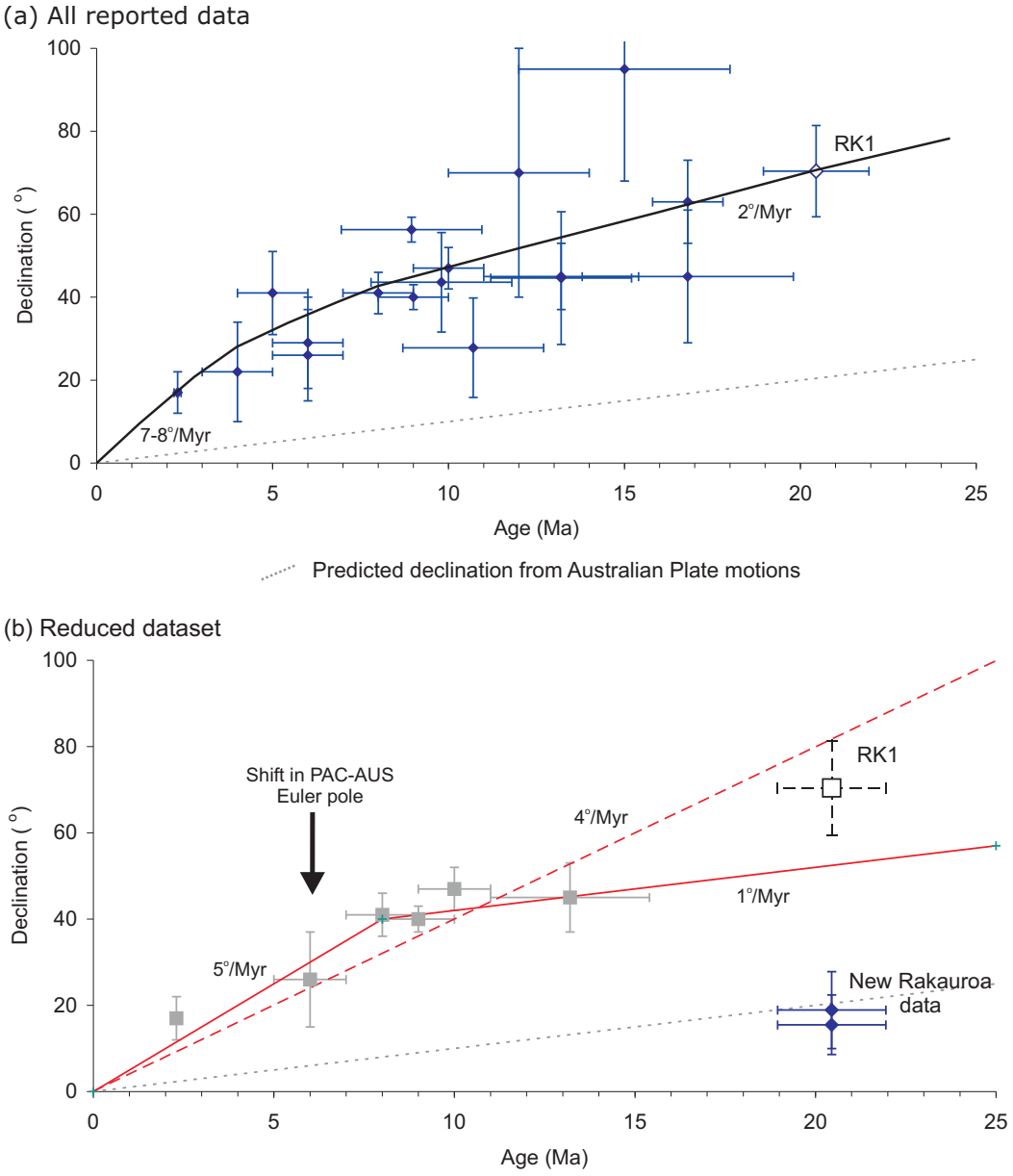

Figure 4.12: (a) Previously published paleomagnetic declinations for the Wairoa domain (Walcott et al., 1981; Walcott and Mumme, 1982; Mumme and Walcott, 1985; Wright and Walcott, 1986; Thornley, 1996) plotted versus age. Some sites have been re-dated by Mazengarb (pers. comm., 2002). The best-fit interpretation of Wright and Walcott (1986) and Walcott (1989) (solid line) is significantly constrained by the RK1 declination. (b) Same as (a), but including only localities with demonstrably reliable paleomagnetic data (see text for details). Exclusion of the RK1 declination anomaly (open square with dashed error bars) allows an interpretation requiring no rotation with respect to the Australian plate prior to 5-10 Ma (solid line).

Much of the published paleomagnetic data for the Wairoa domain predates widespread recognition of the need for detailed stepwise demagnetization to ensure the reliable isolation of primary remanence directions; samples were commonly only subjected to blanket AF or thermal demagnetizations at low fields or temperatures. We have shown that these techniques do not adequately isolate a ChRM in the presence of a strong secondary overprint. This raises the possibility that other published declination anomalies may be unreliable due to the incomplete removal of such overprints. In Fig. 4.12b, we exclude localities where these uncertainties exist (refer to Table 4.1 for details). It is unlikely that all of the excluded data are unreliable, because strong overprints are not ubiquitous: samples from the HR1 locality (Walcott and Mumme, 1982; resampled by Mumme and Walcott, 1985) are not appreciably overprinted, which allows reasonable confidence in the published declination anomaly - the position of this locality (Fig. 4.11) also means that reliable paleomagnetic data are still consistent with the boundary between the Raukumara and Wairoa domains being placed between the Rakauroa and Waerengaokuri faults. However, the limited availability of complete demagnetization data precludes detailed assessment of many localities. The majority of the data remaining are from Wright and Walcott (1986), who employed more rigorous stepwise thermal demagnetizations that allowed them to remove a strong viscous overprint. Antipodal normal and reversed polarity ChRM directions were also identified at each of their localities, which provide a robust reversals test.

Geodetic measurements show that the Hikurangi margin is currently rotating at a rate of 2–4°/Myr with respect to the Australian plate (Wallace et al., 2004). The velocity field derived from known Quaternary fault slip rates provides a minimum estimate of 3–4°/Myr (Beanland and Haines, 1998). The reduced paleomagnetic dataset (Fig. 4.12b) suggests that the Wairoa domain has rotated at rates of 4–5°/Myr with respect to the Pacific plate (3–4°/Myr with respect to the Australian plate) since the Late Miocene (5–10 Ma), which is within the range of geodynamic estimates. Sparse reliable data for the Middle and Early Miocene make any interpretation of the rotation history during this earlier time interval tentative; it is possible that rotations have occurred at a similar rate throughout the Neogene. However, a marginally better fit to the data requires no rotation of the margin with respect to the Australian plate before 10 Ma (Fig. 4.12b). Whilst this interpretation is constrained purely by data that are demonstrably reliable, with the exclusion of the erroneous RK1 declination anomaly, it is a reasonable fit for the whole data set (Fig. 4.12). Nevertheless, reliable paleomagnetic data from Early and Middle Miocene strata are needed to confirm any interpretation.

It is illuminating to compare this potential rotation history for the Wairoa

Table 4.1: Reported declinations from the Wairoa region of the Hikurangi margin.

Locality	Source	Age(Ma)	Declination(°)	Retained	Rationale
RK1	MW	20.5±1.5[1]	70±11	No	Blanket demagnetization, incompletely removing a strong overprint (see text)
HR1	**WM/MW**	**13.2±2.2**[1]	**45±8**	**Yes**	**Blanket demagnetization but data indicate negligible overprint**
WK1	WM	12±2	70±30	No	Blanket demagnetization; data unavailable
MK1	WM	17±1[1]	63±10	No	”
MK2	WM	17±3[1]	45±16	No	”
MK3	WM	15±3	95±27	No	”
MK4	WM	4±1	22±12	No	”
MK5	WM	5±1	41±10	No	”
MK6	WM	6±1	29±11	No	”
MK7	**WW**	**10±1**	**47±5**	**Yes**	**Stepwise demagnetization, reversals test**
MK8	**WW**	**9±1**	**40±3**	**Yes**	”
MK9	**WW**	**8±1**	**41±5**	**Yes**	”
MK10	**WW**	**6±1**	**26±11**	**Yes**	”
WH1	**WW**	**2.3±0.1**	**17±5**	**Yes**	”

Those data proven to be reliable and included on Fig. 4.12b are highlighted in bold. WM = Walcott and Mumme (1982); MW = Mumme and Walcott (1985); WW = Wright and Walcott (1986). [1]Site redated by Mazengarb (pers. comm. 2002). The unpublished data of Thornley (1996) are also considered to be unreliable, and have been excluded from Fig. 4.12b.

domain with data from the southern Hikurangi margin. Based on the data of Roberts (1992, 1995a), Little and Roberts (1997) described clockwise vertical axis rotations of 30–50° since the early Pliocene (∼4 Ma) in northeastern Marlborough, hinged about a northwest-trending kink in the structural trend of basement rocks. A second crustal scale boundary farther to the east appears to have accommodated another 50° of Early-Middle Miocene clockwise rotation (using data from Vickery and Lamb (1995)). The most recent of these two phases of rotation has a clear correlative in the revised rotation history of the Wairoa domain proposed here. In both cases, the beginning of large-scale rotations may have been associated with an abrupt shift in the position of the Pacific-Australian Euler rotation pole at 5–6.5 Ma (Cande et al., 1995; Sutherland, 1995; Walcott, 1998), which increased convergence across the plate boundary in the New Zealand region. This event coincided with a number of tectonic events, including a southward shift in the locus of strike-slip displacement on the Marlborough fault system (King, 2000) and a period of rapid uplift in the Wairoa region (Buret et al., 1997). In the Early and Middle Miocene, rotations with respect to the Australian plate may have been much more spatially restricted, possibly being absent in the Wairoa region, and confined to a much smaller area near the coast in northeast Marlborough. However, this interpretation remains speculative until additional early Neogene paleomagnetic data are obtained from the Wairoa region. The rotation history of the intervening Wairarapa region is also currently unconstrained.

4.6 Conclusions

Early Miocene rocks from the Rakauroa area have not been rotated with respect to the Australian plate during the Neogene, and are therefore part of the Raukumara domain, in agreement with observed structural trends. The large declination anomaly previously reported from this area resulted from the use of low-field, blanket AF demagnetization that failed to remove a strong secondary overprint. Our reconciliation of paleomagnetic data with regional geology will aid attempts to locate and characterise the nature of the tectonic boundary between the unrotated Raukumara and rotated Wairoa domains.

Reassignment of the Rakauroa locality to the Raukumara domain also requires a reappraisal of the rotation history of the Wairoa domain. A reduced paleomagnetic dataset, excluding data from early studies that utilised potentially unreliable blanket demagnetization techniques, suggests that clockwise vertical axis rotations of 4–6°/Myr have occurred since the Late Miocene (5–10 Ma), with possibly no rotations other than those expected from large-scale plate motions before this. This interpretation remains reasonable even when potentially unreliable Wairoa

domain data are reintroduced to the dataset. On the Hikurangi margin, the only reliable data that indicate vertical axis rotations with respect to the Australian plate in the Early and Middle Miocene are now restricted to a small coastal area in northeastern Marlborough (Vickery and Lamb, 1995; Little and Roberts, 1997). It is possible that rotations during this period were local to the intersection between the Hikurangi subduction interface and the Alpine-Wairau Fault.

The difficulties with secondary overprints encountered in this study re-emphasise the need for caution when interpreting paleomagnetic data from New Zealand Cenozoic mudstones. A stable reversed polarity ChRM was isolated in only 16% of samples; the combination of a weak NRM, strong viscous overprints, and the effects of thermal alteration resulted in a ChRM that was at best observable over a 100°C temperature range. Detailed stepwise demagnetization of samples is therefore essential if reliable results are to be obtained.

Chapter 5

Tectonic and geochronological implications of variably timed magnetizations carried by authigenic greigite in marine sediments from New Zealand

This chapter appeared in *Geology* Volume 33, Rowan, C. J., and A. P. Roberts, Tectonic and geochronological implications of variably timed magnetizations carried by authigenic greigite in marine sediments from New Zealand, pages 553-556.

Abstract Detailed scanning electron microscope observations, coupled with elemental microanalysis, confirm the presence of a chemical remanent magnetization carried by authigenic greigite (Fe_3S_4) in uplifted Neogene marine sediments from the Hikurangi margin of New Zealand. Normal polarity samples from the studied section have declinations that are deflected ∼60° clockwise of reversed polarity samples, indicating the presence of two distinct magnetizations separated by several million years of tectonic rotation about a vertical axis. However, although multiple generations of iron sulphide growth are observed petrographically, we see no clear differences in the relative timing of greigite formation between samples carrying these two magnetizations. Not only can the diagenetic growth of greigite in fine-grained marine sediments occur long after deposition, obscuring tectonic and magnetostratigraphic information, but such remagnetizations are also difficult to distinguish from a more primary signal in the absence of constraints from field tests. Our observations emphasize that considerable care is necessary when interpreting paleomagnetic data from greigite bearing sediments.

5.1 Introduction

The ferrimagnetic iron sulphide greigite (Fe_3S_4) is being increasingly reported as a carrier of remanent magnetizations in marine sediments (Roberts and Weaver, 2005, and references therein). Greigite is an authigenic mineral that forms as a metastable precursor to framboidal pyrite (Wilkin and Barnes, 1997). Pyritization occurs in anoxic sedimentary environments in the presence of dissolved iron, and sulphide (H_2S, HS^-) released by sulphate reduction during the microbial degradation of organic matter (Berner, 1984). When reactive iron is abundant and dissolved sulphide concentrations are low, pyritization can be arrested and greigite can be preserved (Kao et al., 2004), creating a chemical remanent magnetization (CRM). In many environments, anoxic conditions can exist only a few millimetres below the sediment-water interface, allowing greigite to form soon after deposition and to preserve a syn-depositional paleomagnetic signal. However, this is not necessarily the case; recent studies have identified inconsistent polarity records (e.g. Florindo and Sagnotti, 1995; Roberts and Weaver, 2005; Sagnotti et al., 2005) and even contradictory polarities within the same horizon (e.g. Jiang et al., 2001) which demonstrate late diagenetic growth of greigite.

We identify here two distinct CRMs carried by greigite, in tectonically uplifted Neogene marine sediments from the Hikurangi margin, North Island, New Zealand. Parts of this region have experienced up to 90° of tectonic rotation about a vertical axis during the Neogene (Rait et al., 1991). Paleomagnetic data have been extensively used to constrain the location, rates, and timings of these rotations

(Walcott, 1989), and are crucial in linking past deformation to the contemporary vertical-axis rotations revealed by geodetic studies (Beavan and Haines, 2001). In addition, thick successions in this region, dated by magnetostratigraphy, provide standard mid-latitude sections for foraminiferal biostratigraphy. To assure the reliability of such studies, the identification of late-forming CRMs in these sediments is essential. At the locality studied here, paleomagnetic analysis reveals a patchy development of the later CRM, with a much earlier remanence still preserved in parts of the outcrop. This provides an excellent opportunity to examine the petrographic differences resulting from differently timed magnetizations. We have undertaken detailed scanning electron microscope (SEM) observations, coupled with elemental microanalysis, to examine iron sulphide growth textures and to establish whether early- and late-forming CRMs involving greigite can be reliably distinguished.

5.2 Sampling and methods

Standard paleomagnetic cores (25 mm diameter) were taken from the base of cliffs on Waihau Beach, 35 km northeast of Gisborne (178.2°E, 38.3°S), as part of a larger sampling program to investigate the tectonic evolution of the Hikurangi margin. Samples ∼1 km north of this locality were previously reported to have a reversed polarity magnetization with a small declination anomaly, indicating that this part of the margin has not experienced vertical-axis rotations (Thornley, 1996). Our sampling was along strike (beds measured at 194/23 W) and was thus at approximately the same stratigraphic level. The lithology consisted of massive, grey mudstone with interbedded tuffaceous layers of variable thickness (up to 30 cm). The rocks are early Late Miocene (8.8–11.0 Ma) in age (Mazengarb and Speden, 2000).

Forty-two cores were collected over a total stratigraphic thickness of 7.8 m, including from two tuff beds (Fig. 5.1a); weathered surficial material was removed from the outcrop prior to sampling. Cores were stored and transported to the laboratory in a mu-metal shield. Stepwise demagnetization of the samples was undertaken with a 2G-Enterprises cryogenic magnetometer, situated in a magnetically shielded room at the National Oceanography Centre, Southampton. Samples were demagnetized using both thermal (20–60° steps to 400°C) and alternating field (5–10 mT steps to 60 mT) techniques. Where thermal demagnetization was used, low-field bulk magnetic susceptibility was measured after each heating step to monitor thermal alteration. Vector-component diagrams were used to identify samples where characteristic remanent magnetization (ChRM) directions could be isolated and analysed using principal component analysis (Kirschvink, 1980).

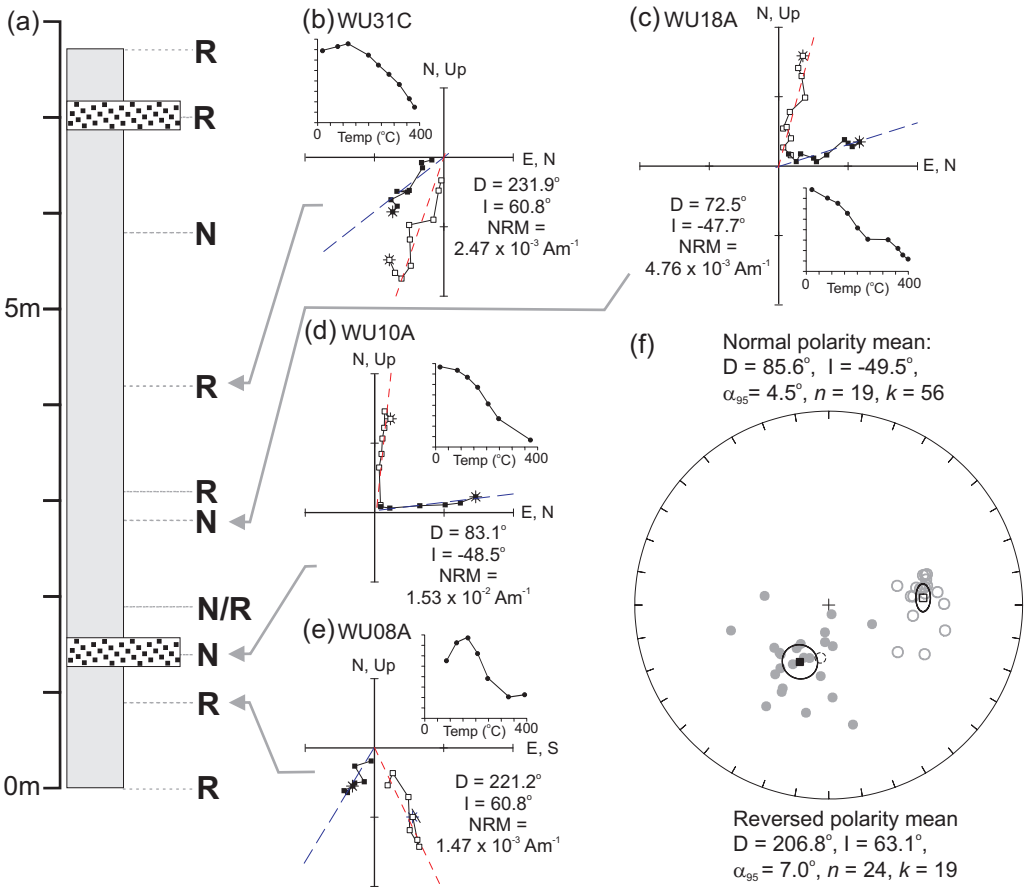

Figure 5.1: (a) Stratigraphic column of the sampled Waihau Beach locality, showing the distribution of reversed and normal polarity remanent magnetizations through the section. (b-e) Representative vector demagnetization plots and anchored best-fit ChRM determinations (blue = declination, red = inclination) showing (c, d) normal polarity and large clockwise declination rotations, and (b, e) reversed polarity and small rotations. Solid symbols denote declinations; open symbols denote inclinations. (f) Equal area stereographic plot of ChRM directions in tilt-corrected coordinates, showing the non-antipodal distribution of normal and reversed polarity directions. The mean direction of Thornley (1996) is plotted for comparison (small dashed error ellipse).

Resin-impregnated polished sections were prepared for SEM analysis from paleomagnetic samples that had not been thermally demagnetized. Sedimentary microtextures were examined with a JEOL JSM-6360LV SEM, operated at 15 keV with an 18 pA acceleration voltage, at the Institute of Earth Sciences, Academia Sinica, Taipei, Taiwan. Mineral phases were identified with an Oxford Instruments Ltd INCA-300 energy dispersive spectrometer (EDS), with a pyrite (FeS_2) calibration standard. The high atomic mass of iron sulphides allows them to be easily identified by their high electron backscatter. It is possible to distinguish between greigite and pyrite from examination of the iron to sulphur ratio: Fe/S = 0.5 for pure pyrite, whereas for greigite, Fe/S = 0.75. Several studies have demonstrated that, with careful analysis, different sedimentary iron sulphides can be clearly distinguished (e.g. Jiang et al., 2001; Roberts and Weaver, 2005; Sagnotti et al., 2005). In this study, the grain size of the iron sulphides being analyzed was often small with respect to the diameter of the electron beam ($\sim$1 μm), so elemental ratios reflected an average of several grains and the matrix between them. Careful examination was required to establish whether intermediate ratios ($0.5 \leq \text{Fe/S} \leq 0.75$) were due to a mixture of pyrite and greigite, rather than pyrite oxidation (which also leads to Fe/S > 0.5). Oxidation was inferred in analyses where large oxygen peaks occurred in the absence of silicate minerals.

5.3 Results

The natural remanent magnetization (NRM) of the samples ranged from 1×10^{-4} to 2×10^{-2} Am^{-1}, although only the tuff samples had values exceeding 5×10^{-3} Am^{-1}. ChRMs were isolated from both thermally and alternating field demagnetized samples, with the samples exhibiting unblocking temperatures of 280–380°C and median destructive fields of 50–60 mT; thermal treatment generally yielded better-defined demagnetization trajectories. Both normal (Figs. 5.1c, d) and reversed (Figs. 5.1b, e) polarity directions were isolated; in all but one instance, polarities are consistent within a sampling level (Fig. 5.1a). In tilt-corrected co-ordinates, the normal polarity samples give a mean direction of declination (D) = 85.6°, inclination (I) = -49.5°, α_{95} = 4.5°; the reversed polarity samples give a mean direction of D = 206.8°, I = 63.1°, α_{95} = 7.0° (Fig. 5.1f). These directions are clearly not antipodal to one another, and the shallow dip of the beds means that they cannot be made so by unfolding (in geographic coordinates, the mean directions are D = 66.8°, I = -70.2° and D = 163.9°, I = 59.3°, respectively); nor do the normal polarity directions result from a present day overprint (D = 21°, I = -64°).

In the absence of local tectonic rotation, the expected declination for localities

of 10 Ma age on the Australian plate is ∼10°. The reversed polarity direction has a declination of 27 ± 7°, which is close to that previously reported from nearby sediments (Thornley, 1996) (Fig. 5.1f) and suggests minimal vertical-axis rotation. However, the large declination anomaly exhibited by the normal polarity samples indicates substantial tectonic rotation. This discrepancy can be explained if the normal polarity samples carry a magnetization that was acquired much earlier than that in the reversed polarity samples, with a significant period of rotation in the interim.

Normal and reversed polarity samples were studied with the SEM; representative back-scattered electron images are shown in Figures 5.2 and 5.3. Iron sulphides appear to be more abundant in the normal polarity samples but are present throughout all the samples studied, generally occurring in large aggregates representing several generations of iron sulphide growth, interpreted to represent progressively remineralised fragments of organic matter. In the normal polarity samples, which document a large vertical-axis rotation, the first sulphide generation (marked P) consists of either euhedral pyrite crystals (Figs. 5.2a, d) or framboidal pyrite that often has euhedral overgrowths (Fig. 5.2c). Both forms can be observed in close proximity to each other (Fig. 5.2b), but their temporal relationship to each other is unclear. This first generation of iron sulphides is then surrounded by later growth of both greigite and at least one space-filling pyrite generation (P2); two phases of growth (P2 and P3) may be indicated by different grain sizes in the case of Fig. 5.2e. Whereas in some cases greigite appears to post-date formation of P2 (Figs. 5.2a, e), in others the P2 phase has grown around the greigite (Fig. 5.2c). This suggests that the greigite and P2 formed penecontemporaneously; the greigite possibly formed as a precursor to P2, but in some places has been preserved, presumably due to incomplete pyritization.

In the reversed polarity samples, which indicate minimal rotation, the first iron sulphide phase consists exclusively of framboidal pyrite, commonly with euhedral overgrowths (Figs. 5.3b, c, d). Greigite neoformation is observed at the edges of these framboids (Figs. 5.3b, e) and in isolated patches (Figs. 5.3c, d, e); in all cases this growth appears to have preceded a later space-filling generation of pyrite (P2). In contrast to the paleomagnetic data, SEM observations indicate no clear differences in the mode of occurrence of remanence-bearing greigite in the differently magnetized samples; in all cases it appears to have grown at an intermediate or late stage within authigenic iron sulphide aggregates that have undergone multiple generations of growth.

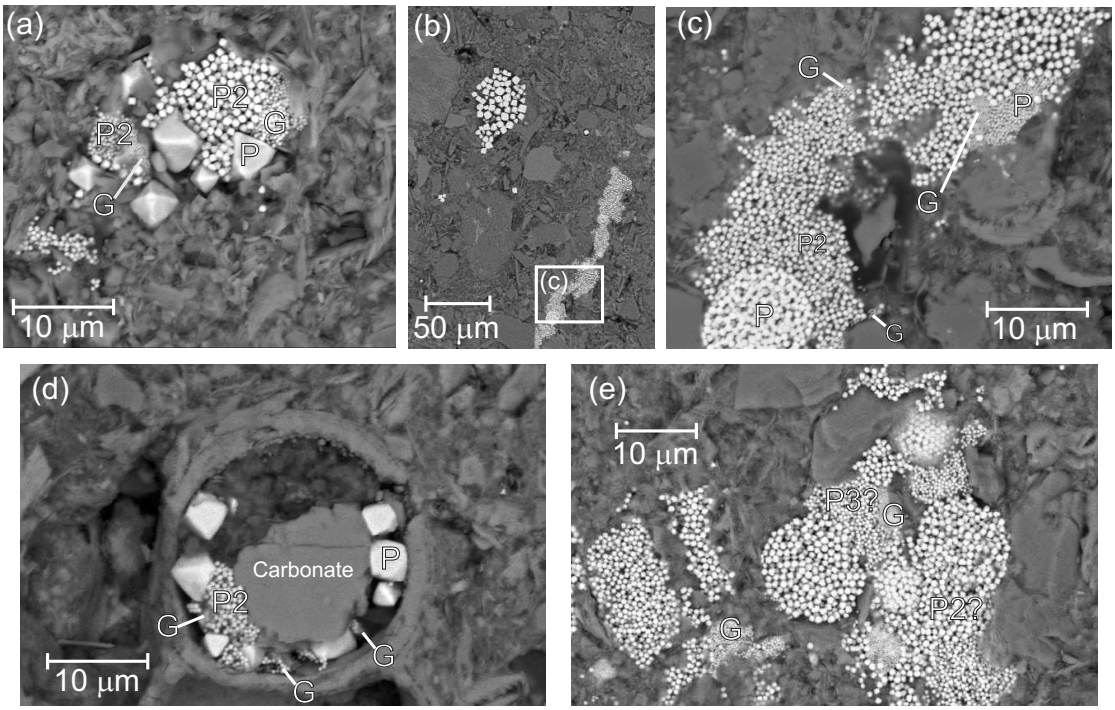

Figure 5.2: Back-scattered electron images illustrating microtextures of several generations of authigenic greigite (G) and pyrite (P), from a sample with a normal polarity, highly rotated, characteristic remanent magnetization direction. (a) Small iron sulfide aggregate consisting of an early growth of euhedral pyrite P, followed by framboidal and space-filling pyrite P2 and neoformed greigite. (b) Euhedral pyrite filling microfossils close to a polyframboidal aggregate. (c) Close-up view of the aggregate in (c). Neoformation of greigite is associated with the space-filling P2 phase. (d) Limited iron sulphide growth within a microfossil that has been partially infilled with carbonate cement. P2 pyrite and greigite have formed after euhedral pyrite (P). (e) Close-up view of a polyframboidal aggregate; different grain sizes possibly indicate two space-filling pyrite phases, tentatively labeled P2 and P3. Greigite neoformation is associated with these later phases.

5.4 Discussion and conclusions

Elemental analysis confirms the presence of authigenic greigite at the studied locality, in association with larger aggregations of authigenic iron sulphides. The demagnetization behaviour of all samples is also consistent with the properties of greigite (Roberts, 1995b; Sagnotti and Winkler, 1999), particularly the ∼300–350°C unblocking temperature, and higher coercivites than would be expected for magnetite. Additionally, the normal polarity samples, which contain a greater abundance of iron sulphides, have higher NRM intensities (Figs. 5.2b-e). Combined, these observations establish that greigite is the carrier of both the normal and reversed polarity magnetizations. No sample appears to contain both components; the formation of the later CRM appears to have destroyed or completely obscured the earlier remanence.

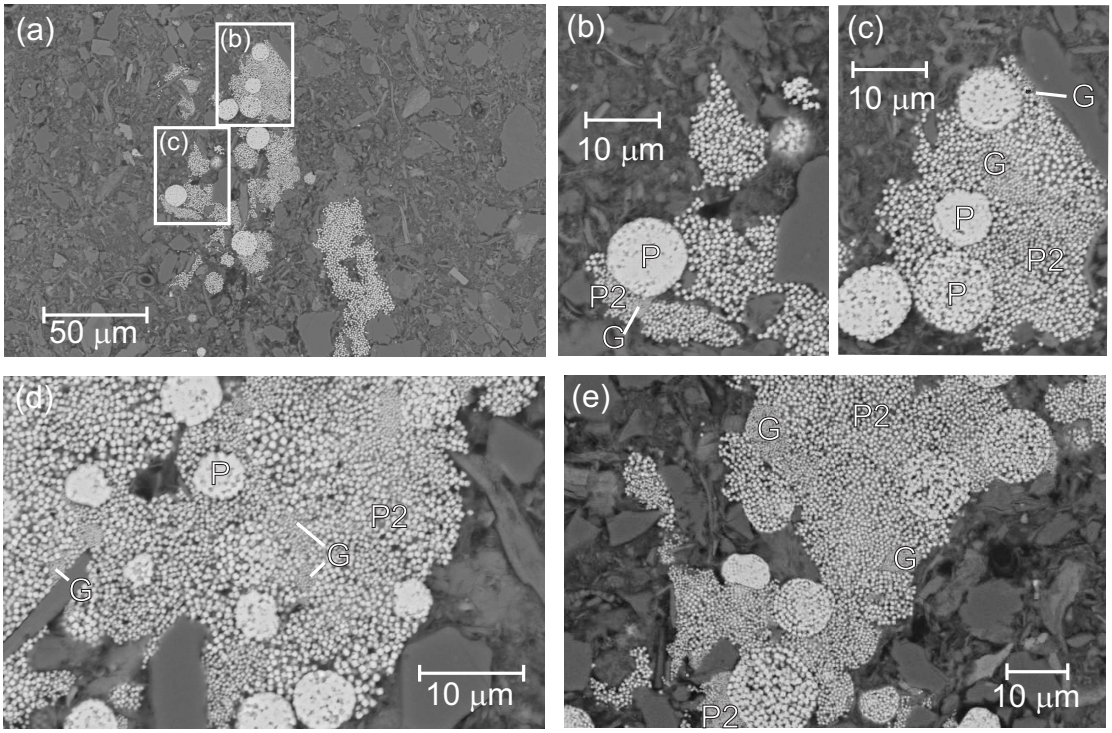

Figure 5.3: Back-scattered electron images from a reversed polarity sample with a small declination anomaly. (a) Polyframboidal aggregate. (b) Close-up view of area indicated in (a), showing greigite neoformation on the surface of an early framboid with euhedral overgrowth P, surrounded by space-filling pyrite (P2). (c) Close-up view of area indicated in (a). Greigite growth has occurred in a patch between recrystallized framboids (P), and on the edge of a silicate grain, before growth of P2. (d) Close-up view of a polyframboidal aggregate. The first generation of framboidal pyrite (P) shows euhedral overgrowth. Isolated patches of greigite are surrounded by growth of pyrite P2. (e) Close-up view of a polyframboidal aggregate; greigite has formed on the edge of early framboids, and in isolated patches, before growth of the space-filling pyrite phase (P2).

The magnetic properties and demagnetization behaviour described above are also consistent with those reported from Cenozoic marine mudstones elsewhere in New Zealand (Turner, 2001, and references therein). These sediments have been through multiple episodes of uplift, erosion, redeposition and reductive diagenesis, which have led to the dissolution of detrital magnetic minerals such as magnetite and growth of abundant pyrite. Greigite has previously been documented in similar sediments in New Zealand by Roberts and Turner (1993), who concluded that it formed near the time of deposition rather than during later diagenesis. Our results indicate that this is not always the case. The presence of a remanent magnetization carried by a potentially late-forming authigenic mineral phase clearly has implications for the reliability of paleomagnetic studies in this region, and also in other regions with similar lithologies. For example, abundant greigite has been reported from Italian Neogene sequences (e.g. Sagnotti and Winkler, 1999), which

also provide important mid-latitude biostratigraphic zonations.

The locality reported here is important because a late remagnetization has only patchily overprinted an earlier CRM. In contrast to a similar case recently reported by Sagnotti et al. (2005), in which the early magnetization was carried by magnetite, here both early and late magnetizations are carried by greigite. The shallow tilt of the beds sampled means that the 60° difference in declination can only be due to several million years of vertical-axis rotation occurring between the times of acquisition of the two magnetizations. Worryingly, samples showing both types of paleomagnetic behaviour exhibit several generations of sulphide growth, with greigite forming at an intermediate to late stage. Thus, the relative timing of formation of the remanence-bearing phases appears to be similar, although the absolute timing clearly differs. It may therefore be difficult to discriminate between late and early magnetizations at sites where greigite is the dominant magnetic mineral. The section sampled by Thornley (1996), nearby on the same beach, records only the later magnetization reported here; as a result this area was mistakenly considered to be unaffected by Neogene tectonic rotations. Tectonic information has been lost in this case, and magnetostratigraphic data from these sediments would also be unreliable. Our results suggest that this is unlikely to be obvious from SEM observations.

If greigite is a common magnetic carrier in New Zealand Cenozoic mudstones, late-forming CRMs may potentially impact much of the data pertaining to the Neogene rotation of the Hikurangi margin, as well as Cenozoic magnetostratigraphy. Any such studies should routinely incorporate petrographic observations to establish whether iron sulphides are present; in such cases, both in this region and in other regions where greigite is the dominant magnetic mineral, an early date for remanence acquisition should not be assumed in the absence of firm evidence, such as fold tests, reversals tests, or other field tests.

Chapter 6

Magnetite dissolution, diachronous greigite formation, and secondary magnetizations from pyrite oxidation: Unravelling complex magnetizations in Neogene marine sediments from New Zealand

This chapter appeared in *Earth and Planetary Science Letters* Volume 241, Rowan, C. J. and A. P. Roberts, Magnetite dissolution, diachronous greigite formation, and secondary magnetizations from pyrite oxidation: Unravelling complex magnetizations in Neogene marine sediments from New Zealand, pages 119-137.

Abstract Detailed rock magnetic and electron microscope analyses indicate that the magnetic signature of Neogene marine sediments from the east coast of New Zealand is dominated by the authigenic iron sulphide greigite. The greigite is present as a mixed population of stable single domain and superparamagnetic grains, which is consistent with authigenic growth from solution. This growth can result from pyritization reactions soon after deposition, which also leads to dissolution of most detrital magnetite; however, where constrained by field tests, our data suggest that remanence acquisition can occur >1 Myr after deposition, and can vary in timing at the outcrop scale. Strong viscous overprints result from oxidation of the iron sulphides, probably during percolation of oxic ground water. This process can sometimes destroy any ancient remanent magnetization. This complex magnetic behaviour, particularly the presence of late-forming magnetizations carried by greigite, means that the remanence in New Zealand Cenozoic sediments, and in similar sediments elsewhere, cannot be assumed to be primary without confirmation by field tests. The reversals test should be employed with caution in such sediments, as patchy remagnetizations can lead to false polarity stratigraphies.

6.1 Introduction

Thick sequences of tectonically uplifted, fine-grained Cenozoic marine sediments from the Hikurangi margin, on the east coast of New Zealand (Fig. 6.1a), provide standard mid-latitude sections for foraminiferal biostratigraphy. Since the 1970s, paleomagnetic data have been used to tie these sequences to the geomagnetic polarity timescale (Lienert et al., 1972; Kennett and Watkins, 1974; Roberts et al., 1994), enabling precise correlation of Neogene paleoclimatic variations in the southwest Pacific with changes in the Mediterranean and elsewhere (Roberts et al., 1994). Paleomagnetic data have also revealed substantial tectonic rotations of the Hikurangi margin during the Neogene (Walcott et al., 1981; Mumme and Walcott, 1985; Wright and Walcott, 1986; Lamb, 1989; Mumme et al., 1989; Walcott, 1989; Roberts, 1992; Little and Roberts, 1997), and are crucial in linking past deformation to contemporary vertical axis rotations revealed by geodetic measurements (Beavan and Haines, 2001; Wallace et al., 2004). However, despite over 30 years of paleomagnetic research, longstanding questions concerning the origin of the magnetic signal in these sediments remain unanswered. Magnetic extractions often fail to clearly identify any remanence bearing phases that could be the carrier of their weak (typically 10^{-5}–10^{-3} Am^{-1}) natural remanent magnetization (NRM) (Turner, 2001). Alternating field (AF) demagnetization is often unsuccessful in isolating a stable characteristic remanent magnetization (ChRM), and the results

of thermal demagnetization indicate low unblocking temperatures (250–350°C) that are consistent with a wide range of possible magnetic minerals. Establishing the origin of a strong, widespread, present-day field overprint has also proven problematic.

Neogene sedimentary sequences from the Hikurangi margin were principally deposited in marginal basin settings since the initiation of subduction at 23–20 Ma (Rait et al., 1991; King, 2000), and ongoing shortening along the subduction system has led to their uplift above sea level. The sediments were chiefly sourced from uplifted Triassic-Cretaceous basement rocks of the Torlesse Supergroup, which have been through repeated cycles of uplift, erosion and redeposition (Mackinnon, 1983); exposure to anoxic diagenetic conditions during such cycles makes these rocks a poor source of detrital magnetic iron oxides such as magnetite (Smale, 1990; Roberts and Turner, 1993). Since the mid-Miocene, increasing amounts of detrital iron oxides have been supplied to marginal basins by volcanic activity on the Coromandel Penisula, and, since 2 Ma, from the Taupo Volcanic Zone (Carter et al., 2003). Evidence of recent volcanic activity is apparent in the magnetic signature of Holocene sediments from the continental slope east of the North Island (Figs. 6.1a, 6.2), where peaks in NRM intensity at the top of core MD972121 (Fig. 6.2a) correlate to ash layers rich in detrital magnetic minerals (Carter et al., 2002). However, below 4.7 m depth no such peaks occur, and from 4.2 to 4.7 m there is also a substantial, permanent drop in the background NRM intensity (Fig. 6.2a), accompanied by a significant decrease in its median destructive field (MDF) below 3 m (Fig. 6.2b). Following the onset of anoxic conditions, iron-bearing minerals such as magnetite will react with H_2S, produced by bacterial reduction of sulphate during the decomposition of organic matter, forming pyrite (FeS_2) (Berner, 1984) (Fig. 6.2c). Within about 12,000 years of deposition most detrital magnetic minerals in core MD972121, even in the magnetite-rich ash layers, have been dissolved, particularly magnetically stable single domain (SD) grains. All that remains is a sparse population of multi-domain grains (with low MDFs) that are unlikely to record a stable remanent magnetization. As reported by Karlin and Levi (1983, 1985) and Karlin (1990), this type of signature is common in organic-rich, terrigenous sediments from continental margins.

The effects of pyritization are not only evident in modern sediments. Pyrite is abundant in the uplifted Neogene sequences of New Zealand, and magnetic extractions have yielded abundant paramagnetic ilmenite, which is more resistant to dissolution than ferrimagnetic iron oxides (Canfield et al., 1992), but only minor amounts of titanomagnetite (Roberts and Turner, 1993; Wilson and Roberts, 1999; Turner, 2001) (occasional exceptions exist, e.g. Little and Roberts (1997)

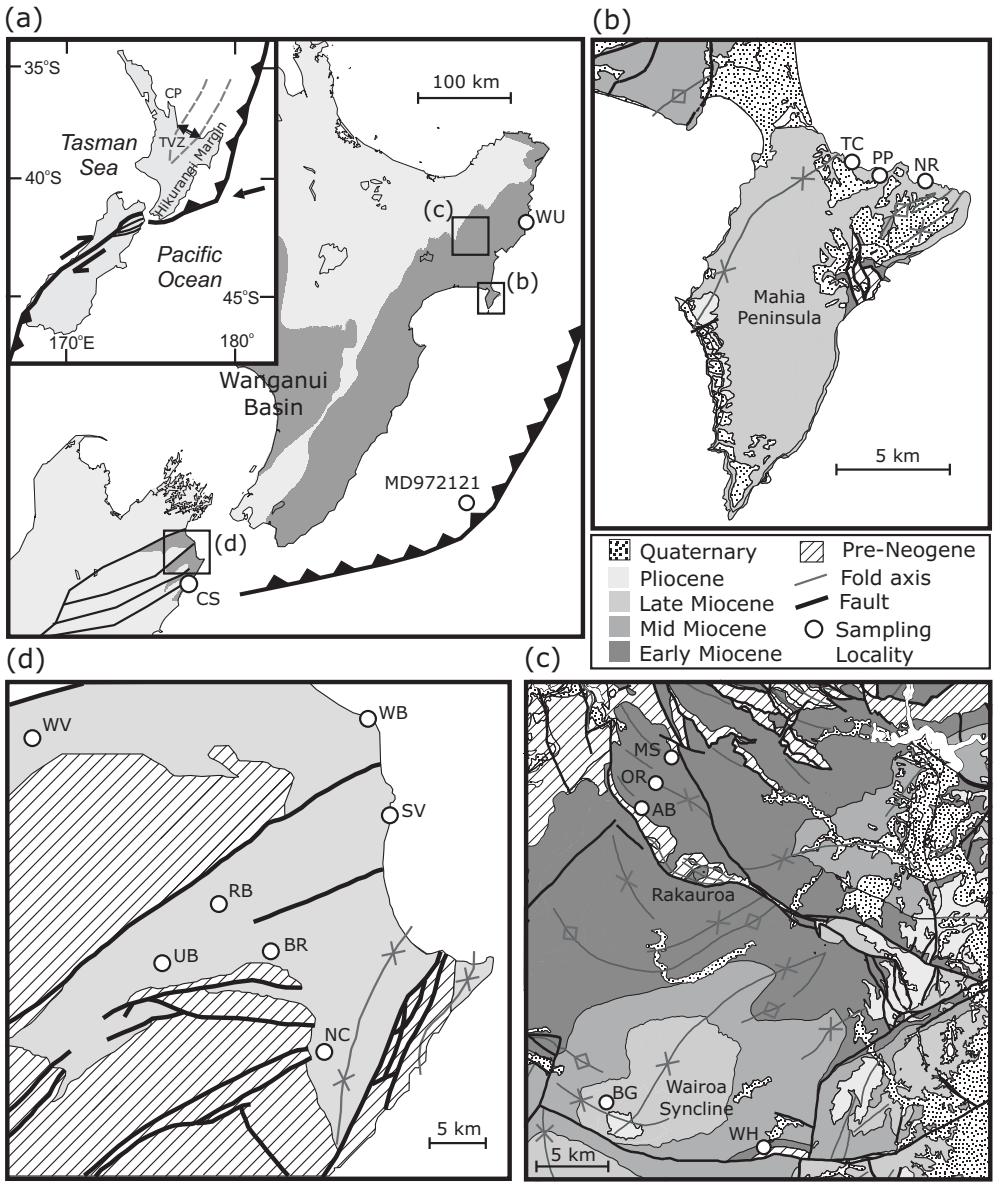

Figure 6.1: Distribution of sampling localities. (a) Tectonic setting of the New Zealand region. Inset: boundary between the Australian and Pacific plates. TVZ = Taupo Volcanic Zone, CP = Coromandel Peninsula. Main figure: shaded regions delineate Neogene marginal basins. WU = Waihau Beach, CS = Camp Stream. The location of piston core MD972121 (Carter et al., 2002) is also shown. (b) Gently folded Late Miocene sequences on the Mahia Peninsula. TC = Te Waipera Cemetary, PP = Putiki Point, NR = Nukutaurua Road. (c) Early Miocene-Pliocene sequences in the vicinity of the Wairoa Syncline. MS = Matawai Station, OR = Oliver Road, AB = Anzac Bridge, BG = Burgess Road, WH = Waterfall Hill. (d) Late Miocene–Pliocene (not subdivided on map) Awatere Group sediments, bounded by faults of the Marlborough fault system. WV = Waihopai Valley, WB = White Bluffs, SV = Sea View, RB = Richmond Brook, UB = Upton Brook, BR = Blind River, NC = Needles Creek. Figures (b) and (c) are adapted from the QMAP data set (Mazengarb and Speden, 2000), and (d) is modified from Roberts (1992).

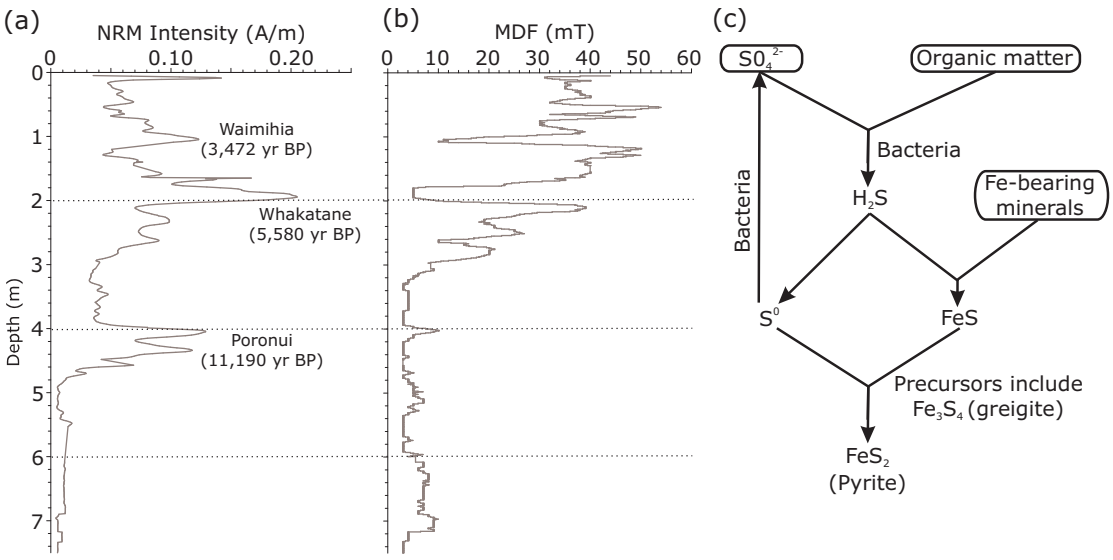

Figure 6.2: Down-core profiles of (a) NRM intensity, and (b) median destructive field (MDF) for piston core MD972121 (Carter et al., 2002). In the upper 4.7 m of the core, NRM peaks and corresponding MDF minima correlate with dated ash layers rich in coarse magnetic minerals. Below 4.7 m, NRM and MDF both decrease significantly, indicating dissolution of detrital magnetic minerals; susceptibility profiles for the entire 35 m core (not shown) indicate that this reduction is permanent. (c) Pyritization reactions, after Berner (1984).

reported magnetite in sediments that were probably partially sourced from Cretaceous volcanics). Typical depositional environments in marginal basins of the Hikurangi margin have apparently been consistently inimical to the preservation of detrital magnetite since the Early Miocene, and it is therefore unlikely to be a significant contributor to the remanence of most of these sediments.

Pyritization proceeds via a series of precursors that include the ferrimagnetic iron sulphide greigite (Fe_3S_4) (Berner, 1984; Wilkin and Barnes, 1997). Although it is generally regarded as metastable, instances of greigite carrying a stable ChRM are increasingly being recognized in the geological record (Roberts and Weaver, 2005). It has been shown that where reactive iron is abundant and organic carbon is relatively restricted, any dissolved sulphide reacts rapidly with available dissolved iron, which can lead to incomplete pyritization and the preservation of greigite (Kao et al., 2004). Such conditions are particularly likely to arise where the sedimentation rate, and therefore the dilution of organic matter by terrigenous material, is high.

In New Zealand, greigite has previously been reported in a small part of a late Miocene section in Marlborough (Roberts and Turner, 1993) (UB, Fig. 6.1d), and, more recently, in early late Miocene rocks from the northern Hikurangi margin (WU, Fig. 6.1a; see Chapter 5). Greigite has also been inferred to be present in Pleistocene sediments from the Wanganui Basin, western North Island (Roberts

and Pillans, 1993). Although definitive identifications of greigite have only been made in these few instances, the demagnetization behaviour of samples from the localities in question is consistent with that of paleomagnetic samples from similar sediments throughout New Zealand (Turner, 2001), which raises the possibility that authigenic greigite is a common remanence carrier in these rocks. The steady state diagenetic model of Berner (1984) confines pyritization reactions to the top of the sediment column, in which case any remanence carried by greigite will record the geomagnetic field close to the time of deposition. However, increasing reports of later-forming greigite (Florindo and Sagnotti, 1995; Jiang et al., 2001; Roberts and Weaver, 2005; Sagnotti et al., 2005), including one instance within New Zealand itself (Chapter 5), make it clear that external forcing events can potentially change pore water chemistry and trigger greigite formation at any time after deposition, not just during initial reductive diagenesis. In New Zealand, paleomagnetic data from Cenozoic sediments are rarely constrained by rigorous field tests; if greigite is a common remanence carrier, the possibility of late-forming magnetizations becomes an issue of real concern.

In this study, we discuss paleomagnetic results from samples collected along the length of the Hikurangi margin. The complex behaviour observed, particularly the abundance of late forming magnetizations, is consistent with the presence of an authigenic mineral; we present rock magnetic and scanning electron microscope (SEM) observations that confirm in all cases that this mineral is greigite. Later oxidation of iron sulphides can also be implicated in the formation of strong viscous overprints. We then address the implications of these results, not only for paleomagnetic studies in New Zealand but also in similar tectonically active marginal basins around the Pacific, the Mediterranean, and other areas that are host to rapidly deposited terrigenous sediments and reducing diagenetic environments.

6.2 Sampling and methods

The majority of the results presented here come from a comprehensive paleomagnetic sampling program undertaken in 2002/03 in order to study the tectonic evolution of the Hikurangi margin. Paleomagnetic analysis of samples from over 40 localities was performed using a 2G-Enterprises cryogenic magnetometer, situated in a magnetically shielded laboratory at the National Oceanography Centre, Southampton (NOCS). Samples were stepwise demagnetized using both thermal (40° steps from 80°C to 400°C) and AF (5 mT steps to 60 mT) techniques. These measurements reveal a wide range of paleomagnetic behaviours, including strong present-day field overprints (Chapter 4) and differently timed magnetizations separated by several Myr (Chapter 5). We have focused on a subset of

these localities, chosen to reflect this variety, for further investigations of magnetic mineralogy (Fig. 6.1; Table 6.1). Samples from earlier studies in the Marlborough region (Fig. 6.1d) (Roberts, 1992; Roberts et al., 1994) are also included. Three types of analysis were performed: (a) measurement of the bulk magnetic hysteresis properties of $\sim$1 cm^3 sub-samples, using a Princeton Measurements Corporation Micromag 3900 vibrating sample magnetometer (VSM) at NOCS. Values of saturation magnetization M_s, saturation remanent magnetization M_r, and coercive force B_c were obtained from hysteresis loops (0.5 T saturating field); the coercivity of remanence B_{cr} was determined from back-field remanence curves. (b) Measurement of first-order reversal curves (FORCs), which are a class of partial hysteresis loop measured by cycling between a positive saturation field and a reversal field B_a (Pike et al., 1999; Roberts et al., 2000), using the same VSM. A series of FORCs with different B_a values provides a more complete sampling of the magnetic response of the sample than a single hysteresis loop; this information is commonly represented on a FORC diagram, which can be thought of as a contour plot of the coercivity distribution of magnetic particles and their interaction field strengths (Pike et al., 1999; Roberts et al., 2000). We measured 140 FORCs for each sample, with a field spacing of 1.85 mT and an averaging time of 250 ms, in a 0.5 T saturating field. FORC distributions were calculated using a smoothing factor (SF) of 5. (c) SEM observations of resin-impregnated polished sections, combined with elemental analysis of mineral phases using an X-ray energy dispersive spectrometer (EDS). Principal observations were made at NOCS using a LEO 1450VP SEM, operated at 10–20 keV with an acceleration voltage of 17–20 pA, and a Princeton Gamma Tech (IMIX-PTS) EDS system. Some supplementary analyses were made with a JEOL JSM-6360LV SEM, operated at 15 keV with an 18 pA acceleration voltage, and an Oxford Instruments Ltd INCA-300 EDS, at the Institute of Earth Sciences, Academia Sinica, Taipei, Taiwan. Observations focused on iron sulphides, which are easily identified by their high electron backscatter. Careful analysis of EDS measurements, calibrated with a pyrite standard, allows different phases such as greigite and pyrite to be distinguished by their distinctive iron to sulphur ratios (Fe/S = 0.75 and = 0.5, respectively) (Jiang et al., 2001; Roberts and Weaver, 2005; Sagnotti et al., 2005; see also Chapter 5).

6.3 Paleomagnetic data

The diverse paleomagnetic behaviour of the studied sediments reflects the wide range of processes that have contributed to their complex magnetization. Results from the localities described below are representative examples of these various processes.

6.3.1 Differentially timed synfolding magnetizations, Mahia Peninsula

Three localities were sampled within a thick sequence of fine-grained mudstones, interbedded with tuffs and reworked tuffaceous beds, on the north coast of Mahia Peninsula (Fig. 6.1b). The rocks are all of late Miocene (6.5–11.0 Ma) age (Mazengarb and Speden, 2000) and are distributed across a syncline formed during early Pliocene folding (Buret et al., 1997).

Near Te Waipera Cemetery (locality TC), we sampled a 24.0 m sequence consisting of massive, dark grey, fine-grained mudstones, overlain by interbedded mudstones and tuffaceous beds, with one primary tuff (Fig. 6.3a). The bedding attitude is 203/10 NW (Fig. 6.1b). NRMs are strong, with intensities $>5 \times 10^{-4}$ Am^{-1} in 89% of samples (Table 6.1), and a minimally overprinted, normal polarity ChRM was almost universally recovered (Fig. 6.3b, c). Thermal and AF demagnetizations were both effective, although AF treated samples from the lower part of the section often developed a strong gyroremanent magnetization (GRM) above 40 mT (Fig. 6.3c). After correction for bedding tilt, 48 samples yielded a mean paleomagnetic direction of declination (D) = 57.5°, inclination (I) = 53.8°, and α_{95} = 2.8° (Fig. 6.3d).

At Putiki Point (locality PP), the 16.5 m sequence sampled consists of shallowly dipping (bedding attitude 239/11 NW) white, ash-rich mudstones, with minor reworked tuff beds (Fig. 6.3e). In comparison to TC, samples had weaker NRMs, with 76% of samples having intensities $<5 \times 10^{-4}$ Am^{-1} (Table 6.1), and AF demagnetization was generally ineffective. A reversed polarity ChRM was isolated from 24 samples, producing a mean direction in tilt-corrected coordinates of D = 237.8°, I = 64.5°, and α_{95} = 5.0° (Fig. 6.3h). The ChRM was overprinted to various degrees by a normal polarity component (Fig. 6.3f, g), which was so strong at three sampling levels that a stable endpoint could not be isolated (marked by crosses in Fig. 6.3e).

At the end of Nukutaurua Road (locality NR), we sampled an 81.5 m sequence of more steeply dipping (bedding attitude 240/48 NW) pale grey mudstones, regularly interbedded with white reworked tuffs (Fig. 6.3i). NRMs were generally weak (81% of samples $<5\times10^{-4}$ Am^{-1}) and noisy demagnetization paths were common; at three horizons, the remanence was so unstable that reliable directions could not be isolated (Fig. 6.3i). Both normal and reversed polarity ChRMs were identified in this section (Fig. 6.3j, k). After tilt correction, a mean direction of D = 99.7°, I = -62.8°, and α_{95} = 4.7° was determined from 16 normal polarity samples; the mean reversed polarity direction was D = 256.9°, I = 65.9°, and α_{95} = 5.0° from 24 samples (Fig. 6.3l).

Table 6.1: Magnetic properties of samples analysed in this study.

		NRM			Hysteresis ratios	
Locality	n	Intensity ($\times 10^{-4}$ Am^{-1})	$> 5 \times 10^{-4}$ Am^{-1}	n	M_r/M_s	B_{cr}/B_c
Mahia Peninsula (Fig. 6.1b)						
TC	54	2.7–34	89%	15	0.12–0.52	1.35–3.90
PP	42	0.5–12	24%	4	0.20–0.24	3.23–3.72
NR	83	0.2–64	19%	21	0.03–0.20	3.13–17.47
Rakauroa (Fig. 6.1c)						
MS	60	0.1–2.2	0%	2	0.12–0.13	2.93–3.21
OR	81	0.5–7.6	9%	2	0.17–0.18	2.70–2.85
AB	42	0.5–1.8	0%	2	0.12–0.14	3.64–3.84
Coast North of Gisborne (Fig. 6.1a)						
WU	60	0.2–15	7%	8	0.13–0.19	3.38–3.87
Wairoa Syncline (Fig. 6.1c)						
WH	16	2.2–5.3	6%	2	0.13–0.14	3.67–3.99
BG	11	3.4–7.8	44%	2	0.11–0.13	4.96–5.61
Marlborough (Fig. 6.1a, d)						
SV	12	16–41	100%	3	0.28–0.41	1.64–2.59
UB	19	1.3–93	55%	6	0.14–0.59	1.27–3.46
WB	14	0.3–22	7%	3	0.23–0.49	1.38–2.56
BR	9	1.5–4.1	0%	2	0.14–0.16	3.51–3.75
CS	12	1.0–44	58%	2	0.36–0.45	1.46–1.75
RB	12	1.1–27	75%	3	0.22–0.44	1.35–2.34
WV	12	1.1–16	42%	2	0.14–0.15	3.19–3.20
NC	10	1.9–26	70%	3	0.14–0.33	1.78–3.60

Locality names are abbreviated as in Fig. 6.1. n = number of samples analysed; NRM = natural remanent magnetization; M_r = saturation remanent magnetization; M_s = saturation magnetization; B_{cr} = coercivity of remanence; B_c = coercive force.

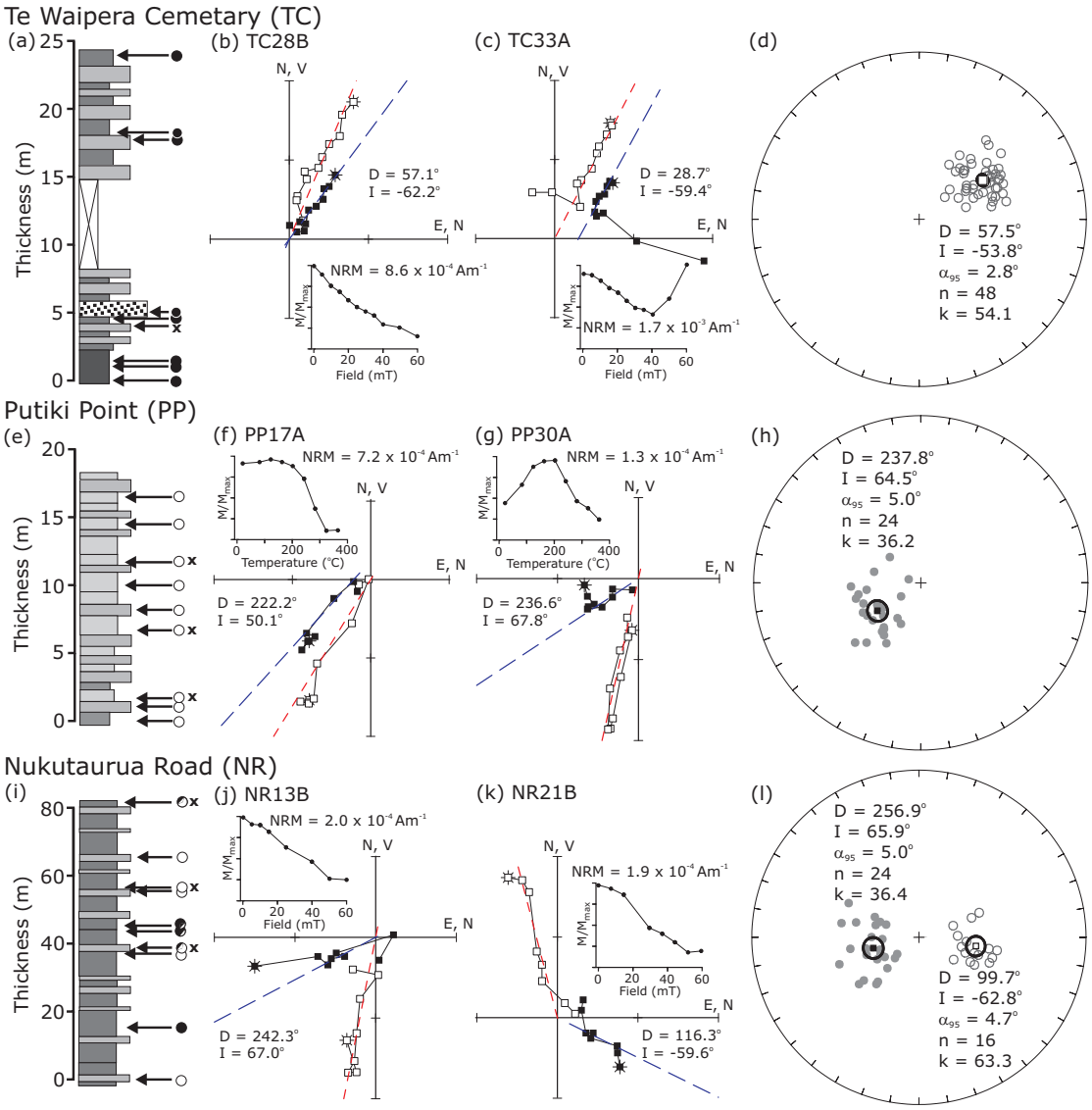

Figure 6.3: Demagnetization data from Mahia Peninsula. (a) Sequence sampled at TC. Arrows mark sampling horizons in mudstones (black/dark grey) and tuffaceous beds (light grey, stipple for primary tuff), with normal polarity (solid circle) or unstable magnetizations (cross) indicated. (b) Vector component plot of AF demagnetization data for sample TC28B. Solid symbols denote declinations, open symbols inclinations, dashed lines best-fit directions from principal component analysis. (c) AF demagnetization data for sample TC33A, with GRM acquisition above 40 mT. (d) Equal area stereographic projection of normal polarity ChRM directions (open circles) from TC, with calculated mean direction and α_{95} error ellipse (bold). (e) Sequence sampled at PP. All sampling horizons had reversed polarity magnetizations (open circles), with unstable ChRMs at three levels (crosses). (f) Thermal demagnetization data for sample PP17A. (g) Thermal demagnetization data for sample PP30A, with a strong normal polarity overprint and reversed ChRM. (h) Stereoplot of reversed polarity ChRMs (closed circles) from PP, with mean direction. (i) Sequence sampled at locality NR, showing normal and reversed polarity, and unstably magnetized horizons. Partially open/closed circles mark horizons with samples of both polarities. (j) AF demagnetization data for reversed polarity sample NR13B. (k) AF demagnetization data for normal polarity sample NR21B. (l) Stereoplot of normal and reversed polarity ChRMs from NR, with mean directions.

In tilt-corrected coordinates, the normal and reversed polarity mean directions from NR fail the reversals test (critical angle at 95% confidence level = 7.0°; observed angle between means = 10.3°) (McFadden and McElhinny, 1990). The reversed polarity direction is close to that isolated at PP, although it fails the test for a common mean (critical angle = 6.2°; observed angle = 8.1°) (Fig. 6.4a), but the normal polarity direction has a significantly higher declination than the mean direction from TC. Reversing the tilt correction restores the mean directions from the moderately tilted NR locality closer to those from the other two localities (Fig. 6.4a), but less tilting is required to reconcile the reversed polarity data. This suggests that the two polarities represent differently timed, synfolding magnetizations. The presence of sister samples with different polarities in several horizons in the middle of the NR section (Fig. 6.3i) suggests that the polarity sequence is not primary, which supports the hypothesis of differential timing. Applying the fold test of Tauxe and Watson (1994) separately to the normal and reversed polarity directions (Fig. 6.4b, c) produces a clear difference at the 95% confidence level: the reversed polarity directions are in best agreement at 79% unfolding, while the normal polarity directions cluster at 44% unfolding. The normal polarity magnetization was therefore acquired demonstrably later, although both polarities are clearly associated with the same folding episode; there is no trace of a syn-depositional remanence at any of the Mahia localities. Paleomagnetic mean directions after partial unfolding combine to give a declination of 49 ± 5° for the Mahia Peninsula localities; large-scale motion of the Australian plate accounts for ∼1°/Myr of clockwise rotation (Idnurm, 1985), leaving a declination anomaly of 44 ± 5° since folding at 4–6 Ma.

6.3.2 Early forming magnetization, Rakauroa region

As reported in Chapter 4, resampling of three Early Miocene localities in the Rakauroa region (Fig. 6.1c) established that a previously reported large declination anomaly (Mumme and Walcott, 1985) was the result of incomplete removal of a large viscous overprint. At Oliver Road (OR) and Matawai Station (MS), more rigorous analysis yielded tectonically unrotated, reversed polarity declinations (Table 6.2), which are shown by field tests to predate early folding. At Anzac Bridge (AB), the remaining site, no stable ChRM could be isolated beneath the overprint. The OR and MS localities represent a clear instance of an early-forming remanence that preserves a retrievable ChRM despite strong overprinting. NRM intensities were $<5\times10^{-4}$ Am^{-1} for almost all samples at these localities.

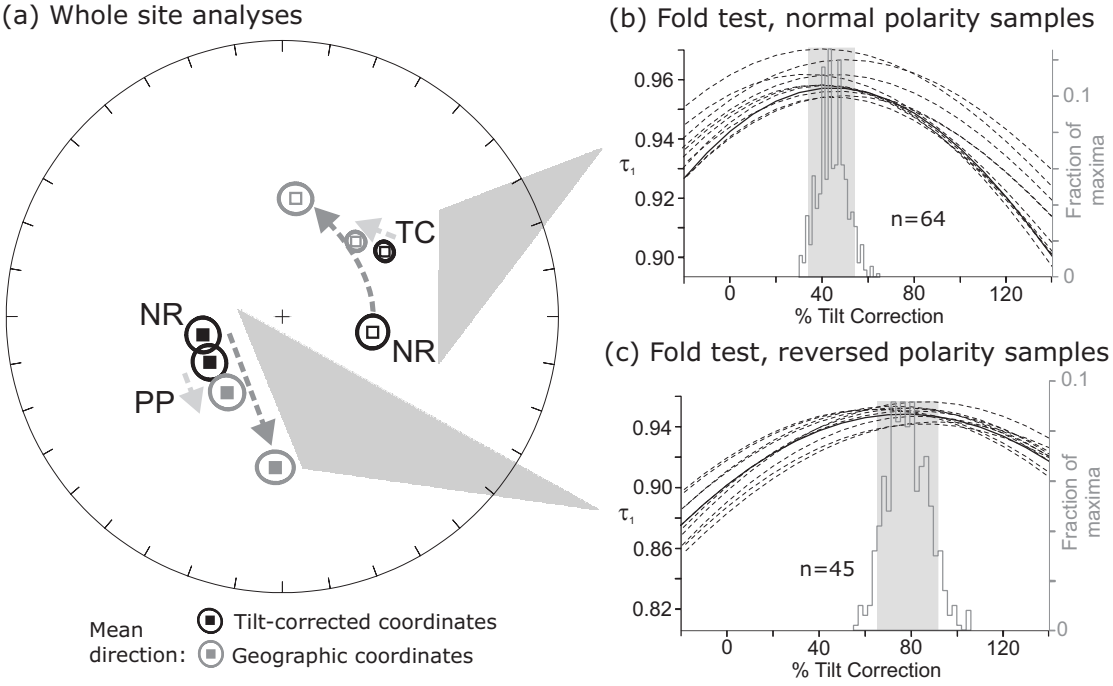

Figure 6.4: (a) Calculated mean directions and α_{95} error ellipses in both geographic and tilt-corrected coordinates for the TC, PP, and NR localities, Mahia Peninsula. Dashed arrows demonstrate how the directions from the different localities are brought into better agreement by reversing the tilt correction. (b) Bootstrap fold test of Tauxe and Watson (1994), applied to normal polarity ChRMs from TC and NR. Variation of the principal eigenvector τ_1 with various degrees of unfolding is depicted with dashed lines for different para-data sets; the distribution of maxima for these data sets is shown by the histogram. The 95% confidence interval (grey shading) puts the maximum at 34–54% unfolding, indicating a synfolding magnetization. (c) Fold test applied to reversed polarity ChRMs from PP and NR. The 95% confidence interval for the maximum value of τ_1 is at 65–92% unfolding, indicating a synfolding magnetization acquired earlier than the normal polarity remanence.

Table 6.2: Summary of paleomagnetic results from localities included in this study.

Locality	D (°)	I (°)	α_{95} (°)	k	Reference
Mahia Peninsula (Fig. 6.1b)					
TC[1]	57.5	-53.8	2.8	54.1	this study
NR[1]	99.7	-62.8	4.7	63.3	this study
	256.9	65.9	5.0	36.4	
PP[1]	237.8	64.5	5.0	36.2	this study
Rakauroa (Fig. 6.1c)					
MS	198.9	43.3	8.1	12.6	Chapter 4
OR	195.5	47.5	5.8	16.3	Chapter 4
AB		PDF			Chapter 4
Coast North of Gisborne (Fig. 6.1a)					
WU	85.6	-49.5	4.5	55.5	Chapter 5
	206.8	63.1	7.0	18.7	
Wairoa Syncline (Fig. 6.1c)					
WH		PDF			this study
BG		PDF			this study
Marlborough (Fig. 6.1a, d)					
SV	223.5	58.7	3.1	67.1	Roberts (1992)
UB	201.3	59.0	1.8	48.2	Roberts (1992)
WB	204.2	67.0	3.6	58.1	Roberts (1992)
BR	212.6	59.5	2.0	37.5	Roberts (1992)
CS	174.8	59.3	2.8	50.8	Roberts (1992)
RB	211.6	61.8	3.9	56.5	Roberts (1992)
WV	199.6	60.6	2.4	84.6	Roberts (1992)
NC	215.4	59.8	3.5	61.1	Roberts (1992)

Mean directions are given in tilt-corrected coordinates. [1]Localities with synfolding magnetizations; these directions are therefore not indicative of tectonic rotations.

6.3.3 Early and late magnetizations, Waihau Beach

Two distinct magnetizations with opposite polarity, both with weak NRM intensities (7% of samples having intensities $>5\times10^{-4}$ Am^{-1}), and with a 60° difference in declinations, were reported from a section of massive, grey mudstone, with interbedded tuffaceous layers, at Waihau Beach (WU) (Fig. 6.1a; Table 6.2). The large discrepancy in declinations can only be accounted for if several Myr of vertical-axis rotation has occurred between the acquisition of these two magnetizations (Chapter 5). The later-forming, reversed polarity remanence has only patchily grown within the section, which results in an apparent reversal sequence. SEM observations confirm that both polarities are chemical remanent magnetizations (CRMs) carried by greigite (Chapter 5).

6.3.4 Strong present-day field overprint, Wairoa Syncline

Two localities were sampled across the Wairoa Syncline (Fig. 6.1c): a roadside outcrop of interbedded silty mudstones and sandstones, with a steep northwest dip, near Waterfall Hill (WH); and a section of massive, sandy mudstone with occasional sandstone beds exposed on the northern bank of the Hangaroa River near Burgess Road (BG). NRM intensities of samples from BG were higher than at WH (with 44% and 6% of samples $>5\times10^{-4}$ Am^{-1}, respectively). However, demagnetization data indicate that both localities are dominated by a low temperature, low coercivity remanence component, which aligns with the present-day field direction (D = 20°, I = -64°) before tilt correction, indicating that it is a viscous overprint (Fig. 6.5). The low MDF and unblocking temperatures indicate that, in contrast to the nearby Rakauroa localities, no older paleomagnetic signal has been preserved, which is a common phenomenon in this region (Mumme et al., 1989).

6.3.5 Marlborough

Extensive paleomagnetic sampling of fine-grained Late Miocene to Pliocene sediments has been undertaken in the Marlborough region, at the southern end of the Hikurangi margin (Fig. 6.1a, d), for tectonic (Roberts, 1992; Little and Roberts, 1997) and stratigraphic (Turner et al., 1989; Roberts et al., 1994) studies. Vertical axis rotations inferred from paleomagnetic data correlate well with deviations in the strike of a vertical structural fabric in the underlying Late Jurassic to Early Cretaceous Torlesse basement rocks (Little and Roberts, 1997), which suggests relatively early remanence acquisition dates.

Previously unanalysed paleomagnetic samples from the collection of Roberts (1992) provide a larger data set for interpreting the magnetic properties of Neogene sediments from New Zealand. Samples were stepwise AF demagnetized before

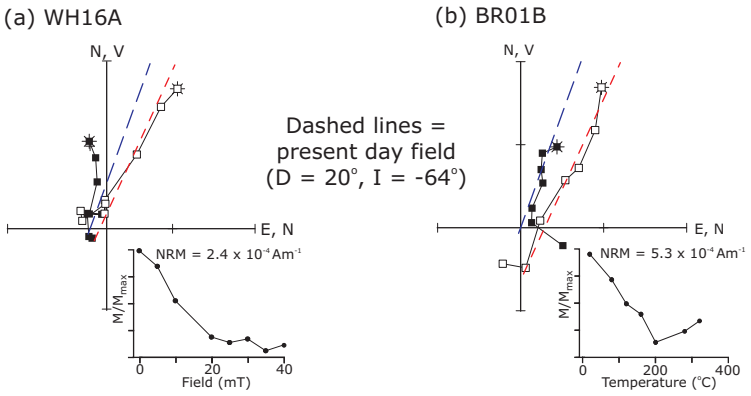

Figure 6.5: Vector component plot of (a) AF demagnetization data for sample WH16A, and (b) thermal demagnetization data for sample BG01B (symbols as in Fig. 3). Data are plotted before correction for bedding tilt, and show only a low coercivity, low temperature component aligned with the present day field (dashed lines) which is interpreted as a viscous overprint.

preparation for VSM and SEM analyses. NRM intensities were generally higher than those observed in localities from the northern Hikurangi margin, with an average of 51% of samples having intensities $>5\times10^{-4}$ Am^{-1} (Table 6.1). Although AF demagnetization was found to be generally ineffective in the original studies (Turner et al., 1989), directions comparable to previously published thermal demagnetization data (Table 6.2) were obtained from Upton Brook (UB), Sea View (SV), White Bluffs (WB), and Waihopai Valley (WV). At other localities, particularly Richmond Brook (RB), Needles Creek (NC) and Camp Stream (CS), lengthy storage (15 years) in an unshielded environment appears to have led to the development of strong secondary overprints.

6.4 Rock magnetic and SEM observations

Greigite has already been clearly identified as a remanence carrier in samples from Upton Brook (UB) and Waihau Beach (WU), by X-ray diffraction (XRD) on magnetic separates (Roberts and Turner, 1993) and SEM analyses of polished sections (Chapter 5), respectively; this provides a useful starting point for our rock magnetic measurements. The FORC distribution for sample UB192A (Fig. 6.6a), which is from close to the stratigraphic interval where greigite was reported by Roberts and Turner (1993) indicates a large population of strongly interacting SD grains with a peak coercivity of ∼60 mT, which is typical of greigite (Roberts et al., 2000). In contrast, the distribution for sample WU21A lies closer to the origin of the FORC diagram, with a slight peak at ∼20 mT (Fig. 6.6b, d). Such low coercivities have not previously been considered indicative of sedimentary greigite, which is generally associated with high coercivities of the type indicated in Fig. 6.6a (Roberts, 1995b). A large peak at the origin of the FORC distribution in

both samples, most easily seen in profiles along the B_c axis (Fig. 6.6c, d), indicates a significant reversible component of magnetization due to paramagnetic and superparamagnetic (SP) particles (Pike, 2003). Pike et al. (2001) demonstrated that thermal relaxation in a population of single domain (SD) grains will progressively shift a FORC distribution to lower B_c; in the extreme case of a sample dominated by SP particles, the FORC distribution will be centred on the origin of the FORC diagram (Pike et al., 2001). It therefore appears that in addition to stable SD greigite, sample WU21A contains a substantial SP population, which causes the FORC distribution to shift to lower coercivities and also contributes to a large reversible ridge (Fig. 6.6d).

Large SP populations will also alter bulk hysteresis parameters, decreasing M_r/M_s and markedly increasing B_{cr}/B_c (Tauxe et al., 1996; Dunlop, 2002), which is consistent with the position of sample WU21A on a Day et al. (1977) plot (Fig. 6.6e). A similar range of magnetic properties is exhibited by all samples in this study, which also have FORC distributions with a measurable reversible ridge at the origin consistent with the presence of a sizeable SP (or paramagnetic) contribution. On a Day plot, the samples follow a trend that resembles theoretical SD-SP mixing curves for (titano)magnetite (Dunlop, 2002) (Fig. 6.6e). Although strict numerical comparison with the results of Dunlop (2002) cannot be made, the magnetic behaviour of SD–SP greigite mixtures broadly resembles that expected for (titano)magnetite mixtures. Changes in magnetic properties amongst these samples therefore appear to be linked to a change in the relative proportions of thermally stable SD and unstable SP grains. This relationship is made clear by data from TC (Fig. 6.7), which establish an explicit linkage between demagnetization behaviour, hysteresis properties, and the FORC distribution. As shown in Fig. 6.7a, stably magnetized samples that acquire GRMs at high AFs (TC08B; see also Fig. 6.3c) have low B_{cr}/B_c (<1.5) and $M_r/M_s \approx 0.5$, approaching SD-like values, whilst their FORC distributions also indicate a large population of magnetostatically interacting stable SD grains (GRM acquisition by SD greigite during AF demagnetization is a well-established phenomenon (e.g. Snowball, 1997)). Samples that still have a stable ChRM, but which do not acquire a GRM (TC28A; see also Fig. 6.3b) have elevated B_{cr}/B_c (≈ 3.5) and a FORC distribution similar to that seen for sample WU21A, with a large reversible ridge, thermal relaxation of the SD assemblage, and reduced magnetostatic interactions. Finally, samples from an unstably magnetized horizon (Fig. 6.3a), with no clear ChRM and $B_{cr}/B_c \geq 7$ (TC23A), have a FORC distribution almost exclusively consisting of thermally relaxed SP particles. Increasing B_{cr}/B_c also corresponds with wasp-waisted hysteresis loops (Fig. 6.7b), a further indication of an increasingly

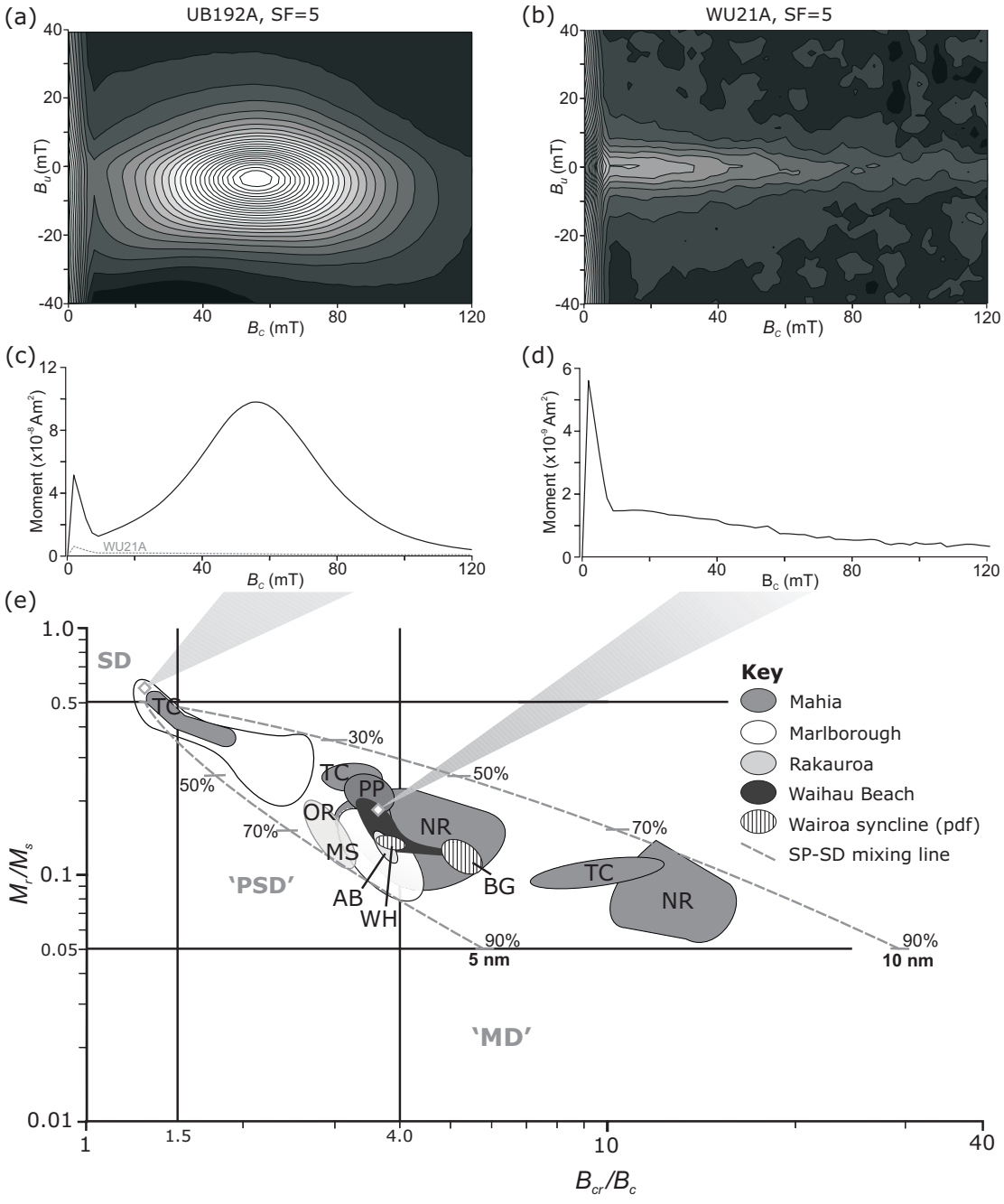

Figure 6.6: (a, b) FORC distributions for samples UB192A and WU21A, which are both known to contain greigite, interpreted as (a) a population of SD greigite with strong magnetostatic interactions, and (b) a smaller population of SD greigite, with minimal interactions and a coercivity distribution shifted toward the origin by thermal relaxation. (c, d) Profiles through the FORC distribution at $B_u = 0$ for both samples, illustrating the large reversible ridges at $B_c = 0$. (e) Hysteresis parameters for all samples in this study, plotted according to Day et al. (1977). Compared to the SD-like values of sample UB192A, the large SP population of sample WU21A has reduced M_r/M_s and increased B_{cr}/B_c; many other samples from the Hikurangi margin also plot in the same region. Theoretical curves for mixtures of SD and SP (titano)magnetite (Dunlop, 2002) have been plotted for 5 nm and 10 nm SP grains (% refers to % SP grains), although the assumption of a constant SP grain size is probably not valid in this case.

dominant SP contribution (Tauxe et al., 1996). Normalised FORC profiles for representative samples from each of these groups (Fig. 6.7c) clearly show that as the relative height of the stable SD peak decreases, thermal relaxation effects become more dominant, shifting the higher coercivity distribution from a clear peak centred at ∼60 mT to a flatter profile with lower B_c values. All of these observations are consistent with the increase in SP content indicated by comparison to theoretical SD–SP mixing curves (Fig. 6.7a), as is the increased relative magnitude of the reversible ridge (RR) in the profiles of Fig. 6.7c. A variable paramagnetic contribution due to lithological changes in the TC section (Fig. 6.3a) cannot be ruled out as the cause of variations in the magnitude of RR. Nevertheless, the increasing ratio between the two peaks of the FORC distribution (RR/SD, see inset in Fig. 6.7a) seems to provide a qualitative measure of the increasing SP component.

Further support for a common magnetic mineralogy in these samples comes from SEM observations (Fig. 6.8): abundant iron sulphides are seen in all samples, commonly forming aggregates with at least two distinct growth phases. The first generation consists of framboidal pyrite (P), often with euhedral overgrowths resulting from progressive recrystallization in evolving pore waters during early diagenesis (Raiswell, 1982). Later generations of space-filling pyrite (P2) and greigite (G) have then grown around these framboids. The greigite invariably has a finer grain size than P2, and appears to have formed by neoformation on the surfaces of the earlier framboids (Fig. 6.8b, c, e, i), and also as isolated patches between silicate grains (Fig. 6.8c, l) or within the space filling matrix (Fig. 6.8e, k). These growth relationships suggest that the greigite either formed earlier than, or penecontemporaneously with, P2.

At OR, which is one of the localities where early remanence acquisition is verified by a fold test (Chapter 4), early framboidal pyrite P is partially or completely surrounded by amorphous silica cement (Figs. 6.8e, f), which appears to have limited the growth of later generations of iron sulphides. Where P2 and G have developed, the growth relationships appear to be similar to that described above; however, an earlier generation of greigite is also present as framboids rimmed by neoformed pyrite (Fig. 6.8f).

Greigite neoformation between the cleavages of detrital sheet silicates (Fig. 6.8h) is also common in many samples. This has implications for the timing of remanence acquisition because, compared to magnetite, iron-bearing phyllosilicates are relatively unreactive to sulphide, requiring thousands of years for partial dissolution to occur (Canfield et al., 1992; Jiang et al., 2001; Roberts and Weaver, 2005).

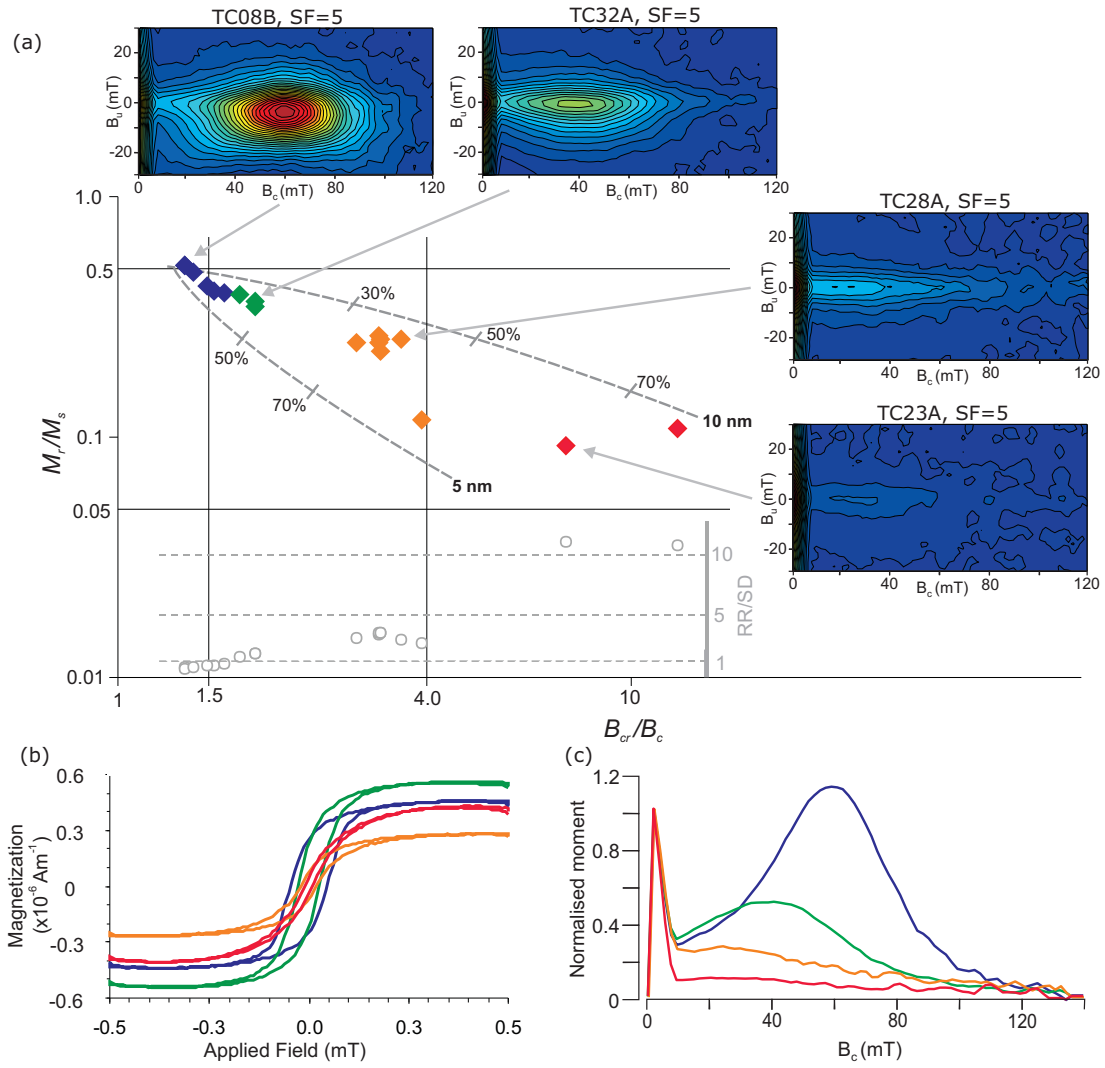

Figure 6.7: (a) Day plot illustrating the relationship between varying hysteresis ratios and the FORC distributions of selected samples from locality TC. SD-SP mixing curves (Dunlop, 2002) are again plotted for reference. Decreasing M_r/M_s and increasing B_{cr}/B_c, consistent with an increase in SP content, accompany the lower coercivity distribution and increased thermal relaxation of the stable SD population on the FORC distribution. The relative magnitude of the reversible ridge at $B_u = 0$ also increases, as shown by the inset plot of RR/SD, the ratio of the heights of the reversible ridge and the SD peak. (b) Hysteresis loops for selected samples from (a), with the paramagnetic slope corrected. Samples with higher B_{cr}/B_c (TC23A, 28A) are more wasp-waisted than samples with more SD-like values (TC08B, 32A), which is diagnostic of a larger SP contribution (Tauxe et al., 1996). (c) Profiles along the B_c axis of FORC distributions from (a), normalised to the peak of the reversible ridge at $B_c = 0$. As the SD peak gets proportionally smaller, it also shifts toward the origin, due to thermal relaxation of the proportionally larger SP population.

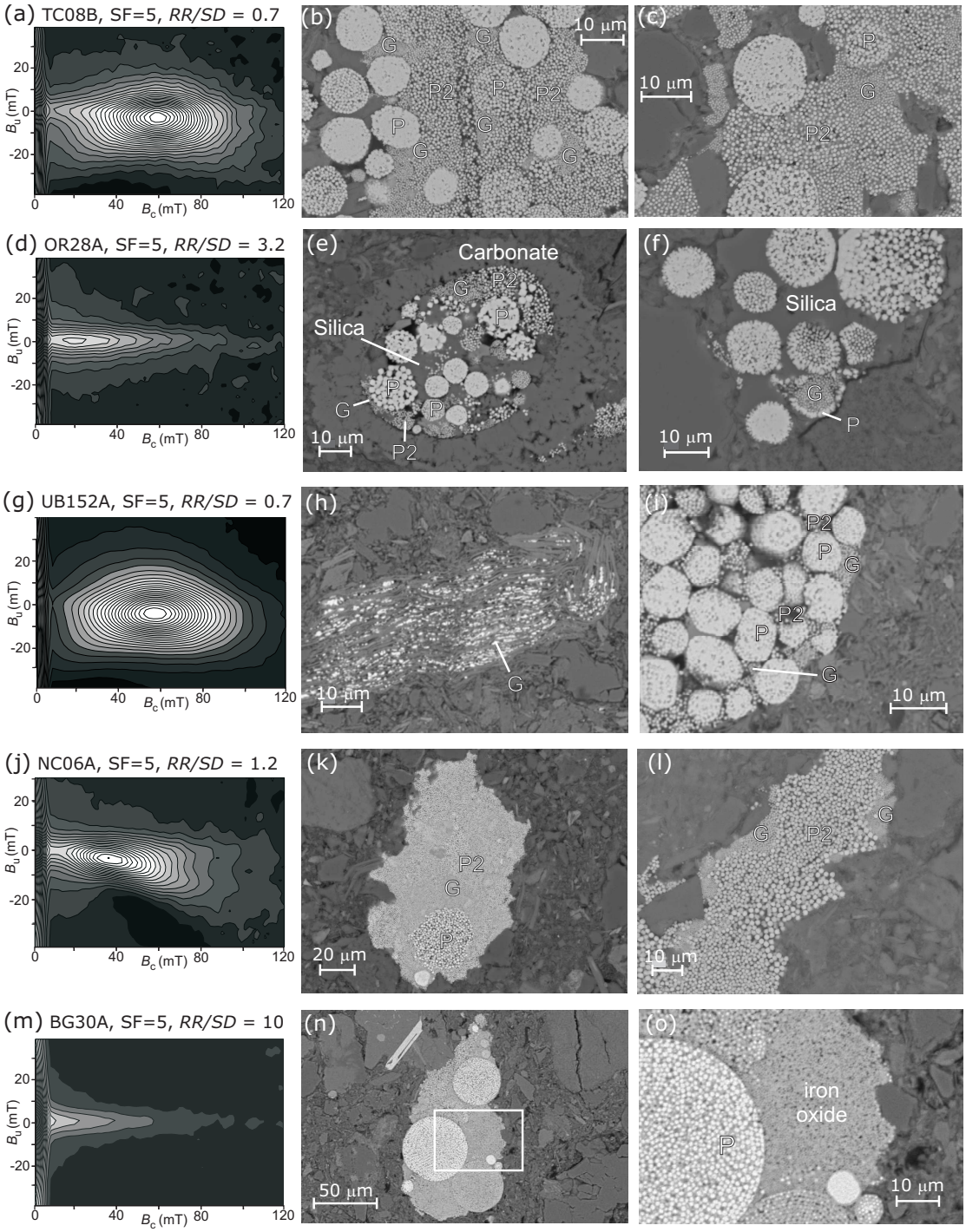
(a) TC08B, SF=5, RR/SD = 0.7
(b)
(c)
(d) OR28A, SF=5, RR/SD = 3.2
(e)
Carbonate
Silica
(f)
Silica
(g) UB152A, SF=5, RR/SD = 0.7
(h)
(i)
(j) NC06A, SF=5, RR/SD = 1.2
(k)
(l)
(m) BG30A, SF=5, RR/SD = 10
(n)
(o)
iron oxide
G
P
P2
10 µm
20 µm
50 µm
B_u (mT)
B_c (mT)

In many samples, EDS analyses of the iron sulphides reveal elevated Fe:S ratios and measurable oxygen peaks in the absence of silicate and carbonate minerals, suggesting that they are oxidised to some degree. At sites where there is no trace of an ancient paleomagnetic signal, this oxidation has extensively degraded later iron sulphides, replacing them with amorphous iron oxide (Fig. 6.8n, o). The FORC distributions for such samples are dominated by a large reversible component of magnetization (Fig. 6.8m).

6.5 Discussion

Paleomagnetic data demonstrate that the magnetizations of Neogene sediments from New Zealand are often complex. The late-forming (>1 Myr after deposition) CRMs on Mahia Peninsula and Waihau Beach require involvement of an authigenic phase, such as greigite, but our SEM observations also link greigite with early-forming remanences in the Rakauroa and Marlborough region. The samples share certain aspects of their demagnetization behaviour, particularly magnetic unblocking above 250°C, the onset of thermal alteration at ∼350°C, and a general unresponsiveness to AF treatment, with many other New Zealand Cenozoic mudstones, which suggests that fine-grained greigite may be common in these rocks.

Figure 6.8 ***(preceding page)*:** Representative FORC distributions and backscattered electron microscope images illustrating microtextures of authigenic greigite (G) and pyrite (P, P2). (a-c) Sample TC08AB, which (a) is dominated by thermally stable SD greigite, with strong magnetostatic interactions. A low RR/SD value indicates a small SP contribution (low reversible component of magnetization). (b) Typical iron sulphide aggregate, with neoformed greigite (G) on the surface of recrystallized early pyrite framboids (P), and a later space-filling pyrite generation (P2). (c) Higher magnification view of another aggregate with similar textural relationships. (d-f) Sample OR28A, showing (d) thermal relaxation of SD greigite due to a large SP population, indicated by elevated RR/SD. (e) Iron sulphide growth within a calcareous microfossil. Amorphous silica cement has grown around early pyrite (P), restricting growth of later iron sulphides (G, P2). (f) An early greigite framboid (G) rimmed by pyrite (P) and surrounded by silica cement. (g-i) Sample UB152A, which (g) contains thermally stable SD greigite. (h) Neoformation of greigite (G) between the cleavages of a detrital sheet silicate. (i) Aggregate consisting almost entirely of recrystallized pyrite framboids (P), with limited greigite neoformation (G) on their surfaces. (j-l) Sample NC06A, with (j) slight thermal relaxation of the SD population. (k) Iron sulphide aggregate volumetrically dominated by later iron sulphide generations (G, P2). (l) Greigite (G) neoformed on the surfaces of detrital silicate grains, and surrounded by space-filling pyrite (P2). (m-o) Sample BG30A, which (m) is dominated by a large reversible component of magnetization, with negligible stable SD greigite. (n) Oxidised iron sulphide aggregate. (o) Close-up of the aggregate in (n) where later iron sulphide generations have been replaced by amorphous iron oxide. Early pyrite framboids (P) have also been partially affected.

Our observations contrast with previous studies, which have generally failed to definitively identify the dominant magnetic carrier (Roberts and Turner, 1993; Wilson and Roberts, 1999; Turner, 2001). Because the remanence is generally carried by small amounts of greigite, obtaining sufficiently clean magnetic extracts to enable detection by XRD would be difficult. The FORC profile of sample UB192A (Fig. 6.6c), where greigite was detected by XRD (Roberts and Turner, 1993), has an absolute magnetic moment that is an order of magnitude higher than that of most other samples, exemplified by sample WU21A (Fig. 6.6c, d); clear identification of greigite is therefore much simpler for samples like UB192A. However, such high concentrations of thermally stable greigite appear to be relatively rare in New Zealand sediments. Greigite is also typically a fine-grained component in the space-filling matrix of iron sulphide aggregates (Fig. 6.8), which might not survive the extraction process intact, leaving the more robust and/or volumetrically more significant pyrite framboids. This may explain the presence of pyrite in magnetic extracts, just as observations of greigite within chlorite cleavages (Fig. 6.8h) might explain the common occurence of chlorite in extracts in which greigite has been identified (Roberts and Turner, 1993).

The magnetic properties of these sediments are dominantly controlled by variable mixtures of SP and stable SD material, with a large SP component being common. The lack of any other identified magnetic minerals strongly suggests that greigite is also responsible for the SP signal. Greigite formation involves *in situ* nucleation and growth of ferrimagnetic grains; any individual grain must therefore initially be small and magnetically SP, before growing through the stable SD blocking volume and becoming capable of preserving a thermally stable ChRM. During the early stages of growth, most particles will be SP, with only a small number of larger grains having SD magnetic properties (Fig. 6.9a). With unlimited growth, all particles will eventually become SD; however, even when the average grain size moves past the SD threshold volume, significant amounts of SP material can remain in the rock (Fig. 6.9b). The magnetic signature of these samples is therefore consistent with populations of authigenic greigite, with variable grain size distributions ranging across the critical boundary for SP/SD behaviour. Differing proportions of SP and SD grains (Fig. 6.6e) appear to have resulted from greigite growth being arrested at slightly different times. A plot of the ratio RR/SD against B_{cr}/B_c for all studied samples (Fig. 6.9d) indicates that in the majority of cases, growth appears to have been arrested at a relatively early stage, resulting in the preservation of large amounts of SP greigite, FORC distributions centred near the origin, and elevated B_{cr}/B_c ratios. The relatively small amounts of stable SD greigite lead to weak NRMs. In some horizons at TC, and

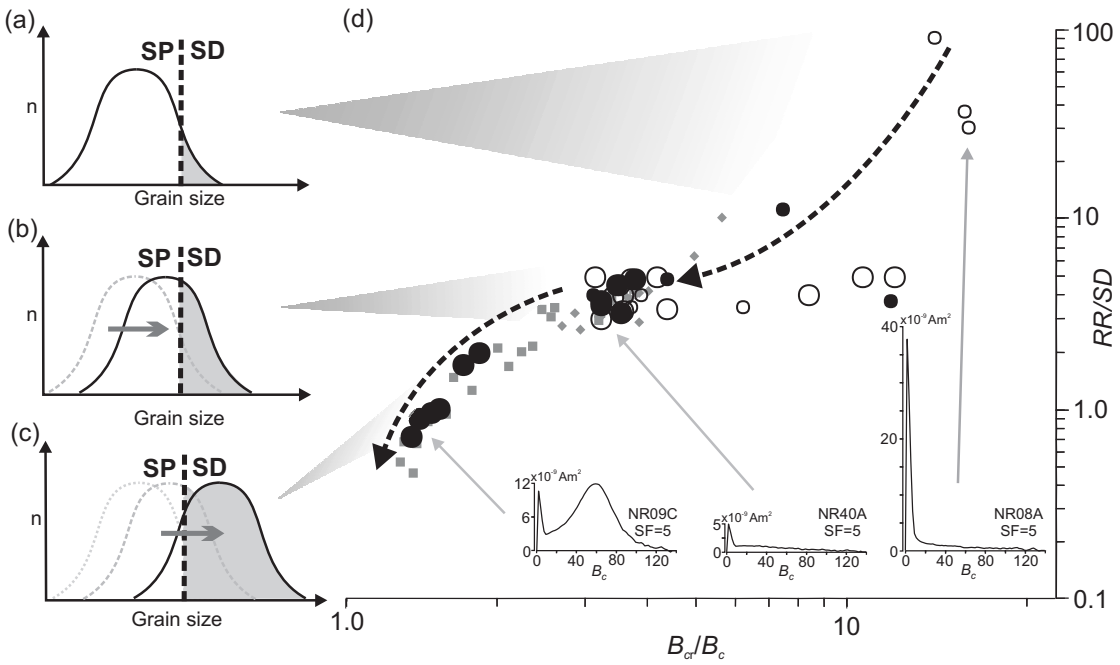

Figure 6.9: (a-c) Illustration of the progressive authigenic growth of greigite. (a) Just after initiation of growth all grains are small, and most will therefore be SP. (b) As the average grain size increases with further growth, a larger amount of greigite attains the blocking volume for stable SD behaviour, and can potentially retain a ChRM. A large SP population remains, however. (c) After the average grain size has moved past the blocking volume, SD grains begin to dominate the mixture. These distributions are linked to the relevant region of (d), a plot of B_{cr}/B_c against RR/SD, which is a qualitative measure of the relative proportions of SP and SD material in a sample. FORC profiles of samples at each stage of growth are inset for further clarification. Data from Mahia Peninsula (closed circles = normal polarity samples, open circles = reversed polarity, small circles = unstably magnetized) and Marlborough (squares) have been separated from data for other localities from the east coast of the North Island (diamonds). Greigite in most samples is still dominantly SP, apparently due to the early arrest of authigenic growth.

at many of the Marlborough localities, growth of greigite has progressed further, such that SD particles begin to dominate (Figs. 6.6a, 6.8a, 6.8g, 6.9c). At the other extreme, samples from unstably magnetized horizons at TC and NR have high RR/SD ratios and large reversible components on their FORC distributions (e.g. NR08A, Fig. 6.9d), which is consistent with the presence of a large population of SP grains, and may therefore represent greigite populations 'frozen' in the early stages of growth (Fig. 6.9a). The ability of rock magnetic measurements to constrain the varying proportions of SD and SP greigite in these rocks is of great potential importance; more detailed SEM analysis of grain size distributions may allow the threshold size for stable SD behaviour of greigite, which is currently poorly constrained, to be determined.

The factors governing the arrest of pyritization and consequent preservation

of greigite in these sediments are still not fully understood. There are clearly some lithological controls on this process, however. On the Mahia Peninsula, the older, reversed polarity, CRM is generally found in beds rich in volcanic material, whereas the later, normal polarity magnetization is associated with mudstone units (e.g. Fig. 6.3i). Futhermore, localities with abundant stable SD greigite tend to consist of very fine-grained mudstones, rather than the coarser siltstones and mudstones that dominate elsewhere in the Neogene sedimentary basins of New Zealand. These observations suggest that authigenic growth is being limited by underlying chemical controls. Geochemical analyses of fine-grained sediments from Taiwan that are magnetically dominated by stable SD greigite suggest that greigite preservation is favoured by a combination of limited organic carbon, which limits microbial production of dissolved sulphide, and high concentrations of reactive iron (Kao et al., 2004). In later diagenetic sulphidization events, sulphate limitation, resulting from closure of the system to seawater due to burial, may also be a factor. Geochemical analyses of New Zealand sediments are required to identify the mechanisms controlling greigite growth and grain size.

SEM analyses have also cast light on the source of the strong viscous overprints that are common in New Zealand Cenozoic sediments. In previous studies, unanchored demagnetization paths have indicated the presence of a high temperature magnetic component, that is thought to be carried by iron oxides such as hematite (Turner, 2001). Our observations of iron oxides replacing authigenic iron sulphides (Fig. 6.8n, o) demonstrate that these oxides, although not necessarily hematite, also have an authigenic origin, and that they are most likely a product of pyrite oxidation in percolating oxic ground water. Greigite, as the finest-grained iron sulphide phase, will also be highly reactive; the oxidation process will therefore involve replacement of SP and SD greigite, as well as paramagnetic pyrite, by SP iron oxides. As discussed above, authigenic growth produces large populations of SP grains, and magnetic viscosity associated with high concentrations of SP hematite is a well-documented phenomenon (Creer, 1961). Samples from the Rakauroa localities, and from WH and BG (Fig. 6.1c), where a strong viscous overprint is observed, have reduced M_r/M_s, which is consistent with the presence of additional SP hematite (Fig. 6.6e). Furthermore, at localities AB, WH and BG, where there is no identifiable ChRM beneath the overprint, samples have FORC distributions with a negligible SD component (Fig. 6.8m) and progressively increased B_{cr}/B_c indicative of increasing SP grain size (Fig. 6.6e); these changes are consistent with continued growth of SP iron oxides at the expense of SD greigite. Unfortunately, however, these variations are within the range observed at localities lacking a significant viscous component (Fig. 6.6e); strongly overprinted samples

therefore cannot be identified by rock magnetic measurements alone.

Perhaps the most significant results of our study relate to the timing of greigite formation. In two instances we have clearly shown that remanence acquisition post-dates deposition by >1 Myr; caution is therefore required when using paleomagnetic data for tectonic studies of the Hikurangi margin. For example, when properly corrected, synfolding magnetizations from the Mahia Peninsula indicate $44 \pm 5^{\circ}$ of tectonic rotation since 4–6 Ma, which requires a much higher rate of rotation than has been previously inferred (Wright and Walcott, 1986; Walcott, 1989). Late-forming greigite may be common, and if it is not identified both the rate and magnitude of tectonic rotations will be underestimated; this was the case at WU, where an earlier study found only the late-forming magnetization and incorrectly assumed that it was primary (Chapter 5; Thornley, 1996).

However, even at localities where greigite appears to have formed relatively early, multiple generations of iron sulphide growth, with later generations often being volumetrically dominant (e.g. Fig. 6.8b, k), as well as sulphidisation of phyllosilicates (e.g. Fig. 6.8h) both appear to require sulphide growth over a significant period of time following deposition, potentially tens of thousands of years in the latter case (Canfield et al., 1992). Such a delay is well within the constraints provided by field tests, which often still allow a considerable period of time for remanence acquisition. The magnetizations at Rakauroa are only constrained to within 1–2 Myr of deposition by a fold test (Chapter 4), although greigite associated with the first generation of framboids at OR (Fig. 6.8f) does suggest early growth. Protection of this early greigite generation by the surrounding amorphous silica cement might have contributed to the preservation of a pre-folding remanence. In Marlborough, paleomagnetically determined crustal rotations are systematically lower than the rotations seen in the underlying Torlesse basement fabric (Little and Roberts, 1997), although both estimates are generally within error of each other. This discrepancy might also be due to delayed remanence acquisition in the Neogene sediments, but other explanations are also possible (e.g. rotations occurring prior to deposition of the sedimentary cover). Nonetheless, our observations suggest that in New Zealand Cenozoic marine sediments a truly syn-depositional paleomagnetic signal is rarely preserved intact. At best, greigite that formed during later phases of sulphide growth is restricted, and is volumetrically dominated by earlier greigite, as has been documented in greigite-bearing sediments in Italy (Roberts et al., 2005).

Delays in remanence acquisition of even a few thousand years have potentially serious consequences for studies of short-period geomagnetic field behaviour. Even more troubling are the implications for magnetostratigraphy of results from the

WU and NR localities, where two differently timed magnetizations are patchily distributed at outcrop scale, producing a spurious apparent reversal sequence. The fact that similar patchy remagnetizations, involving late greigite growth and giving rise to false 'reversal' sequences, have been observed elsewhere (Sagnotti et al., 2005) suggests that this is not an isolated phenomenon. Furthermore, discriminating between earlier and later forming magnetizations appears to be difficult in the absence of paleomagnetic constraints: at WU, neither SEM observations (Chapter 5) nor rock magnetic measurements (Fig. 6.6) provide any clear means of discriminating between horizons with early and late forming greigite. Stably magnetized samples of both polarities at NR also cannot be distinguished by their magnetic properties (Fig. 6.9d). Unlike at WU, the fact that the two polarities formed at different times only became evident following the addition of paleomagnetic data from nearby localities; if samples from this locality were analyzed in isolation, the difference in mean directions is small enough that they might easily be thought to record a primary sequence of reversals.

It is possible that other techniques, particularly geochemical analysis (e.g. laser ablation δ^{34}S analysis on polished sections), might allow early and late forming greigite to be distinguished in these sediments. Currently, however, in the absence of diagnostic indicators from rock magnetic and SEM analyses, the use of paleomagnetic field tests to constrain the age of remanence acquisition of greigite is essential. Furthermore, the reversals test should be used with extreme care: the existence of apparent reversal stratigraphies resulting from patchy, differently timed remagnetizations involving greigite indicate that a positive reversals test is not necessarily diagnostic of an early magnetization.

Late remagnetizations involving greigite are not confined to New Zealand. Inconsistent geomagnetic polarities associated with later-forming greigite have been reported from Plio-Pleistocene sequences in Taiwan (Horng et al., 1998; Jiang et al., 2001) and the New Jersey margin (Oda and Torii, 2004), Miocene glaciomarine sediments from Antarctica (Sagnotti et al., 2005), and fine-grained Neogene sediments on the Italian peninsula (Florindo and Sagnotti, 1995), where ferrimagnetic iron sulphides are widespread (Sagnotti and Winkler, 1999), and where paleomagnetic data from greigite-bearing sediments have also been used to infer tectonic rotations (Speranza et al., 1997). It is becoming apparent that conditions amenable to greigite preservation are common in rapidly deposited continental margin deposits, which are often targeted for high-resolution studies of geomagnetic field behaviour. If greigite is present in these sequences, the possibility that the paleomagnetic record has been compromised by delayed remanence acquisition must be seriously considered.

6.6 Conclusions

Paleomagnetic measurements, combined with detailed rock magnetic and SEM analyses, demonstrate that the authigenic iron sulphide, greigite, which forms during reductive diagenesis, is a common remanence carrier in New Zealand Cenozoic mudstones. Although greigite can form during early diagenesis, in at least two instances authigenic growth has occurred >1 Myr after deposition. The resulting late remagnetizations can be irregularly distributed within an outcrop, and cannot be readily distinguished from earlier magnetizations by either SEM observations or by rock magnetic measurements. Remanent magnetizations are further affected by pyrite and greigite oxidation in oxic ground waters, forming fine-grained iron oxides that carry a dominant viscous overprint. Progressive oxidation of the iron sulphides eventually destroys any older paleomagnetic signal.

Late remagnetizations may seriously impact upon the reliability of magnetostratigraphic and tectonic studies, not only in the New Zealand region but also in similar sequences worldwide. In the light of our observations, *a priori* assumption of early remanence acquisition in sediments where greigite is present is extremely risky in the absence of confirmation from paleomagnetic field tests. Even an apparent reversal sequence can result from patchily distributed, diachronous magnetizations; the most reliable constraints come from structural field tests.

Chapter 7

Neogene tectonic rotations within the Australia-Pacific plate boundary zone, Hikurangi margin, New Zealand

Abstract Large, clockwise, vertical axis tectonic rotations of the Hikurangi margin, East Coast, New Zealand, have been inferred over both geological and contemporary timescales, from paleomagnetic and geodetic data, respectively. Previous interpretations of paleomagnetic data have laterally divided the margin into independently rotating domains, which is not a feature of the short-term velocity field; the domain concept is also difficult to reconcile with the large-scale boundary forces driving the rotation. New paleomagnetic results, rigorously constrained by field tests, demonstrate that late diagenetic growth of the iron sulphide greigite has occurred at up to 65% of sampling localities. When these remagnetizations are accounted for, similar rates, magnitudes, and timing of tectonic rotations are observed for the central and southern Hikurangi margin, which is consistent with all Neogene rotation being driven by realignment of the subducting Pacific plate. Rotations initiated at 8–10 Ma, possibly due to collision of the Hikurangi Plateau, and proceeded at rates of 7–14°/Myr during the Late Miocene and Pliocene before decelerating to the presently observed rates of 3–4°/Myr at 1–2 Ma. This deceleration is linked to initiation of strike slip on the North Island Dextral Fault Belt, when these originally reverse faults rotated into an orientation favourable for accommodating oblique motion. Deformation patterns in the Late Miocene and Pliocene were dominated by shortening in the southern Hikurangi margin and by extension in the north, which drove more rapid tectonic rotations about a pole ∼200 km closer to the plate boundary than the present rotation pole. Overall, the recognition of widespread remagnetizations, the lack of evidence for independently rotating domains, and the observation of tectonic rotation rates substantially higher than previously reported, which have been accommodated by a variety of structures since the Late Miocene, combine to provide a completely new view of the Neogene tectonic evolution of the Hikurangi margin.

7.1 Introduction

The Hikurangi margin structurally links the subduction zone to the north of New Zealand, with associated slab roll-back and back-arc spreading, to a zone of intra-continental transpression on the South Island of New Zealand, where underthrusting of buoyant continental crust (the Chatham Rise) impedes subduction and transfers inter-plate motion to the Marlborough and Alpine-Wairau faults (Fig. 7.1a). This transition is made less abrupt by subduction of anomalously thick oceanic crust of the Hikurangi Plateau (Davy and Wood, 1994; Wood and Davy, 1994) beneath the east coast of the North Island.

Vertical-axis tectonic rotations are an important feature of crustal deformation in this region, on both decadal and geological timescales. The short-term veloc-

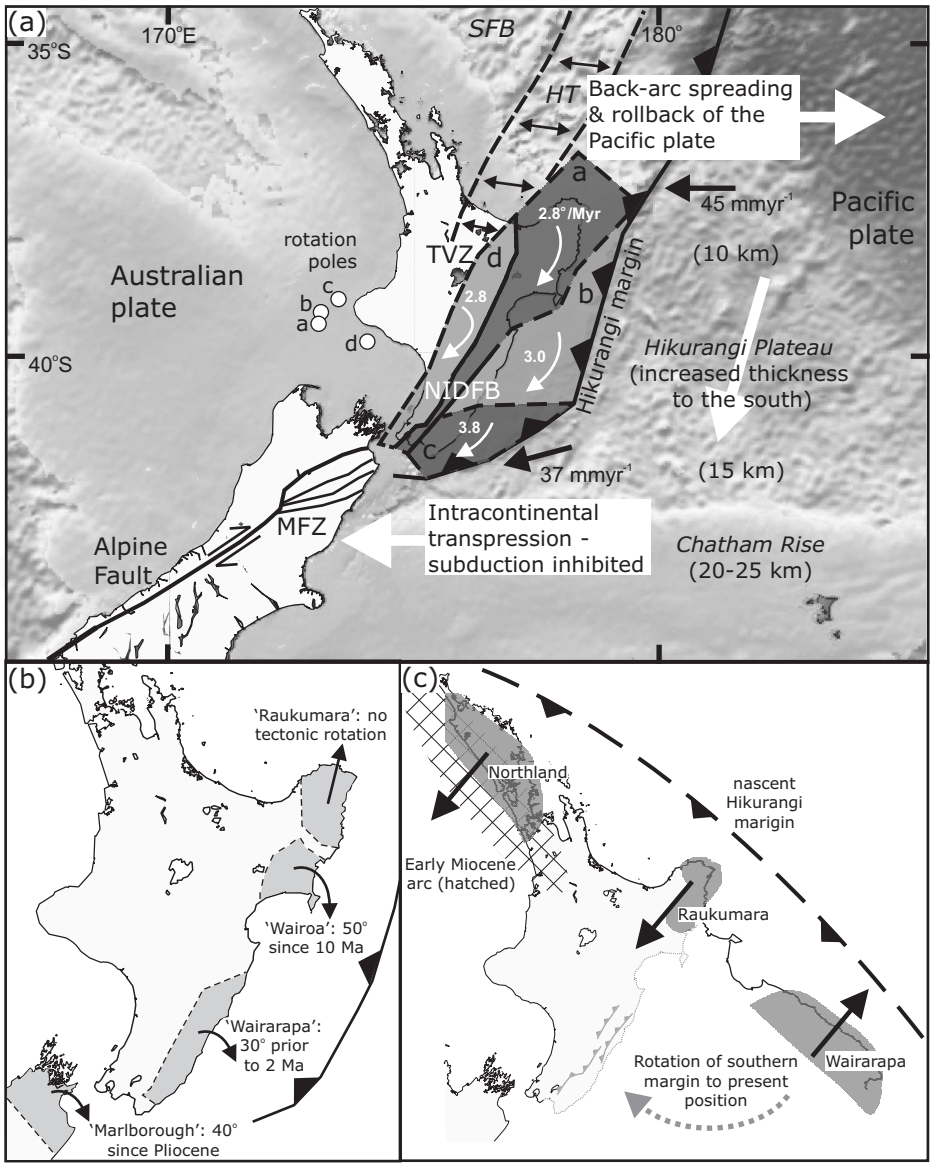

Figure 7.1: (a) Contemporary geodynamics of the New Zealand plate boundary region (bathymetry from Smith and Sandwell (1997)). Subduction of thickened oceanic crust (the Hikurangi Plateau) beneath the Hikurangi margin links subduction and back-arc spreading north of New Zealand with intra-continental transpression on the Alpine and Marlborough fault systems; the Hikurangi margin rotates clockwise in response to this transition. The rotating forearc is divided into a number of separate blocks to account for slip on faults of the North Island Dextral Fault Belt (NIDFB), following Wallace et al. (2004). SFB = South Fiji Basin; HT = Havre Trough; TVZ = Taupo Volcanic Zone; MFZ = Marlborough Fault Zone. (b) Summary of published paleomagnetic data from the Hikurangi margin, showing division into 'domains' based on inferred differences in the rates and magnitudes of tectonic rotations (cf. Walcott, 1989). (c) Early Miocene reconstruction, following Rait et al. (1991). Realignment of thrusts associated with the initiation of subduction forms a NW-SE trending margin that has subsequently rotated up to 90° clockwise.

ity field, derived from a combination of geodetic data and Quaternary fault slip rates (e.g. Beanland et al., 1998; Beavan and Haines, 2001; Wallace et al., 2004), indicates that the entire forearc region is actively rotating clockwise at rates of ∼3–4°/Myr with respect to the Australian plate (Fig. 7.1a). Paleomagnetic studies of tectonically uplifted marine sediments on the east coast of New Zealand (Walcott et al., 1981; Walcott and Mumme, 1982; Mumme and Walcott, 1985; Wright and Walcott, 1986; Mumme et al., 1989; Roberts, 1992, 1995a; Vickery and Lamb, 1995; Thornley, 1996; Little and Roberts, 1997) also routinely report large clockwise declination anomalies (Fig. 7.1b), indicating that tectonic rotations are also a long-term feature of deformation on the Hikurangi margin.

A striking feature of the paleomagnetic data is the apparent lateral variation in the rate and timing of rotations on the Hikurangi margin during the Neogene (Fig. 7.1b). Declination anomalies of 30–40° in Late Miocene (6–11 Ma) sediments from the central part of the Hikurangi margin (Wright and Walcott, 1986) are consistent with the present rate of rotation (Chapter 4). However, Early Miocene sediments from the northeast North Island (Raukumara Peninsula) indicate no tectonic rotation with respect to the Australian plate (Walcott and Mumme, 1982; Mumme et al., 1989; Thornley, 1996), and sparse data from the southern North Island have been interpreted to indicate Late Miocene rotations that had ceased by 2 Ma (Walcott et al., 1981; Lamb, 1988). Additionally, in the Marlborough region (northeast South Island), two distinct periods of rotation, in the Early Miocene and from the early Pliocene (c. 4 Ma) onward, have been observed (Walcott et al., 1981; Lamb, 1988; Roberts, 1992, 1995a; Vickery and Lamb, 1995; Little and Roberts, 1997; Hall et al., 2004). These observations led to the proposal that the margin is divided into discrete, fault-bounded 'domains', with independent tectonic histories (Lamb, 1988; Walcott, 1989) (Fig. 7.1b).

Wallace et al. (2004) modelled contemporary deformation using a number of rotating blocks, bounded by major faults of the North Island Dextral Fault Belt (NIDFB) (Beanland, 1995); however, these blocks do not correlate to the paleomagnetically defined domains (Fig. 7.1a, b). Furthermore, the domain concept greatly complicates attempts to relate long-term tectonic rotations to present geodynamics (e.g. Walcott, 1989). Along the present Hikurangi margin, the thickness of the subducting Hikurangi Plateau increases to the south (Davy and Wood, 1994) (Fig. 7.1a), gradually increasing coupling across the plate interface (Reyners, 1998), and creating a smooth margin-normal shear gradient that is most easily accommodated by bulk clockwise rotation of the entire margin. Whilst this mechanism can account for the similar rates and poles of rotation of the blocks modelled by Wallace et al. (2004) (Fig. 7.1a), it is difficult to reconcile with the

domain model, which requires much smaller scale variation of the forces driving rotation to allow large differential rotations between adjacent crustal blocks. A possible source of this variation, postulated 'tears' in the subducting plate (Reyners, 1983; Smith et al., 1989) that were thought to correlate to the boundaries of the paleomagnetic domains, have since been ruled out by high-resolution surveys of seismicity along the plate boundary (Ansell and Bannister, 1996). Within the forearc itself, structures that could have accommodated large differential rotations between adjacent blocks are also not apparent from surface geology.

Key features of the current tectonic regime, including the NIDFB and the Taupo Volcanic Zone (TVZ), appear to have developed since 1–2 Ma (Beanland, 1995; Wilson et al., 1995; Beanland et al., 1998); prior to this, different structures must have been involved in accommodating inter-plate motion. The apparent mismatch between paleomagnetically and geodetically determined rotations may therefore be a consequence of the ongoing evolution of structures in the New Zealand plate boundary zone. Some support for this hypothesis comes from examination of early Miocene thrust sheets from Northland (Northland Allochthon) (Ballance and Spörli, 1979; Spörli, 1982; Rait, 2000), the northern Raukumara Peninsula (East Coast Allochthon) (Stoneley, 1968; Rait et al., 1991), and the southern Wairarapa (Chanier and Férrière, 1989) (Fig. 7.1c). In their present orientation, the Wairarapa thrust sheets record a northwest-southeast shortening direction; this contrasts with thrusts in Northland and Raukumara, which were emplaced from the northeast. Tectonic reconstructions (King, 2000; Rait et al., 1991) suggest that upon initiation of subduction at 23–20 Ma, all thrusts, and the margin itself, were oriented northwest-southeast, in alignment with the Early Miocene Northland volcanic arc (Herzer, 1995) (Fig. 7.1c). Alignment of the Raukumara thrusts with those in Northland suggests that, in agreement with paleomagnetic data, the northern part of the margin has experienced negligible rotation since the Early Miocene, and that the rotation of this region observed in the present velocity field must have begun recently. However, these reconstructions also suggest that in the same period the southern part of the margin has rotated up to 90° (Fig. 7.1c), which is greater than the maximum rotations recorded by previously published paleomagnetic data from the North Island.

Some of the difficulty in reconciling paleomagnetic data from the Hikurangi margin with both geodetic and other geological data may be due to the questionable reliability of some of the published paleomagnetic results. Widespread use of blanket demagnetization techniques in early studies often failed to completely remove the strong present day field (PDF) overprints that are common in this region (Chapter 4); detailed stepwise demagnetization is necessary to assess whether such

overprints have been successfully removed. Even more significantly, recent observations indicate that the magnetization of New Zealand Neogene marine sediments is commonly carried by the authigenic iron sulphide, greigite (Chapters 5 and 6; see also Roberts and Turner, 1993). Numerous studies of fine-grained sediments have shown that where greigite is present, remanence acquisition can occur during late diagenesis, potentially several Myr after deposition (e.g. Florindo and Sagnotti, 1995; Horng et al., 1998; Roberts and Weaver, 2005; Sagnotti et al., 2005; see also Chapters 5 and 6). Good constraints on the timing of remanence acquisition from paleomagnetic field tests are usually lacking in the published data from the Hikurangi margin. Late remagnetizations may therefore have gone unrecognized, leading to a loss of information regarding tectonic rotations, and compromising attempts to reconstruct the deformation history of the plate boundary region.

In this study, we present a major new paleomagnetic data set from the East Coast of the North Island, New Zealand, which demonstrates that remagnetizations are widespread along the Hikurangi margin. At sites where the timing of remanence acquisition can be properly constrained by structural field tests, the magnetization often post-dates deposition by several Myr. We show that once these remagnetizations are accounted for, a significantly different history of tectonic rotations in the New Zealand plate boundary zone emerges, which can be more easily reconciled with active deformation.

7.2 Sample collection and analysis

Standard (25 mm diameter) paleomagnetic cores were collected from 38 localities in various Neogene sedimentary basins distributed along the Hikurangi margin (Fig. 7.2a; Table 7.1). The approximate stratigraphic intervals sampled at these localities are shown on generalized stratigraphic columns in Figure 7.3. Fine-grained sediments exposed in sequences with unambiguous bedding orientation were targeted in all cases. Continuous exposures of >10 m of section were preferred, in order to ensure that the effects of secular variation were properly averaged. To minimize viscous magnetic overprints, weathered surficial material was removed from the outcrop prior to sampling, and, upon retrieval, cores were immediately placed in a mu-metal shield. Cores were cut into samples of 21 mm length; paleomagnetic measurements were then made using a 2G-Enterprises cryogenic magnetometer (sensitivity of $\sim 10^{-12}$ Am^2), situated in a magnetically shielded laboratory at the National Oceanography Centre, Southampton (NOCS). Both thermal (40° steps from 80°C to 400°C) and alternating field (AF) (5 mT steps to 60 mT) demagnetization techniques were used; the low-field bulk magnetic susceptibility was measured for thermally demagnetized samples after each heating step to monitor for thermal alteration.

Characteristic remanent magnetization (ChRM) directions were calculated using principal component analysis of stepwise demagnetization data (Kirschvink, 1980). Mean directions and confidence limits for stably magnetized localities were calculated according to Fisher (1953). If great circle demagnetization paths were observed at localities where strong overprints were prevalent, they were used to augment ChRM data (McFadden and McElhinny, 1988) in order to better constrain the mean direction. Where localities of similar age were distributed across well-defined structures, fold tests were applied to ChRM data in an attempt to constrain the timing of remanence acquisition.

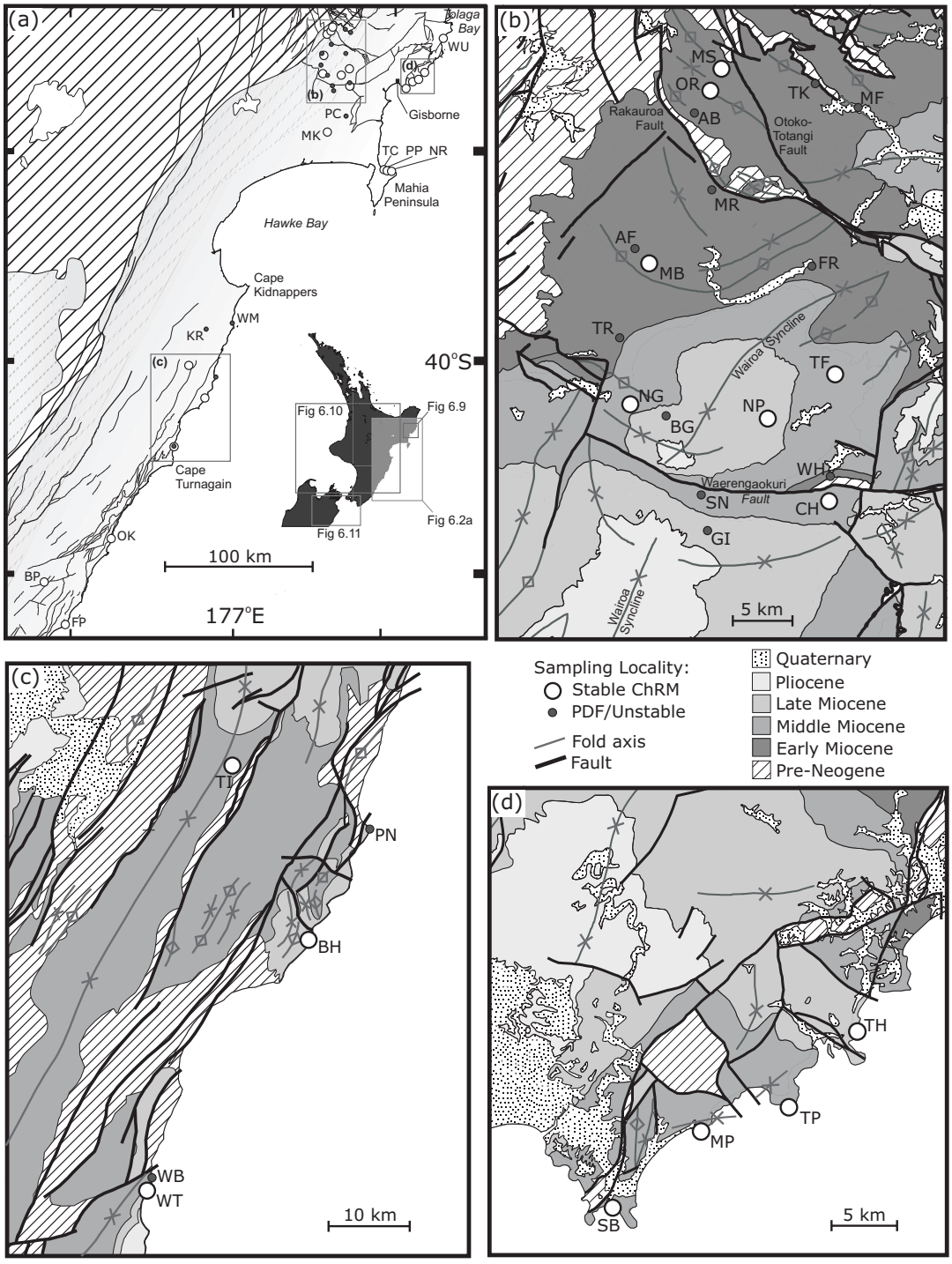

Figure 7.2: Distribution of sampling localities on the Hikurangi margin. Densely sampled areas in (b) the Wairoa Syncline and environs, (c) Southern Hawke Bay, and (d) the coastal region between Gisborne and Tolaga Bay (pre-Neogene outcrop in this area is the result of smectite diapirism), are enlarged to show more detail. Full locality names are given in Table 1; (b) and (d) are adapted from the QMAP dataset (Mazengarb and Speden, 2000); (c) is modified from Kingma (1962).

Table 7.1: Location and geological details of sampling localities in this study.

Locality	Grid Reference	Age (Ma)	Principal Lithology	Average Bedding	Sampled Section	Behaviour
			Rakauroa (Fig. 7.2b)			
MB *Mokonui Bridge*	X17/074860	16.8±0.8	Dark, calcareous mud/siltstones	027/18 SE	33 m	S
MS *Matawai Station*[1]	X17/128009	20.4±1.4	Blue-grey mudstones, sandstones	088/54 S	47 m	SO
OR *Oliver Road*[1]	X17/118988	20.4±1.4	Grey and brown sandy mud/siltstones	067/12 SE	27 m	SO
MR *Makaretu Road*	X17/118917	17.5±1.5	Fine blue-grey sandstones	086/30 S	11 m	U
FR *Falkner Road*	X17/191864	16.8±0.8	Sand-rich siltstones	105/29 S	3 m	PDF
AF *Atea Ford*	X17/063871	16.8±0.8	Sand-rich mudstones, sandstones	017/12 E	41 m	PDF
TK *Te Koawa*	X17/196994	17.5±1.5	Light grey calcareous mudstones	309/56 NE	46 m	PDF
AB *Anzac Bridge*[1]	X17/096972	20.4±1.6	Massive blue-grey mudstones	298/57 NE	53 m	PDF
MF *Maharahara Farm*	X17/223976	20.4±1.6	Mudstones and fine sandstones	090/32 S	22 m	PDF
			Wairoa Syncline (Fig. 7.2b)			
MK *Mangapoike River*	X19/071449	6±1	Massive, light grey mudstones	187/30 W	16 m	S
NP *Ngatara-Poha*	X18/160749	9.9±1.1	Sand-rich mudstones, sandstones	186/23 W	82 m[4]	S
TF *Te Korau Farm*	X18/205761	13.1±2.1	Dark, sandy mud/siltstones	199/20 W	13 m	S
NG *Ngatimita*	X18/063762	13.5±2.5	Mud/siltstones and sandstones	084/43 S	21 m	SO
CH *Cheviot Hills*	X18/204688	14.2±1	Mudstones and sand-rich mudstones	072/56 S	17 m	SO
PC *Paparatu Cottage*	X18/175529	15.6±0.5	Mud/siltstones and fine sandstones	183/21 W	19 m	SO
GI *Glen Innes*	X18/116668	7.6±1.1	Sand-rich siltstones, sandstones	085/44 S	19 m	PDF
BG *Burgess Road*[2]	X18/088752	9.9±1.1	Sand-rich mudstones	064/42 SE	14 m	PDF
SN *Strathblane Farm*	X18/111696	14.2±1	Brown mud/siltstones and sandstones	146/27 SW	25 m	PDF
TR *Taumata Road*	X17/053807	15.6±0.5	Massive grey mud/siltstones	348/19 E	47 m	PDF
WH *Waterfall Hill*[2]	X18/204706	21.4±1.2	Mudstones and massive sandstones	238/63 NW	28 m	PDF

Coast North of Gisborne (Fig. 7.2d)						
TH *Turihaua Point*	Y18/608739	8.8±2.3	Massive, dark grey mudstones	038/19 SE	14 m	S
WU *Waihau Beach*[3]	Z17/719916	9.9±1.1	Massive grey mudstones and tuffs	194/23 W	7 m	S
MP *Makarori Point*	Y18/541693	14.6±1.4	Turbidites with blue-grey pelagic interbeds	307/14 NE	10 m	S
TP *Tatapouri Point*	Y18/574705	14.6±1.4	Turbidites with blue-grey pelagic interbeds	273/32 N	19 m	S
SB *Sponge Bay*	Y18/498658	14.6±1.4	Turbidites with blue-grey pelagic interbeds	353/47 E	43 m	SO
Mahia Peninsula (Fig. 7.2a)						
TC *Te Waipera Cemetary*[2]	Y19/362233	7.6±1.1	Dark mudstones and tuff beds	203/10 NW	24 m	S
PP *Putiki Point*[2]	Y19/379226	7.6±1.1	White, ash-rich mudstones	239/11 NW	17 m	SO
NR *Nukutaurua Road*[2]	Y19/402222	8.8±2.3	Pale grey mudstones and reworked tuffs	240/48 NW	82 m	S
Southern Hawke Bay (Fig. 7.2c)						
BH *Blackhead*	V23/359074	8.8±2.3	Massive light grey mud/siltstones	067/23 SE	13 m	SO
WT *Whangaehu Tuff*	V24/186826	8.8±2.3	Tuff bed within sand-rich siltstones	051/38 SE	10 m	SO
TI *Titoki Road*	V23/281249	14.2±1	Brown and grey mud/siltstones	201/30 W	23 m	S
PN *Paoanui Point*	V23/420182	12.1±1.1	Dark, blue-grey mudstones	033/61 SE	47 m	PDF
WB *Whangaehu Beach*	V24/185829	12.1±1.1	Black and grey mudstones	054/73 SE	44 m	PDF
KR *Kahuranaki Road*	V22/380435	13.5±2.5	Mudstones, fine siltstones, sandstones	196/65 W	32 m	U
WM *Waimarama Beach*	W22/519461	22.1±3.1	Light blue grey mudstones, welded tuffs	285/46 N	13 m	PDF
South Wairarapa (Fig. 7.2d)						
BP *Brancepeth*	T26/485148	8.8±2.3	Light grey calcareous mudstones	229/18 NW	35 m	SO
FP *Flat Point*	T27/587925	19.6±2.1	Blue-grey mudstones, glauconitic sands	223/41 NW	14 m	SO
OK *Okau*	U26/840361	21.9±1.6	Fine-grained turbidites	207/50 W	22 m	S

Grid references are from NZMS 260 sheets. Bedding measurements are given as strike and dip with dip direction. Demagnetization behaviour is classified as follows: S = stable ChRM with negligible overprint, SO = ChRM strongly overprinted by present day field, but still recoverable, PDF = no ChRM evident beneath present day field component, U = magnetization difficult to interpret. [1–3] Data from these localities are presented fully in [1]Chapter 4, [2]Chapter 6, [3]Chapter 5. [4] Sampling at NP was in two 6–7 m sections separated by an interval with no exposure.

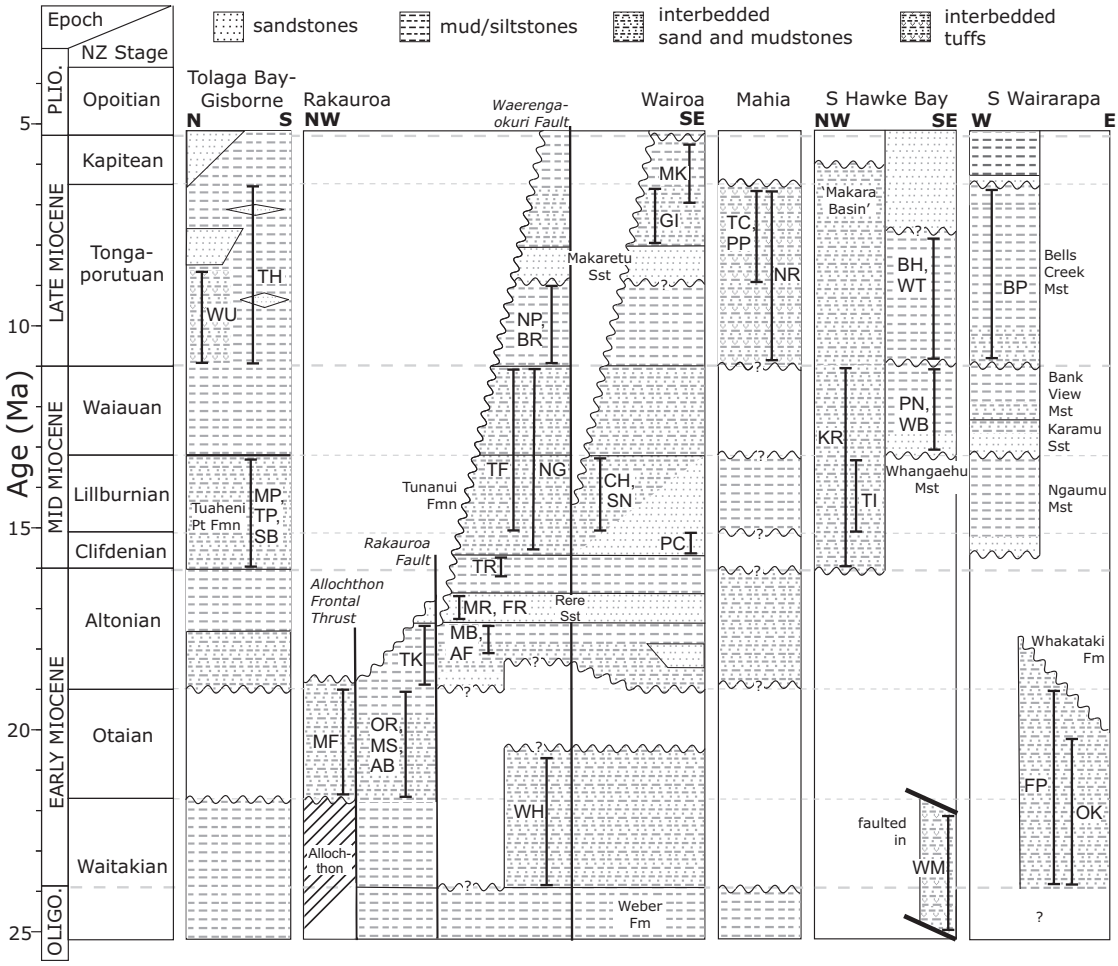

Figure 7.3: Generalized stratigraphy of the East Coast region, with the stratigraphic ranges of the sampling sites within simplified lithological columns. Adapted from Field et al. (1997) with additional information from Neef (1992), Davies et al. (2000), Mazengarb and Speden (2000) and Francis et al. (2004).

7.3 Results

7.3.1 Demagnetization behaviour

Rock magnetic and scanning electron microscope observations of the studied sediments, which have been discussed in Chapters 5 and 6, indicate that they commonly contain variable mixtures of single domain and superparamagnetic greigite, which grew authigenically within the sediments at various stages of diagenesis. Thermal demagnetization behaviour, including unblocking at 250–350°C and the onset of thermal alteration (indicated by large increases in low-field bulk magnetic susceptibility) above 350°C, is also consistent with the presence of greigite in many of our samples (cf. Roberts, 1995b).

The natural remanent magnetization (NRM) of all samples was weak (typically $<10^{-4}$ Am^{-1}). In geographic coordinates, a PDF overprint (Declination (D) = 20°, Inclination (I) = -64°) was also commonly observed. This overprint can be linked to

pyrite oxidation that is probably associated with modern groundwater percolation (Chapter 6), and its variable strength exerts a major control on demagnetization behaviour, which fell into three main classes (Fig. 7.4; Table 7.1).

Class S At 12 of the 38 studied localities (33%), the viscous overprint is weak and is removed at low temperatures (<150°C) and AFs (<20 mT), allowing a stable ChRM to be easily isolated (Fig. 7.4a, b). At many of these localities, both AF and thermal demagnetization appear to be equally effective.

Class SO At 11 further localities (29%), the viscous overprint is much stronger, and AF demagnetization was generally ineffective, as has often been the case for similar Cenozoic sediments from New Zealand (Turner et al., 1989; Pillans et al., 1994; Roberts et al., 1994; Turner, 2001). Thermal demagnetization data often follow great circle paths toward the ChRM (Fig. 7.4c, d), although in many cases a stable endpoint is not reached (e.g. Fig. 7.4d).

Class PDF At 13 localities (34%), no ChRM appears to be present; progressive removal of the PDF overprint reveals no stable component at higher temperatures or at higher applied fields (Fig. 7.4e, f). Iron sulphide oxidation, which is inferred to be responsible for the overprint (Chapter 6), has evidently also destroyed any ancient magnetization.

Demagnetization data for two remaining localities (4%; class U = uncertain in Table 7.1) proved difficult to interpret, having no obvious PDF overprint and anomalous ChRM directions with shallow inclinations.

7.3.2 Mean paleomagnetic directions

Mean paleomagnetic directions for type S and SO localities are listed in both geographic and tilt-corrected coordinates in Table 7.2; ChRM data for these localities, along with representative great circle demagnetization paths where appropriate, are plotted in Figure 7.5. The reliability of the mean directions calculated for some type SO localities may be questionable due to the small amount of data available, which makes it difficult to assess whether the strong PDF overprint has been completely removed (e.g. FP, PC; see also discussion in Chapter 4).

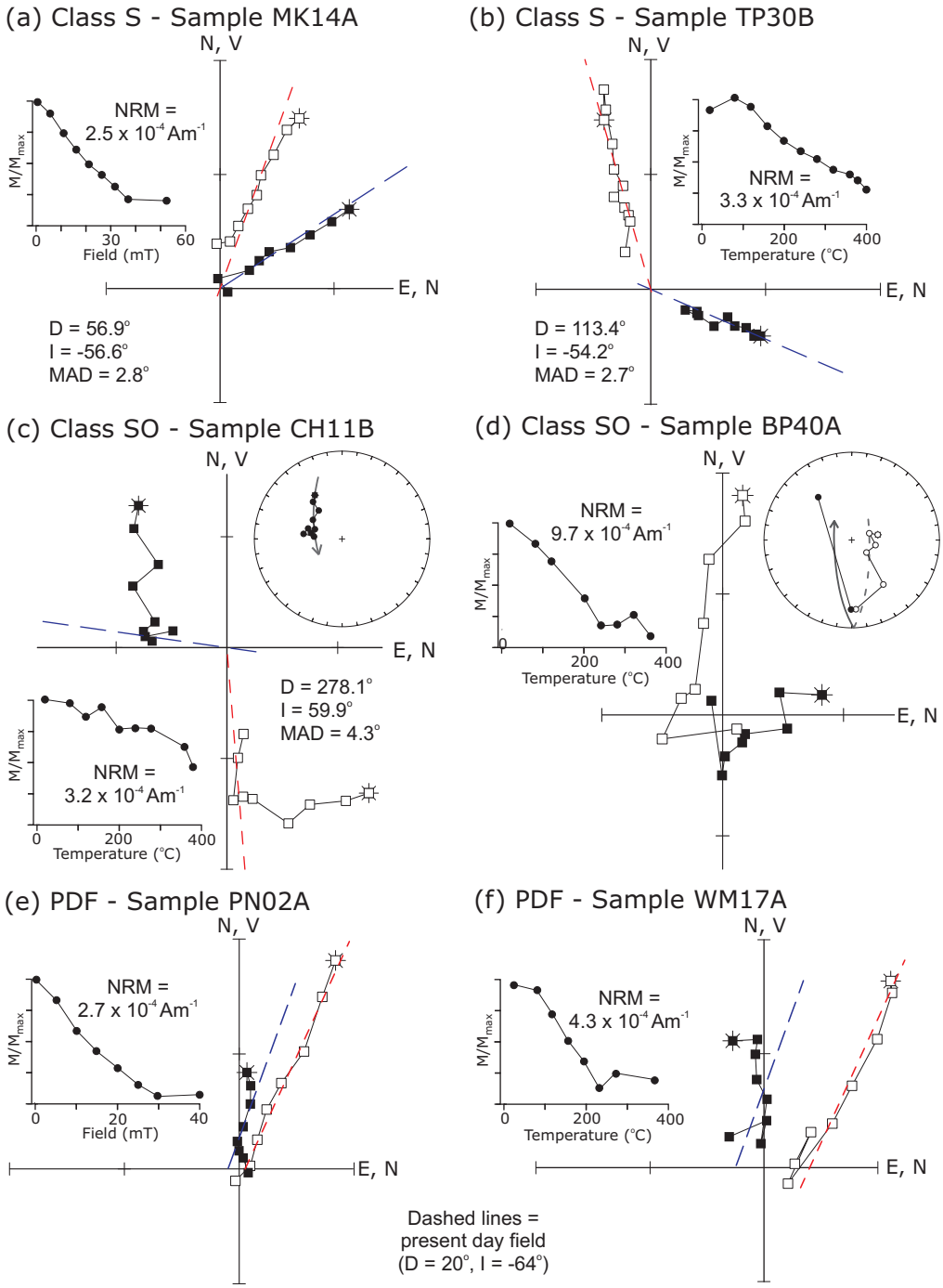

Figure 7.4: Vector component plots of representative AF and thermal demagnetization behaviour. Solid symbols denote declinations, open symbols denote inclinations, dashed lines indicate best-fit directions from principal component analysis. Demagnetization behaviour is subdivided according to the variable strength of the PDF overprint. Class S samples (a, b) have a stable ChRM with a weak viscous overprint. Class SO samples (c, d) have a much stronger PDF overprint that overlaps the ChRM, resulting in great circle demagnetization paths (see inset equal area stereoplots) and sometimes preventing the isolation of a stable end point (e.g. d). Class PDF samples (e, f) are also strongly overprinted, but there is no sign of an underlying ChRM. Data are plotted in tilt-corrected coordinates for (a–d), and in geographic coordinates for (e–f).

Table 7.2: Paleomagnetic mean directions and constraints on timing of remanence acquisition.

Locality (Behaviour)	n	Mean directions Geographic D(°)	Geographic I(°)	Tilt-corrected D(°)	Tilt-corrected I(°)	α_{95}	k	Timing of remanence acquisition Constraint	Untilting	Age (Ma)	Corrected declination
Central Hikurangi margin (Rakauroa)											
MB (S)	38	37.9	-52.4	14.2	-52.3	6.3	14.5	no constraint			
MS (SO)	27[12]	298.0	72.0	198.9	43.3	8.1	12.6	before Early Miocene folding	100%	19.0–21.7	18.9 ± 6.5°
OR (SO)	39[30]	206.1	56.2	195.5	47.5	5.8	16.3			19.0–21.7	15.5 ± 4.7°
Central Hikurangi margin (Wairoa Syncline)											
MK (S)	26	21.8	-63.8	64.5	-49.3	3.2	79.6	no constraint			
NP (S)	15	16.5	-74.5	64.0	-60.2	7.3	28.4	no constraint			
TF (S)	22	15.3	-65.5	53.5	-59.7	3.5	80.0	before Pliocene folding	100%	5.0–15.2	53.5 ± 2.4°
NG (SO)	31	297.9	47.6	241.5	53.1	5.1	26.4			5.0–16.0	61.5 ± 4.1°
CH (SO)	20	313.4	27.8	258.3	65.2	5.6	35.3	prob. before Pliocene folding	100%	5.0–15.2	78.3 ± 4.5°
PC (SO)	13[7]	58.7	-76.6	79.1	-57.1	7.7	31.5	no constraint			
Central Hikurangi margin (coast)											
TC (S)	48	44.3	-58.6	57.5	-53.8	2.8	54.1	during Late Miocene–Pliocene folding	44%	4.0–6.0	49.1 ± 5.4°
NR (S)	16	6.5	-54.5	99.7	-62.8	4.7	63.3				
	24	182.6	44.6	256.9	65.9	5.0	36.4		79%		
PP (SO)	24	216.1	62.3	237.8	64.5	5.0	36.2				
WU (S)	19	66.8	-70.2	85.6	-49.5	4.5	55.5	early (large declination)	100%	? –11.0	85.6 ± 3.6°
	24	163.9	59.3	206.8	63.1	7.0	18.7	late (small declination)	100%	0.8– ?	26.8 ± 5.4°
MP (S)	44	77.2	-56.0	96.5	-65.1	3.7	35.3	between Miocene–Pliocene deformation episodes	0%	3.6–8.8	51.2 ± 2.2°
TP (S)	37	49.8	-59.2	115.8	-66.1	3.9	37.3				
SB (SO)	22	56.9	-11.7	39.3	-51.4	6.7	22.1	prob. before Late Miocene–Pliocene diapirism	100%	3.6-16.0	39.3 ± 5.3°
TH (S)	23	73.4	-44.9	53.4	-53.2	5.5	30.7	no constraint			

Locality (Behaviour)	n	Mean directions Geographic D(°)	I(°)	Tilt-corrected D(°)	I(°)	α_{95}	k	Timing of remanence acquisition Constraint	Untilting	Age (Ma)	Corrected declination
Southern Hikurangi margin (S Hawke Bay)											
BH (SO)	$24^{(12)}$	264.6	59.9	224.5	58.8	6.6	21.1	during Late Miocene–Pliocene folding	56%	3.6-8.8	60.2 ± 2.3°
WT (SO)	5	79.2	-50.1	28.3	-52.6	5.8	176				
TI (S)	37	31.2	-64.4	71.3	-47.8	3.0	64.6				
Southern Hikurangi Margin (Wairarapa)											
BP (SO)	$33^{(33)}$	210.6	57.8	240.3	58.8	4.5	32.8	no constraint			
FP (SO)	$13^{(7)}$	214.6	44.2	250.8	36.2	6.9	36.8	no constraint			
OK (S)	37	339.7	-58.5	75.9	-57.4	4.3	31.2	prob. before Early Miocene folding	100%	16.0-23.9	75.9 ± 3.4°

n = number of samples; superscript number = number of great circle arcs used to constrain the mean direction according to McFadden and McElhinny (1988). Errors on corrected declinations are calculated according to Demarest (1983).

Paleomagnetic declinations (from tilt-corrected mean directions, with errors calculated according to Demarest (1983)) are plotted against depositional age for all localities in Figure 7.6. There is a large amount of scatter in these data, both temporally and spatially: tectonic rotations that differ by as much as 80° are recorded at localities of comparable age and position along the Hikurangi margin. Additionally, rotations of >90° are recorded by Late Miocene sediments, which would require tectonic rotation at substantially higher rates than are presently observed in the short-term velocity field (e.g. Wallace et al., 2004). However, as stated above, the assumption that the ChRM dates from the time of deposition is invalid for at least some, and possibly many, of these localities, due to the widespread occurrence of authigenic greigite in the studied sediments. In several cases greigite has formed during late diagenesis, 1 Myr or more after deposition (Chapters 5, 6). Taking the declination-age plot in Figure 7.6 at face value could therefore be highly misleading; rigorous constraints on the timing of magnetization are required to develop a more accurate picture of the rotation history of the Hikurangi margin.

7.3.3 Constraints on the timing of remanence acquisition

Attempts to establish the age of the ChRM using paleomagnetic field tests, primarily the fold test of Tauxe and Watson (1994), was in many cases frustrated by the prevalence of strong PDF overprints, which led to the loss of useful data at critical sites. However, careful analysis enables constraints to be placed on the timing of remanence acquisition at 16 of the 23 stably magnetized localities, although in some cases the age constraints remain broad (Table 7.2). Constraints on individual localities are discussed in more detail in the following sections, which are subdivided according to their position on the Hikurangi margin; the 'central' and 'southern' regions are roughly equivalent to the Wairoa and Wairarapa domains of Walcott (1989) (Fig. 7.1b).

Central Margin

Rakauroa region A reversed polarity magnetization in Early Miocene (Otaian) sediments at Oliver Road (OR) and Matawai Station (MS) (Fig. 7.2b) has been shown by a fold test to pre-date Early Miocene (Altonian) folding (Chapter 4). The small declinations observed (<20°; Fig. 7.5) are consistent with expected values for the Australian plate (Idnurm, 1985) (Fig. 7.6), indicating negligible tectonic rotations in this area during the Neogene. This contrasts with the large declination anomaly reported from this region by Mumme and Walcott (1985), which resulted from incomplete removal of a PDF overprint (Chapter 4). Although many more localities were sampled in this area, most were compromised by strong PDF overprints (Table 7.1). A stable ChRM was isolated from Early Miocene sediments

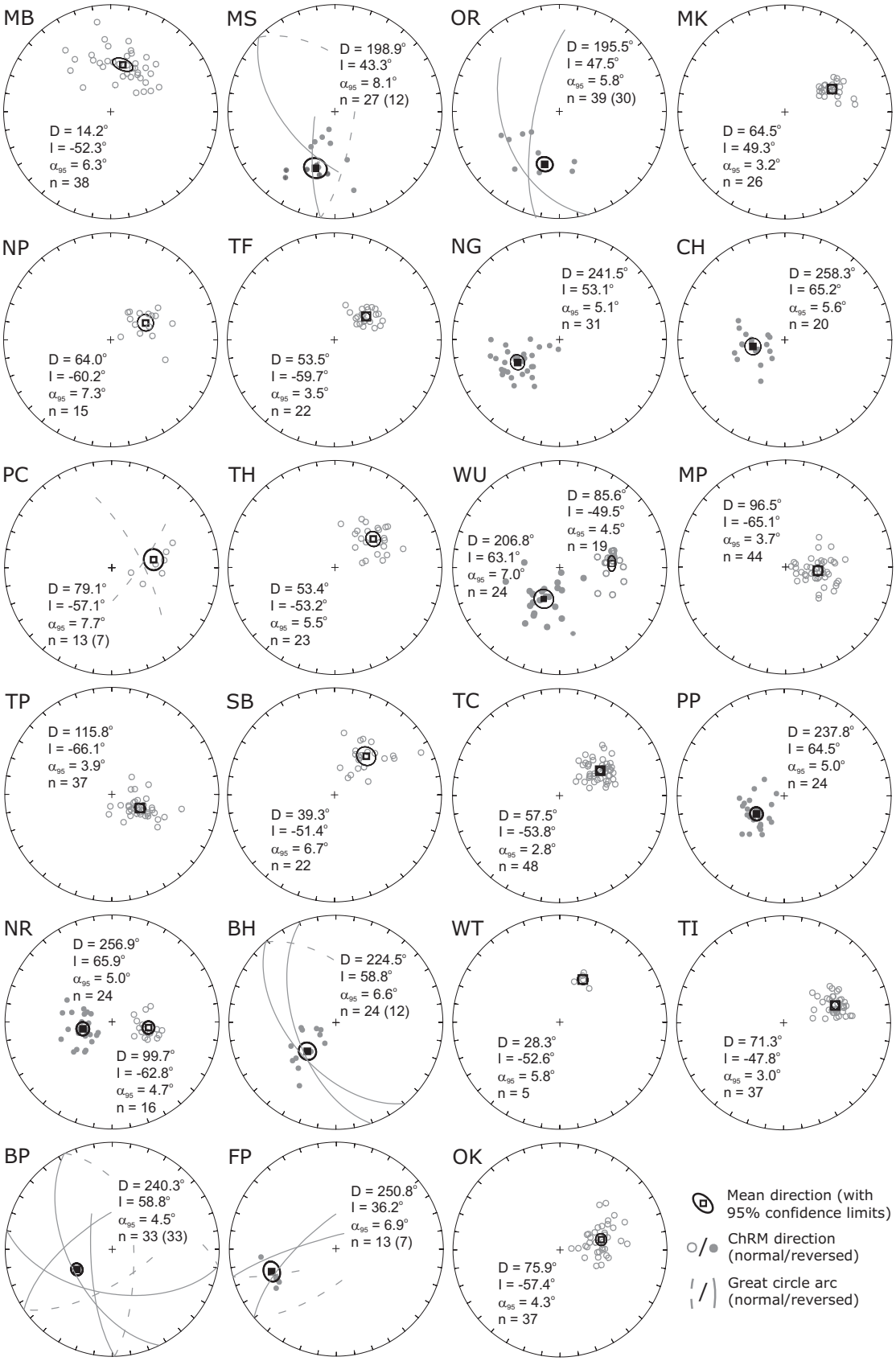
MB
D = 14.2°
I = -52.3°
α95 = 6.3°
n = 38
MS
D = 198.9°
I = 43.3°
α95 = 8.1°
n = 27 (12)
OR
D = 195.5°
I = 47.5°
α95 = 5.8°
n = 39 (30)
MK
D = 64.5°
I = 49.3°
α95 = 3.2°
n = 26
NP
D = 64.0°
I = -60.2°
α95 = 7.3°
n = 15
TF
D = 53.5°
I = -59.7°
α95 = 3.5°
n = 22
NG
D = 241.5°
I = 53.1°
α95 = 5.1°
n = 31
CH
D = 258.3°
I = 65.2°
α95 = 5.6°
n = 20
PC
D = 79.1°
I = -57.1°
α95 = 7.7°
n = 13 (7)
TH
D = 53.4°
I = -53.2°
α95 = 5.5°
n = 23
WU
D = 85.6°
I = -49.5°
α95 = 4.5°
n = 19
D = 206.8°
I = 63.1°
α95 = 7.0°
n = 24
MP
D = 96.5°
I = -65.1°
α95 = 3.7°
n = 44
TP
D = 115.8°
I = -66.1°
α95 = 3.9°
n = 37
SB
D = 39.3°
I = -51.4°
α95 = 6.7°
n = 22
TC
D = 57.5°
I = -53.8°
α95 = 2.8°
n = 48
PP
D = 237.8°
I = 64.5°
α95 = 5.0°
n = 24
NR
D = 256.9°
I = 65.9°
α95 = 5.0°
n = 24
D = 99.7°
I = -62.8°
α95 = 4.7°
n = 16
BH
D = 224.5°
I = 58.8°
α95 = 6.6°
n = 24 (12)
WT
D = 28.3°
I = -52.6°
α95 = 5.8°
n = 5
TI
D = 71.3°
I = -47.8°
α95 = 3.0°
n = 37
BP
D = 240.3°
I = 58.8°
α95 = 4.5°
n = 33 (33)
FP
D = 250.8°
I = 36.2°
α95 = 6.9°
n = 13 (7)
OK
D = 75.9°
I = -57.4°
α95 = 4.3°
n = 37
Mean direction (with 95% confidence limits)
ChRM direction (normal/reversed)
Great circle arc (normal/reversed)

at Mokonui Bridge (MB) (Figs. 7.2b, 7.5), but the timing of the magnetization cannot be constrained in this case.

Wairoa Syncline Many localities distributed across the Wairoa Syncline, to the south of Rakauroa (Fig. 7.2b), were also affected by strong PDF overprints, which often obscured the primary magnetic signal (Table 7.1). Of the six localities from which a stable ChRM was retrieved, no constraints could be placed on the timing of magnetization at Ngatara-Poha (NP), Paparatu Cottage (PC) and Mangapoike River (MK); mean directions from these localities are plausible both before and after tilt correction (Table 7.2). Only Te Korau Farm (TF) and Ngatimita (NG) could be subjected to a fold test; the results indicate that remanence acquisition occurred before folding of the Wairoa Syncline (Fig. 7.7a, b). These localities yielded tilt-corrected declinations of 54 ± 2° and 62 ± 4°, respectively (Fig. 7.5). South of the Waerengaokuri Fault, a large, reversed polarity declination of 78 ± 5° at Cheviot Hills (CH) also appears to record a pre-folding magnetization: in geographic coordinates the mean direction is unrealistic, with a large declination requiring 140° of tectonic rotation, and a shallow inclination (Fig. 7.7a, Table 7.2). Unfortunately, at all of these localities a large time window exists between deposition in the Middle Miocene and folding from the Pliocene onward (Field et al., 1997), meaning that constraints on the age of their magnetizations remain broad. Declinations at TF and NG are 20° smaller than at CH (Table 7.2), which may indicate late and early-forming magnetizations, respectively; this discrepancy could also be due to differential rotations across the Waerengaokuri Fault, but there is no indication that this structure has substantially altered the trend of the earlier-forming Wairoa Syncline, as would be expected if this was the case (Fig. 7.2b).

Coast Coastal sampling between Mahia Peninsula and Tolaga Bay (Fig. 7.2a, d) proved particularly successful, with most localities having easily removable PDF overprints and stable paleomagnetic directions (Tables 7.1, 7.2). However, remagnetizations are common. Fold tests indicate that the normal and reversed polarity magnetizations recorded in a Late Miocene sequence on Mahia Peninsula (local-

Figure 7.5 ***(preceding page)*****:** Equal area stereographic plots of individual ChRM directions, and mean directions with 95% confidence limits, for all localities in this study where a stable magnetization was isolated. n = number of samples used in calculation; the bracketed number, if present, records the number of great circle demagnetization paths that were used to constrain the mean direction (representative great circles are plotted for localities where they were used).

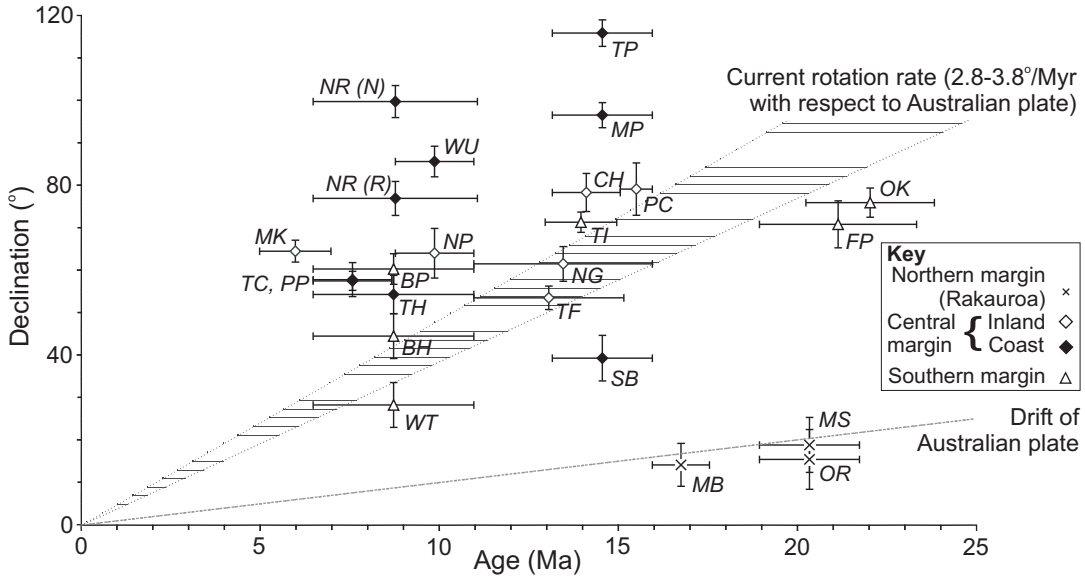

Figure 7.6: Tilt-corrected declinations plotted against depositional age at all localities where a stable ChRM was isolated. Localities have been subdivided according to their position on the margin; the northern, central and southern Hikurangi margin are roughly equivalent to the Raukumara, Wairoa and Wairarapa domains of Walcott (1989).

ities TC, PP, NR; Figs. 7.2a, 7.5) were acquired during folding at 4–6 Ma, with the reversed polarity magnetization being acquired demonstrably earlier than the normal polarity magnetization (at 79% and 44% unfolding, respectively; Chapter 6). When properly corrected by partial unfolding, ChRMs from these localities combine to give a mean declination of 49 ± 5° at 4–6 Ma.

Further to the north, two differently timed magnetizations with opposite polarity have also been recorded in Late Miocene sediments near Tolaga Bay (locality WU, Fig. 7.2a). In this case, however, there is a 60° difference in declination between the mean directions of the reversed and normal polarity magnetizations (Fig. 7.5), which requires several Myr of tectonic rotation between their respective acquisition times (Chapter 5). The normal polarity magnetization must therefore date from close to the time of deposition and the reversed polarity magnetization was acquired much later, but before the last polarity reversal at 0.78 Ma.

Four other coastal localities were also sampled from Middle-Late Miocene rocks near Gisborne (Fig. 7.2d), in an area that has undergone at least two separate periods of deformation since the Late Miocene. At Tatapouri Point (TP) and Makarori Point (MP), Middle Miocene sediments of the Tuaheni Point Formation (Fig. 7.3) (Neef, 1992) have been folded into a syncline, which has then been

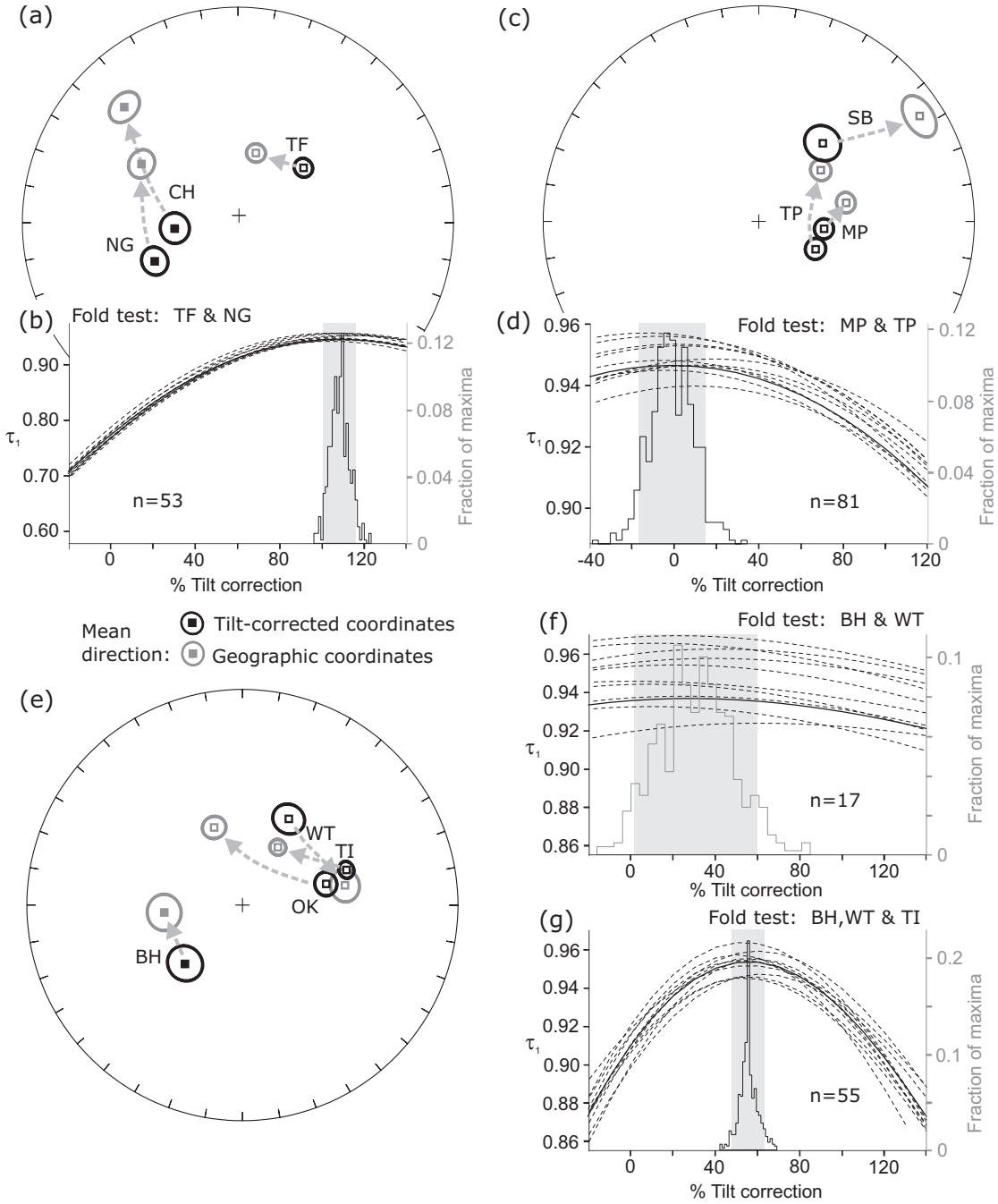

Figure 7.7: Constraints on the timing of remanence acquisition at localities from (a, b) the Wairoa Syncline, (c, d) the coast north of Gisborne, and (e–g) southern Hawke Bay. Stereoplots depict mean directions in tilt-corrected and geographic coordinates. Fold tests follow the method of Tauxe and Watson (1994); variation of the principal eigenvector τ_1 with various degrees of unfolding is depicted with dashed lines for different para-data sets, the distribution of maxima for these data sets is shown by the histogram, and the grey shading represents the 95% confidence interval.

disrupted by emplacement of a smectite diapir, causing a 20–25° clockwise rotation of the fold axis at MP with respect to TP (Fig. 7.2d). In contrast, tilt-corrected paleomagnetic data indicate large (∼100°) clockwise declination anomalies at both sites (Fig. 7.5), but the apparent rotation is larger at TP than at MP. With no tilt correction applied, however, the declination at MP is 27° more rotated than at TP (Table 7.2, Fig. 7.7c); this is much more consistent with the structural evidence, and suggests that remanence acquisition at these sites occurred after folding of the syncline, but before emplacement of the diapir. When the data from MP are corrected for a 25° local rotation, a fold test confirms a post-folding remanence (Fig. 7.7d) with a mean declinaton of 51 ± 2° (Table 7.2). The first generation of folding also affects Late Miocene sediments (Fig. 7.2d), and diapir emplacement occurred in the Late Miocene and Pliocene (Neef, 1992; Field et al., 1997). Remanence acquisition therefore appears to have occurred at the end of the Miocene.

At Sponge Bay (SB), sediments of equivalent age to those sampled at localities MP and TP are steeply tilted as a result of Late Miocene–Pliocene diapir emplacement (Fig. 7.2d). This deformation post-dates the folding at the other two localities, and therefore a fold test cannot be used to constrain the magnetization age. However, a pre-folding remanence appears likely because the mean direction at SB has an unrealistically shallow inclination in geographic coordinates (Fig. 7.7c). The tilt-corrected declination of 39.3 ± 5.3° indicates slightly less rotation than the corrected declination from the MP and TP localities, which suggests, but does not conclusively demonstrate, a late, pre-folding, remagnetization. In contrast, shallow tilting of Late Miocene sediments at Turihaua Point (TH; Fig. 7.2d) cannot be dated with any confidence, so no constraints on remanence acquisition are possible for this locality. A moderate to large tectonic rotation is indicated in both geographic and tilt-corrected co-ordinates (Table 7.2).

Southern Margin

Southern Hawke Bay Five coastal localities sampled between Cape Kidnappers and Cape Turnagain proved to be strongly affected by a PDF overprint (Fig. 7.2a, c; Table 7.1). Even at the two localities where a stable remanence was isolated, from early Late Miocene sediments at Blackhead Beach (BH) and around a tuff horizon of similar age on Whangaehu Beach (WT), few samples yielded reliable ChRMs after demagnetization (Fig. 7.5). A fold test indicates a late syn-folding magnetization, but the paucity of data, and the similar bedding tilt at these two localities (Table 7.1) produces a partial tilt correction with a broad 95% confidence interval of 2–62% (Fig. 7.7f).

Much better data were obtained from Titoki Road (TI) (Fig. 7.2a, c; Ta-

ble 7.2). Although these sediments are Middle Miocene rather than Late Miocene in age, all Miocene strata in this area were folded by the same deformation episode, from the Late Miocene-Pliocene onward (Kelsey et al., 1995; Field et al., 1997) (Fig. 7.2c). To test for the presence of a syn-folding magnetization at TI, a fold test was performed on the combined ChRM data from TI, BH and WT. This indicates a syn-folding magnetization acquired at 48–63% tilt correction (Fig. 7.7g), which is within the 95% confidence interval of the fold test for BH and WT alone (Fig. 7.7f), but is much better constrained due to the inclusion of additional data from TI. These results suggest a similarly timed syn-folding magnetization at all three localities. Applying a partial tilt correction of 56% to the ChRM data from TI, BH, and WT produces a corrected declination of 60 ± 2° for an assumed magnetization age of 4–9 Ma (Table 7.2).

Wairarapa Three localities were sampled in the Wairarapa region (Fig. 7.2a), two of which were affected by a strong PDF overprint. Few samples from Flat Point (FP), and none from Brancepeth (BP), reached a stable end point on demagnetization. The calculation of paleomagnetic mean directions for these two localities therefore relies heavily upon demagnetization great circle data (Fig. 7.5), making these directions potentially unreliable. Furthermore, no ChRM data are available for fold tests to constrain the timing of remanence acquisition. In contrast, at Okau (OK) the PDF overprint was easily removed, allowing a ChRM to be isolated in most samples (Fig. 7.5). The calculated mean direction has an anticlockwise declination anomaly in geographic coordinates (Fig. 7.7e; Table 7.2), which indicates that the magnetization pre-dates Early Miocene (Altonian) folding associated with movement on the nearby Adams-Tinui Fault (Field et al., 1997). In tilt-corrected coordinates, the paleomagnetic declination is 76 ± 3° (Fig. 7.5; Table 7.2), which is similar to those obtained from the potentially less reliable FP and BP localities (Fig. 7.5).

7.3.4 Inferred tectonic rotations

In order to properly reconstruct Neogene deformation of the Hikurangi margin, the paleomagnetic data set has been reduced to those localities where the timing of remanence acquisition can be properly constrained, with appropriately corrected declinations for localities with verified syn-folding magnetizations (Table 7.2; Fig. 7.8a). This reduced data set provides a number of new insights into the pattern of tectonic rotations on the East Coast of New Zealand.

Our data confirm that part of the northern Hikurangi margin has not tectonically rotated over geological timescales. Although substantial tectonic rotations are observed as far north as Tolaga Bay (locality WU) on the coast (Fig. 7.2a),

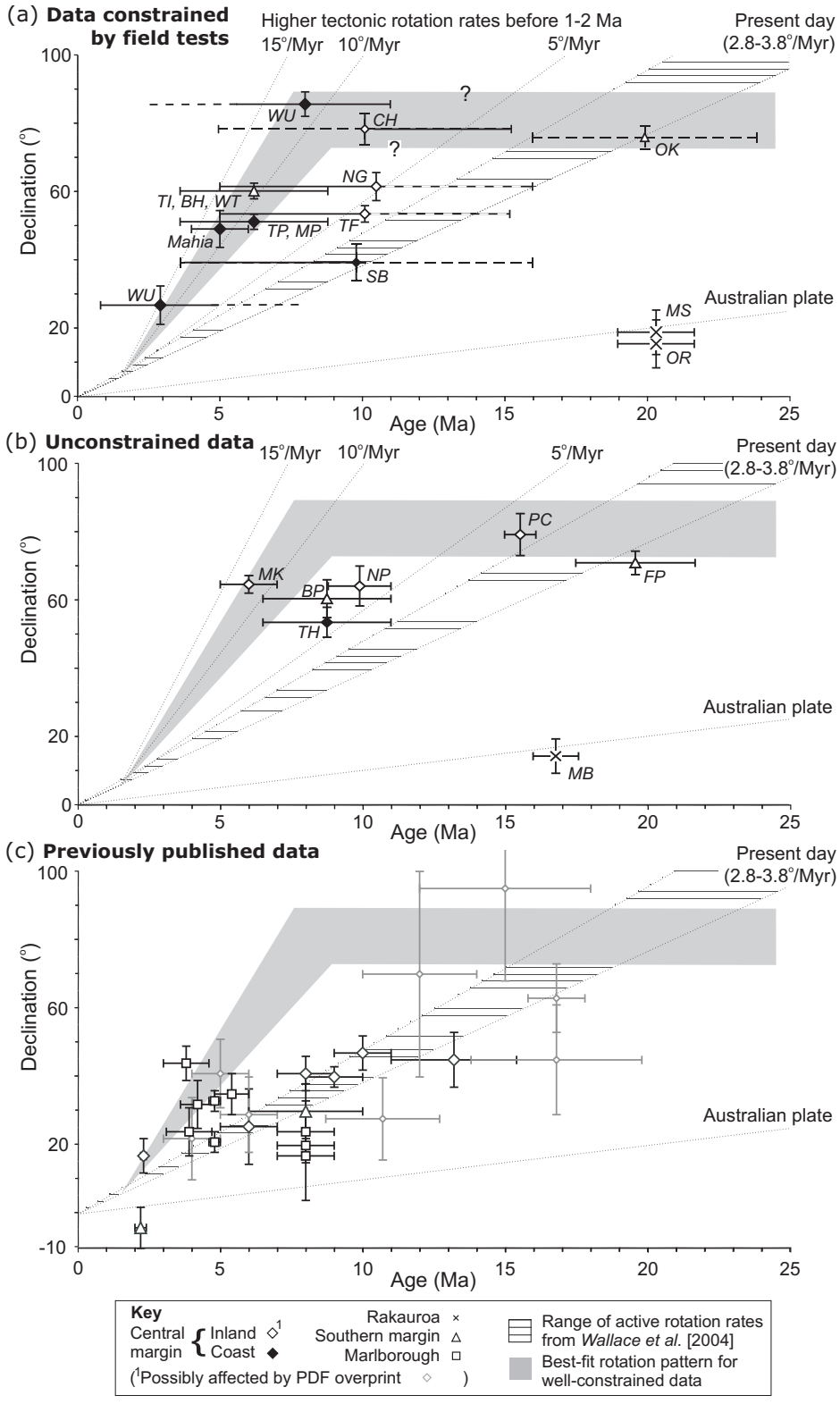
(a) Data constrained by field tests
Higher tectonic rotation rates before 1-2 Ma
15°/Myr
10°/Myr
5°/Myr
Present day (2.8-3.8°/Myr)
Declination (°)
Age (Ma)
WU
CH
OK
NG
TI, BH, WT
TP, MP
TF
Mahia
SB
WU
MS
OR
Australian plate
(b) Unconstrained data
PC
FP
MK
NP
BP
TH
MB
(c) Previously published data
Key
Central margin
Inland
Coast
(1Possibly affected by PDF overprint)
Rakauroa
Southern margin
Marlborough
Range of active rotation rates from Wallace et al. [2004]
Best-fit rotation pattern for well-constrained data

localities further inland (OR and MS; Fig. 7.2b) show no measurable tectonic rotation with respect to the Australian plate during the Miocene (Fig. 7.8a). A similar, small, tilt-corrected declination at locality MB just south of the Rakauroa Fault (Fig. 7.2b) is also consistent with negligible tectonic rotation if it acquired its magnetization close to the time of deposition (Fig. 7.8b); however, in the absence of constraints from field tests, the possibility of a late remagnetization cannot be excluded in this case. The spatial distribution of these localities indicates that the boundary between the unrotated and rotated parts of the Hikurangi margin runs ENE, between the Rakauroa and Waerengaokuri faults, before intersecting the coast between Tolaga Bay and Tokomaru Bay (Fig. 7.9a).

For the central Hikurangi margin (the 'Wairoa' domain of Walcott, 1989), the best-constrained data come from the coastal region. Rotations of 50–60° recorded by Late Miocene–Pliocene remagnetizations of sediments from Mahia Peninsula (TC, PP and NR) and at localities TP and MP, and the 90° declination of the early-forming remanence at WU, cannot be accounted for by long-term rotation of the Hikurangi margin at the presently observed rate of 2.8–3.8°/Myr (Fig. 7.8a). Data from further inland are more difficult to interpret due to large uncertainties in the timing of remanence acquisition; however, the 50–60° of rotation recorded at localities TF and NG appears to be carried by late-forming magnetizations, which formed closer to Pliocene folding than to Middle Miocene deposition (page 122). If this is the case, then assuming that the presently observed deformation pattern has persisted for the Quaternary, a best fit for all of the new data from the central Hikurangi margin requires higher rotation rates of 7–14°/Myr relative to the Australian plate before 1–2 Ma (shaded region on Fig. 7.8a). Futher south along the margin, the declination of 60 ± 2° for a Late Miocene–Pliocene syn-folding magnetization from southern Hawke Bay (localities WT, BH, and TI),

Figure 7.8 *(preceding page)*: (a) Plots of corrected declinations versus magnetization age for localities where the timing of remanence acquisition can be constrained by field tests. Dotted lines indicate predicted declinations from extrapolation of tectonic rotation at present day rates (hatched area) (Wallace et al., 2004), and from higher rates before 1-2 Ma (these rates exclude the 1°/Myr clockwise rotation due to drift of the Australian plate (Idnurm, 1985), which is also plotted). The shaded area represents a best-fit rotation history based on these data. (b) Tilt-corrected declinations plotted against depositional age for localities where the timing of remanence acquisition could not be constrained by field tests. Data for some localities fall below the best-fit rotation history from (a), suggesting that they have been remagnetized. (c) Previously published paleomagnetic data from the Hikurangi margin (Walcott et al., 1981; Walcott and Mumme, 1982; Mumme and Walcott, 1985; Wright and Walcott, 1986; Lamb, 1988; Roberts, 1992; Vickery and Lamb, 1995), plotted against the best-fit rotation history from (a).

an area previously considered to be part of the 'Wairarapa' domain (Fig. 7.1b), is also consistent with higher rates of tectonic rotation during the Late Miocene and Pliocene (Fig. 7.8a). Rather than being divided into discrete regions with separate tectonic histories, a large part of the Hikurangi margin appears to have been rotating coherently since the Late Miocene.

There are scant reliable data in our reduced data set regarding Middle and Early Miocene rotation of the central and southern margin, but there is some evidence of substantially reduced tectonic rotation rates before 8–10 Ma. On the southern Hikurangi margin, the apparently Early Miocene magnetization at locality OK records only 10–15° of additional rotation relative to the Australian plate compared to the Late Miocene-Pliocene magnetization in southern Hawke Bay (Fig. 7.8a). On the central Hikurangi margin, similar declinations of 80–90° are recorded both by the early-forming, Late Miocene magnetization at locality WU and the Middle Miocene sediments at locality CH. Although a Late Miocene remagnetization at CH cannot be ruled out, the large tectonic rotations observed at these localities approach the maximum suggested by tectonic reconstructions; this supports the inference that tectonic rotations of the Hikurangi margin have mostly occurred from the Late Miocene onward.

7.4 Discussion

7.4.1 Comparison with published paleomagnetic data

Difficulties in obtaining good paleomagnetic data from New Zealand Cenozoic sediments, due to their weak magnetization and strong PDF overprints, have been well-documented in previous studies (e.g. Walcott and Mumme, 1982; Mumme et al., 1989; Turner et al., 1989; Pillans et al., 1994; Roberts et al., 1994; Turner, 2001; see also Chapter 4). The results presented in this study re-emphasise these problems. At 39% of the localities sampled, any ancient remanence has been completely destroyed by inferred iron sulphide oxidation. At localities where an ancient ChRM is still preserved, the strength of the PDF overprint makes it difficult to retrieve; stable ChRMs without strong PDFs were routinely isolated at only 33% of all localities. However, another potential difficulty with the paleomagnetic data from the Hikurangi margin, which has not been appreciated in previous tectonic studies, is the presence of late-forming magnetizations in these sediments, which have arisen as a consequence of the widespread growth of authigenic greigite during late diagenesis (Chapters 5, 6). Our results make the scale of this problem clear: at least 9, and possibly 12, of the 16 localities where the timing of remanence acquisition can be constrained have been remagnetized, often several Myr after deposition. At localities where the timing of remanence acqui-

sition could not be established, comparison of tilt-corrected declinations to the best fit rotation history provided by well-constrained data suggests that a further 3 localities (BP, NP, TH) do not record a depositional signal (Fig. 8b). If this is the case, then at least 15 out of the 23 stably magnetized localities reported in this study (65%) appear to carry late-forming magnetizations. The widespread distribution of remagnetized sediments on the Hikurangi margin indicates that the broad scatter of declinations seen in Figure 7.6 occurs because, in many cases, the age of the magnetization does not correlate to the age of the sediments.

The presence of such widespread remagnetizations in the East Coast region raises questions about previous paleomagnetic results from this area (Fig. 7.8c), which usually lack constraints from structural field tests. Earlier studies have suggested accelerating tectonic rotation of the central Hikurangi margin since the Early Miocene (Wright and Walcott, 1986), although a reinterpretation, excluding data that may have been compromised by the incomplete removal of PDF overprints (Chapter 4), indicates a constant rate of rotation, consistent with active deformation, since the Late Miocene (Fig. 7.8c). More importantly, earlier studies have suggested that rotation of the southern Hikurangi margin had ceased by 2 Ma (Lamb, 1988), which is a key observation behind the proposed division of the margin into independently rotating 'domains' (Lamb, 1988; Walcott, 1989). However, the declination anomalies reported by these earlier studies are generally significantly smaller than our own results from the same areas on the North Island (Fig. 7.8a, c). Given that no constraints on the timing of remanence acquisition exist for these older data, it is likely that the apparent conflict is principally a result of unrecognised late-forming magnetizations at many of these previously reported localities. This potentially invalidates interpretations of past deformation in these areas, which have assumed a close to depositional paleomagnetic signal. In contrast, previously published paleomagnetic data from Pliocene sediments in the Marlborough region (Roberts, 1992, 1995a) are more consistent with the rotation history of the Hikurangi margin inferred from this study (Fig. 7.8c). Inferred paleomagnetic rotations in Marlborough also correlate well with deviations in the strike of a vertical structural fabric in the Torlesse basement rocks (Little and Roberts, 1997), which suggests that late remagnetizations may be less common in these younger sediments, even though greigite is still a common remanence carrier in this region (Roberts and Turner, 1993; see also Chapter 6).

7.4.2 Comparison of long-term rotation patterns with active deformation

With our improved data set, it is possible for the first time to rigorously compare long-term patterns of tectonic rotation with those inferred from the present-day

velocity field. Present day rotation of the Australian-Pacific plate boundary in the New Zealand region is driven by a couple arising from the transition from subduction to intra-continental transpression (Fig. 7.1a). Vertical axis rotations on the Australian plate therefore arise as a passive response to the reorientation of the subducting Pacific plate (Walcott, 1989); the dominant role of large-scale boundary forces is reflected by the similar rates of rotation along the whole Hikurangi forearc observed in the short-term velocity field (Wallace et al., 2004) (Fig. 7.1a). Similar forces, acting over geological timescales, would also account for the Neogene tectonic rotations recorded by paleomagnetic studies. Whilst the large differential rotations between adjacent regions suggested by previous interpretations of paleomagnetic data (Lamb, 1988; Walcott, 1989) (Fig. 7.1b) have been difficult to reconcile with this hypothesis, the more rigorously constrained paleomagnetic data presented here indicate similar rates and magnitudes of tectonic rotation along the whole Hikurangi margin south of Tolaga Bay since the Late Miocene. Although data from the southern North Island remain limited, coherent rotation of the entire East Coast region appears to be a feature of both long- and short-term deformation on the Hikurangi margin, which strongly suggests that they are the result of the same driving forces.

However, despite the apparent coherence of tectonic rotations during the Neogene, it is clear that the response of the Australian plate to these driving forces has not remained constant over time. This ongoing tectonic evolution is reflected by apparent changes in the extent and movement of the rotating block, revealed by features of the long-term deformation pattern that still conflict with the short-term velocity field. These features include the negligible Neogene tectonic rotations on the northern Raukumara Peninsula (Fig. 7.9a), which is presently rotating at the same rate as the rest of the Hikurangi margin (Wallace et al., 2004) (Fig. 7.1a), and the more rapid Late Miocene–Pliocene rotation of the central and southern Hikurangi margin, possibly at rates almost three times those presently observed. To properly understand these changes we must identify how tectonic rotation of the Hikurangi margin has been structurally accommodated on the boundaries of the rotating forearc.

7.4.3 Structural accommodation of large rotations

Northern limit of rotation - the Raukumara Peninsula

On the Raukumara Peninsula, extensive paleomagnetic sampling confines the northern limit of Neogene tectonic rotation to a 10-km-wide zone, between the Rakauroa and Waerengaokuri faults, inland, and to a 25 km stretch between Tolaga Bay and Tokomaru Bay on the coast (Fig. 7.9a). The inferred ENE-WSW trend of this rotation boundary contrasts with previous studies, which have pro-

posed a NW-SE-trending boundary running between the Bay of Plenty and Gisborne, with relative rotations being accommodated by dextral strike-slip along the Otoko-Totangi, Rakauroa and Waerengaokuri faults (e.g. Lamb, 1988). The paleomagnetic data also indicate that in this region the boundary between the non-rotating 'Raukumara domain' and the rotating Hikurangi forearc has remained relatively stable; approximately 80° of differential rotation has occurred across this narrow hinge zone in the last 10 Ma.

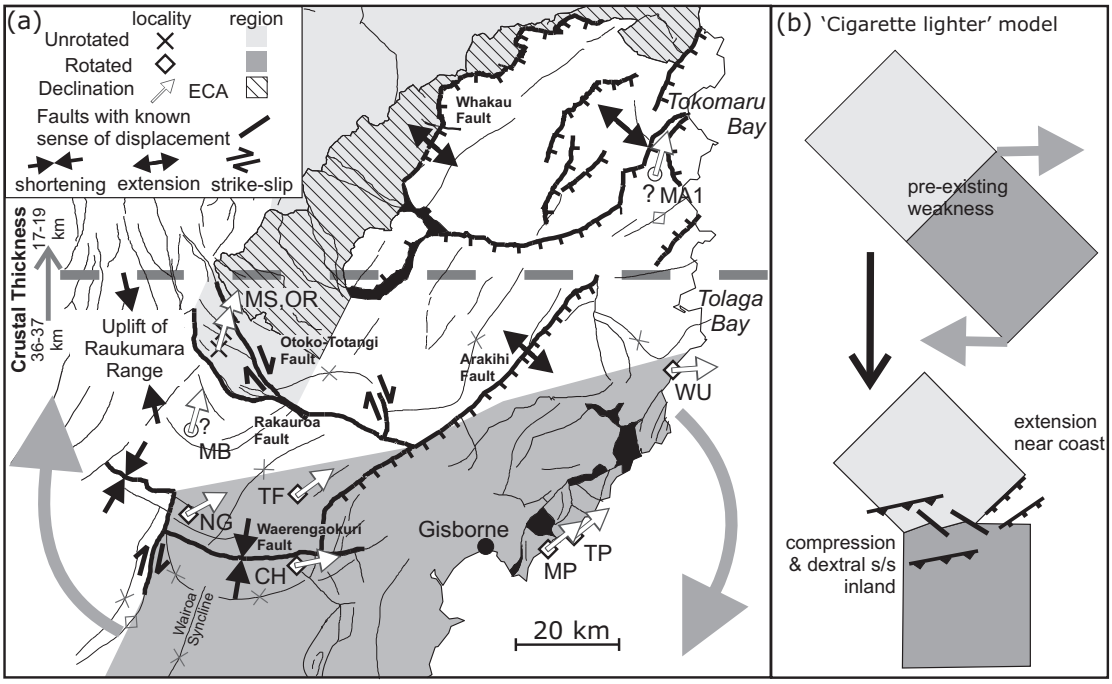

Figure 7.9: (a) Paleomagnetically-defined limits of the rotating and non-rotating parts of the Hikurangi margin on Raukumara Peninsula. Localities with well-constrained magnetizations have been plotted with white arrows depicting their inferred clockwise rotations. The small declination anomaly at MB, and the unrotated, reversed polarity magnetization at locality MA1 reported by Mumme et al. (1989), are not used to constrain the rotation boundary because the ages of remanence acquisition are unconstrained. Inferred senses and directions of horizontal strain have been plotted for active faults (marked in bold). The thick dashed line marks the approximate location of an abrupt change in the thickness of the Australian plate. Early Miocene thrust sheets are defined by the East Coast Allochton (ECA). (b) Schematic representation of a 'cigarette lighter' model, in which differential rotations are being accommodated by a combination of extension near the coast, and compression and dextral strike-slip inland.

The hinge area is structurally complex, and it has proven difficult to establish the sense and timing of movement on the numerous Neogene faults due to uplift and erosion of the sedimentary cover. However, there is a clear change in tectonic style across the paleomagnetically-defined rotation boundary. In the northeast, most faults with large (>100 m) displacements are north- to northeast-trending

normal faults (Thornley, 1996) (Fig. 7.9a); the western limit of this faulting is the east-dipping Whakau Fault, which marks the contact between the Neogene cover sequence and the ECA (Fig. 7.9a). To the south, NE–SW-trending structures such as the Wairoa Syncline begin to dominate (Mazengarb and Speden, 2000) (Fig. 7.2b), indicating margin-perpendicular shortening. Inland between Tolaga Bay and Gisborne, however, structures indicating approximately N-S shortening (e.g. the Waerengaokuri Fault, and the southward plunge of the Wairoa Syncline) and dextral strike-slip (e.g. the Otoko-Totangi Fault) are superimposed on this general pattern (Fig. 7.9a). A combination of extension toward the coast and shortening inland, which may also have contributed to uplift of the Raukumara Range, therefore appear to have accommodated differential rotations in this region, hinged about a zone near the intersection of the Waerengaokuri and Arakihi faults (Fig. 7.9a). This mechanism mimics the opening of a cigarette lighter, as schematically illustrated in Figure 7.9b.

Uncertainty regarding the exact trend and position of the rotation boundary shown in Figure 7.9a make it unclear as to whether the mechanism outlined above is solely responsible for accommodating ∼80° of differential tectonic rotation between the Raukumara Peninsula and the rest of the Hikurangi margin since 10 Ma; paleomagnetic data indicate, however, that the northern limit of tectonic rotation has been confined to this region for most of the Neogene. This rotation boundary also coincides with significant along-strike changes in the structure of the plate boundary. There is an abrupt reduction in crustal thickness on the Australian plate, from 36–37 km to 17–19 km, north of Tolaga Bay (Davey et al., 1997; Reyners et al., 1999), which has reduced the down-dip extent of the seismogenic zone (Reyners, 1998; Reyners and McGinty, 1999). This, combined with the presence of sediments with high pore fluid pressure at the plate interface (Collot et al., 1996; Reyners et al., 1999), produces a sharp decrease in inter-plate coupling between Gisborne and Tolaga Bay (Reyners, 1998), which might play an important role in allowing large differential rotations between the northern Raukumara Peninsula and the rest of the Hikurangi margin. The possible involvement of basement structures, indicated by the abrupt change in crustal thickness on the Australian plate, could have maintained this discontinuity over geological timescales; this is consistent with the fixed geographical position of the hinge zone suggested by paleomagnetic data. The clear change in coupling presently observed in this region, and the Late Quaternary scarps on several of the faults highlighted in Figure 7.9a (Thornley, 1996), suggest that the hinge could still be active today despite contemporary rotation of the Raukumara Peninsula indicated by the short-term velocity field (Wallace et al., 2004). Comparison of geodetic data over different timescales

indicates significant temporal variations in strain rates and directions of principal horizontal stresses on the Raukumara Peninsula in the last century (Àrnadóttir et al., 1999), so it is possible that present day rotations in this region are not representative of long-term deformation.

Western North Island

The geological youth of the TVZ and the NIDFB (Beanland, 1995; Wilson et al., 1995; Beanland et al., 1998) means these features were not involved in accommodating tectonic rotations of the Hikurangi margin in the Late Miocene-Pliocene. We have examined Neogene deformation patterns in an attempt to identify other structures on the western edge of the rotating forearc that may have been involved in accommodating vertical-axis rotations.

From 10 to 5 Ma, the apparent initiation of vertical-axis rotations on the Hikurangi margin coincided with a period of renewed tectonic activity in Taranaki Basin, off the west coast of the North Island (Fig. 7.10a). Cretaceous normal faults in the southern basin were reactivated as reverse faults (the Southern Inversion Zone, Fig. 7.10a) (King and Thrasher, 1992), with up to 3 km of exhumation indicated by offset porosity-depth trends (Armstrong et al., 1998) and thermal modelling (Funnell et al., 1996). This contrasts with extensional faulting in the Northern Graben (Fig. 7.10a), which increased to the north in a manner similar to present extension in the TVZ (King and Thrasher, 1992). This pattern resembles the rotation hinge on the Raukumara Peninsula (Fig. 7.9): shortening in the south, coupled with extension in the north, could have accommodated clockwise tectonic rotation of the Australian plate to the east. However, this implies that during the Late Miocene a much larger region than is presently observed, encompassing the west coast of the North Island and possibly parts of the South Island north of the Alpine-Wairau Fault, was affected by tectonic rotations (Fig. 7.10a). Our paleomagnetic data indicate that the Hikurangi margin has rotated ∼90° since the early Late Miocene, of which 50–60° has occurred since 5–6 Ma (Fig. 7.8a); therefore, if western regions were part of the rotating forearc in the Late Miocene, they would have experienced ∼30° of tectonic rotation. Unfortunately, relevant paleomagnetic data are scarce, making it difficult to test this hypothesis. Mumme and Walcott (1985) reported a range of contradictory small to moderate (-10–40°) declinations from Oligocene–Early Miocene sediments on the western North Island, and a large (80°) declination from Oligocene sediments from east of Nelson on the South Island; however, the use of blanket demagnetization techniques, and the lack of any constraint on the timing of remanence acquisition, mean that the reliability of these data is questionable, and further paleomagnetic sampling is required to verify Late Miocene rotations in these areas. Such rotation could,

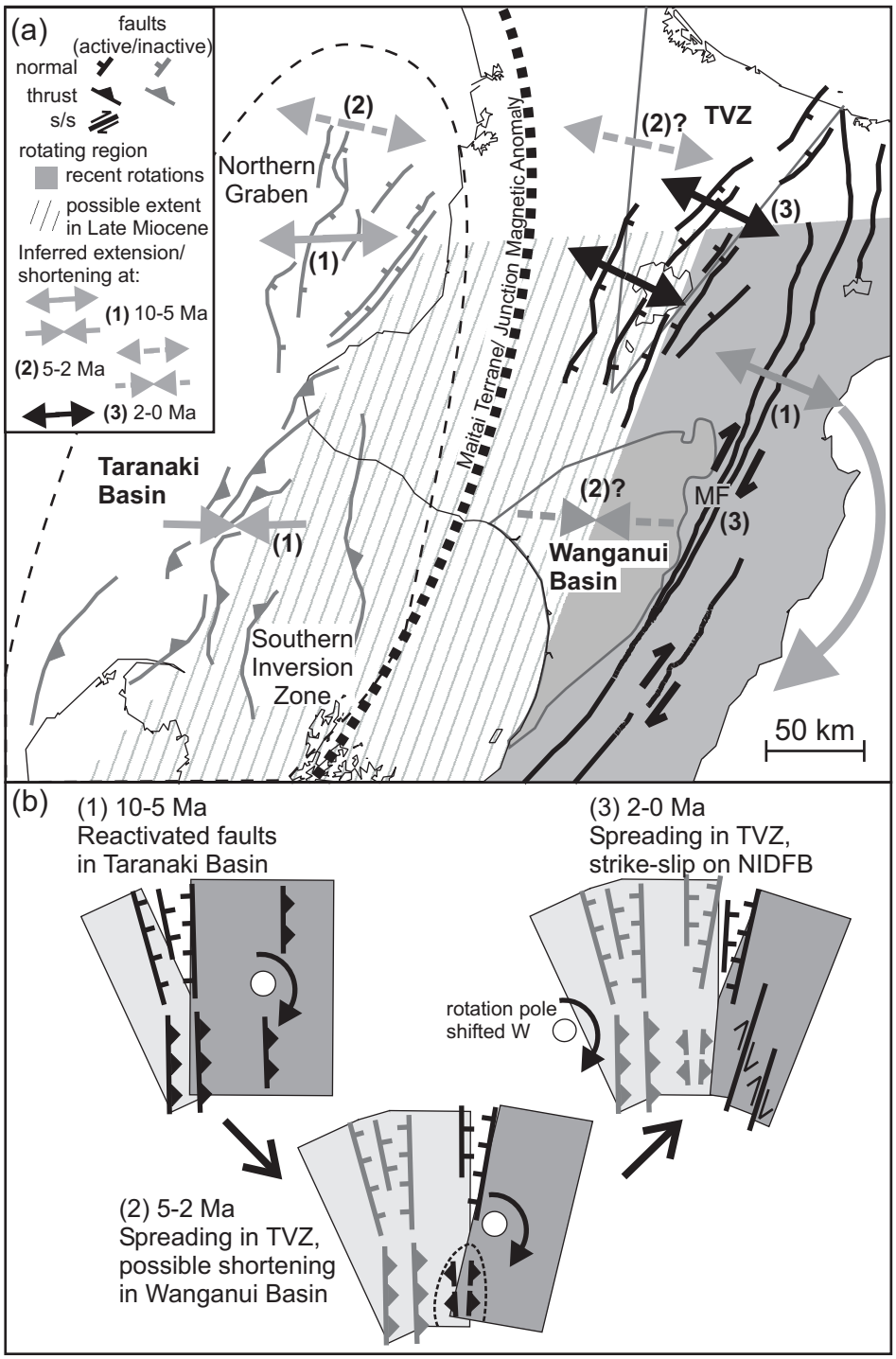

Figure 7.10: (a) Late Neogene deformation patterns on the western North Island of New Zealand. Arrows indicate directions and foci of shortening, extension and strike-slip in (1) the Late Miocene (10-5 Ma), (2) the Pliocene (5-2 Ma), and (3) the Quaternary (2-0 Ma). The boundary of the rotating forearc appears to have migrated eastward over time. TVZ = Taupo Volcanic Zone. MF = Mohaka Fault. (b) Simplified model of Neogene rotations on the Hikurangi margin, showing eastward migration of the limit of rotation and westward migration of the forearc rotation pole.

however, explain the long wavelength curvature of Mesozoic basement terranes through the western North Island, including the Maitai Terrane/Junction Magnetic Anomaly (Sutherland, 1999a) (Fig. 7.10a), the origin and timing of which remains controversial (e.g. Bradshaw et al., 1996; Sutherland, 1999b).

By 5 Ma, shortening had ceased in the Southern Inversion Zone (King and Thrasher, 1992; Armstrong et al., 1998), and the principal focus of tectonic activity on the North Island appears to have shifted eastward. In the south, faults west of the Mohaka Fault (Fig. 7.10a) appear to have accommodated negligible shortening since 5 Ma (Nicol and Beavan, 2003). In contrast, the large negative gravity anomaly associated with the Plio-Pleistocene Wanganui Basin (Fig. 7.10a) indicates lithospheric downwarping, caused by large shear stresses being transferred across a strongly coupled plate boundary (Davey and Stern, 1990; Stern et al., 1993). To the north of New Zealand, extension in the Havre Trough from ∼5 Ma (Wright, 1993) may also have led to some associated extension in the western part of the TVZ (Stern, 1987) (Fig. 7.10a), although structural patterns in this region are ambiguous (King, 2000); there was also further Pliocene extension in the Northern Graben of the Taranaki Basin (King, 2000). Small (<15°) tectonic rotations inferred from the thick Plio-Pliestocene sequences in the Wanganui Basin (Beanland, 1995; Wilson and McGuire, 1995) suggest that at this stage the western boundary of the rotating forearc had also migrated eastward, to a position similar to that presently observed (Fig. 7.10a). However, rotation of the Hikurangi margin to the east appears to have been accommodated by a similar mechanism to that seen in the Late Miocene, with shortening across a strongly coupled plate interface in the south, and extension in the north (Fig. 7.10).

The small strike-slip offsets (<10 km) on the faults of the NIDFB, compared to their large Quaternary slip rates (5–10 mm/yr) (Beanland, 1995; Van Dissen and Berryman, 1996), indicate that they first began to accommodate significant margin-parallel convergence at 1–2 Ma (Beanland, 1995; Beanland et al., 1998), signalling a tectonic reorganization at the end of the Pliocene. Beanland (1995) proposed that the NIDFB is comprised of reactivated Late Miocene reverse faults; clockwise rotation of the Hikurangi margin since 10 Ma has not only increased the obliquity of the margin with respect to the Pacific-Australian convergence vector, but it would also have rotated thrust faults that were originally perpendicular to the convergence direction into a favourable orientation to take up strike-slip displacement. At the same time, extension began in the TVZ (Wilson et al., 1995); the beginning of the Quaternary therefore marks the beginning of the present tectonic regime.

Accommodation of differential rotations at the western edge of the Hikurangi

forearc since the Late Miocene has therefore involved a number of different structures and tectonic styles. These observations are summarized by the block model in Fig. 7.10b, which also demonstrates a further consequence of the deformation patterns in the Late Miocene and Pliocene: the dominance of shortening rather than strike-slip in the southern forearc places the pole of rotation for the Hikurangi margin much closer to the plate boundary, up to 200 km east of the poles for contemporary rotations inferred by Wallace et al. (2004) (Fig. ref6Fig1a). By allowing higher angular velocities from smaller displacements, this configuration could account for the higher rates of tectonic rotation ($\sim$10°/Myr) during the Late Miocene and Pliocene, compared to the present day.

The causes of the other principal change since the Late Miocene, the apparent eastward migration of the rotation boundary, remain unclear. There is a potential link to a similar migration of back-arc spreading and volcanism north of New Zealand, in response to the roll-back of the Pacific plate. This hypothesis is supported by the observation that the largest shift in the location of the western rotation boundary in the Early Pliocene coincides with the initiation of back-arc spreading in the Havre Trough (Wright, 1993). However, the timing of spreading in the back-arc basins to the west of this newest rift is still disputed. The adjacent South Fiji Basin (Fig. 7.1a) is often assigned an Oligocene age based on interpretation of seafloor magnetic anomalies (e.g. Malahoff et al., 1982; Sdrolias et al., 2003), although Mid–Late Miocene spreading in the South Fiji Basin has also been suggested, based on geophysical surveys of the Northland margin (Herzer et al., 2000). Further west still, spreading in the Norfolk Basin may also have continued into the Late Miocene (Sdrolias et al., 2004). However, linking extension in the Taranaki Basin to back-arc spreading to the north of New Zealand remains speculative.

Southern limit of rotation - Cook Strait

Paleomagnetic studies have established that there were no tectonic rotations in the Marlborough region during the Late Miocene (Roberts, 1992). At this time, therefore, the southern limit of the rotating Hikurangi margin was located between the northern South Island and the southern North Island. The most likely position for this rotation boundary is in Cook Strait, which appears to represent a major structural discontinuity (Walcott, 1978) (Fig. 7.11a). The faults of the NIDFB cannot be linked across Cook Strait to those in the Marlborough Fault Zone (Carter et al., 1988), and Mesozoic basement terranes (e.g. the Esk Head subterrane, Fig. 7.11a) are offset by 140 km across what is interpreted to be the eastern termination of the Wairau Fault, which is bent clockwise through Cook Strait (Walcott, 1978; Lewis et al., 1994). This dextral offset probably occurred in

the early Neogene, before the eastern Wairau Fault was isolated by development of the Southern Inversion Zone on the western North Island at 10 Ma (Fig. 7.10a), became inactive, and began to rotate with the rest of the Hikurangi margin to the north (Fig. 7.11b). It is unclear whether structures are preserved in Cook Strait that might have accommodated this rotation; extension associated with the Late Miocene Wairau Basin (Lewis et al., 1994) was probably important, but the deformation style associated with most Late Miocene-Pliocene faulting is poorly constrained (Barnes and Audru, 1999).

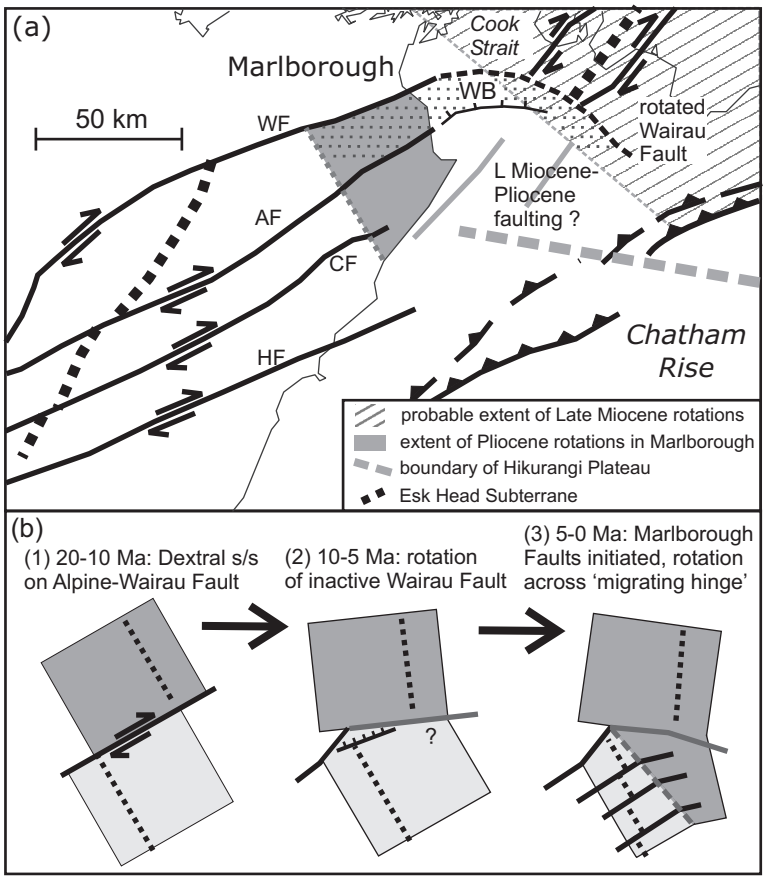

Figure 7.11: (a) Deformation patterns in the Marlborough region, showing major strike-slip faults (WF = Wairau Fault; AF = Awatare Fault; CF = Clarence Fault; HF = Hope Fault) and the probable distribution of Neogene tectonic rotations, the boundary of which is associated with the boundary between the Hikurangi Plateau and continental crust of the Chatham Rise. The inactive eastern termination of the Wairau Fault curves through Cook Strait. WB = Wairau Basin. Figure adapted from Barnes and Audru (1999) according to Little and Roberts (1997). (b) Simplified model of Neogene rotations in this area.

Increased convergence in the plate boundary region, arising from a shift in the Pacific-Australian Euler pole at 5–6 Ma (Sutherland, 1995; Walcott, 1998), could not be accommodated by the rotated Wairau Fault. Instead, the plate boundary propagated southeast into the Pacific plate, with dextral strike-slip initiating on

the Marlborough faults in the early Pliocene. This tectonic reorganization also appears to have shifted the border of the rotating Hikurangi margin southwestward into northern Marlborough, with vertical-axis rotations of 5–7°/Myr since ∼4 Ma indicated by paleomagnetic data (Roberts, 1992, 1995a) (Fig. 7.8c). Little and Roberts (1997) demonstrated that this rotation is also recorded by a regional kink in the underlying Torlesse basement fabric, and proposed that Pliocene rotations can be modelled by northeastward translation of the northern Marlborough region through a 'migrating hinge' (Fig. 7.11b), which is located inland of the boundary between the Hikurangi Plateau and continental crust of Chatham Rise (Fig. 7.11a). A ∼7 km vertical offset in the seismicity associated with the subducting plate indicates an abrupt increase in crustal thickness, and hence inter-plate coupling, across this boundary (Eberhart-Phillips and Reyners, 1997; Reyners, 1998), to the extent that the plate interface off the coast of Marlborough appears to be permanently locked (Collot et al., 1996; Barnes and Mercier de Lepinay, 1997). The intersection of Chatham Rise with the Hikurangi margin therefore marks the southern limit of subduction, and the pivot point of the rotating Pacific plate; tectonic rotations in the forearc cannot occur further south. The southwestward migration of the rotation boundary since the Late Miocene is a consequence of the southward propagation of the subduction zone, probably in response to the transfer of intra-plate slip onto the Marlborough faults since 5 Ma (Little and Roberts, 1997).

7.4.4 Revised Neogene reconstructions for the Hikurangi margin

In Figure 7.12 we have integrated the evidence discussed in the previous section with our paleomagnetically-derived rotation history. These reconstructions focus on defining the borders of the rotating region, effectively treating it as a rigid block. As discussed in section 7.4.2, our paleomagnetic results indicate coherent, long-term deformation of the margin at length scales much greater than the separation between major faults; this approach is therefore justified, although some local refinements to this model may be required to properly account for internal deformation within the forearc, and for localized rotations (e.g. Roberts, 1995a).

Early-Middle Miocene: 23-10 Ma

Although limited paleomagnetic data exist for the Early and Middle Miocene, there is no indication of widespread tectonic rotations on the North Island in this time period, despite subduction of the Pacific plate since 23–20 Ma (King, 2000; Rait et al., 1991). Active rotation of the margin appears to be dependent on the gradual southward increase in coupling at the plate interface (Reyners, 1998), caused by

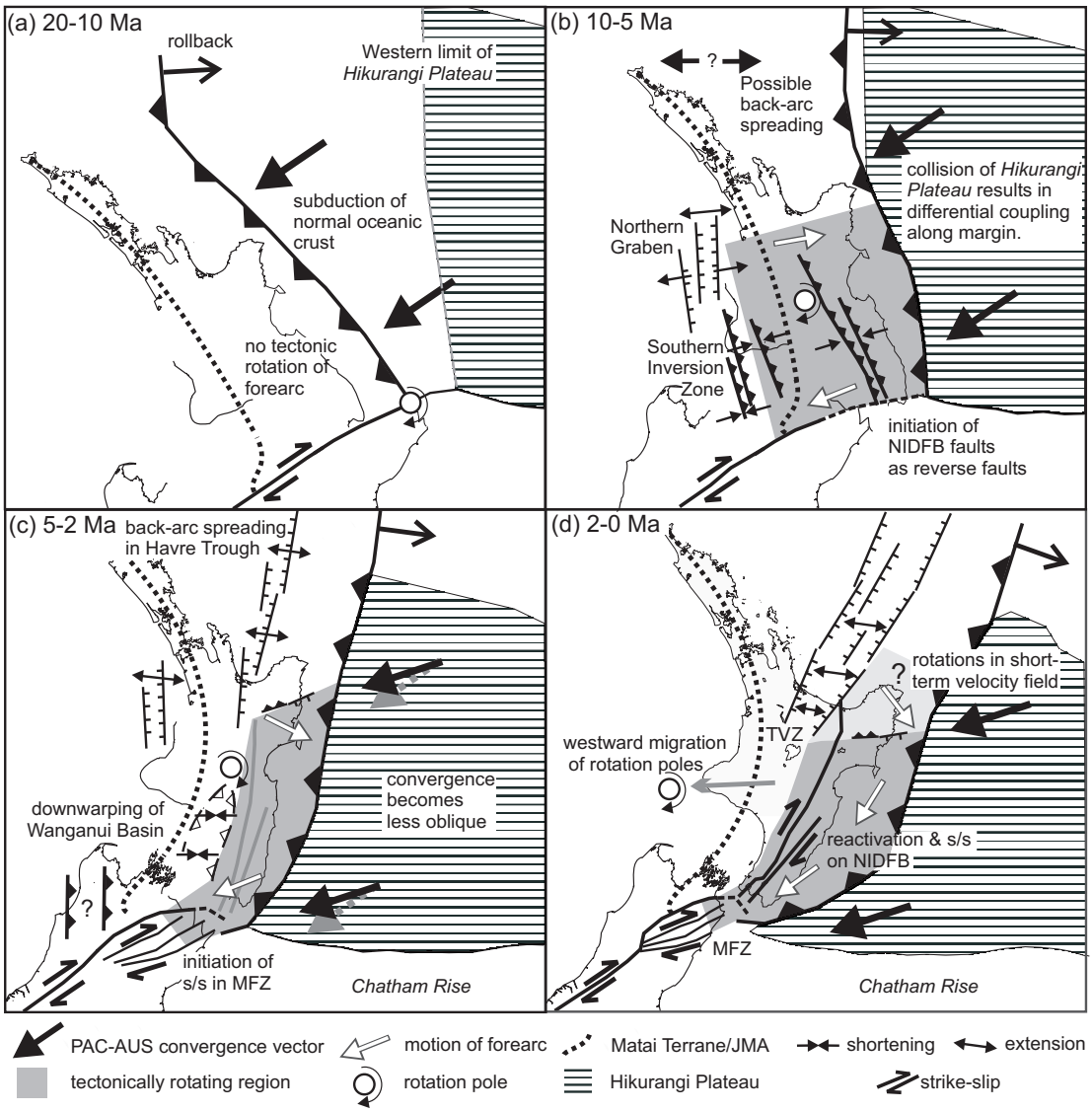

Figure 7.12: Neogene tectonic reconstructions of the New Zealand plate boundary region. (a) Early–Middle Miocene (20–10 Ma) reconstruction, showing normal oceanic crust being subducted along a NW-SE oriented Hikurangi margin. (b) Late Miocene (10–5 Ma) reconstruction. Subduction of the Hikurangi Plateau results in increased inter-plate coupling along the Hikurangi margin and shortening in the southern forearc, driving tectonic rotation of most of the North Island about a central pole. (c) Pliocene (5–2 Ma) reconstruction. The initiation of strike-slip in the Marlborough Fault Zone (MFZ), shortening across the Wanganui Basin, and spreading in the Havre Trough, combine to cause a narrowing of the rotating forearc. (d) Quaternary (2–0 Ma) initiation of strike-slip on the NIDFB causes the rotation pole to migrate westward, reducing the rate of tectonic rotation.

the increasing crustal thickness and buoyancy of the subducting Hikurangi Plateau (Davy and Wood, 1994) (Fig. 7.1a). This inference is supported by numerical models of oblique subduction, which indicate that more abrupt changes in the strength of the subduction thrust would result in discrete zones of margin-normal dextral shear rather than tectonic rotation (Upton et al., 2003).

The down-dip extent of the Hikurangi Plateau is still poorly resolved. Thickened oceanic crust has been inferred on the subducted slab at depths of 15 to 30 km using ScSp conversions (Bourne and Stuart, 2000), and down to depths of 75 km by recent tomographic studies (Reyners et al., 2004). This represents at least 6–8 Myr of subduction, and suggests that subduction of the Hikurangi Plateau commenced in the early Late Miocene. We therefore propose that the Early and Middle Miocene represented a period when normal oceanic crust was being subducted beneath the Hikurangi margin (Fig. 7.12a). In this scenario, the only change in intra-plate coupling would have occurred at the transition to continental crust at the edge of Chatham Rise, where subduction was impeded and the plate boundary changed into a dextral transform fault (the Alpine-Wairau Fault). Such a sharp transition would be unlikely to generate large-scale vertical-axis rotations on the Australian plate. Clockwise rotations of 100–140° recorded by Paleogene to Middle Miocene sediments from the Marlborough coast (Vickery and Lamb, 1995) appear to be spatially restricted, and have been linked to the initial development of the plate boundary region (Little and Roberts, 1997), or to oroclinal bending (Fig. 7.12a) associated with early Neogene strike-slip on the Alpine-Wairau Fault (Hall et al., 2004).

Late Miocene: 10–5 Ma

The initiation of widespread tectonic rotations along the Hikurangi margin in the early Late Miocene followed collision of the Hikurangi Plateau (Fig. 7.12b). Subduction of thickened oceanic crust increased intra-plate coupling along the southern Hikurangi margin, which appears to have triggered shortening over a large area of the southern North Island in the Late Miocene (King, 2000) as convergent motion was transferred onto the Australian plate. The western limit of this region was in the Taranaki Basin (the Southern Inversion Zone of King and Thrasher (1992); see page 136). However, reverse faulting also occurred on faults further east in the forearc region, including those that presently comprise the NIDFB (Beanland, 1995), which at that stage were oriented perpendicular to the plate convergence vector (Fig. 7.12b). With increasing clockwise rotation in the next 5 Ma, the Hikurangi margin became more oblique to the plate convergence vector and margin-parallel motion was transferred into the forearc, which may also have led to Miocene dextral strike-slip faulting (Field et al., 1997, and references

therein). It is interesting to note that this period of regional tectonism appears to be linked to the widespread late remagnetizations of sediments along the Hikurangi margin, many of which formed in the Late Miocene (Table 7.2; Figs. 7.8a, b). Anomalous magnetizations carried by iron sulphides have been linked to migration of gas hydrates (Housen and Musgrave, 1996), or to hydrocarbon seepage (Reynolds et al., 1994), both of which are potential consequences of the convergence and uplift resulting from collision of the Hikurangi Plateau.

As discussed on page 136, during the Late Miocene the boundary of the rotating Hikurangi margin may have extended as far west as the Taranaki Basin, where extension in the Northern Graben, combined with shortening further south, could have accommodated coherent clockwise rotation of most of the North Island. At this stage, large velocity gradients within the forearc meant that the pole of rotation was probably located in the central North Island (Fig. 7.12b), leading to rapid tectonic rotations at $\sim$10°/Myr. The northern limit of this rotation is poorly constrained west of the Raukumara Range, with any Late Miocene structures being obscured by Quaternary volcanism and tectonism in the TVZ. At the southern end of the margin, widening of the active plate boundary region to include structures in the Taranaki Basin isolated the eastern end of the Alpine-Wairau Fault, causing it to become inactive and to rotate clockwise with the rest of the forearc (Fig. 7.11).

Pliocene: 5–2 Ma

A southwestward jump in the location of the Pacific–Australian Euler rotation pole occurred at 5–6 Ma (Cande et al., 1995; Sutherland, 1995; Walcott, 1998), reorienting the plate motion vector toward a more E–W direction and increasing convergence across the plate interface (Fig. 7.12c). Transfer of transpressional plate motion away from the now misaligned Alpine Fault, and initiation of strike-slip on the Marlborough faults, appears to be a direct response to this change. The Hikurangi margin migrated southward to link with the relocated transform boundary, causing the north-eastern South Island to begin rotating with the rest of the margin to the north.

Back-arc rifting in the Havre Trough, in response to continued roll-back of the Pacific plate, also began at $\sim$5 Ma (Wright, 1993), reducing the width of the forearc region to the north of New Zealand. This appears to have forced a similar response on the North Island, where the western boundary of rotation also moved east (Fig. 7.12c), and margin-perpendicular strain was accumulated by long-wavelength plate bending and subsidence in the Wanganui Basin (Stern et al., 1993). The overall pattern of shortening across the southern Hikurangi margin and extension in the north maintained high velocity gradients and drove

rapid tectonic rotations at similar rates to those seen in the Late Miocene, although in a more restricted region. The northern boundary of rotation remained confined to the southern Raukumara Peninsula, with rotations being accommodated by NW–SE extension on the coast, and by compression on inland structures such as the Waerengaokuri Fault (Fig. 7.9).

Quaternary: 2–0 Ma
Further clockwise rotation of the Hikurangi margin in the Pliocene continued to increase its obliquity with respect to the plate motion vector. By the end of the Pliocene, rotations of up to 70° had realigned Late Miocene reverse faults so that they were now in a favourable orientation to be reactivated as strike-slip faults, forming the NIDFB (Beanland, 1995) (Fig. 7.12d). The change to a strike-slip regime reflects a much larger margin-parallel component of motion in the southern forearc compared to the Late Miocene and Pliocene, when margin-perpendicular shortening was dominant (Figs. 7.12b, c). This change would have reduced the lateral velocity gradient along the margin, slowing rotations to their present rate of 3–4°/Myr as the rotation pole migrated westward to its present position off the Taranaki Coast (Fig. 7.12d). Propagation of spreading in the Havre Trough southward into the TVZ at the beginning of the Quaternary may also have been a response to this tectonic adjustment.

The increased obliquity of plate convergence in the Quaternary would also have led to strain partitioning at the weakly coupled plate boundary east of the Raukumara Peninsula, and the transfer of margin-parallel motion into the forearc. This additional component of motion might account for the contemporary rotation of the entire Raukumara Peninsula reported by Wallace et al. (2004) (Fig. 12d). However, as discussed on page 136, it is also possible that the present velocity field is not representative of deformation over longer timescales.

7.5 Conclusions

New paleomagnetic results from New Zealand, when properly constrained by field tests, have provided important new insights into the patterns of clockwise tectonic rotation on the Hikurangi margin during the Neogene. Our data indicate that large-scale plate boundary forces drive coherent, long-term rotational deformation of the margin at length scales much greater than the separation between major faults, in agreement with the short-term velocity field. There is no evidence for independently rotating 'domains'; previously reported lateral variations in the rate and magnitude of tectonic rotations are probably an effect of unrecognized late remagnetizations involving the iron sulphide greigite, which have affected up to 65% of the stably magnetized localities reported here.

Clockwise rotations of up to 90° have occurred since 8–10 Ma, possibly following collision of the Hikurangi Plateau with the subduction zone. In the north and south, the margin has pivoted about two relatively fixed hinges, on the Raukumara Peninsula and in Cook Strait, respectively, where major lateral changes in basement structure along the plate boundary zone have maintained long-term discontinuities in intra-plate coupling. In contrast, the western limits of rotation may have shifted over time, with deformation on the Australian plate being confined to a much narrower zone, closer to the plate boundary, since 5 Ma. Rates of rotation also appear to have been much higher before 1–2 Ma, with rates of 7–14°/Myr required to account for rotations of 50–60° since 5–6 Ma. Deformation patterns in the Late Miocene and Pliocene were dominated by shortening in the southern Hikurangi margin and by extension in the north, which created steep velocity gradients in the forearc and drove rapid tectonic rotations. Initiation of strike-slip on the NIDFB, as convergence became more oblique in the Quaternary, has reduced these gradients, resulting in slower rotation about a more distant pole.

The difficulties in obtaining reliable paleomagnetic data, due to widespread late remagnetizations and strong PDF overprints, mean that rotation of the Hikurangi margin before the Late Miocene remains relatively unconstrained. Further work is also needed to test for hypothesised Late Miocene rotation of the western North Island.

Chapter 8

Summary and conclusions

8.1 Summary and conclusions

The research presented in this thesis has focussed on interpreting a substantial new paleomagnetic data set from New Zealand, which has produced a new picture of deformation patterns since the initiation of subduction in the Early Miocene, and has provided new insights into how vertical-axis rotations are accommodated within continental crust. A key component in producing a coherent tectonic interpretation has been the improved understanding of the complex magnetic signature of New Zealand Cenozoic marine mudstones, which has emphasised the paleomagnetic importance of iron sulphides such as greigite. In addition to the discussion and conclusions at the end of Chapters 4 to 7, the principal conclusions of this research, and the wider implications stemming from them, are summarised below.

8.1.1 The ubiquity of greigite and the consequences of late remagnetizations

The rock magnetic and SEM analyses presented in Chapters 5 and 6 demonstrate that authigenic greigite is an important remanence carrier in New Zealand Neogene marine mudstones. In some respects this is not a surprising discovery: stably magnetized greigite is being increasingly recognized in the geological record, particularly in rapidly deposited marine sediments (Roberts and Weaver, 2005, and references therein) that are similar to those deposited along the Hikurangi margin since the Early Miocene. It is not even the first time that late growth of greigite, possibly millions of years after deposition of the host sediments, has been documented to have caused inconsistent and contradictory magnetic polarity records within marine sequences (e.g. Florindo and Sagnotti, 1995; Jiang et al., 2001; Roberts and Weaver, 2005; Sagnotti et al., 2005). What is unique about the New Zealand paleomagnetic data set, however, is the sheer abundance of remagnetized sediments, revealed by the rigorous application of field tests undertaken in Chapter 7. This abundance, coupled with the existence of late remagnetizations, which can vary significantly in timing even at the outcrop scale, obviously presents serious problems for magnetostratigraphic and tectonic studies in New Zealand. It is not yet clear whether the scale of remagnetization seen on the Hikurangi margin is the result of late diagenetic processes that are likely to have affected rapidly deposited marine sequences elsewhere, or whether it is a unique consequence of New Zealand tectonic history (see page 150); ascertaining this will require a much better understanding of the mechanisms that cause the late diagenetic growth of greigite, and more detailed study of greigite-bearing sediments in other areas (e.g. Taiwan and Italy). Regardless, in any sediments where greigite is present, the assumption of a primary remanence should be made with extreme caution, prefer-

ably following confirmation from paleomagnetic field tests. However, although these observations may lead to some degree of pessimism, the recognition that many sequences on the Hikurangi margin were remagnetized was *the* key insight in this research, without which a consistent tectonic interpretation would probably have been beyond reach.

8.1.2 The non-existence of paleomagnetic 'domains'

Prior to this study, recent work on the tectonics of the North Island of New Zealand has focussed mainly on characterising Quaternary deformation, particularly the short-term deformation field constructed from GPS and other geodetic data (e.g. Beanland and Haines, 1998; Wallace et al., 2004). Although these studies have provided valuable insights, applying this understanding to reported tectonic rotations earlier in the Neogene has been frustrated by the obvious conflict between the 'domain' hypothesis and the more coherent rotation seen in the short-term velocity field. This contradiction can now be addressed. The new paleomagnetic data presented in Chapter 7 indicate coherent rotation of the entire Hikurangi margin, with the exception of the northern Raukumara Peninsula, since the Late Miocene. Detailed geophysical investigations of the present structure of the Hikurangi margin (Chapter 2) also support this interpretation: major changes in basement structure occur at either end of the rotating margin, but there is no evidence for any further lateral subdivision that might allow differential rotation between adjacent parts of the margin. The independently rotating 'domains' proposed by Lamb (1989) and Walcott (1989) therefore appear to have been an artefact of the limited distribution of paleomagnetic data, particularly in the southern Hikurangi margin, and the unrecognized effects of late-forming magnetizations and incompletely removed present-day field overprints (e.g. Chapter 4). Instead, the large-scale boundary forces responsible for contemporary rotation appear to have also driven large-scale, coherent rotations over geological timescales.

8.1.3 The evolving tectonic regime

Key elements of the present tectonic regime, such as the NIDFB and TVZ, were not active before 2 Ma. Prior to this, therefore, different structures must have been involved in accommodating rotation of the Hikurangi margin. The well-constrained history of Neogene tectonic rotation described in Chapter 7 indicates that despite the apparent spatial coherence of tectonic rotations during the Neogene, there is a clear temporal variation in the rate and extent of these rotations, with three main periods apparent.

- Early and Middle Miocene (20–10 Ma): subduction with no rotation.
- Late Miocene and Pliocene (10–2 Ma): rapid (7–14°/Myr) rotation.

- Quaternary (2–0 Ma): continued rotation, but at a reduced rate (3–4°/Myr).

The lateral extent of the rotating region has also changed over time, extending into the Marlborough region since 5 Ma, and possibly onto the Raukumara Peninsula in the last few 100,000 years. Many of these changes can be correlated to the development of new structures in the New Zealand plate boundary zone during the Neogene. The initiation of widespread tectonic rotations at ∼10 Ma coincides with a period of extensive Late Miocene shortening on the southern Hikurangi margin, which stretched as far west as the Taranaki Basin. Rotations in Marlborough from the Pliocene onward appear to have been related to the initiation of strike-slip on the MFZ, caused by the southward propagation of the subduction zone. Finally, reduced rates of rotation at the end of the Pliocene are linked to the activation of strike-slip on the NIDFB, in response to the increasing obliquity of the margin with respect to the plate motion vector. Other aspects of the reconstructions presented in Chapter 7, such as proposed Late Miocene rotations west of the Axial Ranges, need to be verified by future work. Overall, the research presented in this thesis represents significant progress in documenting the evolving response of the Australian plate to large-scale plate boundary forces, and in describing how the 80–90° Neogene rotation of the Hikurangi margin has been accommodated.

8.1.4 Collision of the Hikurangi Plateau: a key tectonic event?

The gradual southward increase in intra-plate coupling along the Hikurangi margin, resulting from subduction of the Hikurangi Plateau, is a key control on contemporary rotation of the forearc; large-scale, regional rotation would not occur if normal oceanic crust was being subducted. The lack of tectonic rotation in the Early and Middle Miocene indicated by paleomagnetic data therefore suggest that subduction of the Hikurangi Plateau did not begin until 8–10 Ma. This interpretation is supported by recent tomographic constraints on the down-dip extent of thickened oceanic crust on the Pacific plate which suggest up to 8 Myr of subduction (Reyners et al., 2004).

In addition to causing the initiation of tectonic rotations, the collision of the Hikurangi Plateau with the subduction zone would have led to increased intra-plate coupling, causing the increased transfer of horizontal strain into the over-riding Australian plate, and uplift of the Hikurangi margin. One potential consequence of this increased tectonism and basement faulting is the migration of methane derived from gas hydrates, hydrocarbons, and other fluids through the Neogene basins on the East Coast of New Zealand. By altering the redox conditions within the sediment pore fluid, such migration events could potentially trigger the late

diagenetic growth of greigite (e.g. Roberts and Weaver, 2005); the large number of remagnetized localities where the age of remanence acquisition is constrained to 5–10 Ma (Figure 7.8; Table 7.2), may therefore also be a consequence of Late Miocene collision of the Hikurangi Plateau

8.1.5 Length scales of deformation

The results presented in Chapter 7 indicate that deformation is occurring over two distinct length scales in this region. Coherent rotation of the entire forearc is occurring over length scales of hundreds of kilometres, in response to rotation of the underlying Pacific plate. However, it is also clear that simply treating the forearc as a large rotating 'microplate' does not provide a full description of the kinematics in the plate boundary zone; distributed deformation is occurring within the forearc region (Section 1.5), principally on large basement faults with a separation of ∼50 km (e.g. Figs. 7.10, 7.11). Paleomagnetic and geodetic data both indicate no significant differential rotations between the blocks defined by these faults, but the substantial slip rates on some of them will result in substantial changes in the shape of the rotating forearc region over geological timescales.

These observations suggest that although large regions of continental crust can show 'plate-like' behaviour, in that they move coherently in response to boundary forces, the boundaries of such 'plates' can be fairly dynamic, quickly changing in shape in response to internal deformation, and also in extent in response to boundary forces (e.g. page 139). This is probably a consequence of the weakness of continental crust with respect to oceanic crust.

8.2 Further work

The research presented in this thesis opens two potentially important avenues for further research, one specific to New Zealand, and the other more general. Within New Zealand, paleomagnetic sampling of Miocene sediments on the west coast of the North Island, and the Nelson region on the South Island, is needed to test the more speculative aspects of the reconstructions presented in Chapter 7, particularly the proposed more spatially extensive Late Miocene rotations. Furthermore, the possibility that much previously published paleomagnetic data may be contaminated by both unrecognised late-forming magnetizations, and also incompletely removed present-day field overprint, means that it would be profitable to revisit some of these localities, testing new samples against published data to assess their reliability. By taking advantage of more sensitive magnetometers and stepwise demagnetization techniques, and using field tests to rigorously constrain the age of remanence acquisition, useful tectonic information may be recoverable at many of these localities. As discussed in Chapter 6, patchily distributed remagnetiza-

tions are of particular concern in sequences where magnetostratigraphy has been used to correlate New Zealand foraminiferal biozones to the geomagnetic polarity timescale (e.g. Lienert et al., 1972; Kennett and Watkins, 1974; Wright and Vella, 1988; Roberts et al., 1994), and reappraisal of these sequences should be a particular priority.

Similar studies of greigite bearing sequences worldwide is also necessary, not only to assess the potential scale of the problems caused by late remagnetizations, but also to assess the geochemical factors that may influence the timing of greigite formation. In some reported occurrences of greigite, it has grown millions of years after deposition; in others, growth has occurred close to the time of deposition, enough to record and preserve a detailed record of a geomagnetic reversal (Roberts et al., 2005). Previous studies have suggested that the preservation of greigite is dependent on the relative concentrations of reactive iron and organic carbon (Kao et al., 2004); similar underlying geochemical controls may also determine the susceptibility of these sediments to remagnetization. Further geochemical analyses of patchily remagnetized sediments might shed some light on the processes that have promoted the late growth of greigite. For example, late reductive diagenesis, linked to e.g. gas hydrate migration, might produce sulphides with distinctive $\delta^{34}S$ signatures, which would allow early- and late-forming magnetizations to be distinguished. In addition, the timing of, and controls on, early greigite growth could be examined by combined rock magnetic, electron microscope and geochemical analyses of sediment cores from areas of rapid marine sedimentation. Fundamental studies of this type provide the background necessary for detailed tectonic (and other) interpretations of paleomagnetic data.

References

Acocella, V., Spinks, K., Cole, J., Nicol, A., 2003. Oblique back arc rifting of Taupo Volcanic zone, New Zealand. *Tectonics, 22*, 1045, doi:10.1029/2002TC001447.

Adams, R. D., Ware, D. E., 1977. Subcrustal earthquakes beneath New Zealand: Locations determined with a laterally inhomogeneous velocity model. *New Zealand Journal of Geology and Geophysics, 20*, 59–83.

Aitchison, J. C., Clarke, G. L., Meffre, S., Cluzel, D., 1995. Eocene arc-continent collision in New Caledonia and implications for regional southwest Pacific tectonic evolution. *Geology, 23*, 161–164.

Ansell, J. H., Bannister, S. C., 1996. Shallow morphology of the subducted Pacific plate along the Hikurangi margin, New Zealand. *Physics of the Earth and Planetary Interiors, 93*, 3–20.

Armstrong, P. A., Allis, R. G., Funnell, R. H., Chapman, D. S., 1998. Late Neogene exhumation patterns in Taranaki Basin (New Zealand): Evidence from offset porosity-depth trends. *Journal of Geophysical Research, 103*, 30269–30282.

Àrnadóttir, T., Thornley, S., Pollitz, F. F., Darby, D. J., 1999. Spatial and temporal strain rate variations at the northern Hikurangi margin, New Zealand. *Journal of Geophysical Research, 104*, 4931–4944.

Ballance, P. F., Ablaev, A. G., Pushchin, I. K., Pletnev, S. P., Birylina, M. G., Itaya, T., Follas, H. A., Gibson, G. W., 1999. Morphology and history of the Kermadec trench-arc-backarc basin-remnant arc system at 30 to 32°S: Geophysical profile, microfossil and K–Ar data. *Marine Geology, 159*, 35–62.

Ballance, P. F., Spörli, K. B., 1979. Northland Allochthon. *Journal of the Royal Society of New Zealand, 9*, 259–275.

Barnes, P. M., Audru, J. C., 1999. Quaternary faulting in the offshore Flaxbourne and Wairarapa Basins, southern Cook Strait, New Zealand. *New Zealand Journal of Geology and Geophysics, 42*, 349–367.

Barnes, P. M., Mercier de Lepinay, B. M., 1997. Rates and mechanics of rapid frontal accretion along the very obliquely convergent southern Hikurangi margin, New Zealand. *Journal of Geophysical Research, 102*, 24931–24952.

Barnes, P. M., Mercier de Lepinay, B. M., Collot, J. Y., Delteil, J., Audru, J. C., 1998. Strain partitioning in the transition area between oblique subduction and continental collision, Hikurangi margin, New Zealand. *Tectonics, 17*, 534–557.

Beanland, S., 1995. *The North Island Dextral Fault Belt, Hikurangi subduction margin, New Zealand*. Unpublished PhD. thesis, Victoria University of Wellington.

Beanland, S., Haines, J., 1998. The kinematics of active deformation in the North Island, New Zealand, determined from geological strain rates. *New Zealand Journal of Geology and Geophysics, 41*, 311–323.

Beanland, S., Melhuish, A., Nicol, A., Ravens, J., 1998. Structure and deformational history of the inner forearc region, Hikurangi subduction margin, New Zealand. *New Zealand Journal of Geology and Geophysics, 41*, 325–342.

Beavan, J., Haines, J., 2001. Contemporary horizontal velocity and strain rate fields of the Pacific–Australian plate boundary zone through New Zealand. *Journal of Geophysical Research, 106*, 741–770.

Berner, R. A., 1984. Sedimentary pyrite formation - an update. *Geochimica et Cosmochimica Acta, 48*, 605–615.

Bourne, M., Stuart, G., 2000. ScSp observed on North Island, New Zealand: Implications for subducting plate structure. *Geophysical Journal International, 142*, 925–932.

Bradshaw, J. D., Weaver, S. D., Muir, R. J., 1996. Mid-Cretaceous oroclinal bending of New Zealand terranes. *New Zealand Journal of Geology and Geophysics, 39*, 461–468.

Buret, C., Chanier, F., Férrière, J., Proust, J. N., 1997. Individualization of a forearc basin during the active margin evolution: Hikurangi subduction margin, New Zealand. *Comptes Rendus de l'Academie des Sciences - Series IIA, 325*, 615–621.

Butler, R. F., 1992. *Paleomagnetism: Magnetic domains to geologic terranes*. Blackwell Scientific Publications, 238pp.

Cande, C., Raymond, C. A., Stock, J., Haxby, W. F., 1995. Geophysics of the Pitman Fracture Zone and Pacific–Antarctic plate motions during the Cenozoic. *Science, 270*, 947–953.

Cande, S. C., Kent, D. V., 1995. Revised calibration of the Geomagnetic Polarity Timescale for the Late Cretaceous and Cenozoic. *Journal of Geophysical Research, 100*, 6093–6095.

Canfield, D. E., Raiswell, R., Bottrell, S., 1992. The reactivity of sedimentary iron minerals toward sulfide. *American Journal of Science, 292*, 659–683.

Carter, L., Lewis, K. B., Davey, F., 1988. Faults in Cook Strait and their bearing on the structure of central New Zealand. *New Zealand Journal of Geology and Geophysics, 31*, 431–446.

Carter, L., Manighetti, B., Elliot, M., Trustrum, N., Gomez, B., 2002. Source, sea level and circulation effects on the sediment flux to the deep ocean over the past 15 ka off eastern New Zealand. *Global and Planetary Change, 33*, 339–355.

Carter, L., Shane, P., Alloway, B., Hall, I. R., Harris, S. E., Westgate, J. A., 2003. Demise of one volcanic zone and birth of another - a 12 m.y. marine record of major rhyolitic eruptions from New Zealand. *Geology, 31*, 493–496.

Chanier, F., Férrière, J., 1989. On the existence of major tangential movements in the East Coast Range of New Zealand - their significance within the framework of Pacific plate subduction. *Comptes Rendus de l'Academie des Sciences Series II, 308*, 1645–1650.

Cole, J. W., Lewis, K. B., 1981. Evolution of the Taupo–Hikurangi subduction system. *Tectonophysics, 72*, 1–21.

Collot, J. Y., Davy, B., 1998. Forearc structures and tectonic regimes at the oblique subduction zone between the Hikurangi Plateau and the southern Kermadec margin. *Journal of Geophysical Research, 103*, 623–650.

Collot, J. Y., Delteil, J., Lewis, K. B., Davy, B., Lamarche, G., Audru, J. C., Barnes, P., Chanier, F., Chaumillon, E., Lallemand, S., deLepinay, B. M., Orpin, A., Pelletier, B., Sosson, M., Toussaint, B., Uruski, C., 1996. From oblique subduction to intra-continental transpression: Structures of the southern Kermadec–Hikurangi margin from multibeam bathymetry, side-scan sonar and seismic reflection. *Marine Geophysical Researches, 18*, 357–381.

Cooper, R. A., 2004. *New Zealand Geological Timescale 2004/2 wallchart*. Vol. 64 of Institute of Geological and Nuclear Sciences information series. Insitute of Geological and Nuclear Sciences Limited, Lower Hutt, New Zealand.

Creer, K. M., 1961. Superparamagnetism in red sandstones. *Geophysical Journal of the Royal Astronomical Society, 5*, 16–28.

Davey, B., Collot, J. Y., 2000. The Rapuhia scarp (northern Hikurangi Plateau) - its nature and subduction effects on the Kermadec Trench. *Tectonophysics, 328*, 269–295.

Davey, F. J., Henrys, S., Lodolo, E., 1997. A seismic crustal section across the East Cape convergent margin, New Zealand. *Tectonophysics, 269*, 199–215.

Davey, F. J., Stern, T. A., 1990. Crustal seismic observations across the convergent plate boundary, North Island, New Zealand. *Tectonophysics, 173*, 283–296.

Davies, E. J., Frederick, J. B., Leask, W. L., Williams, T. J., 2000. East Coast Drilling Results. *New Zealand Petroleum Conference Proceedings*.

Davy, B., Wood, R., 1994. Gravity and magnetic modelling of the Hikurangi Plateau. *Marine Geology, 118*, 139–151.

Day, R., Fuller, M., Schmidt, V. A., 1977. Hysteresis properties of titanomagnetites: Grain size and composition dependence. *Physics of the Earth and Planetary Interiors, 13*, 260–266.

Delteil, J., Morgans, H. E. G., Raine, J. I., Field, B. D., Cutten, H. N. C., 1996. Early Miocene thin-skinned tectonics and wrench faulting in the Pongaroa district, Hikurangi margin, North Island, New Zealand. *New Zealand Journal of Geology and Geophysics, 39*, 271–282.

Delteil, J., Ruellan, E., Wright, I., Matsumoto, T., 2002. Structure and structural development of the Havre Trough (SW Pacific). *Journal of Geophysical Research, 107*, 2143, doi:10.1029/2001JB000494.

Demarest, H. H., 1983. Error analysis for the determination of tectonic rotation from paleomagnetic data. *Journal of Geophysical Research, 88*, 4321–4328.

DeMets, C., Gordon, R. G., Argus, D. F., Stein, S., 1994. Effect of recent revisions to the geomagnetic reversal time-scale on estimates of current plate motions. *Geophysical Research Letters, 21*, 2191–2194.

Dunlop, D. J., 1979. On the use of Zijderveld vector diagrams in multicomponent paleomagnetic samples. *Physics of the Earth and Planetary Interiors, 20*, 12–24.

Dunlop, D. J., 2002. Theory and application of the Day plot (M_{rs}/M_s versus H_{cr}/H_c) 1. Theoretical curves and tests using titanomagnetite data. *Journal of Geophysical Research, 107*, 2056, doi:10.1029/2001JB000486.

Eberhart-Phillips, D., Reyners, M., 1997. Continental subduction and three-dimensional crustal structure: The northern South Island, New Zealand. *Journal of Geophysical Research, 102*, 11843–11861.

Eberhart-Phillips, D., Reyners, M., 1999. Plate interface properties in the north-east Hikurangi subduction zone, New Zealand, from converted seismic waves. *Geophysical Research Letters, 26*, 2565–2568.

Field, B. D., Uruski, C. I., et al., 1997. *Cretaceous-Cenozoic Geology and Petroleum Systems of the East Coast Region*. Vol. 19 of Institute of Geological and Nuclear Sciences Monograph. Insitute of Geological and Nuclear Sciences Limited, Lower Hutt, New Zealand.

Fisher, R. A., 1953. Dispersion on a sphere. *Proceedings of the Royal Society, London, 217A*, 295–305.

Florindo, F., Sagnotti, L., 1995. Palaeomagnetism and rock magnetism in the upper Pliocene Valle Ricca (Rome, Italy) section. *Geophysical Journal International, 123*, 340–354.

Fournier, M., Jolivet, L., Huchon, P., Sergeyev, K. F., Oscorbin, L. S., 1994. Neogene strike-slip faulting in Sakhalin and the Japan Sea opening. *Journal of Geophysical Research, 99*, 2701–2725.

Francis, D., Bennett, D., Courteney, S., 2004. Advances in understanding of onshore East Coast Basin structure, stratigraphic thickness and hydrocarbon generation. *New Zealand Petroluem Conference Proceedings*.

Funnell, R., Chapman, D., Allis, R., Armstrong, P., 1996. Thermal state of the Taranaki Basin, New Zealand. *Journal of Geophysical Research, 101*, 25197–25215.

Gaina, C., Muller, D. R., Royer, J. Y., Stock, J., Hardebeck, J., Symonds, P., 1998. The tectonic history of the Tasman Sea: A puzzle with 13 pieces. *Journal of Geophysical Research, 103*, 12413–12433.

Hall, L. S., Lamb, S. H., MacNiocaill, C., 2004. Cenozoic distributed rotational deformation, South Island, New Zealand. *Tectonics, 23*, TC2002, doi:10.1029/2002TC001421.

Hall, R., 2002. Cenozoic geological and plate tectonic evolution of SE Asia and the SW Pacific: Computer-based reconstructions, model and animations. *Journal of Asian Earth Sciences, 20*, 353–431.

Herzer, R. H., 1995. Seismic stratigraphy of a buried volcanic arc, Northland, New Zealand and implications for Neogene subduction. *Marine and Petroleum Geology, 12*, 511–531.

Herzer, R. H., Mascle, J., Davy, B., Ruellan, E., Mortimer, N., Laporte, C., Duxfield, A., 2000. New constraints on the New Zealand-South Fiji Basin continent-back-arc margin. *Comptes Rendus de l'Academie des Sciences - Series IIA, 330*, 701–708.

Holt, W. E., Haines, A. J., 1995. The kinematics of northern South Island, New Zealand, determined from geologic strain rates. *Journal of Geophysical Research, 100*, 17991–18010.

Hornafius, J. S., 1985. Neogene tectonic rotation of the Santa-Ynez Range, western Transverse Ranges, California, suggested by paleomagnetic investigation of the Monterey Formation. *Journal of Geophysical Research, 90*, 2503–2522.

Hornafius, J. S., Luyendyk, B. P., Terres, R. R., Kamerling, M. J., 1986. Timing and extent of Neogene tectonic rotation in the western Transverse Ranges, California. *Geological Society of America Bulletin, 97*, 1476–1487.

Horng, C. S., Torii, M., Shea, K. S., Kao, S. J., 1998. Inconsistent magnetic polarities between greigite- and pyrrhotite/magnetite-bearing marine sediments from the Tsailiao-chi section, southwestern Taiwan. *Earth and Planetary Science Letters, 164*, 467–481.

Housen, B. A., Musgrave, R. J., 1996. Rock-magnetic signature of gas hydrates in accretionary prism sediments. *Earth and Planetary Science Letters, 139*, 509–519.

Idnurm, M., 1985. Late Mesozoic and Cenozoic palaeomagnetism of Australia. 1. a redetermined apparent polar wander path. *Geophysical Journal of the Royal Astronomical Society, 83*, 399–418.

Jackson, J., Molnar, P., 1990. Active faulting and block rotations in the western Transverse Ranges, California. *Journal of Geophysical Research, 95*, 22073–22087.

Jiang, W. T., Horng, C. S., Roberts, A. P., Peacor, D. R., 2001. Contradictory magnetic polarities in sediments and variable timing of neoformation of authigenic greigite. *Earth and Planetary Science Letters, 193*, 1–12.

Johnson, B., Gordon, R., 1996. Recent Pacific Plate standstill? A 32 Ma paleomagnetic pole for the Pacific Plate determined from magnetic anomaly skewness and implications for motion of the Pacific hotspots relative to the spin axis since mid-Tertiary. *Eos Trans. AGU, 77*, F157.

Kao, S. J., Horng, C. S., Roberts, A. P., Liu, K. K., 2004. Carbon-sulfur-iron relationships in sedimentary rocks from southwestern Taiwan: Influence of geochemical environment on greigite and pyrrhotite formation. *Chemical Geology, 203*, 153–168.

Karlin, R., 1990. Magnetite diagenesis in marine sediments from the Oregon continental margin. *Journal of Geophysical Research, 95*, 4405–4419.

Karlin, R., Levi, S., 1983. Diagenesis of magnetic minerals in recent haemipelagic sediments. *Nature, 303*, 327–330.

Karlin, R., Levi, S., 1985. Geochemical and sedimentological control of the magnetic properties of hemipelagic sediments. *Journal of Geophysical Research, 90*, 373–392.

Kelsey, H. M., Cashman, S. M., Beanland, S., Berryman, K., 1995. Structural evolution along the inner forearc of the obliquely convergent Hikurangi margin, New Zealand. *Tectonics, 14*, 1–18.

Kennett, J. P., Watkins, N. D., 1974. Late Miocene-Early Pliocene paleomagnetic stratigraphy, paleoclimatology, and biostratigraphy in New Zealand. *Geological Society of America Bulletin, 85*, 1385–1398.

King, P. R., 2000. Tectonic reconstructions of New Zealand: 40 Ma to the present. *New Zealand Journal of Geology and Geophysics, 43*, 611–638.

King, P. R., Thrasher, G. P., 1992. Post-Eocene development of the Taranaki Basin, New Zealand: Convergent overprint of a passive margin. In: Watkin, J. S., Zhiqiang, F., McMillen, K. J. (Eds.), Geology and Geophysics of Continental Margins,. Vol. 53 of *American Association of Petroleum Geologists Memoir,*. pp. 93–118.

Kingma, J. T., 1962. Sheet 11 Dannevirke, *Geological Map of New Zealand 1:250,000*. Department of Scientific and Industrial Research, Wellington, New Zealand.

Kirschvink, J. L., 1980. The least squares line and plane and the analysis of palaeomagnetic data. *Geophysical Journal of the Royal Astronomical Society, 62*, 699–710.

Kissel, C., Laj, C., 1988. The Tertiary geodynamical evolution of the Aegean arc - a paleomagnetic reconstruction. *Tectonophysics, 146*, 183–201.

Kissel, C., Laj, C., Poisson, A., Savascin, Y., Simeakis, K., Mercier, J. L., 1986. Paleomagnetic evidence for Neogene rotational deformations in the Aegean domain. *Tectonics, 5*, 783–795.

Lamb, S., 1989. Rotations about vertical axes in part of the New Zealand plate boundary zone, theory and observation. In: Kissel, C., Laj, C. (Eds.), *Paleomagnetic Rotations and Continental Deformation*. Kluwer, pp. 473–488.

Lamb, S. H., 1988. Tectonic rotations about vertical axes during the last 4 Ma in part of the New Zealand plate boundary zone. *Journal of Structural Geology, 10*, 875–893.

Lee, J. M., Begg, J. G., 2002. Geology of the Wairarapa Area. 1: 250 000 geological map 11. Institute of Geological and Nuclear Sciences Limited, Lower Hutt, New Zealand.

Lewis, K. B., Carter, L., Davey, F. J., 1994. The opening of Cook Strait - interglacial tidal scour and aligning basins at a subduction to transform plate edge. *Marine Geology, 116*, 293–312.

Lewis, K. B., Pettinga, J. R., 1993. The emerging, imbricate frontal wedge of the Hikurangi Margin. In: Ballance, P. F. (Ed.), *Sedimentary basins of the World 2: South Pacific sedimentary basins*. Elsevier, Amsterdam, pp. 225–229.

Lienert, B. R., Christoffel, D. A., Vella, P., 1972. Geomagnetic dates on a New Zealand Upper Miocene-Pliocene section. *Earth and Planetary Science Letters, 16*, 195–199.

Little, T. A., Roberts, A. P., 1997. Distribution and mechanism of Neogene to present-day vertical axis rotations, Pacific-Australian plate boundary zone, South Island, New Zealand. *Journal of Geophysical Research, 102*, 20447–20468.

Mackinnon, T. C., 1983. Origin of the Torlesse Terrane and coeval rocks, South Island, New Zealand. *Geological Society of America Bulletin, 94*, 967–985.

Malahoff, A., Feden, R. H., Fleming, H. S., 1982. Magnetic anomalies and tectonic fabric of marginal basins north of New Zealand. *Journal of Geophysical Research, 87*, 4109–4125.

Mazengarb, C., Speden, I. G., 2000. Geology of the Raukumara Area. *1: 250 000 geological map 6*. Institute of Geological and Nuclear Sciences Limited, Lower Hutt, New Zealand.

McElhinny, M. W., 1964. Statistical significance of the fold test in paleomagnetism. *Geophysical Journal of the Royal Astronomical Society, 8*, 338–40.

McFadden, P. L., 1990. A new fold test for paleomagnetic studies. *Geophysical Journal International, 103*, 163–169.

McFadden, P. L., McElhinny, M. W., 1988. The combined analysis of remagnetisation circles and direct observations in palaeomagnetism. *Earth and Planetary Science Letters, 87*, 161–172.

McFadden, P. L., McElhinny, M. W., 1990. Classification of the reversal test in palaeomagnetism. *Geophysical Journal International, 103*, 725–729.

Molnar, P., 1988. Continental tectonics in the aftermath of plate tectonics. *Nature, 335*, 131–137.

Mortimer, N., Herzer, R., Gans, P., Parkinson, D., Seward, D., 1998. Basement geology from Three Kings Ridge to West Norfolk Ridge, southwest Pacific Ocean: Evidence from petrology, geochemistry and isotopic dating of dredge samples. *Marine Geology, 148*, 135–162.

Mortimer, N., Parkinson, D., 1996. Hikurangi Plateau: A Cretaceous large igneous province in the southwest Pacific Ocean. *Journal of Geophysical Research, 101*, 687–696.

Moskowitz, B. M., 1991. The Hitchiker's Guide to Magnetism. First presented at Environmental Magnetism Workshop, Institute for Rock Magnetism. URL `http://www.geo.umn.edu/orgs/irm/hg2m/hg2m_index.html`

Mumme, T. C., Lamb, S., Walcott, R. I., 1989. The Raukumara paleomagnetic domain: Constraints on the tectonic rotation of the East Coast, N Island, New Zealand, from paleomagnetic data. *New Zealand Journal of Geology and Geophysics, 32*, 317–326.

Mumme, T. C., Walcott, R. I., 1985. Paleomagnetic studies at Geophysics Division 1980–1983. *Geophysics Division Research Report, 204*, Department of Scientific and Industrial Research.

Musgrave, R. J., 1989. A weighted least-squares fit of the Australian apparent polar wander path for the last 100 Myr. *Geophysical Journal International, 96*, 231–243.

Neef, G., 1992. The Cenozoic geology of the Gisborne area (1:50 000 metric sheet Y18AB), North Island, New Zealand. *New Zealand Journal of Geology and Geophysics, 35*, 515–531.

Néel, L., 1954. Remarques sur la théorie des propriétiés magnétiques des substances dures. *Appl. Sci. Res. B, 4*, 13–24.

Nicol, A., Beavan, J., 2003. Shortening of an overriding plate and its implications for slip on a subduction thrust, central Hikurangi Margin, New Zealand. *Tectonics, 22*, 1070, doi: 10.1029/2003TC001521.

Oda, H., Torii, M., 2004. Sea-level change and remagnetization of continental shelf sediments off New Jersey (ODP Leg 174A): Magnetite and greigite diagenesis. *Geophysical Journal International, 156*, 443–458.

Opdyke, N. D., Channell, J. E. T., 1996. Magnetic Stratigraphy. Academic Press, 346pp.

Petronotis, K. E., Gordon, R. G., Acton, G. D., 1994. A 57Ma Pacific Plate palaeomagnetic pole determined from a skewness analysis of crossings of marine magnetic anomaly 25r. *Geophysical Journal International, 118*, 529–554.

Pike, C. R., 2003. First-order reversal curve diagrams and reversible magnetization. *Physical Review B, 68*, doi:10.1103/PhysRevB.68.104424.

Pike, C. R., Roberts, A. P., Verosub, K. L., 1999. Characterizing interactions in fine magnetic particle systems using first order reversal curves. *Journal of Applied Physics, 85*, 6660–6667.

Pike, C. R., Roberts, A. P., Verosub, K. L., 2001. First-order reversal curve diagrams and thermal relaxation effects in magnetic particles. *Geophysical Journal International, 145*, 721–730.

Pillans, B. J., Roberts, A. P., Wilson, G. S., Abbott, S. T., Alloway, B. V., 1994. Magnetostratigraphic, lithostratigraphic and tephrostratigraphic constraints on Lower and Middle Pleistocene sea-level changes, Wanganui Basin, New Zealand. *Earth and Planetary Science Letters, 121*, 81–98.

Preisach, F., 1934. Über die magnetische Nachwirkung. *Z. Phys., 941*, 277–302.

Raiswell, R., 1982. Pyrite texture, isotopic composition and the availability of iron. *American Journal of Science, 282*, 1244–1263.

Rait, G. J., 2000. Thrust transport directions in the Northland Allochthon, New Zealand. *New Zealand Journal of Geology and Geophysics, 43*, 271–288.

Rait, G. J., Chanier, F., Waters, D. W., 1991. Landward- and seaward- directed thrusting accompanying the onset of subduction beneath New Zealand. *Geology, 19*, 230–233.

Reading, A. M., Gubbins, D., Mao, W., 2001. A multiphase seismic investigation of the shallow subduction zone, southern North Island, New Zealand. *Geophysical Journal International, 147*, 215–226.

Reyners, M., 1983. Lateral segmentation of the subducted plate at the Hikurangi Margin, New Zealand: Seismological evidence. *Tectonophysics, 96*, 203–223.

Reyners, M., 1998. Plate coupling and the hazard of large subduction thrust earthquakes at the Hikurangi subduction zone, New Zealand. *New Zealand Journal of Geology and Geophysics, 41*, 343–354.

Reyners, M., Eberhart-Phillips, D., Stuart, G., 1999. A three-dimensional image of shallow subduction: Crustal structure of the Raukumara Peninsula, New Zealand. *Geophysical Journal International, 137*, 873–890.

Reyners, M., Eberhart-Phillips, D., Stuart, G., Nishimura, Y., 2004. Constraints on subduction and magmatism beneath the central North Island, New Zealand, from seismic tomography. *Geological Society of New Zealand Miscellaneous publication, 117A*, 85–86.

Reyners, M., McGinty, P., 1999. Shallow subduction tectonics in the Raukumara Peninsula, New Zealand, as illuminated by earthquake focal mechanisms. *Journal of Geophysical Research, 104*, 3025–3034.

Reyners, M., Robinson, R., McGinty, P., 1997. Plate coupling in the northern South Island and southernmost North Island, New Zealand, as illuminated by earthquake focal mechanisms. *Journal of Geophysical Research, 102*, 15197–15210.

Reynolds, R. L., Tuttle, M. L., Rice, C. A., Fishman, N. S., Karachewski, J. A., Sherman, D. M., 1994. Magnetization and geochemistry of greigite-bearing Cretaceous strata, North Slope Basin, Alaska. *American Journal of Science, 294*, 485–528.

Roberts, A. P., 1990. *Cainozoic Palaeomagnetism and Tectonics of the Marlborough Region, South Island, New Zealand*. Unpublished PhD. thesis, Victoria University of Wellington, 201 pp.

Roberts, A. P., 1992. Paleomagnetic constraints on the tectonic rotation of the southern Hikurangi margin, New Zealand. *New Zealand Journal of Geology and Geophysics, 35*, 311–323.

Roberts, A. P., 1995a. Magnetic properties of sedimentary greigite (Fe_3S_4). *Earth and Planetary Science Letters, 134*, 227–236.

Roberts, A. P., 1995b. Tectonic rotation about the termination of a major strike-slip fault, Marlborough Fault System, New Zealand. *Geophysical Research Letters, 22*, 187–190.

Roberts, A. P., Jiang, W. T., Florindo, F., Horng, C. S., Laj, C., 2005. Assessing the timing of greigite formation and the reliability of the upper Olduvai polarity transition record from the Crostolo River, Italy. *Geophysical Research Letters, 32*, L05307, doi:10.1029/2004GL022137.

Roberts, A. P., Pike, C. R., Verosub, K. L., 2000. First-order reversal curve diagrams: A new tool for characterizing the magnetic properties of natural samples. *Journal of Geophysical Research, 105*, 28461–28475.

Roberts, A. P., Pillans, B. J., 1993. Rock magnetism of Lower-Middle Pleistocene marine sediments, Wanganui Basin, New Zealand. *Geophysical Research Letters, 20*, 839–842.

Roberts, A. P., Turner, G. M., 1993. Diagenetic formation of ferrimagnetic iron sulphide minerals in rapidly deposited marine sediments, South Island, New Zealand. *Earth and Planetary Science Letters, 115*, 257–273.

Roberts, A. P., Turner, G. M., Vella, P. P., 1994. Magnetostratigraphic chronology of Late Miocene to Early Pliocene biostratigraphic and oceanographic events in New Zealand. *Geological Society of America Bulletin, 106*, 665–683.

Roberts, A. P., Weaver, R., 2005. Multiple mechanisms of remagnetization involving sedimentary greigite (Fe_3S_4). *Earth and Planetary Science Letters, 231*, 263–277.

Sagnotti, L., Roberts, A. P., Weaver, R., Verosub, K. L., Florindo, F., Pike, C. R., Clayton, T., Wilson, G. S., 2005. Apparent magnetic polarity reversals due to remagnetization resulting from late diagenetic growth of greigite from siderite. *Geophysical Journal International, 160*, 89–100.

Sagnotti, L., Winkler, A., 1999. Rock magnetism and palaeomagnetism of greigite-bearing mudstones in the Italian peninsula. *Earth and Planetary Science Letters, 165*, 67–80.

Sdrolias, M., Müller, R. D., Gaina, C., 2003. Tectonic evolution of the Southwest Pacific using constraints from back-arc basins. In: Hillis, R. R., Müller, R. D. (Eds.), Evolution and Dynamics of the Australian Plate. Vol. 372 of *Geological Society of America Special Papers*. pp. 343–359.

Sdrolias, M., Müller, R. D., Mauffret, A., Bernardel, G., 2004. Enigmatic formation of the Norfolk Basin, SW Pacific: A plume influence on back-arc extension. *Geochemistry, Geophysics, Geosystems, 5*, Q06005, doi:10.129/2003GC000643.

Smale, D., 1990. Distribution and provenance of heavy minerals in the South Island - a review. *New Zealand Journal of Geology and Geophysics, 33*, 557–571.

Smith, E. G. C., Stern, T., Reyners, M., 1989. Subduction and back-arc activity at the Hikurangi convergent margin, New Zealand. *Pure and Applied Geophysics, 129*, 203–231.

Smith, W. H. F., Sandwell, D. T., 1997. Global sea floor topography from satellite altimetry and ship depth soundings. *Science, 277*, 1956–1962.

Snowball, I. F., 1997. Gyroremanent magnetization and the magnetic properties of greigite-bearing clays in southern Sweden. *Geophysical Journal International, 129*, 624–636.

Sorlien, C. C., Kamerling, M. J., Mayerson, D., 1999. Block rotation and termination of the Hosgri strike-slip fault, California, from three-dimensional map restoration. *Geology, 27*, 1039–1042.

Speranza, F., Sagnotti, L., Mattei, M., 1997. Tectonics of the Umbria-Marche-Romagna Arc (central-northern Apennines, Italy): New paleomagnetic constraints. *Journal of Geophysical Research, 102*, 3153–3166.

Spörli, K. B., 1982. Review of paleo-strain/stress directions in Northland, New Zealand, and of the structure of the Northland Allochthon. *Tectonophysics, 87*, 25–36.

Stern, T. A., 1987. Asymmetric back-arc spreading, heat flux and structure associated with the Central Volcanic Region of New Zealand. *Earth and Planetary Science Letters, 85*, 265–276.

Stern, T. A., Quinlan, G. M., Holt, W. E., 1993. Crustal dynamics associated with the formation of the Wanganui Basin. In: Ballance, P. F. (Ed.), *Sedimentary Basins of the World, 2: South Pacific Sedimentary Basins*. Elsevier, Amsterdam, pp. 213–223.

Stoneley, R., 1968. A lower Tertiary décollement of the East Coast, North Island, New Zealand. *New Zealand Journal of Geology and Geophysics, 11*, 128–156.

Sutherland, R., 1995. The Australian-Pacific boundary and Cenozoic plate motions in the SW Pacific: Some constraints from Geosat data. *Tectonics, 14*, 819–831.

Sutherland, R., 1999a. Basement geology and tectonic development of the greater New Zealand region: An interpretation from regional magnetic data. *Tectonophysics, 308*, 341–362.

Sutherland, R., 1999b. Cenozoic bending of New Zealand basement terranes and Alpine Fault displacement: A brief review. *New Zealand Journal of Geology and Geophysics, 42*, 295–301.

Sutherland, R., Hollis, C., 2001. Cretaceous demise of the Moa plate and strike slip motion at the Gondwana margin. *Geology, 29*, 279–282.

Takeuchi, T., Kodama, K., Ozawa, T., 1999. Paleomagnetic evidence for block rotations in central Hokkaido-south Sakhalin, northeast Asia. *Earth and Planetary Science Letters, 169*, 7–21.

Tauxe, L., 1998. *Paleomagnetic Principles and Practice*. Kluwer, 299 pp.

Tauxe, L., Mullender, T. A. T., Pick, T., 1996. Potbellies, wasp-waists, and superparamagnetism in magnetic hysteresis. *Journal of Geophysical Research, 101*, 571–583.

Tauxe, L., Watson, G., 1994. The fold test: An eigen analysis approach. *Earth and Planetary Science Letters, 122*, 331–341.

Thatcher, W., 1995. Microplate versus continuum descriptions of active tectonic deformation. *Journal of Geophysical Research, 100*, 3885–3894.

Thornley, S., 1996. *Neogene Tectonics of Raukumara Peninsula, Northern Hikurangi Margin, New Zealand*. Unpublished PhD. thesis, Victoria University of Wellington.

Turner, G. M., 2001. Toward an understanding of the multicomponent magnetization of uplifted marine sediments in New Zealand. *Journal of Geophysical Research, 106*, 6385–6397.

Turner, G. M., Kamp, P. J. J., 1990. Paleomagnetic location of the Jaramillo Subchron and the Matuyama-Brunhes transition in the Castlecliffian stratotype section, Wanganui Basin, New Zealand. *Earth and Planetary Science Letters, 100*, 42–50.

Turner, G. M., Roberts, A. P., Laj, C., Kissel, C., Mazaud, A., Guitton, S., Christoffel, D. A., 1989. New paleomagnetic results from Blind River - revised magnetostratigraphy and tectonic rotation of the Marlborough region, South Island, New Zealand. *New Zealand Journal of Geology and Geophysics, 32*, 191–196.

Upton, P., Koons, P. O., Eberhart-Phillips, D., 2003. Extension and partitioning in an oblique subduction zone, New Zealand: Constraints from three-dimensional numerical modelling. *Tectonics, 22*, 1068, doi:10.1029/2002TC001431.

Van der Voo, R., 1993. *Paleomagnetism of the Atlantic, Tethys and Iapetus Oceans*. Cambridge University Press, 411 pp.

Van Dissen, R. J., Berryman, K. R., 1996. Surface rupture earthquakes over the last ∼1000 years in the Wellington region, New Zealand, and implications for ground shaking hazard. *Journal of Geophysical Research, 101*, 5999–6019.

Vickery, S., Lamb, S., 1995. Large tectonic rotations since the Early Miocene in a convergent plate-boundary zone, South Island, New Zealand. *Earth and Planetary Science Letters, 136*, 43–59.

von Heune, R., Scholl, D. W., 1991. Observations at convergent margins concerning sediment subduction, subduction erosion, and the growth of continental crust. *Reviews of Geophysics, 29*, 279–316.

Walcott, R. I., 1978. Present tectonics and late Cenozoic evolution of New Zealand. *Geophysical Journal of the Royal Astronomical Society, 52*, 137–164.

Walcott, R. I., 1984a. The kinematics of the plate boundary zone through New Zealand: A comparison of short and long-term deformations. *Geophysical Journal of the Royal Astronomical Society, 79*, 613–633.

Walcott, R. I., 1984b. Reconstructions of the New Zealand region for the Neogene. *Palaeogeography, Palaeoclimatology, Palaeoecology, 46*, 217–231.

Walcott, R. I., 1987. Geodetic strain and the deformational history of the North Island of New Zealand during the late Cainozoic. *Philosophical Transactions of the Royal Society of London, Series A, 321*, 163–181.

Walcott, R. I., 1989. Paleomagnetically observed rotations along the Hikurangi Margin of New Zealand. In: Kissel, C., Laj, C. (Eds.), *Paleomagnetic Rotations and Continental Deformation*. Kluwer, Dordrecht, pp. 459–471.

Walcott, R. I., 1998. Modes of oblique compression: Late Cenozoic tectonics of the South Island of New Zealand. *Reviews of Geophysics, 36*, 1–26.

Walcott, R. I., Christoffel, D. A., Mumme, T. C., 1981. Bending within the axial tectonic belt of New Zealand in the last 9 Myr from paleomagnetic data. *Earth and Planetary Science Letters, 52*, 427–434.

Walcott, R. I., Mumme, T. C., 1982. Paleomagnetic study of the Tertiary sedimentary rocks from the East Coast of the North Island, New Zealand. *Geophysics Division Research Report* 189, Department of Scientific and Industrial Research, 62 pp.

Wallace, L. M., Beavan, J., McCaffrey, R., Darby, D., 2004. Subduction zone coupling and tectonic block rotations in the North Island, New Zealand. *Journal of Geophysical Research, 109*, B12406, doi:10.1029/2004JB003241.

Weaver, R., Roberts, A. P., Barker, A. J., 2002. A late diagenetic (syn-folding) magnetization carried by pyrrhotite: Implications for paleomagnetic studies from magnetic iron sulphide-bearing sediments. *Earth and Planetary Science Letters, 200*, 371–386.

Weaver, R., Roberts, A. P., Flecker, R., Macdonald, D. I. M., Fot'yanova, L. M., 2003. Geodynamic implications of paleomagnetic data from Tertiary sediments in Sakhalin, Russia (NW Pacific). *Journal of Geophysical Research, 108*, 2066, doi:10.1029/2001JB001226.

Webb, T. H., Anderson, H., 1998. Focal mechanisms of large earthquakes in the North Island of New Zealand: Slip partitioning at an oblique active margin. *Geophysical Journal International, 134*, 40–86.

Wilkin, R. T., Barnes, H. L., 1997. Formation processes of framboidal pyrite. *Geochimica et Cosmochimica Acta, 61*, 323–339.

Wilson, C. J. N., Houghton, B. F., McWilliams, M. O., Lanphere, M. A., Weaver, S. D., Briggs, R. M., 1995. Volcanic and structural evolution of Taupo Volcanic Zone, New Zealand: A review. *Journal of Volcanology and Geothermal Research, 68*, 1–28.

Wilson, G. S., McGuire, D. M., 1995. Distributed deformation due to coupling across a subduction thrust: Mechanism of young tectonic rotation within the south Wanganui Basin, New Zealand. *Geology, 23*, 645–648.

Wilson, G. S., Roberts, A. P., 1999. Diagenesis of magnetic mineral assemblages in multiply redeposited siliciclastic marine sediments, Wanganui Basin, New Zealand. In: Tarling, D. H., Turner, P. (Eds.), Paleomagnetism and diagenesis in sediments. Vol. 151 of *Geological Society Special Publications*. pp. 95–108.

Wood, R., Davy, B., 1994. The Hikurangi Plateau. *Marine Geology, 118*, 153–173.

Wood, R., Lamarche, G., Herzer, R., Delteil, J., Davy, B., 1996. Paleogene seafloor spreading in the southeast Tasman Sea. *Tectonics, 15*, 966–975.

Wright, I. C., 1993. Pre-spread rifting and heterogenous volcanism in the southern Havre Trough back-arc basin. *Marine Geology, 113*, 179–200.

Wright, I. C., Vella, P. P., 1988. A New Zealand Late Miocene magnetostratigraphy - glacioeustatic and biostratigraphic correlations. *Earth and Planetary Science Letters, 87*, 193–204.

Wright, I. C., Walcott, R. I., 1986. Large tectonic rotation of part of New Zealand in the past 5 Ma. *Earth and Planetary Science Letters, 80*, 348–352.

Zijderveld, J. D. A., 1967. A.C. Demagnetization of rocks: Analysis of results. In: Collinson, D. W., Creer, K. M., Runcorn, S. K. (Eds.), *Methods in Paleomagnetism*. Elsevier, Amsterdam, pp. 254–286.

Appendix A

Summary of sampling localities

AB - Anzac Bridge

Details of sampling

Date sampled	16^{th} February 2002
Locality description	Outcrop on the banks of the Waihuka River, located where a tributary joins it 200 m east and downstream of a bridge across State Highway 2 (Anzac Bridge), 2-3 km southeast of the Oliver Road turn-off.
Grid reference	X17/063871
Lithology	Massive, fractured, blue-grey mudstones with rare massive sandstone beds.
Assigned age	Otaian
Bedding attitude	298/57 NE (3 measurements)
Sampling	41 cores from 9 sampling levels, yielding 61 samples.
Stratigraphic thickness	53 metres

Demagnetization data

Samples demagnetized	AF 9 samples, thermal 33 samples.
Demagnetization behaviour	Strong PDF with no evidence of higher stability components
Range of NRMs	0.52–1.8×10^{-4} Am^{-1}
Isolated components	None.

Rock magnetic measurements

Samples analysed	2
Range of M_r/M_s	0.12–0.14
Range of B_{cr}/B_c	3.64–3.84
FORC behaviour	RR/SD 2.8–3.0; small SD peak at ∼20–30 mT.

AF - Atea Ford

Details of sampling

Dates sampled	23^{rd}–24^{th} February 2002
Locality description	Roadside outcrop, close to most easterly of two fords crossing Wharekopae Road west of Rere.
Grid reference	X17/063871
Lithology	Massive sandstones with thinly interbedded mudstones, which are often calcareous and occasionally sandy.
Assigned age	Altonian - stratigraphically below Rere sandstone.
Bedding attitude	017/12 E (2 measurements)
Sampling	37 cores from 10 sampling levels, yielding 35 samples.
Stratigraphic thickness	41 metres

Demagnetization data

Samples demagnetized	AF 9 samples, thermal 26 samples.
Demagnetization behaviour	Variable - some indications of a reversed polarity, rotated ChRM in the lower part of the section, no systematic trends in the middle and strong PDF overprint at the top. Thermal demagnetization slightly more effective than AF.
Range of NRMs	0.52–15$\times 10^{-4}$ Am^{-1}
Isolated components	None.

BH - Blackhead

Details of sampling

Dates sampled	19^{th} March 2003
Locality description	Cliff exposure ∼500 m south of car park on Blackhead Beach, with additional outcrop exposed on a wave-cut platform beneath the cliffs at low tide.
Grid reference	V23/359074
Lithology	Massive, light grey mudstones and siltstones. Decimetre-scale bedding can be seen in the cliff exposure; on the wave-cut platform outcrop is more massive, with discontinuous calcareous concretions following the trend of bedding.
Assigned age	Tongaporutuan
Bedding attitude	067/23 SE (3 measurements)
Sampling	39 cores from 9 sampling levels, yielding 64 samples.
Stratigraphic thickness	13 metres

Demagnetization data

Samples demagnetized	AF 15 samples, thermal 21 samples.
Demagnetization behaviour	Strong PDF overprint that can occasionally be removed to reveal a reversed polarity ChRM, which typically unblocks by 30 mT/300°C. NRMs are weak and demagnetization paths are often noisy.
Range of NRMs	0.1–9.8×10^{-4} Am^{-1}
Isolated components	11 anchored ChRMs, 1 unanchored ChRM, 17 demagnetization great circles.

BP - Brancepeth

Details of sampling

Date sampled	12^{th} March 2003
Locality description	Extensive roadcut exposure on Masterton-Stronvar Road, just east of junction with Ngaumu Road.
Grid reference	T26/485148
Lithology	Light grey, calcareous mudstone, with at least one tuff member.
Assigned age	Tongaporutuan - unit defined as Bells Creek Mudstone.
Bedding attitude	229/18 NW (1 measurement)
Sampling	45 cores from 9 sampling levels, yielding 66 samples.
Stratigraphic thickness	35 metres

Demagnetization data

Samples demagnetized	AF 8 samples, thermal 40 samples.
Demagnetization behaviour	A strong PDF overprint with an underlying reversed polarity ChRM, but no stable endpoints were isolated before the onset of thermal alteration.
Range of NRMs	0.64–4.5$\times 10^{-4}$ Am^{-1}
Isolated components	33 demagnetization great circles.

Rock magnetic measurements

Samples analysed	3
Range of M_r/M_s	0.11–0.20
Range of B_{cr}/B_c	2.99–4.98
FORC behaviour	Large RR with poorly defined, ridge-like SD distribution with minor peaks at 20–40 mT.

BR - Burgess Road

Details of sampling

Dates sampled	22^{nd} April 2002
Locality description	Contiunous exposure on northern bank of Hangaroa River, on Pehiri Tuhunga Road just east of the Burgess Road turn-off.
Grid reference	X18/088752
Lithology	Sand-rich grey mudstones.
Assigned age	Early Tongaporutuan; stratigraphically below Maketu Sandstone.
Bedding attitude	064/42 SE (3 measurements)
Sampling	35 cores from 8 sampling levels, yielding 57 samples.
Stratigraphic thickness	14 metres

Demagnetization data

Samples demagnetized	AF 8 samples, thermal 8 samples.
Demagnetization behaviour	PDF overprint with no discernable higher stablity components.
Range of NRMs	3.4–7.8$\times 10^{-4}$ Am^{-1}
Isolated components	None.

Rock magnetic measurements

Samples analysed	2
Range of M_r/M_s	0.11–0.13
Range of B_{cr}/B_c	4.96–5.61
FORC behaviour	RR/SD 6.3–10.0; large RR with minimal SD distribution.

CH - Cheviot Hills

Details of sampling

Dates sampled	20^{th} April 2002
Locality description	Fairly continuous outcrop on southern verge of SH36, about 1 km west of turn-off onto Pehiri Tahunga Road.
Grid reference	X18/204688
Lithology	Decimetre scale interbedded mudstones and sand-rich mudstones.
Assigned age	Lillburnian
Bedding attitude	072/56 S (4 measurements)
Sampling	27 cores from 8 sampling levels, yielding 33 samples.
Stratigraphic thickness	17 metres

Demagnetization data

Samples demagnetized	AF 20 samples, thermal 13 samples.
Demagnetization behaviour	Strong PDF obscuring a highly rotated, reversed polarity ChRM. AF and thermal treatments were equally effective.
Range of NRMs	0.73–4.7$\times 10^{-4}$ Am^{-1}
Isolated components	15 anchored ChRMs, 5 unanchored ChRMs, 8 demagnetization great circles.

Rock magnetic measurements

Samples analysed	2
Range of M_r/M_s	0.08–0.10
Range of B_{cr}/B_c	4.96–5.41
FORC behaviour	FORCs not run.

FP - Flat Point

Details of sampling

Dates sampled	10^{th} March 2003
Locality description	Outcrop on beach accessed from car park at Flat Point (sampling just to east of river providing access).
Grid reference	T27/587925
Lithology	Blue-grey mudstones with decimetre scale sandstone interbeds, grading into paler, more calcareous mudstone with glauconitic sandstone horizons and less well-defined bedding.
Assigned age	Upper Waitakian to Otaian.
Bedding attitude	223/41 NW (3 measurements)
Sampling	29 cores from 8 sampling levels, yielding 40 samples.
Stratigraphic thickness	14 metres

Demagnetization data

Samples demagnetized	AF 19 samples, thermal 7 samples.
Demagnetization behaviour	Data are quite poor, with noisy demagnetization paths; AF demagnetization appears to be slightly more effective. Most samples appear to have a strong PDF overprint with an underlying reversed polarity ChRM; however, some samples may exhibit signs of a higher stability normal component instead.
Range of NRMs	0.5–15$\times 10^{-4}$ Am^{-1}
Isolated components	8 anchored ChRMs, 9 unanchored ChRMs, 7 demagnetization great circles.

FR - Falkner Road

Details of sampling

Dates sampled	31^{st} January 2003
Locality description	Limited exposure on the eastern bank of the Wharekopae River, at north end of Falkner Road just before Warwick Hills Farm. Some small scale folding evident.
Grid reference	X17/191864
Lithology	Sand-rich, dark grey siltstones.
Assigned age	Upper Altonian; appears stratigraphically equivalent to the Rere Sandstone.
Bedding attitude	105/29 S (1 measurement)
Sampling	21 cores from 5 sampling levels, yielding 22 samples.
Stratigraphic thickness	3 metres

Demagnetization data

Samples demagnetized	AF 5 samples, thermal 5 samples.
Demagnetization behaviour	Some PDF overprints but no indication of an underlying ChRM.
Range of NRMs	3.1–6.9$\times 10^{-4}$ Am^{-1}
Isolated components	None.

GI - Glen Innes

Details of sampling

Dates sampled	19^{th} February 2003
Locality description	Exposure in Hangaroa River, where it runs south and parallel to SH36, heading south toward Tiniroto. Sampled section just before turn-off to Glen Innes farm.
Grid reference	X18/116668
Lithology	Light grey sand-rich siltstones and sandstones.
Assigned age	Upper Tongaporutuan - stratigraphically above Makaretu Sandstone.
Bedding attitude	085/44 S (2 measurements)
Sampling	48 cores from 10 sampling levels, yielding 56 samples.
Stratigraphic thickness	19 metres

Demagnetization data

Samples demagnetized	AF 20 samples, thermal 10 samples.
Demagnetization behaviour	PDF overprints with no indication of higher stability components.
Range of NRMs	9.3–21$\times 10^{-4}$ Am^{-1}
Isolated components	None.

Rock magnetic measurements

Samples analysed	2
Range of M_r/M_s	0.11–0.13
Range of B_{cr}/B_c	4.23–4.58
FORC behaviour	Large RR with negligible SD distribution.

KR - Kahuranaki Road

Details of sampling

Dates sampled	8^{th} April 2002
Locality description	Steep bluffs, with storm gullies providing good exposure, on west side of Kahuranaki Road north of Elsthorpe, opposite a vineyard. Some small-scale (10–20 cm offset) normal faulting is visible.
Grid reference	V22/380435
Lithology	Mudstones and fine siltstones; some minor clay-rich intervals and sandstone lenses.
Assigned age	Southland (Clifdenian–Waiauan)
Bedding attitude	196/65 W (3 measurements)
Sampling	34 cores from 9 sampling levels, yielding 49 samples.
Stratigraphic thickness	32 metres

Demagnetization data

Samples demagnetized	AF 16 samples, thermal 16 samples.
Demagnetization behaviour	Anomalous stable magnetizations which do not align with PDF direction in geographic coordinates, and have anomalous, low inclination directions following tilt correction.
Range of NRMs	1.1–3.8×10^{-4} Am^{-1}
Isolated components	None that are meaningful.

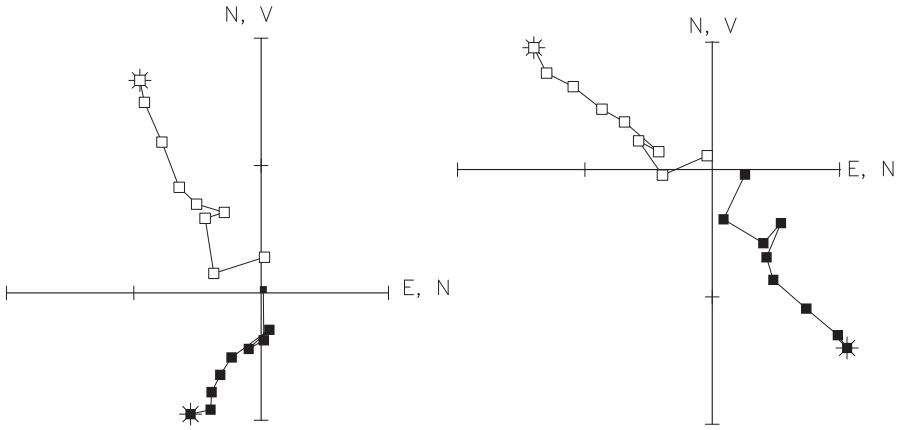

Figure A.1: Vector component plots of demagnetization data for representative sample KR01B, in: (a) geographic co-ordinates, where the ChRM has an unrealistically large normal polarity declination, and (b) tilt-corrected coordinates, where the inclination is anomalously shallow.

Rock magnetic measurements

Samples analysed	2
Range of M_r/M_s	0.09–0.11
Range of B_{cr}/B_c	4.23–4.55
FORC behaviour	FORCs not run.

MB - Mokonui Bridge

Details of sampling

Date sampled	30^{th} January 2003
Locality description	Extensive, smoothly weathering, exposure of shallowly dipping beds in the Wharekopae River, just upstream of a bridge on Mokonui Farm. Sampling was undertaken after a period of little rainfall which substantially increased accessible exposure.
Grid reference	X17/074860
Lithology	Dark calcareous mud and siltstones.
Assigned age	Altonian (probably early); stratigraphically just below Rere Sandstone.
Bedding attitude	027/18 SE (4 measurements)
Sampling	43 cores from 9 sampling levels, yielding 59 samples.
Stratigraphic thickness	33 metres

Demagnetization data

Samples demagnetized	AF 8 samples, thermal 35 samples.
Demagnetization behaviour	Thermal demagnetization is more effective, yielding unrotated normal polarity ChRMs (both anchored and unanchored) which are not completely unblocked before the onset of thermal alteration. Some AF demagnetized samples yielded moderate coercivity components with comparable directions.
Range of NRMs	1.3–4.1$\times 10^{-4}$ Am^{-1}
Isolated components	23 anchored ChRMs, 15 unanchored ChRMs.

MF - Maharahara Farm

Details of sampling

Dates sampled	9^{th}–10^{th} March 2002
Locality description	Steep bluff exposure on southern bank of Waikohu River, visible from Whakarau Road just east of Mahaki Settlement Road turn-off.
Grid reference	X17/223976
Lithology	Often finely-interbedded mudstones and fine sandstones.
Assigned age	Otaian
Bedding attitude	090/32 S (3 measurements)
Sampling	28 cores from 8 sampling levels, yielding 26 samples.
Stratigraphic thickness	22 metres

Demagnetization data

Samples demagnetized	AF 7 samples, thermal 7 samples.
Demagnetization behaviour	No real consistency - some possible indications of a relatively unrotated, reversed polarity component in a few samples but most are quasi-stable at best.
Range of NRMs	1.2–5.5$\times 10^{-4}$ Am^{-1}
Isolated components	None.

Rock magnetic measurements

Samples analysed	2
Range of M_r/M_s	0.08–0.17
Range of B_{cr}/B_c	3.38–5.85
FORC behaviour	Large RR with virtually no SD distribution.

MK - Mangapoike River

Details of sampling

Dates sampled	12^{th} February 2003
Locality description	Cliff exposure on road running parallel to and above Mangapoike River.
Grid reference	X19/071449
Lithology	Massive white and light grey mudstones.
Assigned age	Kapitean (below Opoitian unconformity).
Bedding attitude	187/30 W (3 measurements)
Sampling	26 cores from 6 sampling levels, yielding 32 samples.
Stratigraphic thickness	16 metres

Demagnetization data

Samples demagnetized	AF 6 samples, thermal 20 samples.
Demagnetization behaviour	Good behaviour for both thermal and AF treatment. A minor PDF overprint is easily removed, revealing a stable, normal polarity ChRM.
Range of NRMs	2.4–3.7$\times 10^{-4}$ Am^{-1}
Isolated components	23 anchored ChRMs, 3 unanchored ChRMs.

Rock magnetic measurements

Samples analysed	1
Range of M_r/M_s	0.01
Range of B_{cr}/B_c	4.17
FORC behaviour	Large RR with a minor SD distribution peaking at 20-30 mT.

MP - Makarori Point

Details of sampling

Dates sampled	25^{th}–26^{th} April 2002
Locality description	Cliff exposure around point at north end of Wainui Beach, just north of Gisborne. The ocean is rapidly eroding the shoreline, resulting in fresh exposure. Minor normal faulting and folding is visible along the entire length of the outcrop.
Grid reference	Y18/541693
Lithology	Decimetre scale interbedded mudstones and silt/sandstones, with the latter showing some signs of soft sediment deformation.
Assigned age	Clifdenian–Lillburnian (Tuaheni Point Formation of Neef (1992)).
Bedding attitude	307/14 NE (4 measurements)
Sampling	35 cores from 9 sampling levels, yielding 50 samples.
Stratigraphic thickness	10 metres

Demagnetization data

Samples demagnetized	AF 34 samples, thermal 16 samples.
Demagnetization behaviour	Data are quite noisy but indicate a minimal PDF overprint, overlying a stable normal polarity ChRM, with consistently large rotations indicated. AF and thermal treatments are equally effective.
Range of NRMs	0.85–5.7$\times 10^{-4}$ Am^{-1}
Isolated components	36 anchored ChRMs, 8 unanchored ChRMs.

Rock magnetic measurements

Samples analysed	6
Range of M_r/M_s	0.08–0.25
Range of B_{cr}/B_c	4.48–6.24
FORC behaviour	Large RR with minor, ridge-like SD distribution.

MR - Makaretu Road

Details of sampling

Dates sampled	29^{th} January 2003
Locality description	A roadcut/verge outcrop at Wharekopae turn-off on Makaretu Road, southward off State Highway 2 just past Otoko.
Grid reference	X17/118917
Lithology	Massive m-scale beds of fine, light blue-grey sandstone, some of which have been pervasively weathered
Assigned age	Altonian, probably upper as the sampled unit appears to be stratigraphically equivalent to the Rere Sandstone.
Bedding attitude	086/30 S (3 measurements)
Sampling	32 cores from 7 sampling levels, yielding 40 samples.
Stratigraphic thickness	11 metres

Demagnetization data

Samples demagnetized	AF 7 samples, thermal 20 samples.
Demagnetization behaviour	Samples have strong NRMs and apparently stable magnetizations, with anomalous directions (shallow inclinations after tilt-correction, do not align with PDF in geographic coordinates) which cluster into two distinct groups (one highly rotated, one less so). Both of these components are thermally stable but have low MDFs.
Range of NRMs	17–160$\times 10^{-4}$ Am^{-1}
Isolated components	17 anchored ChRMs, 10 unanchored ChRMs.

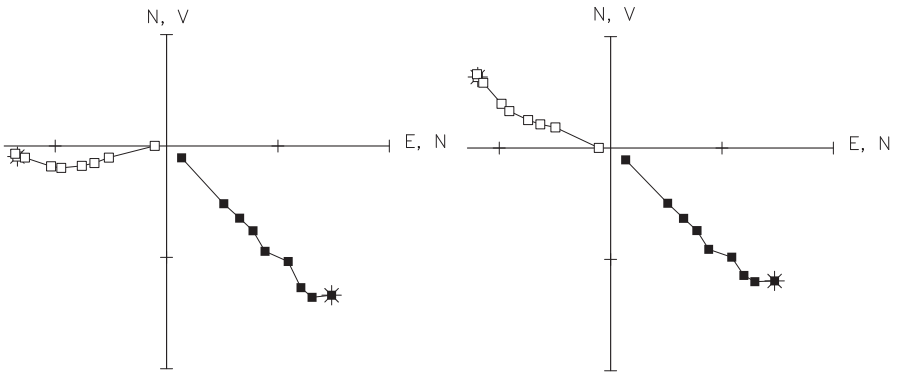

Figure A.2: Vector component plots of demagnetization data for representative sample MR10B, in: (a) geographic co-ordinates, and (b) tilt-corrected coordinates. In both cases the inclination is unrealistically shallow and the declination unrealistically large.

Rock magnetic measurements

Samples analysed	4
Range of M_r/M_s	0.06–0.09
Range of B_{cr}/B_c	4.52–4.99
FORC behaviour	Large RR with negligible SD distribution.

MS - Matawai Station

Details of sampling

Dates sampled	14^{th} February 2002, 25^{th}–26^{th} January 2003
Locality description	A fairly continuous exposure in the bed of the Waikohu River, 100-200 m west and upstream of where it is bridged by Oliver Road north of Matawai Station. Outcrop is fractured, with associated shearing and offsets of up to 10 cm.
Grid reference	X17/128009
Lithology	Light blue-grey calcareous mudstones, with massive sandstone interbeds.
Assigned age	Otaian
Bedding attitude	088/54 S (6 measurements)
Sampling	71 cores from 14 sampling levels, yielding 70 samples.
Stratigraphic thickness	47 metres

Demagnetization data

Samples demagnetized	AF 8 samples, thermal 62 samples.
Demagnetization behaviour	All samples are strongly affected by a PDF overprint. AF demagnetization was ineffective. Thermal demagnetization isolated a stable ChRM in 21% of samples at temperatures of 200–380°C, but in most cases incomplete removal of the overprint resulted in demagnetization great circles.
Range of NRMs	0.13–2.2×10^{-4} Am^{-1}
Isolated components	8 anchored ChRMs, 5 unanchored ChRMs, 36 demagnetization great circles.

Rock magnetic measurements

Samples analysed	2
Range of M_r/M_s	0.12–0.13
Range of B_{cr}/B_c	2.93–3.21
FORC behaviour	RR/SD 2.6–3.0 (small SD peak at ∼20 mT).

NG - Ngatimita

Details of sampling

Dates sampled	23^{rd} April 2002, 14^{th} February 2003
Locality description	Moderately weathered roadside outcrop of steeply dipping beds on Pehiri-Tahunga Road, just east of the turn-off to Ngatimita Farm.
Grid reference	X18/063762
Lithology	Decimetre scale interbedded mudstones and mud-rich sandstones, with rarer coarse sandstone beds.
Assigned age	Southland (Clifdenian–Waiauan)
Bedding attitude	084/43 S (6 measurements)
Sampling	71 cores from 14 sampling levels, yielding 87 samples.
Stratigraphic thickness	21 metres

Demagnetization data

Samples demagnetized	AF 56 samples, thermal 9 samples.
Demagnetization behaviour	Strong PDF overprint obscures a rotated, reversed polarity ChRM, which is successfully isolated in some samples. Thermal and AF demagnetization appear to be equally effective in removing the overprint.
Range of NRMs	0.54–3.1$\times 10^{-4}$ Am^{-1}
Isolated components	30 anchored ChRMs, 1 unanchored ChrM, 23 demagnetization great circles.

Rock magnetic measurements

Samples analysed	3
Range of M_r/M_s	0.06–0.12
Range of B_{cr}/B_c	5.14–6.39
FORC behaviour	Large RR and ridge-like, low coercivity SD distribution, with an additional minor peak at 30-50 mT.

NP - Ngatara-Poha

Details of sampling

Dates sampled	24^{th}April 2002
Locality description	Two separate roadside outcrops with shallowly-dipping beds, about 200 m apart, on Pehiri-Tahunga road between Ngatara and Poha Farms.
Grid reference	X18/160749
Lithology	Interbedded sand-rich mudstones and sandstones.
Assigned age	Early Tongaporutuan, possibly late Waiauan - stratigraphically just beneath the Maketu Sandstone.
Bedding attitude	186/23 W (3 measurements)
Sampling	28 cores from 6 sampling levels, yielding 33 samples.
Stratigraphic thickness	82 metres

Demagnetization data

Samples demagnetized	AF 9 samples, thermal 14 samples.
Demagnetization behaviour	Normal polarity ChRM indicating moderate to large clockwise rotations. No real overprint. AF demagnetization was slightly more effective than thermal treatment.
Range of NRMs	4.1–12$\times 10^{-4}$ Am^{-1}
Isolated components	14 anchored ChRMs, 1 unanchored ChRM, 7 demagnetization great circles.

NR - Nukutaurua Road

Details of sampling

Dates sampled	18^{th} April 2002
Locality description	Extensive shoreline exposure of steeply dipping beds on the beach at the end of Nukutaurua Road, accessed from Mahia East Coast Road just before it turns south away from the northern coast. The beach borders Maori land and as of 2003 may no longer be accessible.
Grid reference	Y19/402222
Lithology	Pale grey mudstones, regularly interbedded with white reworked tuff.
Assigned age	Tongaporutuan
Bedding attitude	240/48 NW (3 measurements)
Sampling	42 cores from 11 sampling levels, yielding 83 samples.
Stratigraphic thickness	82 metres

Demagnetization data

Samples demagnetized	AF 61 samples, thermal 22 samples.
Demagnetization behaviour	Generally weak NRMs and noisy demagnetization paths, with an unstable primary remanence at a number of horizons. Both normal and reversed polarity ChRMs were identified in other parts of the section, sometimes within sister samples from the same core.
Range of NRMs	0.16–6.4$\times 10^{-4}$ Am^{-1}
Isolated components	25 anchored ChRMs, 23 unanchored ChRMs.

Rock magnetic measurements

Samples analysed	21
Range of M_r/M_s	0.03–0.20
Range of B_{cr}/B_c	3.13–17.47
FORC behaviour	RR/SD 3.0–90. Large RRs with minor, low coercivity SD distributions.

OK - Okau

Details of sampling

Dates sampled	9^{th} March 2003
Locality description	Steeply dipping beds prominently exposed on the beach where thr road running north from Whakataki and Castlepoint rejoins the shore.
Grid reference	U26/840361
Lithology	Calcareous fine sandstones and siltstones interbedded between more massive graded sandstones (turbidite sequence).
Assigned age	Late Waitakian–early Otaian (Whakataki Formation).
Bedding attitude	207/50 W (4 measurements)
Sampling	38 cores from 9 sampling levels, yielding 50 samples.
Stratigraphic thickness	22 metres

Demagnetization data

Samples demagnetized	AF 8 samples, thermal 36 samples.
Demagnetization behaviour	Minimal overprint - normal polarity ChRM, which can sometimes be anchored to the centre of the demagnetization plot but in many samples it misses the origin by a large amount, indicating a higher stability component. AF treatment often leads to noisy demagnetization paths.
Range of NRMs	0.91–3.3$\times 10^{-4}$ Am^{-1}
Isolated components	12 anchored ChRMs, 25 unanchored ChRMs.

Rock magnetic measurements

Samples analysed	2
Range of M_r/M_s	0.13–0.14
Range of B_{cr}/B_c	3.65–3.83
FORC behaviour	Ridge-like SD distribution extending to 50–60 mT.

OR - Oliver Road

Details of sampling

Dates sampled	15^{th} February 2002, 27^{th} January 2003
Locality description	A roadcut/verge outcrop on the highest point on Oliver Road before it descends to Matawai Station.
Grid reference	X17/118988
Lithology	Moderately weathered, shallowly dipping grey and brown sandy mudstones and siltstones
Assigned age	Otaian
Bedding attitude	067/12 SE (3 measurements)
Sampling	70 cores from 16 sampling levels, yielding 81 samples.
Stratigraphic thickness	27 metres

Demagnetization data

Samples demagnetized	AF 9 samples, thermal 72 samples.
Demagnetization behaviour	Most samples are strongly affected by a PDF overprint, and AF demagnetization is ineffective. Thermal demagnetization mostly results in demagnetization great circles. Stable ChRMs are only isolated where no obvious overprint is observed; this component had mostly unblocked by 400°C.
Range of NRMs	0.47–7.7×10^{-4} Am^{-1}
Isolated components	6 anchored ChRMs, 3 unanchored ChRMs, 41 demagnetization great circles.

Rock magnetic measurements

Samples analysed	2
Range of M_r/M_s	0.17–0.18
Range of B_{cr}/B_c	2.70–2.85
FORC behaviour	RR/SD 2.7–3.2 (small SD peak at ∼20 mT).

PC - Paparatu Cottage

Details of sampling

Dates sampled	10^{th} February 2003
Locality description	Stream bed and bank exposure in the Mangapoike River, behind the managers cottage for Paparatu Station, on Waingake-Mangapoike Road.
Grid reference	X18/175529
Lithology	Mudstones and siltstones with rare fine sandstone members.
Assigned age	Clifdenian; part of Tunanui Formation?
Bedding attitude	183/21 W (44 measurements)
Sampling	33 cores from 8 sampling levels, yielding 33 samples.
Stratigraphic thickness	19 metres

Demagnetization data

Samples demagnetized	AF 14 samples, thermal 15 samples.
Demagnetization behaviour	Very strong PDF overprint, which in a few samples is removed enough to allow a highly rotated, normal polarity ChRM to be isolated.
Range of NRMs	0.56–2.1×10^{-4} Am^{-1}
Isolated components	5 anchored ChRMs, 1 unanchored ChRM, 7 demagnetization great circles.

Rock magnetic measurements

Samples analysed	2
Range of M_r/M_s	0.09–0.12
Range of B_{cr}/B_c	3.90–4.98
FORC behaviour	Ridge-like SD distribution extending to 40–60 mT.

PN - Paoanui Point

Details of sampling

Dates sampled	20^{th} March 2003
Locality description	Wave-cut platform exposed at Paoanui Point, ∼2 km north along the beach from Pourerere carpark.
Grid reference	V23/420182
Lithology	Dark blue-grey mudstone with massive, discontinuous sandstone interbeds, particularly toward the top of the section.
Assigned age	Waiauan
Bedding attitude	033/61 SE (3 measurements)
Sampling	37 cores from 9 sampling levels, yielding 53 samples.
Stratigraphic thickness	47 metres

Demagnetization data

Samples demagnetized	AF 25 samples, thermal 8 samples.
Demagnetization behaviour	Strong PDF overprint with no discernable higher stability components.
Range of NRMs	2.3–3.9×10^{-4} Am^{-1}
Isolated components	None.

PP - Putiki Point

Details of sampling

Dates sampled	15^{th}–16^{th} April 2002
Locality description	Low cliff exposure of shallowly dipping beds on the beach beneath Mahia East Coast Road, just before it crosses Whangawehi Stream.
Grid reference	Y19/379226
Lithology	White, ash-rich mudstones, with minor reworked tuff beds.
Assigned age	Tongaporutuan (probably late).
Bedding attitude	239/11 NW (3 measurements)
Sampling	35 cores from 9 sampling levels, yielding 57 samples.
Stratigraphic thickness	17 metres

Demagnetization data

Samples demagnetized	AF 8 samples, thermal 34 samples.
Demagnetization behaviour	Strong PDF overprint which is generally not effectively removed by AF demagnetization. Thermal treatment allows a reversed polarity ChRM to be isolated.
Range of NRMs	0.63–8.3$\times 10^{-4}$ Am^{-1}
Isolated components	22 anchored ChRMs, 14 unanchored ChRMs, 3 demagnetization great circles.

Rock magnetic measurements

Samples analysed	4
Range of M_r/M_s	0.20–0.24
Range of B_{cr}/B_c	3.23–3.72
FORC behaviour	RR/SD 3.9–4.8; ridge-like SD distribution with peak at 20-30 mT.

SB - Sponge Bay

Details of sampling

Dates sampled	3^{rd}–4^{th} February 2003
Locality description	Beach exposure on the eastern side of a cove accessed from car park at the end of Sponge Bay Road.
Grid reference	Y18/498658
Lithology	Fine dark blue-grey mudstones with interbedded coarse turbidites.
Assigned age	Clifdenian–Lillburnian (Tuaheni Point Formation of Neef (1992)).
Bedding attitude	353/47 E (7 measurements)
Sampling	42 cores from 12 sampling levels, yielding 43 samples.
Stratigraphic thickness	43 metres

Demagnetization data

Samples demagnetized	AF 18 samples, thermal 18 samples.
Demagnetization behaviour	Data are quite noisy, but appear to indicate a minimally overprinted, normal polarity ChRM with moderate declination anomaly.
Range of NRMs	0.36–2.7$\times 10^{-4}$ Am^{-1}
Isolated components	18 anchored ChRMs, 3 unanchored ChRMs.

Rock magnetic measurements

Samples analysed	2
Range of M_r/M_s	0.10–0.11
Range of B_{cr}/B_c	4.18–5.57
FORC behaviour	Ridge-like SD distribution with minor peak at 30–40 mT.

SN - Strathblane Farm

Details of sampling

Dates sampled	11^{th} February 2003
Locality description	Weathered roadside outcrop on Bushy Knoll Road ∼1 km southwest of Hangaroa, on a rise overlooking Strathblane Farm.
Grid reference	X18/111696
Lithology	Brown mudstones and siltstones with interbedded sandstones.
Assigned age	Lillburnian
Bedding attitude	146/27 SW (3 measurements)
Sampling	31 cores from 8 sampling levels, yielding 35 samples.
Stratigraphic thickness	25 metres

Demagnetization data

Samples demagnetized	AF 23 samples, thermal 8 samples.
Demagnetization behaviour	Strong PDF overprint; some inconclusive indications of an underlying normal polarity component but, if present, it cannot be reliably isolated.
Range of NRMs	1.8–4.6×10^{-4} Am^{-1}
Isolated components	None.

Rock magnetic measurements

Samples analysed	2
Range of M_r/M_s	0.06–0.09
Range of B_{cr}/B_c	4.05–5.53
FORC behaviour	Large RR with minor, ridge-like SD distribution to 30–40 mT.

TC - Te Waipera Cemetary

Details of sampling

Dates sampled	2^{nd}–3^{rd} April 2002
Locality description	Shoreside end of a promontory close to a settlement and small cemetary at Te Waipera, about 1 km east along the coast road from Mahia.
Grid reference	Y19/362233
Lithology	Massive, dark grey, fine-grained mudstones, overlain by interbedded mudstones and reworked tuffaceous beds, with one primary tuff.
Assigned age	Tongaporutuan (probably late)
Bedding attitude	203/10 NW (3 measurements)
Sampling	34 cores from 9 sampling levels, yielding 54 samples.
Stratigraphic thickness	24 metres

Demagnetization data

Samples demagnetized	AF 37 samples, thermal 17 samples.
Demagnetization behaviour	Strong NRMs with a minimally overprinted, normal polarity ChRM that is recoverable from most samples. Thermal and AF treatments are both effective, but strong GRMs above 40 mT were observed for AF treated samples from the lower part of the section.
Range of NRMs	2.7–34$\times 10^{-4}$ Am^{-1}
Isolated components	32 anchored ChRMs, 16 unanchored ChRMs.

Rock magnetic measurements

Samples analysed	15
Range of M_r/M_s	0.12–0.52
Range of B_{cr}/B_c	1.35–3.90
FORC behaviour	RR/SD 0.7–11; SD distribution ranging between strong peaks at ∼60 mT, ridge-like distributions peaking at ∼20 mT, and a negligible SD components of magnetization.

TF - Te Korau Farm

Details of sampling

Dates sampled	13^{th} February 2003
Locality description	Fairly weathered stream bed/bank exposure east of bridge on Stafford Road, just north of Te Korau Farm.
Grid reference	X18/205761
Lithology	Dark, fairly sandy calcareous mudstone with thin sandstone interbeds.
Assigned age	Llilburnian-Waiauan
Bedding attitude	199/20 W (3 measurements)
Sampling	28 cores from 7 sampling levels, yielding 27 samples.
Stratigraphic thickness	13 metres

Demagnetization data

Samples demagnetized	AF 6 samples, thermal 15 samples.
Demagnetization behaviour	A minimally overprinted, normal polarity ChRM is recoverable from most samples. Thermal treatment was superior to AF demagnetization.
Range of NRMs	3.4–9.5$\times 10^{-4}$ Am^{-1}
Isolated components	21 anchored ChRMs.

Rock magnetic measurements

Samples analysed	2
Range of M_r/M_s	0.21–0.44
Range of B_{cr}/B_c	1.41–3.37
FORC behaviour	Significant SD distributions with strong–moderate peaks at 50–60 mT.

TH - Turihaua Point

Details of sampling

Dates sampled	7^{th} February 2003
Locality description	Shoreline exposure on a wave cut platform on the beach running alongside SH35, ∼1 km north of Turihaua Point.
Grid reference	Y18/608739
Lithology	Massive, dark grey mudstones with rare massive sandstone interbeds.
Assigned age	Tongaporutuan
Bedding attitude	038/19 SE (3 measurements)
Sampling	37 cores from 8 sampling levels, yielding 54 samples.
Stratigraphic thickness	14 metres

Demagnetization data

Samples demagnetized	AF 28 samples, thermal 8 samples.
Demagnetization behaviour	Erratic demagnetization behaviour was observed at some sampling levels, but most samples exhibit a moderately overprinted normal polarity ChRM with clockwise declination anomalies. AF and thermal treatments both appear to be effective, although thermally demagnetized samples occasionally have noisy demagnetization paths.
Range of NRMs	1.3–33$\times 10^{-4}$ Am^{-1}
Isolated components	19 anchored ChRMs, 4 unanchored ChRMs, 2 demagnetization great circles.

TI - Titoki Road

Details of sampling

Dates sampled	18^{th} March 2003
Locality description	Extensive stream bank exposure visible to the south from the road to Blackhead and Paoanui Point, just before the junction with Titoki Road.
Grid reference	V23/281249
Lithology	Dark brown and grey mudstones and siltstones with rare massive sandstone beds. Weathered ash fragments are present in some beds.
Assigned age	Lillburnian (probably part of Makara Formation).
Bedding attitude	201/30 W (5 measurements)
Sampling	44 cores from 9 sampling levels, yielding 63 samples.
Stratigraphic thickness	23 metres

Demagnetization data

Samples demagnetized	AF 38 samples, thermal 9 samples.
Demagnetization behaviour	Normal polarity ChRM with a small PDF overprint. AF treatment is generally superior to thermal; however, some AF treated samples acquire large GRMs above 20-30 mT, which could have been the result of a temporary fault with the demagnetizing coils.
Range of NRMs	2.8–9.6$\times 10^{-4}$ Am^{-1}
Isolated components	18 anchored ChRMs, 20 unanchored ChRMs.

Rock magnetic measurements

Samples analysed	2
Range of M_r/M_s	0.15–0.16
Range of B_{cr}/B_c	3.31–3.37
FORC behaviour	Large RR and moderate SD distribution at 20-30 mT.

TK - Te Koawa

Details of sampling

Dates sampled	20^{th} and 22^{nd}–23^{rd} March 2002
Locality description	Outcrop in stream bed and banks, south/downstream of where it fords Whakarau Road, east of Te Koawa.
Grid reference	X17/196994
Lithology	Decimetre-scale beds of light grey, calcareous mudstone.
Assigned age	Altonian
Bedding attitude	309/56 NE (7 measurements)
Sampling	31 cores from 10 sampling levels, yielding 35 samples.
Stratigraphic thickness	46 metres

Demagnetization data

Samples demagnetized	AF 10 samples, thermal 10 samples.
Demagnetization behaviour	Thermal treatment appears to be more effective than AF, but neither technique removed much of what appears to be a strong PDF overprint. Some possible indications of a relatively unrotated, reversed polarity component in a few samples but nothing conclusive.
Range of NRMs	0.65–2.0$\times 10^{-4}$ Am^{-1}
Isolated components	None.

TP - Tatapouri Point

Details of sampling

Dates sampled	5^{th}–6^{th} February 2003
Locality description	Cliff and beach exposure about 1 km east along coast from Makarori, just west of Tatapouri Point.
Grid reference	Y18/574705
Lithology	Fine dark blue-grey mudstones with interbedded coarse turbidites.
Assigned age	Clifdenian–Llilburnian (Tuaheni Point Formation of Neef (1992)).
Bedding attitude	273/32 N (4 measurements)
Sampling	41 cores from 10 sampling levels, yielding 46 samples.
Stratigraphic thickness	19 metres

Demagnetization data

Samples demagnetized	AF 17 samples, thermal 22 samples.
Demagnetization behaviour	AF and thermal treatments were both effective, but thermally demagnetized samples can have noisy demagnetization paths. A minimally overprinted, normal polarity ChRM indicates large clockwise rotations.
Range of NRMs	0.69–5.0$\times 10^{-4}$ Am^{-1}
Isolated components	27 anchored ChRMs 10 unanchored ChRMs.

Rock magnetic measurements

Samples analysed	2
Range of M_r/M_s	0.07–0.16
Range of B_{cr}/B_c	3.16–4.99
FORC behaviour	Large RRs; one sample has a moderate SD peak at 30–40 mT, the other a more ridge-like SD distribution at lower coercivities.

TR - Taumata Road

Details of sampling

Dates sampled	12^{th}–13^{th} March 2002
Locality description	Cliff and bank exposure in a stream running parallel to Taumata Road, between two bridges southwest of Wharekopae Field Station.
Grid reference	X17/053807
Lithology	Fairly massive grey mud and siltstones.
Assigned age	Clifdenian
Bedding attitude	348/19 E (4 measurements)
Sampling	55 cores from 15 sampling levels, yielding 70 samples.
Stratigraphic thickness	47 metres

Demagnetization data

Samples demagnetized	AF 13 samples, thermal 15 samples.
Demagnetization behaviour	No clear primary component underneath a strong PDF overprint.
Range of NRMs	1.3–2.6$\times 10^{-4}$ Am^{-1}
Isolated components	None.

WB - Whangaehu Beach

Details of sampling

Dates sampled	6^{th}–7^{th} March 2002
Locality description	Exposure of near vertical beds below cliffs ∼100 m south of car park at Whangaehu Beach.
Grid reference	V24/185829
Lithology	Thinly interbedded grey and black (organic rich) mudstones.
Assigned age	Lliburnian–Waiauan; part of Whangaehu Mudstone.
Bedding attitude	054/73 SE (4 measurements)
Sampling	36 cores from 9 sampling levels, yielding 53 samples.
Stratigraphic thickness	44 metres

Demagnetization data

Samples demagnetized	AF 46 samples, thermal 8 samples.
Demagnetization behaviour	Consistently strong overprint that is being removed toward reversed polarity primary direction , but no stable endpoints can be isolated. In geographic co-ordinates the overprint has a normal polarity with a westerly declination, so it may not be a PDF. AF and thermal treatments are equally effective.
Range of NRMs	0.51–4.3×10^{-4} Am^{-1}
Isolated components	None.

WH - Waterfall Hill

Details of sampling

Dates sampled	18^{th}–19^{th} February 2002
Locality description	Roadside outcrop on Pehiri-Tahunga Road about 2 km north of the SH 36 turnoff.
Grid reference	X18/204706
Lithology	Massive, metre-scale sandstone beds with thinner interbedded mudstones.
Assigned age	Late Waitakian–Altonian (probably early, as the late Altonian is generally missing in this region).
Bedding attitude	238/63 NW (2 measurements)
Sampling	27 cores from 8 sampling levels, yielding 37 samples.
Stratigraphic thickness	28 metres

Demagnetization data

Samples demagnetized	AF 8 samples, thermal 8 samples.
Demagnetization behaviour	No clear primary component underneath a strong PDF overprint.
Range of NRMs	2.2–5.3$\times 10^{-4}$ Am^{-1}
Isolated components	None.

Rock magnetic measurements

Samples analysed	2
Range of M_r/M_s	0.13–0.14
Range of B_{cr}/B_c	3.67–3.99
FORC behaviour	Large RR with a ridge-like, low coercivity SD distribution.

WM - Waimarama Beach

Details of sampling

Dates sampled	17^{th}–18^{th} March 2003
Locality description	Beach outcrop just south of the car park at the southern end of the beach access road. There is an extensive outcrop of fault melange 50-100 m south along the beach, and small-scale faulting and folding is also observable within the outcrop.
Grid reference	W22/519461
Lithology	Massive, fractured, light blue-grey mudstone interbedded with thick welded tuffs, with internal lamination.
Assigned age	Waitakian–Altonian
Bedding attitude	W22/519461 (5 measurements)
Sampling	38 cores from 8 sampling levels, yielding 61 samples.
Stratigraphic thickness	13 metres

Demagnetization data

Samples demagnetized	AF 9 samples, thermal 8 samples.
Demagnetization behaviour	Strong PDF overprint, with no clear systematic behaviour at higher temperatures or fields; some samples look like they might have a normal polarity primary direction, whilst others possibly have a reversed polarity.
Range of NRMs	1.7–6.5$\times 10^{-4}$ Am^{-1}
Isolated components	None.

WT - Whangaehu Tuff

Details of sampling

Dates sampled	14^{th} April 2002
Locality description	Sequence exposed in cliffs just around a spit ∼200 m south from Whangaehu Beach car park - not accessible at high tide.
Grid reference	V24/186826
Lithology	Massive, light grey, sandy siltstones containing a single tuff bed.
Assigned age	Tongaporutuan
Bedding attitude	051/38 SE (2 measurements)
Sampling	28 cores from 7 sampling levels, yielding 49 samples.
Stratigraphic thickness	10 metres

Demagnetization data

Samples demagnetized	AF 7 samples, thermal 14 samples.
Demagnetization behaviour	Strong PDFs, with no higher-stability components discernable except from tuffaceous samples, from which a normal polarity ChRM could be isolated.
Range of NRMs	0.96–4.3×10^{-4} Am^{-1}
Isolated components	4 anchored ChRMs, 1 unanchored ChRM.

WU - Waihau Beach

Details of sampling

Dates sampled	27^{th}–28^{th} March 2002
Locality description	Shallowly dipping exposure at the base of the cliffs, about 1.5 km south of car park on Waihau Beach.
Grid reference	Z17/719916
Lithology	Massive steel-grey mudstones with interbedded, discontinuous tuff horizons up to 30 cm thick.
Assigned age	Early Tongaporutuan
Bedding attitude	194/23 W (4 measurements)
Sampling	41 cores from 11 sampling levels, yielding 85 samples.
Stratigraphic thickness	7 metres

Demagnetization data

Samples demagnetized	AF 26 samples, thermal 34 samples.
Demagnetization behaviour	ChRMs isolated by both thermal (unblocking temperatures of 280–380°C) and AF (MDFs of 50–60 mT) demagnetization; thermal treatment is generally better. Normal and reversed polarity directions were both isolated, and polarities are generally consistent within a sampling level.
Range of NRMs	0.15–7.1×10^{-4} Am^{-1}
Isolated components	33 anchored ChRMs, 11 unanchored ChRMs, 2 demagnetization great circles.

Rock magnetic measurements

Samples analysed	8
Range of M_r/M_s	0.11–15
Range of B_{cr}/B_c	3.38–3.87
FORC behaviour	RR/SD 3.8–5.0; a large reversible component of magnetization with a minor, ridge-like SD distribution peaking at 20-40 mT.

Appendix B

Demagnetization and rock magnetic data

The CD inside the back cover of this thesis contains the following data:

- Demagnetization data for all of the samples analysed, in the folder 'Demag'. Sub-folders contain individual files for thermally and AF demagnetized samples, in the form of raw .DAT files, and .txt files with geographic and tilt corrections applied.
- Core orientation measurements from all localities, in the file 'cores.text'. Orientations have been corrected for the local magnetic field declination of 20.5° at the time of sampling.
- Averaged bedding measurements from all localities, in the file 'tilt.txt', again corrected for the local magnetic field declination.
- Rock magnetic data in the folder 'Rockmag'. Raw data for all measured hysteresis loops, back-field remanence curves, and FORC series are stored in separate sub-folders.

Please note that these data are provided for reference purposes only, and the permission of the author should be sought before they are put to any other use.